UNIVERSITÉ DU QUÉBEC À TROIS-RIVIÈRES

MATÉRIAUX HYDROGÉLIFIÉS ET CRYOGÉLIFIÉS À BASE DE CARBOXYMÉTHYLCHITOSANE : UNE APPROCHE DURABLE POUR LA DÉCONTAMINATION DES RÉSIDUS D'ANTIDÉPRESSEURS EN SOLUTION AQUEUSE

THÈSE PRÉSENTÉ(E)
COMME EXIGENCE PARTIELLE
DU DOCTORAT EN SCIENCES ET GÉNIE DES MATÉRIAUX LIGNOCELLULOSIQUES

PAR
GILBERT ROMEO NKANA NKANA

AVRIL 2026

UNIVERSITÉ DU QUÉBEC À TROIS-RIVIÈRES

DOCTORAT EN SCIENCES ET GÉNIE DES MATÉRIAUX LIGNOCELLULOSIQUES

Direction de recherche :

Phuong Nguyen-Tri	
Prénom et nom	directeur de recherche
Bruno Chabot	
Prénom et nom	codirecteur de recherche

Jury d'évaluation

(Selon le type de travail de recherche, deux à cinq membres de jury doivent être identifiés ci-dessous)

Simon Barnabé	Président
Prénom et nom	Fonction du membre de jury
Sasan Sattarpanah Karganroudi	Membre interne
Prénom et nom	Fonction du membre de jury
Aymen Amin Assadi	Membre externe
Prénom et nom	Fonction du membre de jury
Phuong Nguyen-Tri	Membre interne/ directeur de recherche
Prénom et nom	Fonction du membre de jury
Bruno Chabot	Membre interne/ codirecteur de recherche
Prénom et nom	Fonction du membre de jury

Thèse soutenue le 25 03 2026

Avant-propos

Mon intérêt pour la décontamination des eaux polluées par les médicaments psychotropes est né à la suite de la pandémie de Covid-19. Cet « ennemi invisible » a eu pour principale conséquence la hausse de la consommation des antidépresseurs dont le rejet dans l'environnement cause des préjudices irréversibles au biote aquatique. La préservation de l'environnement est un enjeu universel qui requiert notre attention ainsi qu'un investissement collectif.

Cette thèse est une modeste contribution qui propose une solution simple à cette problématique à travers le développement de matériaux fonctionnels capables de fixer ce type de contaminant émergent. Elle reflète à la fois un investissement personnel et un engagement scientifique visant à améliorer la qualité de l'eau contaminée par les antidépresseurs avant son rejet dans l'environnement.

La réalisation de ce projet n'aurait pas été possible sans l'expertise scientifique et l'encadrement des professeurs Phuong Nguyen-Tri et Bruno Chabot à qui je témoigne toute ma gratitude. J'espère que ce travail apportera des éléments pertinents sur l'utilisation des matériaux fonctionnels gélifiés pour l'élimination des antidépresseurs en milieu aqueux et ouvrira de nouvelles perspectives de recherche pour le développement de matériaux adsorbants avancés.

Remerciements

Je tiens tout d'abord à remercier mon Dieu tout-puissant de m'avoir accordé le privilège d'être en santé tout au long de cette aventure enrichissante, et de m'avoir accordé l'ouverture d'esprit nécessaire pour accomplir ce travail. Mes remerciements vont également à l'endroit de ma famille qui a toujours été un soutien inconditionnel dans tout mon processus académique et spécialement à ma conjointe qui m'a accompagné sur tous les plans dans cet exercice intellectuel durant toutes ces années.

J'exprime ma profonde reconnaissance à mon directeur de recherche, Pr. Phuong Nguyen-Tri pour son accompagnement scientifique, son expertise, ses conseils avisés, sa disponibilité et la confiance qu'il m'a accordée tout au long de ce travail. Tout cela a contribué à améliorer la qualité de mes travaux.

Mes remerciements s'adressent également à mon co-directeur, Pr. Bruno Chabot, qui n'a ménagé aucun effort et s'est pleinement investi dans la réalisation de ce projet, à travers sa disponibilité, son expertise, ses commentaires toujours constructifs, sa rigueur et la confiance qu'il m'a toujours accordée. Merci pour le soutien remarquable à chaque étape de mon parcours.

Je souhaite remercier chaleureusement les techniciens de laboratoire Jocelyn Bouchard, Jean-Philippe Marineau, Kéziah Milette, Raphaël Gervais Lavoie pour leur accompagnement dans mes analyses et caractérisations, ainsi qu'Isabelle Boulan pour la fabrication du montage d'extrusion électrostatique, la caractérisation de mes échantillons et l'assistance technique.

J'exprime toute ma gratitude à l'Université du Québec à Trois-Rivières et à l'Institut d'Innovations en Écomatériaux, Écoproduits et Écoénergies pour les ressources matérielles et scientifiques mises à ma disposition dans le cadre de la réalisation de ce projet de recherche.

Je remercie également tous mes collègues de laboratoire, Lahbib Abenghal, Berfai Badredine, Nhu-Nang Vu, Mostafa Eesaee, Cédric Boisvert ainsi tous les membres de l'équipe du laboratoire des matériaux avancés pour l'énergie et l'environnement de

l'UQTR qui ont toujours partager leurs connaissances et leurs expériences dans les domaines de la recherche et de la vie. Cela laissera des souvenirs indélébiles dans mon esprit.

Je remercie enfin le Conseil de recherche en sciences et génie du Canada (CRSNG) pour le soutien financier apporté durant mes études de doctorat.

Ce doctorat, je le dois à vous tous.

Avril 2026

Résumé

La pandémie de COVID-19 a entraîné une hausse importante de la consommation de médicaments psychotropes, notamment des antidépresseurs, dont les résidus se retrouvent dans les stations de traitement des eaux usées (STEP). Parmi eux, la fluoxétine (FLX), un contaminant émergent biologiquement actif, persistant et biorécalcitrant, échappe fréquemment aux procédés conventionnels de traitement et atteint les eaux de surface, où elle représente un risque écotoxicologique pour les écosystèmes aquatiques. Dans ce contexte, le développement de solutions de traitement durables, biosourcées et économiquement viables apparaît essentiel.

Cette thèse vise à évaluer le potentiel d'adsorption de matériaux polymériques poreux pour l'élimination de la fluoxétine en milieu aqueux. À partir de carboxyméthylchitosane obtenu par modification chimique du chitosane, deux familles de matériaux ont été développées : des hydrogels sphériques biosourcés, préparés par extrusion électrostatique, et des cryogels hybrides monolithiques, synthétisés par cryopolymérisation à partir d'une matrice naturelle et d'un réseau synthétique de poly(acrylate) de sodium. Un cryogel hybride à empreinte moléculaire a également été élaboré afin d'améliorer la sélectivité envers la fluoxétine.

Les matériaux obtenus présentent des structures poreuses bien développées, interconnectées et capables de gonfler en milieu aqueux. La carboxyméthylation et l'introduction du poly(acrylate) de sodium ont permis d'augmenter la densité des groupes carboxylates, de favoriser les interactions électrostatiques avec la FLX sous forme cationique et d'améliorer la stabilité des adsorbants lors des cycles d'adsorption/désorption.

Les hydrogels sphériques ont montré des capacités d'adsorption en batch comprises entre 90 et 113 mg/g, avec une adsorption exothermique, bien décrite par une cinétique du pseudo-premier ordre et le modèle de Langmuir. Malgré une efficacité maintenue à 65 % après cinq cycles, une perte de masse et une déformation structurale ont limité leur robustesse. Cette observation a motivé le développement des cryogels hybrides, plus résistants mécaniquement.

Le cryogel hybride macroporeux NaPA4-CMCs a présenté une capacité d'adsorption maximale de 80,6 ± 3,4 mg/g, avec un processus favorable, exothermique et dominé par la physisorption, où les interactions électrostatiques jouent un rôle prépondérant. Son efficacité est restée supérieure à 60 % après trois cycles. Son potentiel a ensuite été validé en mode dynamique en flux continu dans une colonne à lit fixe, afin de simuler des conditions plus réalistes de traitement des eaux usées. Dans les conditions optimales (pH 8,5 ; 10 ppm ; 0,4 cm ; 1,5 mL/min), un rendement d'élimination de 59 % a été atteint. Les modèles de Thomas et de Yoon-Nelson ont bien décrit les courbes de percée. Les essais d'adsorption compétitive ont également mis en évidence une plus forte affinité de la FLX pour le cryogel que le citalopram (CIT) et la venlafaxine (VEN). Enfin, le cryogel hybride à empreinte moléculaire s'est révélé plus sélectif et plus performant que le cryogel non imprimé pour la capture de la fluoxétine.

Dans l'ensemble, cette thèse démontre le fort potentiel des hydrogels et cryogels biosourcés, en particulier des cryogels hybrides à empreinte moléculaire, comme matériaux adsorbants innovants, sélectifs et prometteurs pour le traitement des eaux contaminées par des résidus pharmaceutiques.

Avril 2026

Mots Clés

Hydrogel, cryogel hybride, cryopolymérisation, gélification, extrusion électrostatique, cavités mémoire, fluoxétine, adsorption.

Table des Matières

Liste des Figures

Liste des Tableaux

Liste des Équations

Liste des Abréviations

AMI	Amitriptyline
APS	Peroxydisulfate d'ammonium (ammonium peroxydisulfate)
ATC	Antidépresseurs tricycliques
C_0	Concentration initiale
CIT	Citalopram
CLSM	Microscopie confocale à balayage laser (Confocal laser scanning microscopy)
CRIBIQ	Consortium de Recherche et d'Innovation en Bioprocédés Industriels au Québec
CRSNG	Conseil de recherche en sciences naturelles et en génie du Canada
CS	Chitosane
DD	Degré de désacétylation
DS	Degré de substitution
EDTA	Acide éthylène diamine tétraacétique
FA	Groupe amine libre (Free amine group)
FLX	Fluoxétine
FTIR	Spectroscopie infrarouge à transformée de Fourier (Fourier Transform Infrared Spectroscopy)
H NMR	Résonance magnétique nucléaire du proton (proton Nuclear Magnetic Resonance)
HPLC	Chromatographie liquide haute performance (High Performance Liquid Chromatography)
I2E3	Institut d'Innovation en Écomatériaux, Écoproduits et Écoénergies
IEP	Point isoélectrique (Isoelectric point)
IPD	Diffusion intraparticulaire (Intraparticle diffusion)
IRSN	Inhibiteurs de la recapture de la sérotonine et de la noradrénaline
ISRS	Inhibiteurs sélectifs de la recapture de la sérotonine
IUPAC	International Union of Pure and Applied Chemistry
K_d	Coefficient de distribution solide-eau
KPS	Persulfate de Potassium (Potassium persulfate)
Log K_{OW}	Coefficient de partage octanol-eau
M2EBA	International Conference on Materials for Environment, Energy, and Bioresource Application
N, O-CMCs	N, O-Carboxyméthylechitosane
NaCMCS	Carboxyméthylchitosane de sodium
OCDE	Organisation de Coopération et de Développement Économiques
O-CMCs	O-Carboxyméthylchitosane
OMS	Organisation mondiale de la santé
PEG	Polyéthylène Glycol
PFO	Pseudo-premier ordre (Pseudo-First order)
POA	Procédés d'oxydation avancés
PSO	Pseudo-second ordre (Pseudo-second order)
q_m	Capacité d'adsorption maximale
R	Constante universelle des gaz
R^2	Coefficient de détermination

R^2_{adj}	Coefficient de détermination ajustée
R_L	Facteur de séparation
RMSE	Erreur quadratique moyenne (Root Mean Square Error)
RT	Température ambiante (Room Temperature)
SEM	Microscopie électronique à balayage (Scanning Electron Microscopy)
SMS	Métabisulfite de sodium (Sodium Métabisulfite)
STEP	Station d'épuration des eaux usées (WasteWater Treatment Plant: WWTP)
SW	Gonflement (Swelling)
t_b	Temps de percée
t_e	Temps d'épuisement
TEMED	N, N, N`,N`- Tétraméthylènediamine
UQTR	Université du Québec à Trois-Rivières
USD	Dollar américain (United States Dollar)
VEN	Venlafaxine
ZP	Potentiel Zêta (Zêta Potential)
ZTM	Zone de transfert de masse
$\Delta G°$	Énergie libre de Gibbs
$\Delta H°$	Enthalpie de réaction
$\Delta S°$	Entropie

Chapitre 1 - Introduction

1.1 Contexte

La recrudescence des troubles de santé mentale dans le monde constitue un problème sanitaire, socio-économique et environnemental qui se pose avec acuité. Cet état de fait déjà précaire a été accentué pendant la pandémie de Covid-19, qui a été une source d'anxiété et de stress pour les personnes vulnérables. Selon l'Organisation mondiale de la santé (OMS), en 2019, une personne sur huit dans le monde souffrait d'un trouble mental: 301 millions de personnes souffraient d'anxiété et 280 millions de personnes souffraient de dépression. En 2020, les estimations mondiales de l'augmentation des cas d'anxiété et de dépression rapportés étaient de 26 % et 28 % respectivement [1]. Au Canada, le taux de prévalence est passé de 15.4 % à 16.4 % entre 2019 et 2023, avec une augmentation marquée au Québec, passant de 13.9 % à 16.5 % pour la même période [2]. La hausse des cas de troubles mentaux observés a eu pour effet direct une croissance remarquable de la consommation mondiale de médicaments psychotropes, notamment des antidépresseurs (Figure 1.1). Cette consommation est liée à la prévalence croissante des troubles dépressifs et anxieux. En 2021, au plus fort de la pandémie de Covid-19, le marché mondial des antidépresseurs était évalué à 15.87 milliards USD et en 2025, il représente environ 17.82 milliards USD [3]. Au Canada, en 2022, il représentait environ 1.3 milliards USD et pourrait atteindre 2.08 milliards USD en 2030 [4]. Cette hausse de la consommation d'antidépresseurs n'est pas sans conséquences. Elle contribue majoritairement à l'entrée en continu de ces polluants émergents dans les stations d'épuration (STEP) à travers les eaux usées urbaines à la suite de leur excrétion par les organismes à l'état initial ou de métabolites [5,6]. À cela s'ajoutent les rejets hospitaliers et ceux de l'industrie pharmaceutique. De nombreuses études rapportent la présence d'antidépresseurs tels que la fluoxétine, le citalopram et la venlafaxine dans les effluents urbains, les eaux de surface et même les eaux souterraines [7]. Cela met en lumière l'inefficacité des méthodes conventionnelles pour éliminer les antidépresseurs présents dans les eaux usées, en raison de leur complexité [8]. Ces molécules sont conçues pour être biologiquement actives à faibles concentrations, stables et persistantes, ce qui leur confère la capacité de

s'accumuler dans les milieux récepteurs [9,10]. Cette situation est une problématique environnementale majeure qui soulève des inquiétudes et interpelle aussi bien les scientifiques que les politiques quant aux risques liés à l'augmentation des rejets d'antidépresseurs dans l'environnement.

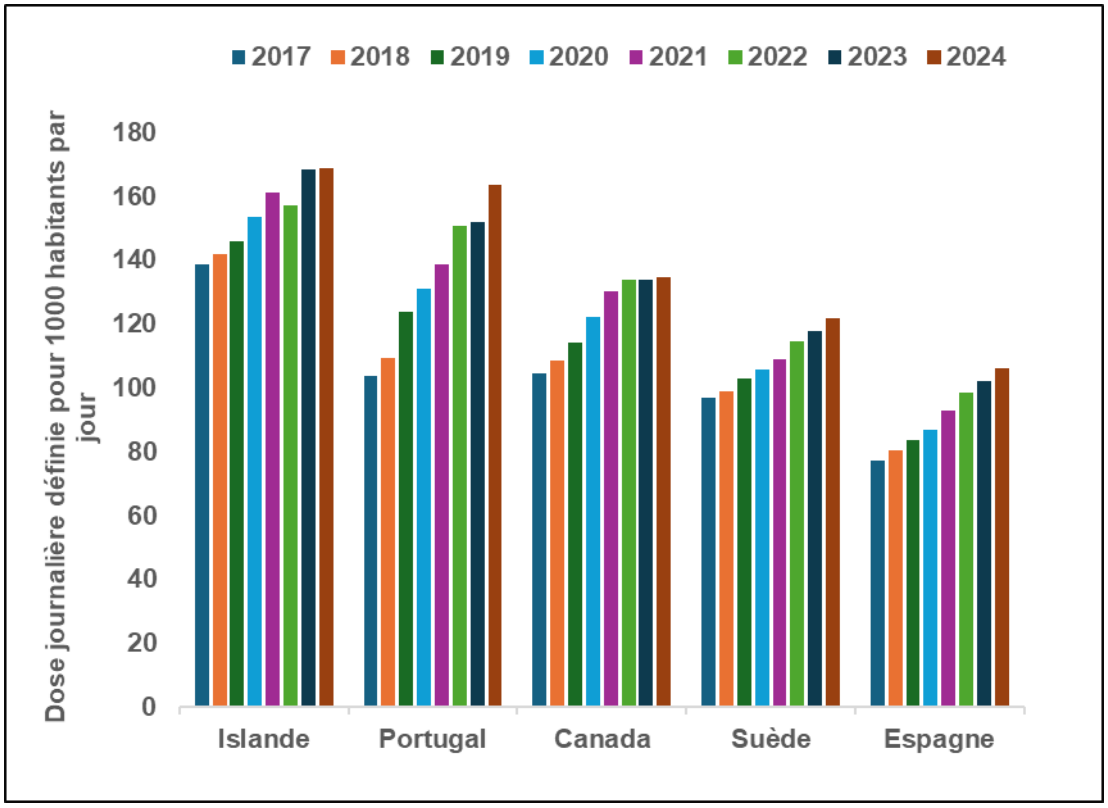

Figure 1.1 Pays membres de l'organisation de coopération et de développement économiques (OCDE) ayant les niveaux de consommation des antidépresseurs les plus hauts (2017-2024) [11]

L'impact des antidépresseurs sur l'écosystème aquatique est de plus en plus répertorié. Des études révèlent leur toxicité à l'égard des organismes aquatiques non ciblés présents dans les milieux récepteurs. Même à de très faibles concentrations, de l'ordre du ng/L dans certains cas et du µg/L dans d'autres, leur bioaccumulation dans des organismes aquatiques peut entraîner des effets néfastes sur la biodiversité aquatique [10]. Ils provoquent le trouble du comportement, une altération des neurotransmetteurs, une perturbation de la reproduction, une altération de l'activité enzymatique, une modification de l'expression génétique, une perturbation endocrinienne, des malformations embryonnaires et des troubles du développement cardiaque [12]. Bien que détecté à l'état

de trace dans l'eau potable, aucun effet négatif sur la santé humaine n'a été rapporté à notre connaissance [13]. La nécessité de mettre au point des méthodes de traitement efficace et durable capable d'éliminer complètement les antidépresseurs dans les eaux usées est une urgence. Cela empêcherait leur rejet dans les plans d'eau par les STEP après le traitement des eaux usées. Cette action permettrait de préserver l'équilibre des écosystèmes aquatiques, garantirait la disponibilité de certaines ressources halieutiques propres à la consommation humaine et éviterait leur accumulation dans les ressources en eau utilisées par l'homme. C'est une nécessité d'autant plus que les ressources en eau encore disponibles s'amenuisent en raison des changements climatiques et nous imposent donc la protection et la préservation de celles-ci face à toute forme de pollution.

1.2 Problématique

Les méthodes de traitement classiques des eaux usées sont peu efficaces face aux antidépresseurs et ne peuvent pas assurer l'élimination complète de leurs polluants émergents. Cela est dû à la complexité de ces molécules attribuée à leurs propriétés physico-chimiques particulières. D'autre part, les procédés d'oxydation avancés (POA) ont démontré une efficacité remarquable pour éliminer ce type de contaminant. Malheureusement, ces techniques sont confrontées à des limitations importantes. Elles sont énergivores, complexes, dispendieuses et génèrent des sous-produits susceptibles de mettre l'environnement en danger. L'adsorption est une alternative attrayante face aux inconvénients que présentent les POA. C'est une méthode simple, efficace, durable et peu onéreuse qui suscite de plus en plus d'intérêt pour l'élimination efficace des antidépresseurs. Toutefois, les matériaux comme les charbons activés utilisés comme adsorbants par excellence souffrent d'une sélectivité limitée, d'une régénération énergivore et des coûts conséquents, environ 0.34 - 22 USD/kg. De plus, la demande énergétique moyenne et les émissions moyennes de gaz à effet de serre liées à la production du charbon actif sont à prendre en compte (97 MJ/kg et 6.6 kg CO_2 eq/kg, respectivement) [14]. Une alternative aux contraintes liées à l'utilisation des charbons actifs est le biochar, de plus en plus utilisé pour la purification de l'eau. Les biochars, adsorbants bon marché et durables, ont une capacité d'adsorption qui dépend notamment du type de matière première et des conditions de fabrication [14,15]. Ce type d'adsorbant

a démontré une efficacité d'adsorption de certains polluants qui est comparable à celle des charbons actifs voir meilleure dans certains cas [14]. Le choix de la matière première est un enjeu sérieux car les métaux lourds parfois contenu dans la biomasse pourrait demeurer dans le biochar après fabrication ou être volatilisé sous forme de gaz lors de la pyrolyse [16]. Les composés organiques volatils et les hydrocarbures aromatiques polycycliques générés à cette étape constituent un danger pour l'environnement [17]. On note qu'une étape de prétraitement est parfois nécessaire pour éliminer les métaux lourds, ce qui accroît les coûts de production. De même, la pyrolyse lente, la méthode la plus utilisée pour obtenir de meilleurs rendements en poids de biochar, nécessite des temps de dégradation thermique de la biomasse plus longs, ce qui rend le processus plus énergivore et plus onéreux [18,19]. Les défis de reproductibilité constituent également un obstacle supplémentaire à leur utilisation à grande échelle.

Dans ce contexte, il apparaît nécessaire de rechercher des alternatives novatrices, abordables et durables capables de concilier plusieurs exigences afin de garantir une élimination efficace des antidépresseurs dans l'eau. Il s'agit notamment de :

- Une bonne affinité vis-à-vis des molécules d'antidépresseurs à des concentrations environnementales (µg/L – mg/L).
- Une cinétique d'adsorption rapide permettant un bon transfert de masse en fonctionnement dynamique.
- Une bonne stabilité chimique et mécanique en milieu aqueux.
- Une compatibilité avec les procédés d'adsorption par lot, ainsi qu'avec le traitement dynamique dans une colonne à lit fixe, facilement transposable à l'échelle industrielle.
- Une régénération facile.
- Une bonne reproductibilité

Le développement de matériaux adsorbants durables à haute valeur ajoutée, conformes à ces exigences, constitue un défi d'actualité dans un contexte de pollution accrue des plans d'eau par les antidépresseurs. L'une des formes d'adsorbants qui attirent l'attention est le gel, qui possède des caractéristiques physico-chimiques requises pour des applications ciblées. Les hydrogels et les cryogels hybrides à base de biopolymères et/ou de polymères

synthétiques constituent une piste prometteuse, de plus en plus explorée. La combinaison de ces deux types de polymères permet de tirer le meilleur parti de chacun, afin d'obtenir un matériau flexible, à bonne stabilité mécanique et chimique, doté de groupes fonctionnels modifiables chimiquement pour optimiser les interactions avec les molécules cibles. D'autre part, la macroporosité de ces matériaux développée grâce aux méthodes de fabrication favorise le transfert de masse dans la structure des matériaux [20–22]. Cependant, à notre connaissance, ce type de matériau n'a pas encore été étudié pour l'élimination des antidépresseurs en solution avant nos travaux. De plus, les mécanismes régissant l'adsorption des antidépresseurs, tels que la fluoxétine, par de tels matériaux, dans différentes conditions d'adsorption et en présence d'un solvant mixte (eau/méthanol), restaient jusque-là inexplorés. Ces observations suscitent des interrogations quant à la manière de concevoir et d'évaluer un hydrogel biosourcé et un cryogel hybride partiellement biosourcé, capables d'éliminer efficacement les antidépresseurs. Quelle serait l'efficacité d'élimination des antidépresseurs, notamment de la fluoxétine, sous différentes conditions d'adsorption à partir d'un hydrogel à base de carboxyméthylchitosane et d'un cryogel hybride à base de polyacrylate de sodium/carboxyméthylchitosane? Quels seraient les mécanismes d'interaction responsables de cette adsorption?

Le choix du carboxyméthylchitosane s'appuie sur la disponibilité du biopolymère précurseur (le chitosane), issu de la chitine, l'un des biopolymères les plus abondants après la cellulose, à partir duquel de nombreux adsorbants écoresponsables sont développés. L'avantage de ce biopolymère est qu'il est non toxique, biodégradable, doté de groupes fonctionnels qui peuvent être modifiés chimiquement afin d'optimiser la sélectivité et peut être extrait des déchets de la biomasse [23–25]. Le choix du polyacrylate de sodium repose sur sa compatibilité avec les biopolymères afin de fabriquer des matériaux hybrides présentant de meilleures propriétés mécaniques et hydrophiles. De plus, il est doté de fonctionnalités requises pour une sélectivité accrue. Sa disponibilité commerciale et son coût abordable rendent son usage intéressant pour de potentielles applications à grande échelle dans le domaine du traitement des eaux usées. La méthode de gélification qui combine la réticulation ionique et la réticulation chimique des chaînes de polymère est retenue pour la fabrication des hydrogels, tandis que la méthode de cryopolymérisation ou

de polymérisation cryotopique est retenue pour la fabrication du cryogel hybride. Ce sont des méthodes simples qui permettent d'obtenir des matériaux poreux présentant une bonne surface spécifique, dont la morphologie peut être contrôlée. La forme sphérique des hydrogels a été obtenue par extrusion électrostatique tandis que les monolithes cryogels hybrides ont été formé en utilisant des seringues comme moule.

1.3 Objectifs

L'objectif principal de ce travail consiste à fabriquer un hydrogel sphérique et un cryogel hybride monolithique, capables d'éliminer efficacement les antidépresseurs, notamment la fluoxétine, dans un milieu aqueux, à partir du carboxyméthylchitosane pour l'un, et de la combinaison polyacrylate de sodium / carboxyméthylchitosane pour l'autre. Pour cela, les objectifs spécifiques qui orientent notre travail se déclinent comme suit:

1. Effectuer la modification chimique du chitosane par carboxyméthylation et caractériser le produit de synthèse.
2. Développer les hydrogels sphériques à partir du carboxyméthylchitosane par extrusion électrostatique en utilisant la méthode combinée de réticulation ionique et réticulation chimique des chaînes de polymères.
3. Évaluer les performances d'adsorption de la fluoxétine, antidépresseur ciblé en solution aqueuse, à l'aide d'une technique d'adsorption en cuvée (batch).
4. Développer un cryogel hybride monolithique par cryopolymérisation à partir du mélange monomère acrylate de sodium et carboxyméthylchitosane puis effectuer la caractérisation du matériau.
5. Évaluer les performances d'adsorption de la fluoxétine par lot et en fonctionnement dynamique dans une colonne à lit fixe de cryogel hybride.
6. Réaliser des essais préliminaires d'adsorption compétitive de trois antidépresseurs (fluoxétine, venlafaxine et citalopram) afin d'évaluer le pouvoir sélectif du cryogel hybride développé.
7. Évaluer la sélectivité du cryogel hybride à empreinte moléculaire par rapport au cryogel hybride non imprimé dans un milieu comportant le la FLX et le CIT.

1.4 Hypothèse de recherche

À partir de leur structure hautement poreuse qui facilite l'accès aux sites actifs, de leur hydrophilie qui les rend compatibles avec les milieux aqueux et de la présence de groupes fonctionnels polaires, les hydrogels à base de carboxyméthylchitosane et les cryogels hybrides à base de polyacrylate de sodium / carboxyméthylchitosane seraient des adsorbants performants et sélectifs pour l'élimination de la fluoxétine. Leur efficacité d'adsorption aussi bien en cuvée qu'en conditions dynamiques pourrait concurrencer celle des adsorbants standards (charbon actif, biochar, zéolithe) et serait adaptée pour des applications d'adsorption dans les conditions aqueuses réelles. La fluoxétine, plus lipophile dans un contexte d'adsorption compétitive avec la venlafaxine et le citalopram, moins lipophile, interagira différemment avec le cryogels hybride. L'introduction de cavité mémoire pourrait accroître la sélectivité du cryogel hybride.

1.5 Importance de la thèse

La présence des antidépresseurs dans les effluents des STEP et le risque qu'ils représentent pour l'écosystème aquatique, en raison de leur persistance, de leur bioaccumulation potentielle et de leurs effets écotoxicologiques, constituent un problème environnemental. Bien que des adsorbants classiques aient été étudiés pour leur élimination, ceux-ci présentent toutefois des limites notables, à savoir une sélectivité limitée, des coûts élevés, une production et une régénération énergivores, une empreinte carbone non négligeable et des risques environnementaux potentiels. Dans ce contexte, cette thèse propose une alternative aux biosorbants standards afin de réduire la dépendance envers ces derniers en assurant une élimination efficace de leurs polluants émergents, notamment la fluoxétine (FLX). Nos travaux constituent une contribution originale qui explore le potentiel des gels (hydrogel et cryogel hybride) à base de carboxyméthylchitosane, ainsi que de la combinaison polyacrylate de sodium/carboxyméthylchitosane, respectivement, pour l'élimination de la FLX dans un milieu aqueux contenant une faible proportion de méthanol (5 %). L'originalité de ce travail réside dans la modification chimique du biopolymère de départ et la macroporosité développée grâce aux techniques de fabrication, qui permettent de moduler l'hydrophilie afin d'optimiser les interactions avec

la FLX ionisée pour le premier, et de favoriser un bon transfert de masse pour le second. Cette approche permet de rehausser l'efficacité de ce type d'adsorbant, qui pourrait concurrencer les biosorbants standards utilisés jusqu'ici, et ouvrir la voie à des procédés d'épuration plus ciblés, portant sur une gamme plus large de polluants pharmaceutiques. Cette étude apporte également des connaissances sur les mécanismes régissant l'adsorption de la FLX sur de tels matériaux, dans diverses conditions expérimentales. Cette thèse vise à démontrer non seulement l'efficacité d'adsorption, mais aussi la pertinence de l'utilisation de gels (hydrogels/cryogels hybrides) biosourcés ou partiellement biosourcés comme adsorbants innovants et alternatives durables à approfondir. Ceux-ci pourraient potentiellement être transférables vers des procédés industriels pour la dépollution des eaux et la préservation de l'écosystème aquatique.

1.6 Organisation de la thèse

La présente thèse repose sur quatre articles scientifiques (deux publiés et deux soumis) et s'articule en huit chapitres. Le chapitre 1 aborde le contexte général, puis la problématique, les objectifs et les hypothèses de recherche. Le chapitre 2 est consacré à la revue de la littérature. Il présente succinctement la situation des antidépresseurs dans les plans d'eau, le risque pour l'environnement aquatique et l'urgence de développer des technologies écoresponsables à haut potentiel, simples et accessibles, qui s'inscrivent dans une optique de développement durable. Il évoque également l'état de l'art des technologies actuelles d'adsorption des antidépresseurs dans l'eau et présente de manière générale les aspects théoriques de l'adsorption en cuvée et de l'adsorption dynamique (mécanismes d'adsorption, isothermes d'adsorption, cinétique d'adsorption et aspects énergétiques des processus). Dans ce chapitre, sont aussi présentés les polymères utilisés pour la fabrication des hydrogels et cryogels hybrides (caractéristiques et propriétés), et leurs méthodes de fabrication. Le chapitre 3 présente le matériel, la démarche méthodologique et les techniques de caractérisation des matériaux utilisés dans ce travail. Les principaux résultats obtenus sont présentés aux chapitres 4, 5, 6 et 7 sous la forme de quatre articles scientifiques. La conclusion générale est présentée au chapitre 8.

1.7 Références

[1] World Health Organization (WHO), Troubles mentaux, (2022).

[2] IQVIA.2024. Snapshot Prevalence and Treatment of Mental Health Disorders. https://www.canada.ca/en/health-canada/services/healthy-living/your-health/diseases/mental-health-anxiety-disorders.html.

[3] Antidepressants Market Report 2025 - Research and Markets. https://www.researchandmarkets.com/reports/5734971/antidepressants-market-report#tag-pos-3 (accessed September 1, 2025).

[4] Canada Anti-Depressants Drugs Market Report 2022 to 2030. https://www.insights10.com/report/canad-anti-depressants-drugs-market-analysis/ (accessed September 1, 2025).

[5] C. Castillo-Zacarías, M.E. Barocio, E. Hidalgo-Vázquez, J.E. Sosa-Hernández, L. Parra-Arroyo, I.Y. López-Pacheco, D. Barceló, H.N.M. Iqbal, R. Parra-Saldívar, Antidepressant drugs as emerging contaminants: Occurrence in urban and non-urban waters and analytical methods for their detection, Science of the Total Environment 757 (2021). https://doi.org/10.1016/j.scitotenv.2020.143722.

[6] L. dan Ma, J. Li, J. jun Li, M. Liu, D. zhi Yan, W. yan Shi, G. Xu, Occurrence and source analysis of selected antidepressants and their metabolites in municipal wastewater and receiving surface water, Environ Sci Process Impacts 20 (2018) 1020–1029. https://doi.org/10.1039/C8EM00077H.

[7] L.J.G. Silva, C.M. Lino, L.M. Meisel, A. Pena, Selective serotonin re-uptake inhibitors (SSRIs) in the aquatic environment: An ecopharmacovigilance approach, Science of the Total Environment 437 (2012) 185–195. https://doi.org/10.1016/J.SCITOTENV.2012.08.021.

[8] A. Lajeunesse, S.A. Smyth, K. Barclay, S. Sauvé, C. Gagnon, Distribution of antidepressant residues in wastewater and biosolids following different treatment processes by municipal wastewater treatment plants in Canada, Water Res 46 (2012) 5600–5612. https://doi.org/10.1016/j.watres.2012.07.042.

[9] P. Arnnok, R.R. Singh, R. Burakham, A. Pérez-Fuentetaja, D.S. Aga, Selective Uptake and Bioaccumulation of Antidepressants in Fish from Effluent-Impacted

Niagara River, Environ Sci Technol 51 (2017) 10652–10662. https://doi.org/10.1021/ACS.EST.7B02912.

[10] W. Wang, J. Zhang, M. Hu, X. Liu, T. Sun, H. Zhang, Antidepressants in wastewater treatment plants: Occurrence, transformation and acute toxicity evaluation, Science of The Total Environment 903 (2023) 166120. https://doi.org/10.1016/J.SCITOTENV.2023.166120.

[11] OCDE. OCDE Data Explorer.2025, Pharmaceutical Consumption. https://data-explorer.ocde.org/vis (accessed December 1, 2025).

[12] A. Puga, M.M. Moreira, M.A. Sanromán, M.M. Pazos, C. Delerue-Matos, Antidepressants and COVID-19: Increased use, occurrence in water and effects and consequences on aquatic environment. A review, Science of the Total Environment 953 (2024). https://doi.org/10.1016/j.scitotenv.2024.175993.

[13] C.D. Metcalfe, S. Chu, C. Judt, H. Li, K.D. Oakes, M.R. Servos, D.M. Andrews, Antidepressants and their metabolites in municipal wastewater, and downstream exposure in an urban watershed, Environ Toxicol Chem 29 (2010) 79–89. https://doi.org/10.1002/etc.27.

[14] H.A. Alhashimi, C.B. Aktas, Life cycle environmental and economic performance of biochar compared with activated carbon: A meta-analysis, Resour Conserv Recycl 118 (2017) 13–26. https://doi.org/10.1016/J.RESCONREC.2016.11.016.

[15] M. Dong, M. Jiang, L. He, Z. Zhang, W. Gustave, M. Vithanage, N.K. Niazi, B. Chen, X. Zhang, H. Wang, F. He, Challenges in safe environmental applications of biochar: identifying risks and unintended consequence, Biochar 7 (2025) 1–20. https://doi.org/10.1007/S42773-024-00412-4/FIGURES/7.

[16] B. Li, S. Ding, H. Fan, Y. Ren, Experimental Investigation into the Effect of Pyrolysis on Chemical Forms of Heavy Metals in Sewage Sludge Biochar (SSB), with Brief Ecological Risk Assessment, Materials 2021, Vol. 14, Page 447 14 (2021) 447. https://doi.org/10.3390/MA14020447.

[17] Y. Hu, K. Tong, Q. Guo, B. Zhang, L. Jiao, M. Li, Z. Zhang, Effect of controlled temperature and biomass addition on the formed environmental persistent free radicals (EPFRs) in sewage sludge-based biochar from pyrolysis treatment, J Anal Appl Pyrolysis 162 (2022) 105460. https://doi.org/10.1016/J.JAAP.2022.105460.

[18] A. Ajien, J. Idris, N. Md Sofwan, R. Husen, H. Seli, Coconut shell and husk biochar: A review of production and activation technology, economic, financial aspect and application, Waste Management & Research 41 (2023) 37–51. https://doi.org/10.1177/0734242X221127167.

[19] D. Mohan, A. Sarswat, Y.S. Ok, C.U. Pittman, Organic and inorganic contaminants removal from water with biochar, a renewable, low cost and sustainable adsorbent – A critical review, Bioresour Technol 160 (2014) 191–202. https://doi.org/10.1016/J.BIORTECH.2014.01.120.

[20] M.B. Agustin, M. Lehtonen, M. Kemell, P. Lahtinen, E. Oliaei, K.S. Mikkonen, Lignin nanoparticle-decorated nanocellulose cryogels as adsorbents for pharmaceutical pollutants, J Environ Manage 330 (2023). https://doi.org/10.1016/j.jenvman.2022.117210.

[21] A. Izadpanah, S. Nemati, S. Nojavan, A comprehensive review on synthesis and applications of cryogel-based sorbents in solid-phase extraction techniques, TrAC - Trends in Analytical Chemistry 180 (2024). https://doi.org/10.1016/j.trac.2024.117899.

[22] P. Patel, P. Thareja, Hydrogels differentiated by length scales: A review of biopolymer-based hydrogel preparation methods, characterization techniques, and targeted applications, Eur Polym J 163 (2022). https://doi.org/10.1016/j.eurpolymj.2021.110935.

[23] M. Jamali, A. Akbari, Facile fabrication of magnetic chitosan hydrogel beads and modified by interfacial polymerization method and study of adsorption of cationic/anionic dyes from aqueous solution, J Environ Chem Eng 9 (2021). https://doi.org/10.1016/j.jece.2021.105175.

[24] H. Jing, X. Huang, X. Du, L. Mo, C. Ma, H. Wang, Facile synthesis of pH-responsive sodium alginate/carboxymethyl chitosan hydrogel beads promoted by hydrogen bond, Carbohydr Polym 278 (2022) 118993. https://doi.org/10.1016/J.CARBPOL.2021.118993.

[25] G. Crini, G. Torri, E. Lichtfouse, G.Z. Kyzas, L.D. Wilson, N. Morin-Crini, Dye removal by biosorption using cross-linked chitosan-based hydrogels, Environ Chem Lett 17 (2019) 1645–1666. https://doi.org/10.1007/s10311-019-00903-y.

Chapitre 2 - Revue de littérature

2.1 Les antidépresseurs comme source de pollution-État de la situation

2.1.1 Généralité

De nombreux déterminants d'une mauvaise santé mentale, présents avant la pandémie de Covid-19, ont été aggravés par celle-ci et continuent d'affecter la santé mentale des populations à l'échelle mondiale. L'anxiété et la dépression font partie des troubles mentaux les plus répandus. Le traitement des troubles mentaux passe entre autres par la consommation de médicaments psychotropes [1]. Les antidépresseurs sont un choix populaire, et la prévalence de leur utilisation indique une tendance à la hausse dans divers pays, notamment au Canada [2–4]. Les antidépresseurs couramment prescrits appartiennent à trois classes selon leur mécanisme d'action et leur structure chimique. Il s'agit des antidépresseurs tricycliques (ATC, par exemple amitriptyline (AMI)), des inhibiteurs de la recapture de la sérotonine et de la noradrénaline (IRSN, exemple la venlafaxine (VEN)), et les inhibiteurs sélectifs de la recapture de la sérotonine (ISRS) comme la fluoxétine (FLX) et le citalopram (CIT), qui se distinguent ces dernières années par une présence prépondérante dans les milieux aqueux [5–7]. Ces antidépresseurs correspondaient à des taux de consommation respectifs de 5.7 %, 16.8 % et 64.9 % en 2019 à l'échelle mondiale [8]. Ce sont des molécules organiques synthétiques qui exercent une action pharmacologique spécifique sur l'organisme. Après ingestion, les antidépresseurs sont métabolisés et excrétés dans l'urine et les fèces sous forme inchangée et/ou conjuguée, puis acheminés par les eaux usées municipales jusqu'aux STEP [9]. Les antidépresseurs non utilisés et ceux périmés, éliminés de façon inadéquate, participent également à leur entrée dans les STEP [10,11]. Les eaux usées des milieux hospitaliers et celles issues des industries pharmaceutiques contribuent également à la charge globale des antidépresseurs dans les STEP [12,13]. Des niveaux d'occurrence moyens de (72,62 ng/L à 5011,8 ng/L) ont été signalés pour les antidépresseurs et leurs métabolites dans les influents des STEP de nombreux pays [14]. Au niveau des STEP, des méthodes de traitement conventionnelles sont mises en œuvre pour éliminer les antidépresseurs et leurs métabolites présents dans les eaux usées (coagulation, floculation, biodégradation,

sorption sur les boues ou les particules et filtration) [15]. Toutefois, l'inefficacité de ces méthodes de traitement a été constatée à la suite de la détection d'antidépresseurs et de leurs métabolites dans les effluents des STEP ainsi que dans les eaux réceptrices adjacentes. Par exemple, la FLX a été détectée après un traitement des eaux usées par boues activées, provenant des effluents des STEP et des eaux de surface [16,17]. Au Canada, cette molécule a également été identifiée dans les eaux de rejet de trois STEP dans le sud de l'Ontario [17]. Dans le fleuve Saint-Laurent à Montréal, non loin du point de rejet des effluents de la STEP de cette ville, les antidépresseurs ont été détectés, révélant ainsi le manque d'efficacité des procédés physico-chimiques opérés pour leur élimination complète [1]. L'un de ses métabolites, la nor-fluoxétine, a été détecté dans l'eau de consommation [18,19]. L'épandage sur le sol de biosolide issu des boues des STEP constitue une autre voie d'entrée de ces polluants émergents dans l'environnement [20]. Ces médicaments sont conçus pour être biologiquement actifs même à faibles concentrations, et la plupart de leurs métabolites conservent une activité pharmacologique plus ou moins identique à celle de la molécule parent [21].

2.1.2 Impact des antidépresseurs dans les stations d'épuration et les eaux réceptrices

Les STEP conventionnelles n'ont pas été conçues pour éliminer les produits pharmaceutiques, notamment les antidépresseurs, des eaux usées [24,25]. Par conséquent, les taux d'élimination variables de ces micropolluants sont rapportés dans la littérature et dépendent à la fois de leurs propriétés physico-chimiques et des technologies d'élimination mises en œuvre dans les STEP [24,25]. Leur présence dans les eaux réceptrices reflète l'incapacité des méthodes conventionnelles à les éliminer efficacement, compte tenu des fractions significatives rejetées par les effluents, principaux vecteurs de la pollution des milieux aquatiques par les antidépresseurs [1].

Les caractéristiques structurelles et physico-chimiques des antidépresseurs permettent de prédire leur comportement dans l'environnement. D'autre part, la connaissance des voies de transformation de ces molécules organiques par différents processus, ainsi que des produits de transformation, facilite la compréhension des risques liés à l'exposition du biote aquatique à ce type de polluant [7]. Par exemple, Wang et al., 2023 [15] ont

répertorié les produits de transformation de la FLX, du CIT et de la VEN obtenus par trois voies distinctes au cours du traitement des eaux usées (voir la figure 2.1). Ils ont mis en lumière la formation de produits de dégradation aussi dangereux que les composés parents pour l'écosystème aquatique. Les paramètres tels que le coefficient de partage octanol-eau (log Kow) et le coefficient de distribution solide-eau (K_d) fournissent des informations sur le caractère lipophile ainsi que sur la capacité de sorption des antidépresseurs à des surfaces organiques [26]. Par exemple la FLX présente une valeur du coefficient de partage octanol-eau ($\log K_{ow} > 4$) et une valeur du coefficient de distribution solide-eau ($\log K_d > 2.7$) ce qui indique que cette molécule est lipophile et a un potentiel de sorption élevé sur les sédiments [27]. L'investigation du potentiel de dégradation, de persistance et d'accumulation des ISRS dans les sédiments a été rapportée dans différentes études. Celles-ci mentionnent que la FLX et le CIT étaient rapidement adsorbés par les sédiments et pendant un délai de 30 jours, la FLX n'était quasiment pas dégradée tandis que les concentrations détectées de CIT étaient entre 52 et 63 % de la concentration initiale adsorbée [7,28]. Ces molécules sont stables dans les sédiments, biorécalcitrantes et persistantes, et leur potentiel de bioaccumulation et de bioamplification à différents niveaux trophiques a été signalé par Metcalfe et al., 2010 [10,29]. Ces polluants organiques coexistent dans les milieux aqueux avec d'autres polluants, de même nature ou non, entraînant des interactions directes ou indirectes entre eux.

La dégradation abiotique des antidépresseurs et de leurs métabolites dans l'environnement dépend de certains paramètres tels que la profondeur du cours d'eau, l'intensité de l'irradiation solaire et la composition en matières organiques, entre autres [30]. L'investigation des réactions de photolyse et d'hydrolyse des antidépresseurs a révélé qu'elles constituent les voies principales de dégradation de ces molécules dans les eaux de surface [30]. Cette approche a mis en lumière leur capacité à persister dans l'eau naturelle et les solutions aqueuses étudiées. Par exemple, la photolyse de certains ISRS (FLX et CIT) et d'IRSN (VEN) en conditions simulées en laboratoire ou réelles (eau de rivière naturelle, lac) a été étudiée dans certains travaux de la littérature [7,28]. Les résultats ont révélé que la photodégradation de la FLX dans l'eau pure sous irradiation solaire naturelle est difficile, avec une demi-vie de 7 jours, et génère un photoproduit, la nor-FLX [7]. Une stabilité photolytique, traduite par une dégradation lente aux pH 5 et 7,

a été observée pour le CIT sous irradiation solaire simulée pendant 30 jours d'expérimentation, tandis qu'à un pH plus alcalin (pH 9), la photodégradation était modérée, avec une demi-vie estimée à 65 jours. Dans l'eau humique synthétique, celle-ci était plus rapide avec une demi-vie de 24 jours et variait entre 14 et 43 jours dans les eaux naturelles [28]. Deux produits de dégradation du CIT ont été identifiés : le DCIT et le CIT-N-oxyde. L'augmentation de l'intensité de l'irradiation solaire a favorisé la photodégradation de la VEN. Des demi-vies allant jusqu'à 62 jours, dans des conditions environnementales réelles, ont été rapportées dans la littérature [31]. La faible biodégradation et la stabilité photolytique de ces polluants pharmaceutiques favorisent leur persistance dans les milieux aquatiques et accroissent les risques de bioaccumulation au sein des organismes aquatiques. De plus, les produits formés lors de la photodégradation sont potentiellement bioactifs [32] et constituent un risque pour l'écosystème aquatique, comme les antidépresseurs parents non dégradés.

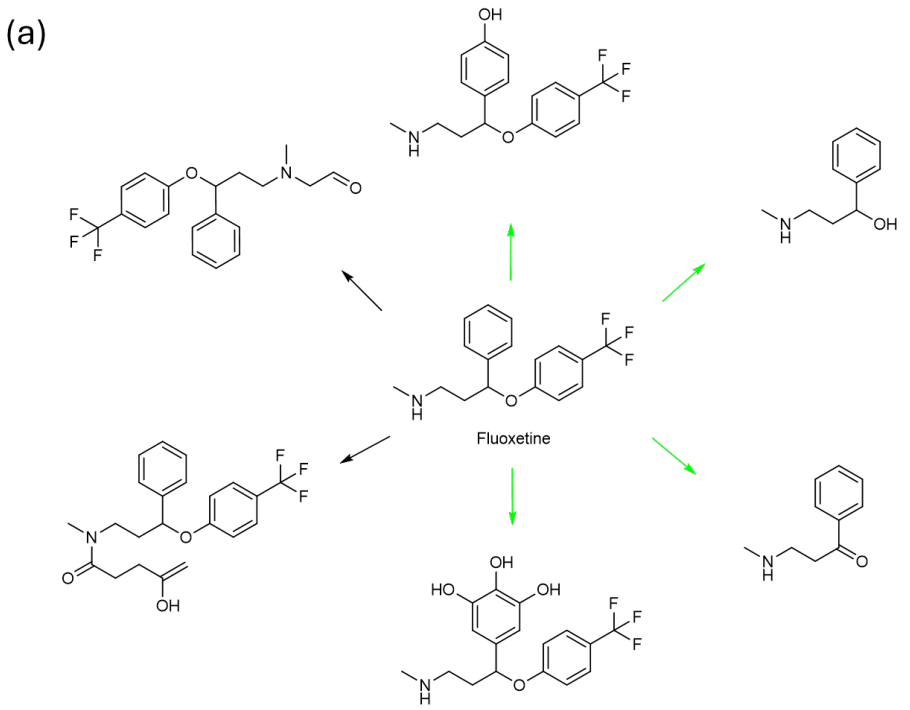

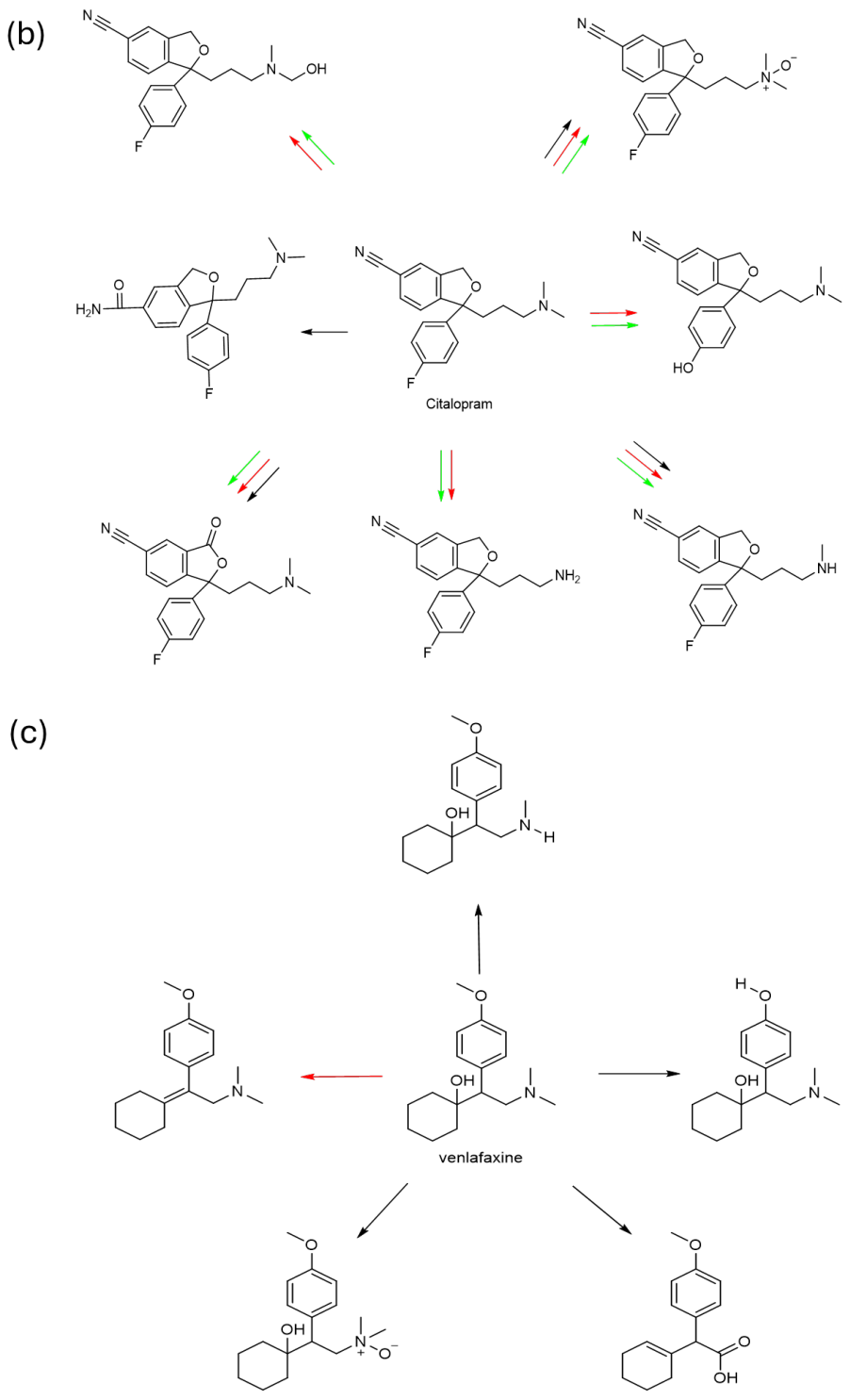

Figure 2.1 **Voies de transformation et produits de transformation de la fluoxétine (a), du citalopram (b) et de la venlafaxine (c) lors des traitements suivants : la biotransformation (flèche noire), l'ozonation (flèche verte) et la chloration (flèche rouge) [15]**

2.1.3 Risques pour l'écosystème aquatique

L'entrée en continu des antidépresseurs dans l'environnement et leur persistance dans les milieux récepteurs peuvent induire des effets indésirables sur les organismes aquatiques exposés à différents niveaux trophiques [33]. Même à de faibles concentrations, ils demeurent bioactifs et ciblent notamment les systèmes de neurotransmission [34]. Les concentrations individuelles d'antidépresseurs, dans certains cas, sont faibles et ne sont pas susceptibles d'induire des effets toxiques chez les espèces aquatiques exposées. Cependant, les effets additifs et/ou synergiques des antidépresseurs de la même classe peuvent compromettre l'écosystème aquatique [35]. Ce sont des molécules capables de traverser les membranes biologiques, et leur accumulation dans les tissus cérébraux et hépatiques des organismes aquatiques exposés a été signalée [20,30,33]. Par exemple, la bioaccumulation des ISRS dans les tissus de poissons notamment le cerveau et le foie a été rapporté [36], la capacité de la VEN à s'accumuler dans le foie, le cerveau, le plasma, les gonades et les muscles a été observé chez la truite arc-en ciel [37]. Les effets négatifs des antidépresseurs sur la biodiversité exposée sont influencés par des facteurs importants, tels que la concentration, la durée d'exposition et l'état d'ionisation des molécules, entre autres. Des études révèlent que, pour les troubles comportementaux, on observe chez les poissons une modification de l'activité locomotrice, avec une lenteur ou une activité accrue, une perturbation de l'alimentation, marquée par une baisse ou une augmentation de l'alimentation, une altération des comportements sociaux (agressivité et prédation) et une réduction de la réaction de fuite face aux prédateurs. Pour ce qui est des effets physiologiques et reproductifs, ils rapportent une perturbation hormonale, une baisse de la fertilité, des anomalies du développement embryonnaire, un retard de la croissance et une diminution des capacités des organismes à lutter contre les infections. On note également, pour les effets biochimiques et cellulaires, une modification de l'expression génique liée à l'altération de la neurotransmission, ainsi qu'à des altérations neuronales et enzymatiques [38,39]. Le risque du transfert de ces micropolluants à travers différents niveaux trophiques a été évoqué dans plusieurs études et des conséquences écologiques globales sur l'écosystème aquatique récepteur ont été mis en exergues tels que la modification de la dynamique des population (moins de reproduction et survie réduite), le déséquilibre trophique et la perte de la biodiversité aquatique à long terme [34].

2.2 Aperçu des approches de traitement de l'eau pour l'élimination des résidus d'antidépresseurs

Les propriétés physico-chimiques des molécules d'antidépresseurs comme la FLX, le CIT et la VEN favorisent leur caractère récalcitrant et persistant vis-à-vis de certaines méthodes d'élimination. Les principales voies recensées dans la littérature pour l'élimination de ces micropolluants sont la biodégradation par des méthodes biochimiques, la minéralisation par des méthodes oxydatives et l'adsorption par des phénomènes de surface.

2.2.1 Dégradation biologique

C'est une approche plus verte qui permet un traitement économique et durable des eaux contaminées par des polluants pharmaceutiques. Elle peut être mise en œuvre selon deux processus. Il s'agit du processus biotique, qui comprend la biosorption, la bioaccumulation et la biodégradation [40,41], ainsi que du processus abiotique, qui comprend l'hydrolyse et la photolyse [42]. Plusieurs stratégies de biodégradation de la FLX ont été signalées dans la littérature et reposent notamment sur l'utilisation de microalgues, de bactéries et de solutions fongiques [41]. L'intérêt, par exemple, pour les microalgues réside dans la charge négative de leur surface, à laquelle la FLX ionisée a une grande affinité. Cela entraîne une biosorption rapide, renforcée par la forte lipophilie de cette molécule (Log K_{ow} = 4.1) [26]. L'immobilisation et la bioaccumulation contribuent à son élimination et des taux de biodégradation entre 41 – 100 % ont été rapporté lorsque la concentration de FLX était comprise entre 10 – 1000 µg/L [41]. Toutefois, la toxicité inhérente à la FLX pour les microalgues a été signalée pour des concentrations seuil supérieures ou égales à 50 µg/L [43].

Des communautés de micro-organismes, notamment les bactéries, ont été utilisées pour la biodégradation de ce type de molécule organique par l'action d'enzymes qui consomment le carbone organique de ces molécules pour produire de l'énergie [40]. Des études de biodégradation de la FLX par cette approche ont mis en lumière la cinétique lente du processus, ce qui la rendrait moins adaptée à des traitements dynamiques et rapides [44]. Des taux de dégradation de 67 à 100 % et de 89 à 100 % ont été rapportés pour

l'élimination des deux énantiomères de la FLX (le S-FLX et le R-FLX), respectivement, lorsque la concentration initiale était comprise entre 0.6 et 2.8 mg/L [44].

Par ailleurs, des solutions fongiques ont également été étudiées pour dégrader la FLX. Les résultats rapportés mettent en exergue le potentiel prometteur de cette approche. Par exemple, une étude a signalé des taux d'élimination supérieurs à 83.1 % en 10 minutes pour la FLX à une concentration initiale de 600 µg/L [45,46].

2.2.2 Traitements physico-chimiques

Les procédés physico-chimiques utilisés pour la décontamination des eaux polluées par des polluants pharmaceutiques, en général, et par des antidépresseurs, en particulier, sont nombreux [47–50]. Il s'agit par exemple des procédés d'oxydation avancés, des procédés électrochimiques, des technologies membranaires et de l'adsorption chacune présentant des avantages et des limites (Tableau 2.1). Les procédés d'oxydation avancés (POA) sont une technologie largement étudiée pour l'élimination efficace des contaminants émergents. Par exemple, la minéralisation de la FLX par ozonation et par photocatalyse hétérogène a été rapportée dans plusieurs travaux. Les radicaux hydroxyles très réactifs ($^{\cdot}OH$, $E° = 2.80$ V) réagissent avec la FLX pour la dégrader selon différents mécanismes [51]. Ce sont des procédés à cinétique rapide et à excellente efficacité, adaptés à des traitements rapides à grande échelle des eaux contaminées. Par exemple, environ 100 % de la FLX (50 mg/L et 5 mg/L) a été éliminée en 120 et 5 minutes, respectivement, avec les systèmes de photocatalyse (TiO_2 P25 et gC_3N_4) et PMS/Fe (III) [52]. Le système O_3/H_2O_2 a réussi à dégrader 86.14 % de la FLX (50 mg/L) après 20 minutes avec 30 mg/L de O_3 et 0.02 mM de H_2O_2 [53]. Toutefois, ces méthodes de traitement génèrent des sous-produits toxiques qui peuvent persister dans le milieu aqueux ce qui limite leur utilisation et nécessite parfois des étapes de traitement supplémentaires qui augmentent les coûts de traitement [54]. De plus, ce sont des méthodes complexes, énergivores et onéreuses comme les technologies électrochimiques [55,56]. Les défis de mise en œuvre de cette dernière méthode sont liés à l'encrassement des surfaces des électrodes et à sa faible sélectivité.

Tableau 2.1 Évaluation comparative des technologies de traitement

Technologies de traitement	Points forts	Limites
Traitement biologique	• Faible coût	• Faible efficacité d'élimination du FLX
	• Peut être intégré à toute technologie de traitement physico-chimique	• Sorption dans les boues
	• Respectueux de l'environnement et durable	
POA	• Haute efficacité d'élimination	• Coûts énergétiques et chimiques élevés
	• Capable de minéralisation du FLX	• Intermédiaires et/ou sous-produits toxiques
	• Rapide et efficace contre les micropolluants	• Complexe
	• Catalyseurs réutilisables	
	• Aucune production de boues	
Procédé électrochimique	• Sélectif et réglable	• Encrassement des électrodes
	• Haute efficacité d'élimination	• Optimisation des paramètres (pH, distance inter-électrodes, courant, matériau des électrodes, électrolyte)
Filtration membranaire	• Aucune transformation chimique	• Forte consommation d'énergie et de coûts
		• Encrassement des membranes
		• Problème d'élimination des concentrés
Adsorption	• Simple et économique	• Stratégies de désorption/régénération parfois complexe
	• Évolutif	• Adsorption compétitive avec des co-contaminants
	• Efficace même à faibles concentrations	• Chute de l'efficacité rapide dès la saturation des sites actifs
	• Aucun sous-produit toxique	• Coûts élevés pour certains adsorbants commerciaux de haute qualité
	• Sélective selon l'adsorbant	• Manque de sélectivité dans certain cas • Cinétique parfois lente • Dépendance aux conditions physico-chimiques • Moins performant pour les molécules très hydrophiles

La technologie membranaire a peu été utilisée pour éliminer la FLX, en mode continu ou discontinu. L'élimination de la FLX par ce procédé dépend de la pression de fonctionnement en plus de la concentration. Elle peut être très énergivore et générer un flux secondaire, bien que, dans certains cas, des taux d'élimination de 84.5 % et une capacité d'adsorption maximale de 2.6 mg/g aient été signalés pour des concentrations de FLX de 1.5 % p/p et de 2 mg/L, en traitement continu et discontinu, respectivement [57].

L'adsorption est une solution écologique exploitant l'affinité des polluants pour la surface des matériaux afin de les éliminer en solution aqueuse, selon la nature des interactions entre le polluant et l'adsorbant. Les enjeux ne concernent pas la méthode mais le choix des matériaux, leur sélectivité et leur régénération, souvent coûteuses et pouvant augmenter l'empreinte environnementale liée au recyclage. Ceci explique l'intérêt accru pour des adsorbants durables. Le tableau 2.2 montre que de nombreux adsorbants, synthétiques ou issus de biomasse, ont été employés pour retirer la FLX en solution aqueuse.

Tableau 2.2 Résultats récents de l'adsorption de la FLX par différents adsorbants en solution aqueuse. (RT*: Room temperature)

Adsorbants commerciaux	q ($mg\ g^{-1}$)	pH	Concentration initiale ($mg\ L^{-1}$)	T (°C)	Réf.
Charbon actif PBFG4	96.2	—	10	25	[58]
Charbon actif granulaire (CAG)	233.5	9	5	25	[59]
NQ40	125.24	7–7.5	1000	—	[60]
Silice	8.54	—	250	—	[62]
Siliaflash® F60	4.25	—	250	—	[62]
Valfor® 100	49	—	250	—	[62]
Dowex® Marathon® C	77.03	—	250	—	[62]
Amberlyst® 15	80.96	—	250	—	[62]
Adsorbants synthétiques					
Nanoparticules de $RuFeO_3$	683.5	7	—	25	[63]
Nanoparticules de $CeFeO_3$	729.6	—	—	—	[63]
Biosorbants					
PS800–10KOH	191.6	—	10	25	[58]
PS800–10NaOH	136.6	—	10	25	[58]
PS800–10$ZnCl_2$	28.4	—	10	25	[58]
Charbon d'arêtes de poisson	55,87	—	100	—	[64]
Biochar d'eucalyptus	6.41	6.5	20	RT*	[59]
Nanofibres AL : PVA 1:1	78.24	—	50	—	[65]
Biochar	—	7.1	50	RT	[66]
Nanocomposite XCM	90.9	7.35	25	28	[67]
PCM nanocomposite	114.9	7.35	25	28	[67]
Hydrochar Alperujo	4.63, 5.95	6.4	30	RT	[68]

2.2.3 Adsorption

L'adsorption est une technologie avancée couramment utilisée pour éliminer des micropolluants organiques récalcitrants des eaux [69]. C'est un phénomène de surface par lequel un adsorbat (molécules, atomes, ions) se fixe à la surface d'un solide ou d'un gel (adsorbant) grâce à différents types d'interactions établies entre l'adsorbat et les sites actifs à la surface de l'adsorbant. Le processus d'adsorption se déroule en quatre étapes : la diffusion externe, le transfert du soluté à travers le film vers la surface de l'adsorbant, la diffusion interne et la réaction d'adsorption (voir la figure 2.2) [70]. Selon les forces d'attraction entre l'adsorbat et l'adsorbant, il existe deux processus d'adsorption : l'adsorption physique, ou physisorption, et l'adsorption chimique, ou chimisorption. La physisorption implique principalement les forces d'attraction faibles de type van der Waals entre l'adsorbat et l'adsorbant, ce qui rend le processus réversible, tandis que pour la chimisorption, des liaisons chimiques plus fortes se forment entre l'adsorbat et l'adsorbant, ce qui rend le processus irréversible [71]. C'est une méthode de traitement flexible, pouvant être combinée à d'autres méthodes. Elle est adaptée à l'élimination des polluants organiques et inorganiques même à de faibles concentrations. Elle est efficace, simple et économique. On note que la capacité d'adsorption maximale à l'équilibre peut être influencée significativement par de nombreux facteurs. Parmi eux on a le type d'adsorbat (nature chimique et la taille des molécules), la morphologie structurale de l'adsorbant notamment la surface spécifique et la porosité (taille, forme et distribution des pores), la charge de surface de l'adsorbant qui dépend à du pH de la solution, la nature des sites actifs (groupes fonctionnels) et leur densité à la surface de l'adsorbant [72]. Les paramètres physico-chimiques peuvent également exercer une influence sur le processus d'adsorption. Il s'agit du pH de la solution, de la température, de la dose d'adsorbant, de la concentration d'adsorbat, de la force ionique, entre autres. Les systèmes adsorbat-adsorbant sont généralement évalués à l'aide de deux modes d'adsorption. Il s'agit du mode discontinu (batch) et du mode continu (colonne) [73,74].

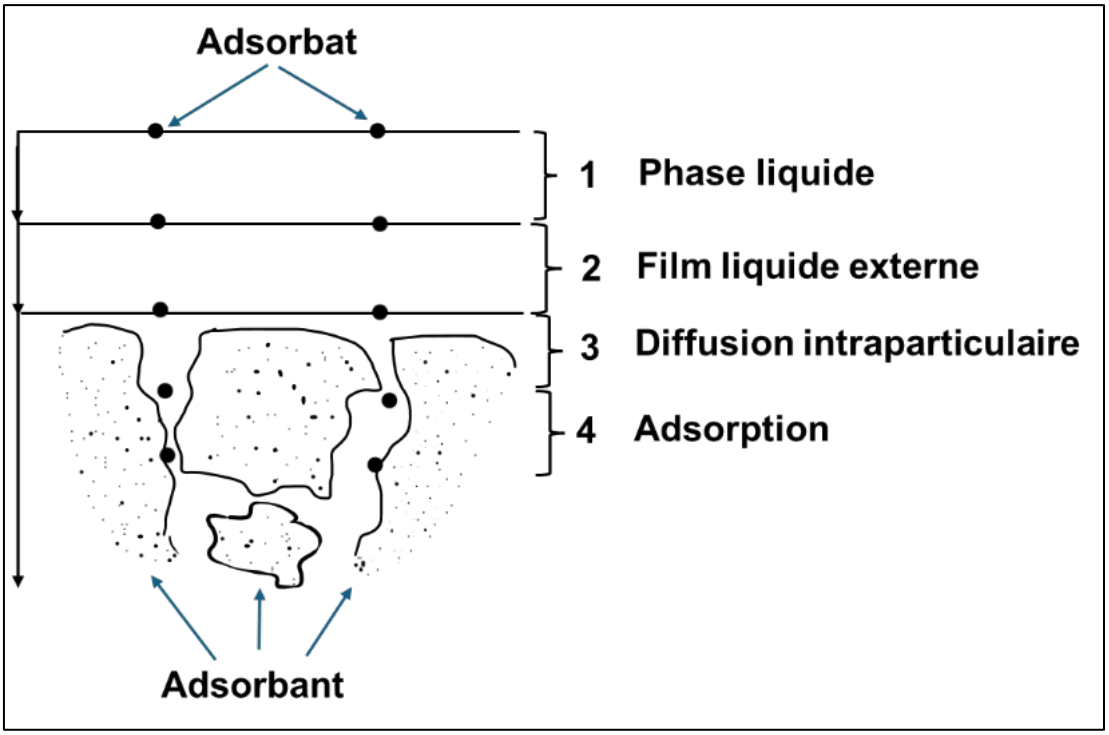

Figure 2.2 Processus d'adsorption [75]

2.2.3.1 Adsorption en cuvée (batch)

L'adsorption en cuvée est une méthode largement utilisée dans la littérature pour éliminer les polluants des eaux usées, qu'elles soient réelles ou synthétiques. Elle repose sur l'agitation à vitesse constante de la solution de polluant, dans laquelle ont été placées des quantités précises d'adsorbant, afin d'optimiser le contact entre l'adsorbat et l'adsorbant jusqu'à atteindre l'équilibre d'adsorption. Elle est adéquate pour évaluer la faisabilité d'un système adsorbat-adsorbant, car elle ne nécessite pas de grand volume de solution, utilise de petites quantités d'adsorbant et est adaptée au traitement de solutions à faible charge polluante. Les essais d'adsorption en cuvée sont généralement étudiés par modélisation des isothermes, de la cinétique et de la thermodynamique [76].

Isothermes d'adsorption

Les modèles isothermes jouent un rôle important dans l'analyse des performances d'un système adsorbat-adsorbant. Les modèles d'isothermes d'adsorption couramment utilisés pour décrire les données expérimentales d'adsorption sont les modèles de Langmuir et de

Freundlich entre autres [77]. Les équations associées à chacun de ces modèles sont répertoriées dans le tableau 2.3. Ces modèles isothermes reposent sur des hypothèses permettant d'interpréter les données expérimentales d'adsorption. Le modèle de Langmuir repose sur des hypothèses physiques qui postulent une adsorption en monocouche, une homogénéité de la surface de l'adsorbant, avec un nombre fini de sites d'adsorption équivalents de même énergie, et ne tient pas compte des interactions entre les molécules adsorbées [78]. Le modèle de Freundlich modélise une adsorption multicouche sur une surface hétérogène et tient compte des interactions moléculaires [79].

Tableau 2.3 Modèles d'isothermes d'adsorption

Isotherme	Équation	Paramètres
Langmuir	$q_e = \frac{q_m K_L C_e}{1 + K_L C_e}$	q_m : Limite théorique de l'adsorption lorsque la surface monocouche est entièrement recouverte d'ions métalliques (mg/g). K_L : Constante de Langmuir (L/mg) liée à l'énergie d'adsorption.
Freundlich	$q_e = K_F C_e^{1/n}$	K_F : Constante de Freundlich, qui prédit la quantité d'ions métalliques par gramme de composite à la concentration d'équilibre (mg/g). n: Une mesure de la nature et de la force du processus d'adsorption, ainsi que de la distribution des sites actifs liés à l'hétérogénéité de surface; plus sa valeur est élevée, plus le système est hétérogène.

Modèles cinétiques

L'étude de la cinétique d'adsorption est une étape essentielle pour la compréhension du processus d'adsorption. Elle permet de déterminer le temps d'atteinte de l'équilibre d'adsorption, facilite la compréhension du mécanisme de transfert de masse et fournit des informations sur la vitesse afin d'identifier l'étape qui limite la cinétique globale du processus d'adsorption. Les modèles cinétiques couramment utilisés pour décrire la vitesse d'adsorption sont le modèle cinétique du pseudo-premier ordre (modèle de Langmuir), le modèle cinétique du pseudo-second ordre (modèle de Ho et McKay) et le modèle de diffusion intraparticulaire (modèle de Weber-Morris) [80]. Les équations et les paramètres sont présentés dans le tableau 2.4.

Tableau 2.4 Équations linéaires et non linéaires des modèles cinétiques du pseudo-premier ordre et du pseudo-deuxième ordre

Modèle	Équation Non-linéaire	Équation Linéaire	Paramètres
Pseudo-premier ordre	$\frac{dq}{dt} = k_1 (q_e - q_t)$	$\log(q_e - q_t) = \log(q_e) - (\frac{k_1}{2.303})t$	q_e: Quantité adsorbée (mg/g) à l'équilibre. q_t: Quantité adsorbée (mg/g) au temps t (min). k_1: Constante de vitesse d'adsorption de pseudo premier ordre (min^{-1}).
Pseudo-deuxième ordre	$\frac{dq}{dt} = k_2 (q_e - q_t)^2$	$\frac{t}{q} = \frac{1}{k_2 q_e^{\ 2}} + \frac{t}{q_e}$	k_2: Constante de vitesse d'adsorption de pseudo deuxième ordre (g/(g min)) ;
Diffusion intraparticulaire	-	$q_t = k_{id} t^{1/2} + C$	k_{id}: Constante de vitesse de diffusion intraparticulaire (g/(g $min^{1/2}$)). C: Épaisseur de la couche limite (mg/g).

Le modèle cinétique du pseudo-premier ordre suppose que le taux d'occupation des sites actifs est proportionnel au nombre de sites disponibles. Ce modèle n'est pas adéquat pour décrire l'ensemble du domaine temporel au cours duquel l'adsorbat est en contact avec l'adsorbant, mais plutôt la phase initiale du processus d'adsorption. La diffusion externe à travers la couche limite contrôle le processus d'adsorption et les interactions de faible énergie sont responsables de la capture de l'adsorbant par les sites actifs. Le modèle cinétique du pseudo-second ordre suppose un taux d'adsorption proportionnel au carré du nombre de sites actifs libres. Il décrit bien l'intégralité du domaine temporel du processus d'adsorption et suggère que la cinétique globale du processus d'adsorption est contrôlée par des réactions chimiques [71,81]. Le modèle de diffusion intraparticulaire permet d'élucider le mécanisme de diffusion à la surface de l'adsorbant. Il suggère que la diffusion de l'adsorbat à l'intérieur des pores est l'étape qui limite le transfert de masse [82].

Thermodynamique

L'étude thermodynamique du processus d'adsorption constitue un outil fondamental qui complète les informations issues de l'analyse des isothermes et de la cinétique d'adsorption. Elle permet de comprendre la nature des interactions, la spontanéité et le mécanisme d'adsorption [76]. L'effet de la température sur le système se manifeste notamment par les valeurs des paramètres thermodynamiques calculés. Il s'agit de l'énergie libre de Gibbs ΔG° (kJ/mol), de l'enthalpie de réaction ΔH° (kJ/mol) et de l'entropie ΔS°. Ces paramètres peuvent être estimés à partir des constantes d'équilibre à différentes températures. La variation d'énergie de la réaction d'adsorption est donnée par les équations 1 et 2 :

$$\Delta G° = -R\,T\,Ln\,K \qquad \text{Équation 2.1}$$

$$\Delta G° = \Delta H° - T\,\Delta S° \qquad \text{Équation 2.2}$$

Où R est la constante universelle des gaz (8.314 $J \cdot mol^{-1} \cdot K^{-1}$), T est la température absolue (K) et K est la constante d'équilibre d'adsorption.

L'énergie libre de Gibbs indique la spontanéité de l'adsorption. Lorsque ses valeurs sont positives, cela indique un processus non spontané tandis que lorsqu'elles sont négatives, cela renvoie à une adsorption spontanée et favorable. Ce cas particulier donne une idée de la nature du processus d'adsorption. Lorsque ΔG° est entre 0 et -20 kJ/mol, l'adsorption est physique et lorsqu'elle est entre -20 et -80 kJ/mol, l'adsorption est chimique. Les valeurs de ΔH° indiquent la capacité du système à libérer de l'énergie ou à adsorber de la chaleur. Des valeurs de ΔH° négatives sont typiques d'une adsorption exothermique favorisée à basse température, où des interactions faibles sont impliquées pour l'adsorption sur les sites actifs (physisorption, ΔH° < 40 kJ/mol), tandis que, lorsque ΔH° est positive, des interactions plus fortes assurent l'élimination du soluté (chimisorption, 40 kJ/mol < ΔH° < 400 kJ/mol). Le processus d'adsorption est favorisé à haute température et est endothermique. L'entropie indique le changement d'ordre du système. Les valeurs négatives de ce paramètre indiquent une adsorption structurée et moins

aléatoire à l'interface solution-adsorbant alors que les valeurs positives indiquent une orientation moins spécifique de l'adsorbat et une augmentation du désordre [83,84].

2.2.3.2 Adsorption continue dans une colonne à lit fixe

L'adsorption dynamique dans une colonne à lit fixe est une méthode de traitement au cours de laquelle l'adsorbat est mis en contact avec le lit de sorbant, par alimentation de la colonne à l'entrée avec un flux continu (débit constant) d'une solution de polluant, qui traverse le lit jusqu'à la sortie [74]. C'est une méthode couramment utilisée pour traiter les eaux présentant une charge polluante importante et qui peut être appliquée en flux descendant ou en flux ascendant. Le principe de cette méthode d'adsorption est simple et se résume à quelques étapes (voir la figure 2.3).

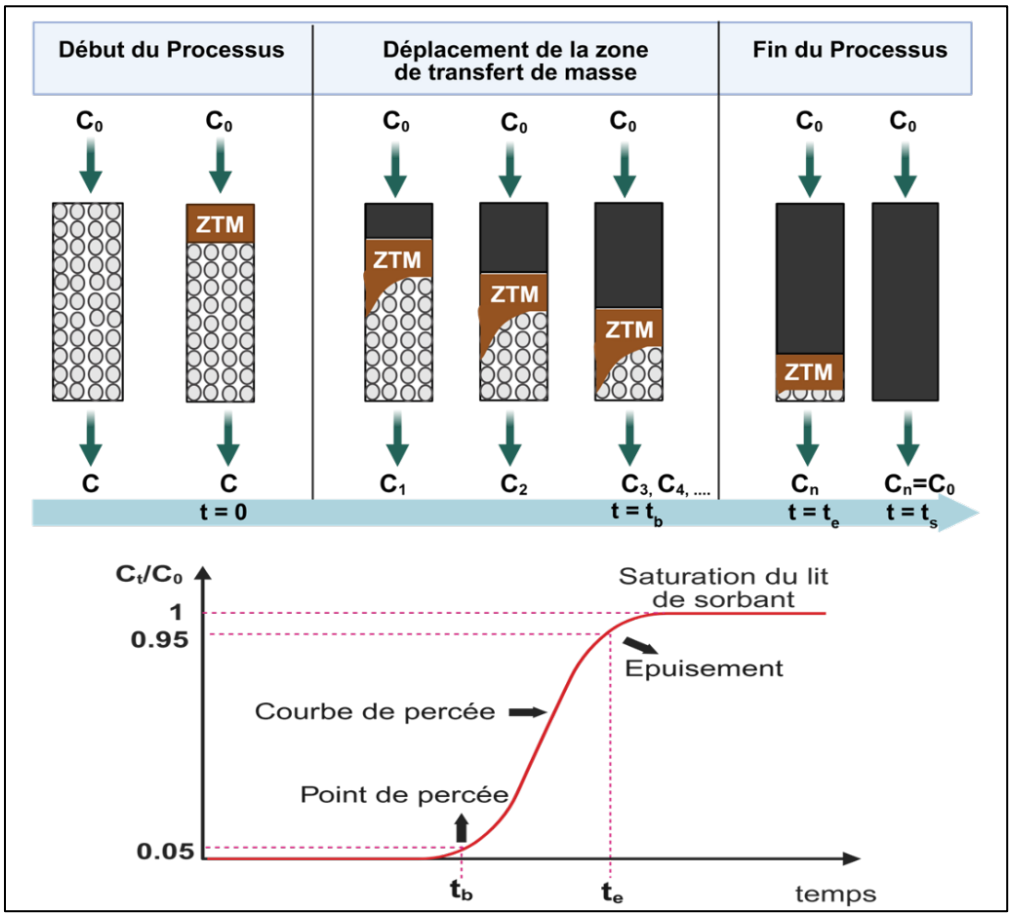

Figure 2.3 Mouvement de la zone de transfert de masse et la courbe de percée associée [70]

La solution contenant le soluté entre par le haut ou par le bas de la colonne, selon que le mode de fonctionnement est ascendant ou descendant, puis migre à travers le lit de la colonne. Au fur et à mesure que les sites d'adsorption se saturent, le front d'adsorption se déplace vers la sortie de la colonne, et lorsque l'adsorbat commence à apparaître dans l'effluent, le point de percée est atteint (la concentration de polluant dans l'effluent à la sortie, au temps t, est égale à 5 % de la concentration initiale du polluant). Tout au long du fonctionnement de la colonne, l'adsorption se fait de manière progressive et se produit exclusivement au niveau de la région du lit de la colonne (adsorbant), directement en contact avec la solution ; c'est la zone de transfert de masse (ZTM). Au-dessus de cette zone, les sites d'adsorption sont occupés et en dessous, ils sont libres. La ZTM se déplace vers la sortie de la colonne et sa vitesse de déplacement peut être affectée par de nombreux paramètres tels que le débit, la concentration initiale, la température, le pH du milieu, la taille des particules et la nature du soluté, entre autres. La courbe de percée est le profil qui décrit la relation entre la concentration de l'effluent et le temps ou le volume traité (C_t/C_0 versus t). L'étude de cette courbe permet d'identifier les moments clés du processus d'adsorption, notamment le temps de percée et le temps d'épuisement. Le temps de percée t_b (min) et le temps d'épuisement t_e (min) correspondent aux moments du fonctionnement où $C_t/C_0 = 0.05$ et $C_t/C_0 = 0.95$. Les modèles de Thomas et de Yoon-Nelson sont des modèles très utilisés pour décrire la dynamique d'adsorption en colonne à lit fixe. Ce sont des outils précieux qui permettent de prédire le comportement de la colonne d'adsorption à partir de ses paramètres respectifs [73]. Ces modèles reposent sur plusieurs hypothèses. Le modèle de Thomas suppose une cinétique d'adsorption gouvernée par une loi du pseudo-second ordre et un transfert de masse dominé par la réaction d'adsorption elle-même, tandis que le modèle de Yoon-Nelson suppose que la diminution de la probabilité qu'une molécule soit adsorbée est proportionnelle à la probabilité qu'elle traverse la colonne sans être adsorbée [85,86]. Les modèles de Thomas et de Yoon-Nelson sont représentés par les équations non-linéaires suivantes

$$C_t/C_0 = 1/\left(1+\exp\left(K_{Th}\left[\left(q_0\, m\right)/Q - C_0\, t\right]\right)\right)$$ Équation 2.3

$$C_t/C_0 = 1/\left(1+\exp\left[K_{YN}\left(\tau - t\right)\right]\right)$$ Équation 2.4

Où K_{Th} (L/mg.min) constante de vitesse de Thomas, q_0 (mg/g) la capacité d'adsorption à l'équilibre, K_{YN} (min^{-1}) constante de vitesse de Yoon-Nelson et τ (min) temps pour une percée de 50 % de polluant, C_0 (mg/L) est la concentration initiale à l'entrée de la colonne et C_t (mg/L) la concentration de l'effluent au temps *t*.

Les courbes de percée sont une représentation graphique de l'évolution progressive de l'adsorption dans le lit de la colonne au cours du temps. Il s'agit du rapport de la concentration du soluté à la sortie de la colonne, en fonction du temps (t), par rapport à la concentration initiale à l'entrée de la colonne (C_t/C_0). Elles permettent d'évaluer les performances d'adsorption du lit de la colonne à partir de paramètres tels que le temps de percée, le temps d'épuisement, la ZTM, la hauteur de la ZTM, le volume de percée et le volume d'épuisement. La saturation du lit de la colonne est atteinte lorsque ce rapport vaut 1. La dispersion axiale affecte le profil de percée. Il s'agit de la diffusion du soluté le long de l'axe de la colonne.

2.2.4 Chitosane et carboxyméthylchitosane

La notion de durabilité a été introduite dans bien des domaines afin de se pencher davantage sur la protection et la préservation de l'environnement. Cela a conduit à l'adoption des biopolymères, tels que les polysaccharides (cellulose, chitosane, alginate, agarose…), au sein de nombreuses stratégies visant à développer des adsorbants durables, notamment les hydrogels et les cryogels [87,88]. Ce choix a été fait au regard des caractéristiques uniques des polymères naturels (biodégradabilité, biocompatibilité, non-toxicité, disponibilité et coûts plus accessibles). Ils sont donc perçus comme une alternative attrayante aux polymères synthétiques [89].

La chitine est un polysaccharide naturel, le plus abondant après la cellulose. Il est extrait des exosquelettes des arthropodes notamment des déchets des carapaces des crustacés et des crabes qui sont plus abondants [90]. C'est un biopolymère dont les applications sont

considérablement limitées en raison de sa structure cristalline hautement organisée, qui le rend insoluble dans les solvants communs tels que l'eau. Pour pallier cette difficulté entre autres, la chitine a été modifiée chimiquement par la réaction de désacétylation partielle en milieu alcalin fort et à haute température pour obtenir un dérivé capable de se dissoudre dans de l'eau acidifiée notamment [90]. Il s'agit du chitosane, dont la structure chimique est dotée de groupes fonctionnels très réactifs (hydroxyles, acétamides et amines) qui se prêtent bien à des modifications chimiques (voir la figure 2.4) [91]. Celles-ci permettent de conserver, d'améliorer ou d'apporter de nouvelles propriétés physico-chimiques aux biopolymères, d'où l'intérêt croissant pour le chitosane.

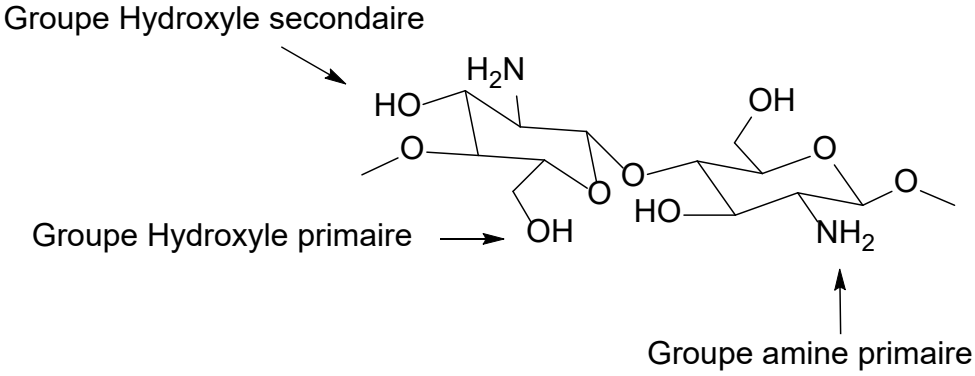

Figure 2.4 Structure chimique du chitosane [91]

Une large gamme de dérivés du chitosane a été obtenue par différentes modifications chimiques, principalement par des réactions de substitution, des modifications enzymatiques et la copolymérisation par greffage, entre autres [92]. La carboxyméthylation est l'une de ces modifications chimiques qui permet d'obtenir lorsqu'un choix judicieux des conditions de la réaction est fait (température, solvants, rapport des réactifs…) trois dérivés distincts du chitosane à savoir le O-carboxyméthylchitosane le N-carboxyméthylchitosane et le N,O-carboxyméthylchitosane (voir la figure 2.5). Cette modification chimique améliore la solubilité du chitosane dans l'eau à pH neutre et alcalin. C'est une réaction simple qui ne nécessite pas l'usage de solvants toxiques, et les dérivés du chitosane obtenus sont amphotères et sensibles à la variation du pH [92]. Cela favorise les interactions avec des ions de charges opposées, d'où l'intérêt de ces dérivés pour le développement de matériaux fonctionnels utilisés dans les domaines biomédicaux et environnementaux.

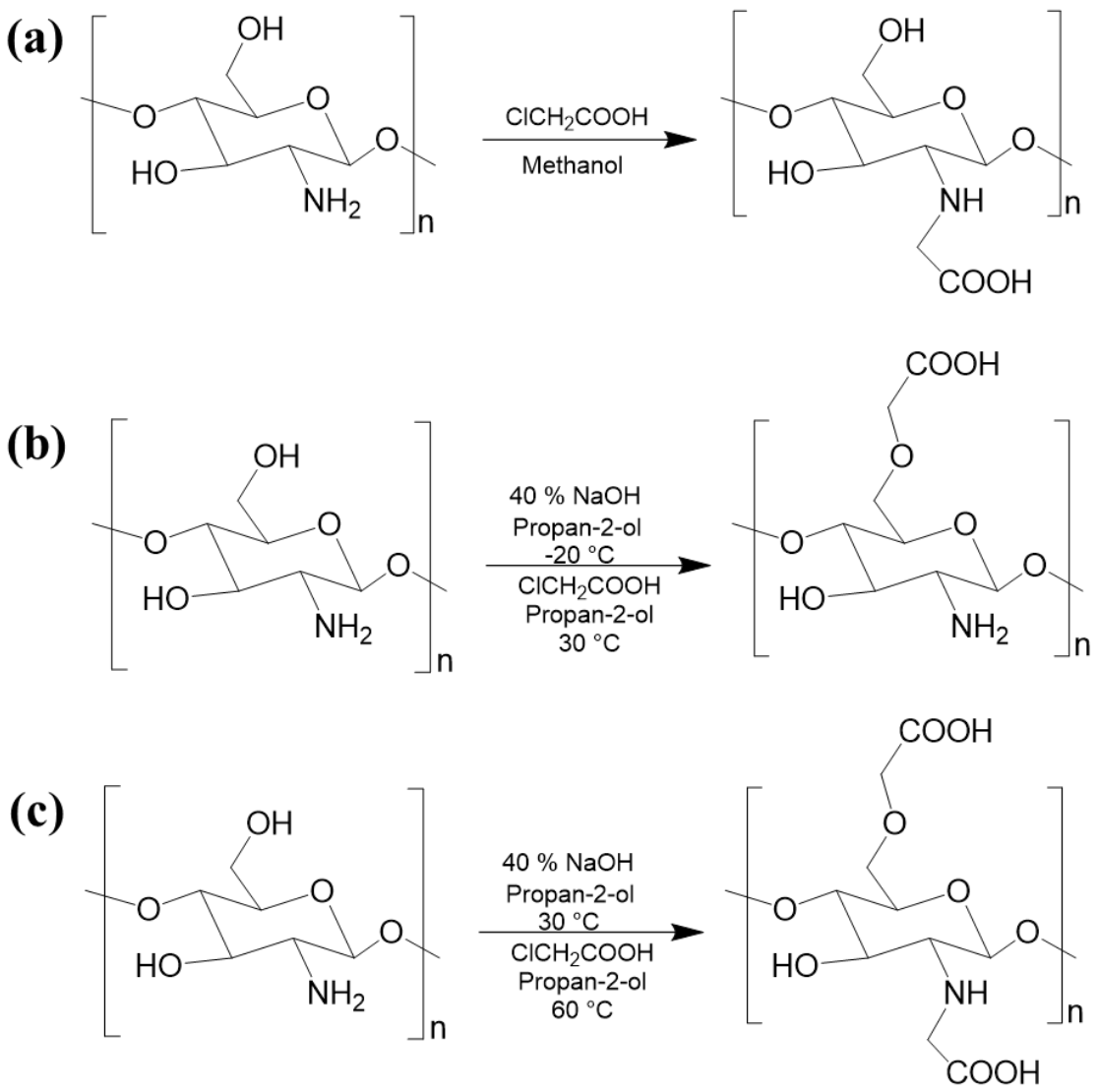

Figure 2.5 Réaction de carboxyméthylation du chitosane : a) formation du N-carboxyméthylchitosane, b) formation du O-carboxyméthylchitosane et c) formation du N,O-carboxyméthylchitosane

De nombreuses études présentent les propriétés du chitosane et du carboxyméthylchitosane et rapportent leur capacité à former des gels (hydrogels et des cryogels) superporeux et "intelligents" dotés d'excellentes propriétés physico-chimiques et mécaniques [93,94]. Les dérivés et composites du chitosane ont été largement utilisés pour la décontamination des résidus pharmaceutiques dans l'eau. Il s'agit notamment des antibiotiques, des anti-inflammatoires, des analgésiques et des antidépresseurs, entre autres (tableau 2.5). Les mécanismes identifiés dans la littérature comme étant responsables de leur élimination par adsorption sont nombreux. On a les interactions

électrostatiques du fait de la présence de charges antagonistes sur la surface du matériaux adsorbants et la molécule pharmaceutique ionisée, les liaisons hydrogènes car la plupart des molécules pharmaceutiques sont dotés de groupes donneurs/accepteurs d'hydrogène, des interactions Π-Π et hydrophobes car pour des molécules comme la fluoxétine qui possède des cycles aromatiques dans sa structure, des interaction faibles peuvent s'établir avec les liaisons Π qui seraient potentiellement présents dans la structure de l'adsorbant à base du chitosane ou du carboxyméthylchitosane.

L'usage de tels matériaux adsorbants, dans différentes conditions opérationnelles, a mis en lumière certains points négatifs (tableau 2.6). On note la faible sélectivité dans les milieux complexes où les micropolluants pharmaceutiques coexistent avec d'autres polluants, la stabilité mécanique dans les conditions réelles, qui n'est pas toujours optimale, et la nécessité de mettre au point de meilleures stratégies de recyclage afin de prolonger leur durée de vie [95]. Il est important de se pencher sur ces différentes lacunes afin de limiter les coûts et de garantir une meilleure durabilité à ce type de matériaux adsorbants car ils ont démontré un potentiel énorme pour l'élimination d'une large gamme de polluants émergents [95,96] Cela passe par la conception de composites "intelligents" et la mise au point des conditions de désorption idéale pour assurer le recyclage de tels matériaux sans le dégrader afin de lui assurer une viabilité à long terme. La fonctionnalisation du précurseur par différentes voies chimiques, la réticulation, l'ajout de nanostructures et l'impression de molécules modèles sont différents moyens optés pour améliorer la sélectivité, la stabilité mécanique, la capacité d'adsorption et la réutilisabilité des matériaux à base de chitosane et de ses dérivés.

La désorption et le recyclage constituent des étapes importantes qui assurent la durabilité de tels adsorbants et favorisent l'économie circulaire et la réduction des coûts. Le processus vise à restaurer les capacités du matériau en évitant d'altérer sa structure de manière significative tout au long des différents cycles de régénération. Pour les matériaux à base de biopolymère, la désorption par voie chimique est la méthode la plus utilisée. Elle nécessite, entre autres, l'usage de solvants organiques, d'acides, de bases et d'agents chélatants [97,98]. L'acide, par exemple, favorise la protonation des groupes amine primaires et des carboxylates de la carboxyméthylchitosane. Il est efficace pour désorber

les cations ayant interagi avec ces sites actifs. L'utilisation d'une base pour la régénération du carboxyméthylchitosane entraîne la déprotonation des groupes carboxyles et des amines primaires protonées, ce qui interrompt les interactions électrostatiques entre les amines primaires protonées et le soluté anionique. L'échange d'ions et la complexation sont également des méthodes de désorption qui nécessitent l'utilisation de solutions de sels (NaCl, $CaCl_2$) et d'un agent chélatant, comme Éthylène diamine tétra-acétique (EDTA), habituellement utilisé pour l'extraction des métaux. Les solvants organiques (méthanol, éthanol et acétone) entre autres ou leur mélange ont été rapporté comme des solvants efficaces pour la désorption de polluants organiques.

Tableau 2.5 Adsorption des résidus pharmaceutiques par des matériaux à base du chitosane et du carboxyméthylchitosane

Résidus pharmaceutiques	Adsorbants	Conditions	Capacité maximale	Cinétique	Isotherme	Thermodynamique	Réf
Enrofloxacine	Hydrogel de chitosane greffé avec de l'acide acrylique	C_0=10-600 mg/L, 1 mM et 10mM de NaCl/$CaCl_2$, pH=2-9	387.7 mg/g	-	-	-	[99]
Chloramphénicol	Polymères à empreinte magnétique à base de microsphères de chitosane	-	52.6 µmol/g	Pseudo-second ordre	Langmuir	-	[100]
Chlortétracycline	Carboxyméthylchitosane modifié Na-montmorillonite	25-45 °C pH = 4-7	271,74 mg/g	Pseudo-second ordre	Freundlich	Exothermique	[101]
Tétracycline	Chitosane réticulé à la génipine/oxyde de graphène-SO3H	25-40 °C pH = 2–12	556.28 mg/g	Pseudo-second ordre	Freundlich	Endothermique	[102]
Ciprofloxacin	Hydrogel de chitosane greffé avec de l'acide acrylique	C_0 = 10-600 mg/L pH = 2-9 (1 mM et 10 mM NaCl/$CaCl_2$)	267,7 mg/g	-	-	-	[99]
	Cryogels de N-(2-carboxyéthyl)chitosane chélatés au Cu (II)	Teneur en Cu (II) : 7-65 mg/g pH = 2,5-10,5	280 mg/g	-	Langmuir	-	[103]
	Cryogels chélatés à l'Al (III) de N-(2-carboxyéthyl)chitosane	pH = 3-10	390 mg/g	-	Langmuir	-	[103]
Diclofénac sodium	Microsphère de chitosane	-	$5,2 \times 10^{-4}$ mol/g	-	Langmuir	Endothermique	[104]
Ibuprofène	Microsphères de chitosane chargées de nanoparticules d'argent	-	390 mg/g	Pseudo-second ordre	Langmuir	-	[105]
Fluoxétine	Billes de carboxyméthylchitosane	C_0 = 50 mg/L pH = 7-8.5, 30-60 °C	90-113 mg/g	Pseudo-premier ordre	Langmuir	Exothermique	[106]
	Cryogel de poly(acrylate) de sodium/carboxyméthylchitosane	C_0 = 50 mg/L pH = 8.5, 30-60 °C	80.6 ± 3.4 mg/g	Pseudo-premier ordre	Langmuir	Exothermique	[107]

Tableau 2.6 Limites structurelles du chitosane et stratégies d'atténuation

Propriétés	Limites	Conséquence sur l'adsorption	Atténuation commune	Réf
Faible surface spécifique et faible porosité	Peu de sites accessibles, adsorption lente et limitation de la capacité d'adsorption maximale	Performances plus faibles (q_{max}) et cinétique plus lente, notamment dans les systèmes à lit fixe	Introduction de porosité (utilisation d'agent porogène, réticulation) fonctionnalisation (impression des modèles, greffage, ajout de nanoparticules,charbon actif, zéolite…)	[108]
Problèmes de solubilité : soluble dans les acides, faible solubilité dans les milieux neutres/basiques	Dissolution ou gonflement entraînant la déformation des particules et mauvaise dispersion à pH neutre/basique, limitant la plage d'utilisation du pH	Performances irrégulières en dehors d'une plage de pH étroite	Réticulation chimique, greffage ou mélange avec des polymères résistants aux acides	[109]
Faible résistance mécanique ou stabilité physique	Les billes/membranes/monolithes se déforment sous l'effet de contraintes mécaniques, faible résistance aux cycles d'adsorption/désorption.	Faible réutilisabilité dans les colonnes et les systèmes dynamiques	Réticulation	[110]
Forte sensibilité au pH de la protonation de $–NH_2$	Les interactions dépendent de la protonation ; l'affinité pour les solutés cationiques diminue fortement à pH plus faible	La fenêtre de pH où l'adsorption de soluté cationiques est optimale pH > pKa chitosane	Greffage des groupes carboxyle, formation des composites	[111]
Faible sélectivité dans les matrices complexes (compétition avec les co-ions/composés organiques)	La liaison non spécifique des amines entraîne une compétition entre les ions coexistants	Perte de capacité en conditions réelles	Fonctionnalisation, impression des modèles	[112]
Régénération et réutilisation limitées	La désorption est souvent incomplète ; les chaînes se dégradent lors de la régénération acide/alcaline	Déclin rapide de la capacité au fil des cycles ; coûts d'exploitation plus élevés	Éluants plus doux ; réticulation robuste ; passage à des formes dérivées/composites	[110]

2.2.5 Hydrogel

Des efforts considérables ont été fourni pour développer des hydrogels pour la décontamination des eau polluées par une grande variété de polluants [113]. Les biopolymères hydrophiles sont des précurseurs de choix pour la conception des hydrogels [93] du fait de leurs propriétés uniques (biodégradabilité, biocompatibilité, faible coût et non-toxicité). La présence des groupes fonctionnels hydrophiles (-OH, -NH_2, -COOH, -$CONH_2$, CONH-, SO_3H) sur les chaînes de polymères leur confère des propriétés uniques telles que le gonflement au contact de l'eau, la flexibilité et, selon la méthode de fabrication, une structure poreuse très développée [114]. Ces points spécifiques faciliteraient la diffusion des fluides dans le réseau tridimensionnel des hydrogels et amélioreraient leur perméabilité, ce qui est un atout majeur pour une application dans le traitement des eaux. Ce sont des matériaux dont le potentiel et les caractéristiques uniques trouvent des applications dans de nombreux domaines et peuvent être classés selon leurs propriétés (voir figure 2.6).

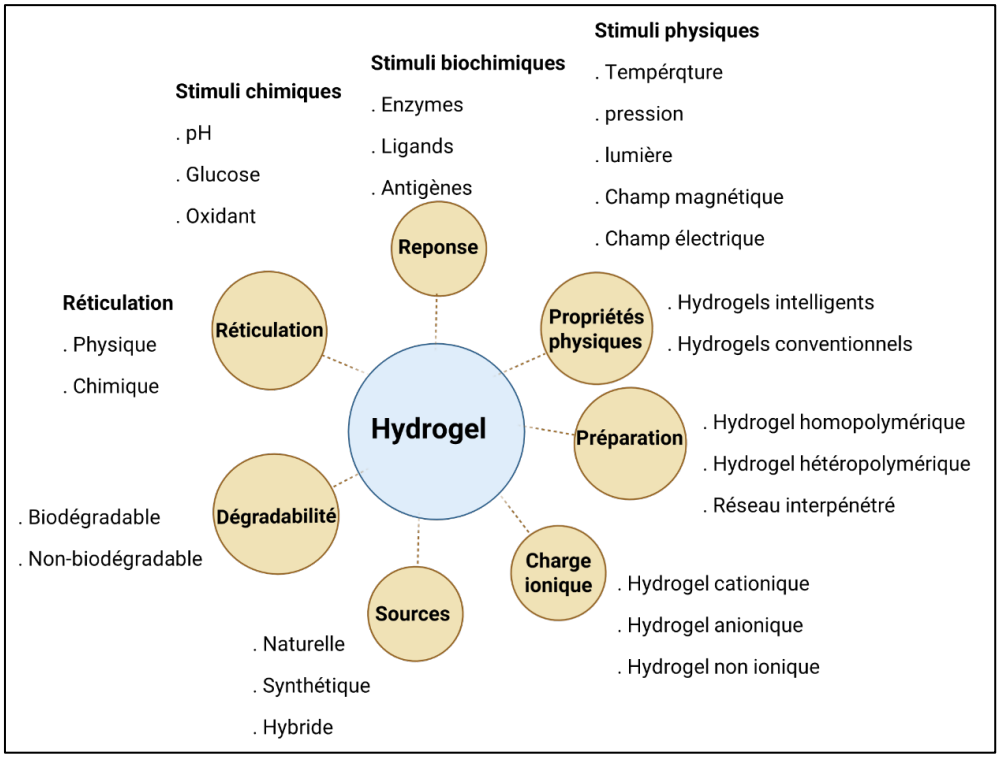

Figure 2.6 Classification des hydrogels en fonction de leurs différentes propriétés [115]

Diverses méthodes permettent de fabriquer des hydrogels poreux. Il s'agit de la méthode de séparation de phases, de la formation de microémulsions, de la porogénation et de la lyophilisation [93]. Ces deux dernières sont les plus utilisées pour élaborer des hydrogels aux tailles de pores variées, allant du micromètre au nanomètre. Le polyéthylène glycol (PEG) de différents poids moléculaires est l'un des porogènes très souvent utilisés pour développer des hydrogels poreux car il est très soluble dans l'eau et peut facilement être éliminé par lavages successifs de l'hydrogel avec de l'eau à la fin du processus [116]. Toutefois, le degré de réticulation affecte également la taille des pores [117].

La réticulation est la formation de ponts physiques ou chimiques entre les chaînes polymériques du réseau des hydrogels [118]. Deux méthodes de réticulation sont utilisées pour préparer les hydrogels (voir la figure 2.7). Il s'agit de la réticulation physique, qui forme des ponts plus courts, et de la réticulation chimique, qui forme des ponts plus longs. La nature hydrosoluble du carboxyméthylchitosane nécessite une réticulation des chaînes pour assurer la stabilité mécanique des hydrogels à base de ce biopolymère lorsqu'ils sont utilisés pour des applications de décontamination en solution aqueuse. Le chlorure de calcium et les biopolymères polyélectrolytes sont généralement utilisés pour la réticulation physique des hydrogels à base de carboxyméthylchitosane où la stabilité réversible du réseau polymérique est assurée grâce aux interactions ioniques, aux liaisons hydrogène et à l'enchevêtrement moléculaire [119]. La réticulation chimique est assurée par des agents chimiques de réticulation comme le glutaraldéhyde, l'épichlorhydrine, le formaldéhyde, l'éther diglycidique d'éthylène glycol et la génipine entre autres [120]. La génipine est une option plus intéressante, car elle est moins toxique que la plupart des agents de réticulation chimique. La réticulation physique confère aux hydrogels une stabilité plus faible tandis que la réticulation chimique leur octroie une stabilité permanente grâce aux liaisons covalentes établies entre les chaînes de polymère

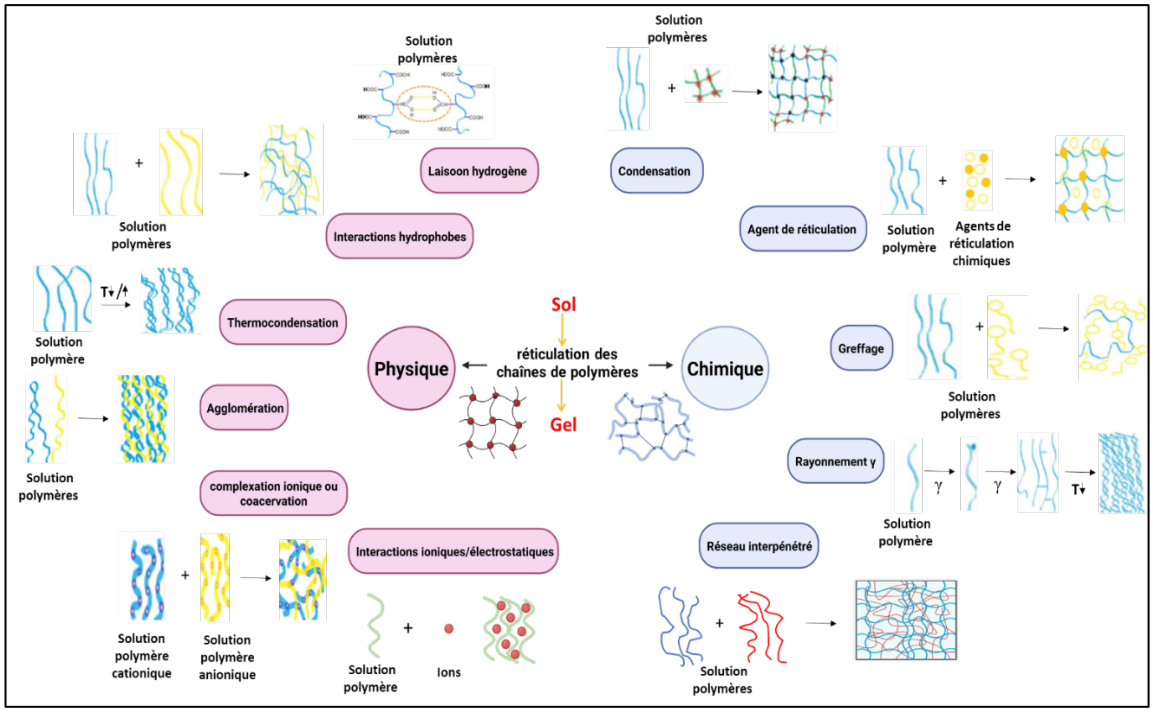

Figure 2.7 Préparation d'hydrogels par des techniques de réticulation physique et chimique [121]

2.2.6 Génipine

La réticulation des chaînes de polymère au cours du processus de fabrication des gels constitue une étape importante, qui a fait l'objet de plusieurs études rapportées dans la littérature. L'intérêt de cette étape réside notamment dans la capacité à moduler certaines propriétés caractéristiques de ce type de matériau en fonction des applications visées. La réticulation chimique et hybride attire davantage l'attention, car les gels réticulés par ces deux méthodes présentent une stabilité irréversible : les liaisons fortes (liaisons covalentes) sont les ponts établis entre les chaînes de polymère, qui assurent la stabilité mécanique du réseau tridimensionnel. Cela facilite, entre autres, leur utilisation dans des milieux acides, neutres ou basiques, d'où leur intérêt pour le traitement des eaux contaminées. Plusieurs agents chimiques de réticulation du chitosane et de certains de ses dérivés comme le carboxyméthylchitosane ont été utilisés pour renforcer les matériaux hydrogels et les cryogels comme le glutaraldéhyde, l'épichlorhydrine, le chlorhydrate de 1-éthyl-3-(3-diméthylaminopropyl) carbodiimide, le poly(N-vinyl-2-pyrrolidone), l'amidon oxydé, le dextrane oxydé et la génipine [122]. La génipine se distingue des

agents de réticulation synthétiques car c'est une alternative plus verte qui a une faible toxicité par rapport aux molécules synthétiques utilisées. La génipine est un composé naturel qui est extrait des fruits des plantes *Genipa americana* et de *Gardenia jasminoides* [124] (figure 2.8).

Figure 2.8 Plante en fleurs (A), fruits mûrissants (B) et fruits secs (C) de Gardenia jasminoides [123]

L'extraction assistée par enzyme est la méthode la plus utilisée pour produire la génipine car elle est plus efficace et fournit un meilleur rendement. L'une des méthodes directes de production de la génipine est l'hydrolyse enzymatique de la geniposide par les β-glucosidases. La cellulase est également une enzyme utilisée dans le processus de biocatalyse pour extraire cette molécule [125]. L'utilisation de cette molécule pour réticuler les polysaccharides ayant un potentiel accru, comme le chitosane et ses dérivés, permet à la fois de stabiliser les gels formés et d'améliorer les propriétés de biocompatibilité de tels matériaux, d'où leur grande utilisation dans le domaine biomédical [126]. Les biopolymères qui possèdent des groupes amines primaires dans leur structure se prêtent bien à une réticulation par la génipine. L'inconvénient de cette réticulation dans la décontamination des eaux par des adsorbants à base de ces biopolymères est la baisse de la capacité d'adsorption. La génipine se lie de manière covalente aux groupes amines primaires, considérés comme des sites actifs à la surface des adsorbants, et réduit par conséquent leur disponibilité pour interagir avec les polluants. Il est donc nécessaire de contrôler le degré de réticulation, la concentration de la génipine et de bien choisir le biopolymère. Pour le carboxyméthylchitosane, par exemple, le greffage du carboxyméthyle exclusivement aux groupes hydroxyles du chitosane est d'autant plus intéressant, car les groupes amines primaires restent disponibles pour la

réticulation avec la génipine. De plus, même si le greffage se fait aussi bien sur les groupes hydroxyles que sur les groupes amines primaires, il existe des cas où l'intégralité des groupes amines n'a pas réagi et demeure suffisante pour participer à la réticulation, de sorte à obtenir des structures polymériques suffisamment stables. Dans ce même domaine, l'avantage de considérer la génipine comme agent chimique de réticulation réside dans la structure des groupes donneurs/accepteurs de liaison hydrogène, ainsi que dans des liaisons carbone-carbone insaturées. Ce qui est idéal pour fixer des molécules organiques dotées de liaisons multiples délocalisées et de groupes donneurs/accepteurs de liaisons hydrogène, comme la fluoxétine. Le pH des solutions, la température et la concentration de génipine sont des paramètres qui influencent la réticulation avec la génipine ainsi que la cinétique du processus. Les méthodes d'extraction de la génipine, ses caractéristiques physico-chimiques et quelques domaines d'application sont présentés dans le tableau 2.7.

Tableau 2.7 Génipine, propriétés physico-chimiques, méthodes d'extraction et domaine d'application

Nom	Génipine	**Réf**
Structure chimique $C_{11}H_{14}O_5$	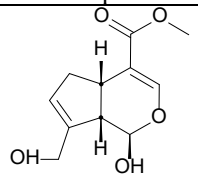	Numéro CAS : 6902-77-8
Masse molaire moléculaire	226.23 g/mol	-
Sources	• Génipa americana • Gardenia jasminoides	[129,130]
Extraction	• Extraction assistée par ultrasons • Traitement à haute pression • Extraction de liquide sous pression • Extraction assistée par enzymes	[129,131, 132]
Caractéristiques physico-chimiques	• Poudre cristalline de couleur blanche - jaune pâle • Soluble dans l'eau, l'alcool, le diméthylsulfoxyde et le diméthylformamide • La réactivité est influencée par le pH, la température et la durée de réticulation et la concentration	[129,131]
Domaines d'application	• Environnement : fabrication d'adsorbants robustes et durables • Agroalimentaire : transformation et emballage des aliments, conservation et préservation des aliments • Biomédicale : renforcement des propriétés anti-inflammatoires et de l'activité antioxydante des gels à base de biopolymères	[130,133,134]

Des pigments bleus sont observés sur les matériaux ayant subi une réticulation par la génipine en milieux faiblement acides et neutres. D'après de nombreuses études, cette

pigmentation bleue serait due à la réaction de la génipine avec les groupes amines primaires des polysaccharides en présence d'oxygène [127]. Le processus se déroule tout d'abord par une attaque nucléophile du carbone oléfinique C3 de la génipine, suivie de l'ouverture du cycle du dihydropyrane. Les groupes esters de cette molécule peuvent également réagir par attaque nucléophile des groupes amines primaires (voir la figure 2.9). Les ponts covalents formés au cours de ce processus de réticulation sont plus courts que ceux obtenus en milieu fortement alcalin, car la génipine subit d'abord une autopolymérisation (condensation aldolique) avant de former des liaisons covalentes avec le polysaccharide. Certaines études rapportent que cette étape préalable serait responsable de la couleur brunâtre observée sur les matériaux réticulés à pH très basique [128].

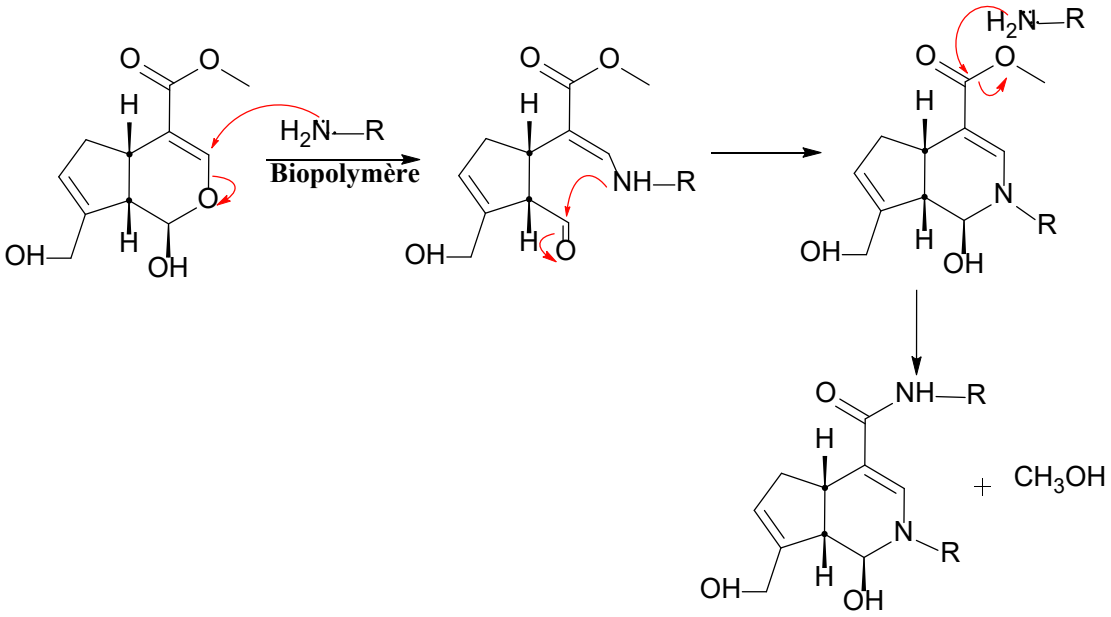

Figure 2.9 Mécanisme possible de la réticulation des biopolymères par la génipine en milieu faiblement acide et neutre.

2.2.7 Formation des hydrogels sphériques

En fonction de leurs applications, les hydrogels sont préparés sous forme de films, de fibres creuses, d'anneaux, de monolithes et de billes par différentes méthodes, telles que le moulage cylindrique et le séchage par coulée, entre autres [87]. La formation des billes d'hydrogel est particulière et ne nécessite ni l'utilisation de moules ni une étape supplémentaire de mise en forme ultérieure. Les sphères se forment simultanément dès

que le polymère entre en contact avec l'agent de réticulation. Pour le cas spécifique des billes d'hydrogel à base de carboxyméthylchitosane, l'absence de réticulation et le poids moléculaire du biopolymère peuvent affecter l'enchevêtrement des chaînes de polymère et influencer la forme des billes [135]. L'utilisation des bains de réticulation d'antisolvant comme le solvant binaire éthanol-eau contenant le $CaCl_2$ comme agent de réticulation physique (figure 2.10) est une solution pour pallier les contraintes observées au cours de la formation de ce type d'hydrogel [136].

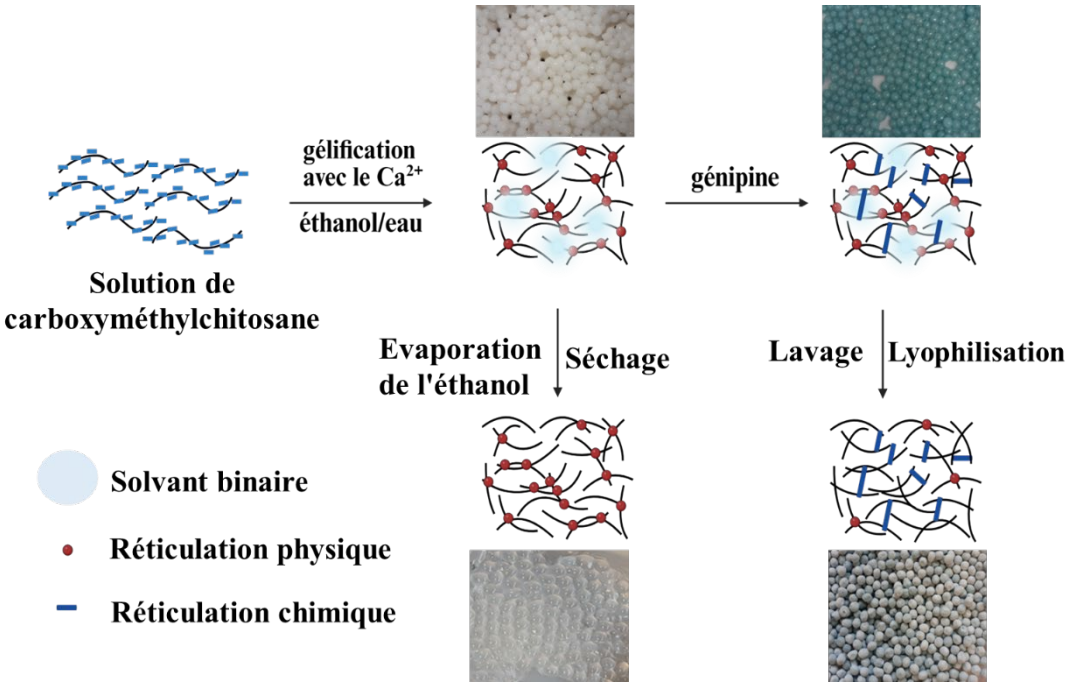

Figure 2.10 Formation des hydrogels sphériques de carboxyméthylchitosane réticulés par la génipine [106]

La formation des billes d'hydrogel peut être influencée par différents facteurs tels que la concentration du biopolymère, la viscosité de la solution polymérique, la température et la composition du solvant, entre autres [114]. L'utilisation de la combinaison de solvants polaires perturbe les liaisons hydrogène entre le biopolymère et l'eau, favorise les interactions entre les chaînes de polymère et crée des interactions hydrophobes plus importantes. Cela accroît l'enchevêtrement des chaînes polymériques, ce qui constitue un facteur important dans la formation des billes sphériques [136]. Toutefois, l'optimisation de la concentration d'alcool dans le solvant binaire alcool-eau, par exemple, et la réticulation physique contribuent grandement à obtenir un réseau polymérique capable de

retenir une quantité suffisante d'eau, ce qui permet de former des billes d'hydrogel parfaitement sphériques. Par exemple, Lin et al., 2005, ont montré que le carboxyméthylchitosane ne pouvait former de billes d'hydrogel que dans une solution aqueuse de $CaCl_2$ [135], Yangchao Luo et al., 2013, ont montré que la variation de la concentration d'éthanol influence la forme des billes d'hydrogel [136]. Cette étude a été la boussole qui a orienté notre démarche dans la fabrication de nos hydrogels sphériques.

Afin d'obtenir des billes d'hydrogel de taille uniforme, la technique d'extrusion électrostatique peut être utilisée [138]. Une technique récente qui permet d'obtenir des microbilles grâce à une force électrostatique appliquée à l'extrémité de la buse métallique par laquelle les gouttelettes de polymère chargées sont extrudées (figure 2.11).

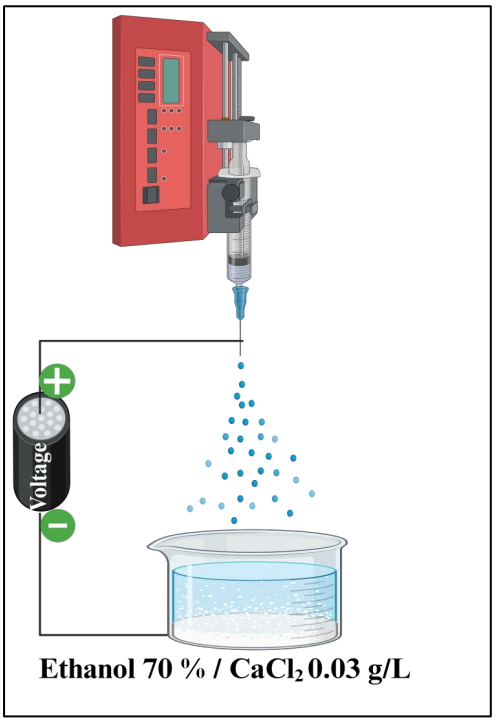

Figure 2.11 Montage d'extrusion électrostatique des solutions de polymère et de réticulation d'hydrogels sphériques dans un bain d'éthanol à 70 % contenant du $CaCl_2$ comme agent de réticulation physique [106]

Elle est avantageuse par rapport aux autres méthodes d'extrusion car les microbilles obtenues sont plus petites et par conséquent possèdent une surface spécifique plus grande ce qui est un point important pour leur utilisation commet adsorbant pour la décontamination des eaux. La taille des billes d'hydrogel obtenues par cette méthode

dépend de la force électrostatique appliquée, du débit d'extrusion appliqué par la pompe, du diamètre du capillaire métallique, de la viscosité de la solution de polymère qui est liée au poids moléculaire et de la concentration des solutions de polymère [139]. Par exemple, Vérica Manojlovic et al., 2008, ont développé des microbilles sphériques d'alginate de taille uniforme (450 ± 20 μm) grâce à cette technique en appliquant une tension de 4,5 kV.

La plupart des hydrogels à base de carboxyméthylchitosane développés ont été orientés principalement vers des applications biomédicales et très peu d'études rapportent leur investigation comme adsorbant pour l'élimination de polluants. À notre connaissance, aucune étude ne mentionne la fabrication d'hydrogels à base de ce biopolymère encore moins ceux réticulés par la génipine pour l'élimination les micropolluants émergents comme les résidus de produits pharmaceutiques. Le tableau 2.8 présente quelques hydrogels à base de carboxyméthylchitosane utilisés pour éliminer les polluants organiques de l'eau.

Tableau 2.8 Hydrogels à base de carboxyméthylchitosane utilisés pour l'élimination de molécules organiques dans les milieux aqueux

Hydrogels	Agents de réticulation	Polluants	Capacité d'adsorption	Réf
O-CM-chitosan	Isothiocyanate	Bleu de méthylène	434.8 mg/g	[140]
CMCS/PVA	$CaCl_2$	Bleu acide 93 (AB)	1666.67 mg/g	[141]
Hydrogel Fe_3O_4 / CMCS -co-p (acide acrylique-acide itaconique)		Vert malachite	608.8 mg/g	[142]
Hydrogel composite d'alginate de sodium/CMCS		Bleu de méthylène	1010 mg/g	[143]
Chitosane/CMCS-PEG		Rouge congo	1053.88 mg/g	[144]
CMCS-PA	-	Orange de méthyle	13.62 mg/g	[145]
SA/CMCS	HCl 0.1 N	Tétracycline ciprofloxacine	51 ± 2% 95 2%	[146]

2.2.8 Les cryogels

L'auto-assemblage, la copolymérisation et la polymérisation (polymérisation par condensation, polymérisation par irradiation et la polymérisation radicalaire) sont des

méthodes qui peuvent être utilisées pour élaborer des gels. Il s'agit de la polymérisation en masse, en suspension et en solution. La polymérisation en solution est plus intéressante car elle est rapide, peu onéreuse et peut facilement être transposée de l'échelle de laboratoire à l'échelle industrielle [147]. Cette méthode nécessite la présence, en solution, de monomères habituellement polaires et, dans certains cas, d'un initiateur de polymérisation et d'un ou plusieurs agents de réticulation. La polymérisation radicalaire fait partie de tels procédés fréquemment utilisé pour la formation des gels [147,148]. Elle nécessite l'utilisation d'un couple initiateur formé d'un système redox et d'un agent réducteur pour la première étape de la réaction. Les solvants non toxiques, tels que l'eau, sont habituellement utilisés pour diluer les réactifs et jouent également le rôle de dissipateurs thermiques. La polymérisation radicalaire est une réaction qui peut être réalisée à des températures supérieures à zéro, où on obtient un hydrogel, ou à des températures inférieures à zéro, où on obtient un cryogel.

2.2.8.1 Fabrication des cryogels

Les cryogels sont des matériaux macroporeux obtenus par la méthode de cryopolymérisation. C'est une technique simple qui repose sur la formation de cristaux de glace et la cryoconcentration du précurseur dans des espaces confinés non gelés, où se déroule la polymérisation (figure 2.12) [149]. Ce processus s'accompagne de la réticulation (Chimique, physique ou hybride) des chaînes polymères pour former un réseau polymère macroporeux. La réticulation des chaînes polymères a un effet direct sur le comportement hydrophile des cryogels. On note que le gonflement des cryogels hydrophiles est bien plus rapide que celui des hydrogels de même type. Cela est dû en partie à la taille des pores, plus grande dans les cryogels que dans les hydrogels. La force osmotique favorisent une diffusion rapide de l'eau à travers les macropores interconnectés dans le réseau de polymère et contribue à l'expansion du réseau polymère des cryogels [150]. Plus le degré de réticulation est important moins l'expansion du réseau polymère pourra être observé ce qui en général a un impact sur la capacité d'adsorption du cryogel [119]. Plusieurs facteurs permettent de moduler les propriétés et la structure des cryogels. Il s'agit de la composition et de la concentration du précurseur (monomères, polymères, agents de réticulation et initiateurs de réaction), qui reste non gelé pendant la

phase de cryogélation. La quantité d'eau, la force ionique, le pH, le gradient de température, la vitesse de congélation et de décongélation et le temps influencent également les propriétés structurales des cryogels [151].

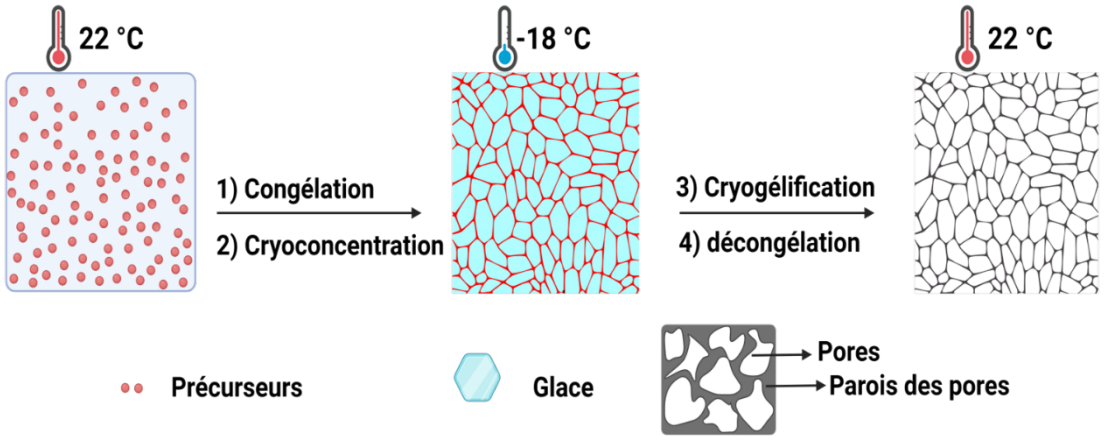

Figure 2.12 Processus de formation des cryogels [152]

2.2.8.2 Formation des pores dans le réseau de polymère

La vitesse de congélation influence la formation des cristaux de glace et, par conséquent, la macroporosité de la structure des cryogels. Cela a un impact direct sur la morphologie de surface des cryogels. La quantité d'eau dans le mélange joue également un rôle prépondérant. Une quantité supérieure à celle du précurseur, au cours de l'étape de congélation, donne lieu à des cristaux de glace plus volumineux, avec des espaces de cryoconcentration plus restreints. La fonte des cristaux de glace laisse derrière elle un réseau interconnecté de pores volumineux (10-300 µm) et les cryogels obtenus sont macroporeux. Les cristaux de glace jouent donc le rôle de porogènes naturels dans la fabrication des cryogels macroporeux [148]. La cryopolymérisation confère aux cryogels des propriétés remarquables par rapport aux hydrogels classiques. On peut noter une excellente porosité, avec des macropores ouverts et interconnectés, qui présentent une faible résistance à l'écoulement des fluides et favorisent le transfert des solutés, même de grande taille. Ils sont plus résilients à des contraintes mécaniques, sont robustes, flexibles et perméables, d'où leur application dans de nombreux domaines tels que le traitement des eaux et le domaine biomédical, entre autres.

2.2.8.3 Précurseurs des cryogels

Les cryogels peuvent être élaborés à partir de polymères synthétiques, de polymères naturels ou, parfois, de leur combinaison [153,154]. Leur utilisation dans la fabrication des cryogels présente des avantages et des inconvénients. Les cryogels à base de polymères synthétiques comme l'acrylamide et ses dérivés, l'acrylonitrile et l'acide acrylique, entre autres, sont mécaniquement résistants, moins sensibles à la dégradation biotique, présentent une bonne résistance chimique et leur production est facilement reproductible. Ils permettent également d'améliorer le contrôle de la porosité des cryogels. Plusieurs points négatifs liés à l'utilisation de polymères synthétiques dans la fabrication des cryogels sont à prendre en compte selon les applications visées. Ce type de cryogel peut être potentiellement toxique et moins écologique ; il n'est presque pas biodégradable et, pour certains, moins performant pour des applications de dépollution des eaux du fait de la présence modérée de groupes fonctionnels réactifs. Les biopolymères hydrophiles ont permis de fabriquer des cryogels présentant des propriétés mécaniques inférieures à celles des cryogel à base de polymères synthétiques, mais qui ont l'avantage d'être biodégradables, biocompatibles et non toxiques. La présence de groupes fonctionnels réactifs dans la structure des biopolymères constitue un atout pour l'utilisation des cryogels à base de ces polymères dans la décontamination des eaux. Quelques travaux rapportent l'utilisation du carboxyméthylchitosane comme précurseur des cryogels de biopolymères. Pan Wu et al., 2024 ont fabriqué un cryogel de carboxyméthylchitosane /alginate pour une hémostase rapide, Bahar Asadi et al., 2023 ont développé un cryogel biomimétique à base de Carboxyméthylchitosane/gélatine/hydroxyapatite et Yuliya Privar et al., 2019 ont fabriqué un cryogel de N-(2-carboxyéthyl) chitosane chélatés par Cu (II) et Al (III) pour adsorber la ciprofloxacine [94,155,156]. Face aux limites que présentent ces cryogels de biopolymères, plusieurs auteurs ont combiné ces deux types de polymères afin d'obtenir des cryogels hybrides avec des propriétés synergiques [157].

2.2.8.4 Cryogels hybrides

Des cryogels hybrides présentant des propriétés supérieures à celles des cryogels à base de polymères synthétiques et à celles des cryogels à base de biopolymères. La synergie entre la stabilité mécanique et la fonctionnalité obtenue en associant des polymères

naturels et synthétiques pour la fabrication de cryogels hybrides permet d'obtenir des matériaux plus robustes, qui résistent mieux aux cycles successifs d'adsorption/désorption et présentent de meilleures performances d'adsorption [158]. De tels matériaux sont durables et, en modulant les proportions de chaque type de polymère dans le mélange de polymères, les caractéristiques finales peuvent être déplacées d'un côté comme de l'autre [159]. Par exemple, pour obtenir un cryogel hybride présentant une capacité d'adsorption élevée pour le polluant, la proportion de biopolymère peut être augmentée jusqu'à un seuil permettant toutefois de le maintenir mécaniquement stable. Dans la littérature, des nanoparticules d'oxydes métalliques, les zéolites, les charbons actifs ainsi que des molécules organiques modèles pour l'impression de polymères ont été incorporés dans les formulations de préparation des cryogels hybrides afin d'accroître leur performance de décontamination ainsi que leur sélectivité [158].

2.2.8.5 Mécanisme d'adsorption sur les cryogels

Les cryogels peuvent être préparés sous différentes formes à partir d'un moulage dans des contenants où la cryogélation a lieu. Parmi ses formes, on peut citer les monolithes, les billes, les disques et les feuilles, entre autres. Dans les cryogel monolithiques, la macroporosité interconnectée du réseau polymère facilite une circulation et une diffusion optimales des solutés, ce qui fait des cryogels monolithiques des adsorbants prometteurs pour des traitements en continu dans des colonnes à lit fixe. Cette particularité est adéquate pour leur intégration dans la conception d'un système de filtration sur mesure. Les cryogels fonctionnalisés peuvent adsorber les polluants par différents mécanismes physiques et chimiques [158,160] (figure 2.13). De nombreuses études rapportent leur utilisation pour éliminer différents types de polluants en solution aqueuse [161] .

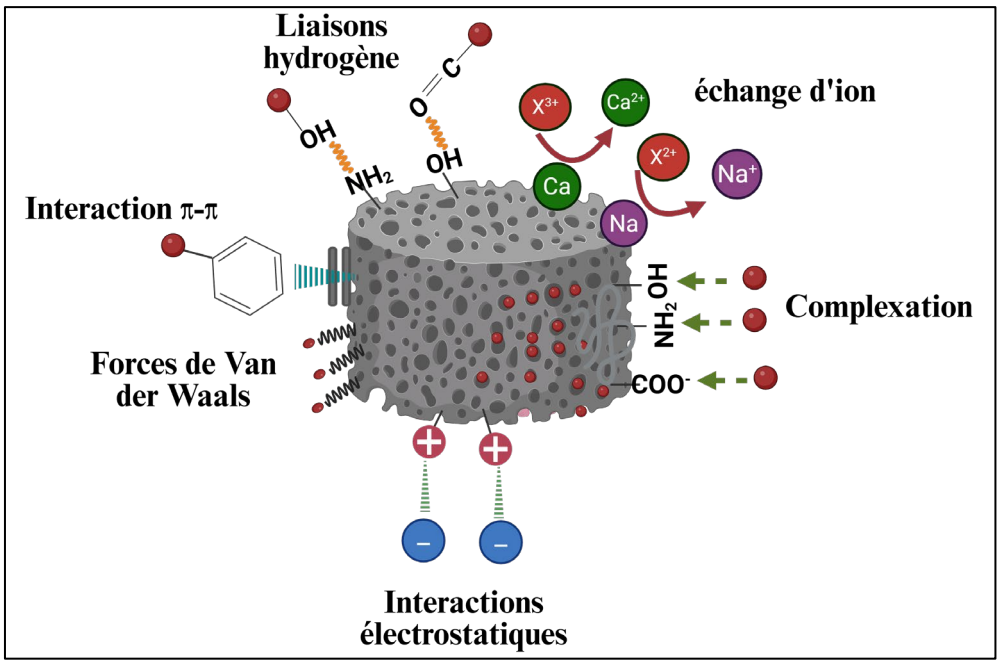

Figure 2.13 Mécanisme d'élimination des polluants par le cryogel fonctionnalisé [162]

2.2.9 Justification du choix des matériaux hydro- et cryogélifiés

Les défis liés à l'utilisation des hydrogels et des cryogels pour le traitement de l'eau, tant à l'échelle pilote qu'à l'échelle industrielle, sont nombreux. Il s'agit de la reproductibilité, de l'absence de sélectivité (adsorption compétitive) dans les solutions aqueuses complexes et du manque de stabilité mécanique, qui affectent négativement l'efficacité d'adsorption, la réutilisabilité et les coûts. Toutefois, il est avantageux de porter son attention sur les hydrogels de biopolymères et les cryogels hybrides monolithiques, car ils constituent des adsorbants prometteurs qui se distinguent des adsorbants classiques sur de nombreux points. Bien qu'ils aient une surface spécifique inférieure à celle des adsorbants commerciaux comme le charbon actif, leur structure poreuse très développée est avantageuse pour une cinétique d'adsorption rapide. De plus, lorsqu'ils sont correctement fonctionnalisés, la forte densité des sites de liaison accroît significativement la capacité d'adsorption des polluants. L'impression moléculaire, l'ajustement de la porosité par optimisation des proportions des précurseurs, ainsi que le degré de réticulation permettent également d'augmenter les performances d'adsorption et constituent des moyens simples d'améliorer l'affinité de ces adsorbants pour des polluants spécifiques. Cela permet

d'accroître leur sélectivité, un point qui fait énormément défaut aux charbons actifs, par exemple. L'utilisation des polyélectrolytes, tels que le carboxyméthylchitosane et le poly(acrylate) de sodium, comme précurseurs de ces matériaux est fondée sur la nature ionique des antidépresseurs ciblés dans cette étude, afin d'optimiser les interactions électrostatiques avec les sites de sorption. Il a été important pour nous, dans notre démarche, de réaliser des essais d'adsorption en cuvée et de relever le matériau, qui n'a pas subi d'effondrement significatif de sa structure tridimensionnelle, afin de le tester en mode continu, facilement transposable à l'échelle pilote. Il faut noter que très peu d'études dans la littérature font état de l'utilisation de matériaux hydrogélifiés et cryogélifiés pour la décontamination de micropolluants émergents en solution aqueuse, et quasiment aucune ne s'est intéressée au cas spécifique des antidépresseurs, qui constituent pourtant un risque réel pour l'équilibre de l'écosystème aquatique.

2.3 Références

[1] A. Lajeunesse, C. Gagnon, S. Sauvé, Determination of Basic Antidepressants and Their N-Desmethyl Metabolites in Raw Sewage and Wastewater Using Solid-Phase Extraction and Liquid Chromatography−Tandem Mass Spectrometry, Anal Chem 80 (2008) 5325–5333. https://doi.org/10.1021/AC800162Q.

[2] T. Oskotsky, I. Marić, A. Tang, B. Oskotsky, R.J. Wong, N. Aghaeepour, M. Sirota, D.K. Stevenson, Mortality Risk Among Patients With COVID-19 Prescribed Selective Serotonin Reuptake Inhibitor Antidepressants, JAMA Netw Open 4 (2021) e2133090–e2133090. https://doi.org/10.1001/JAMANETWORKOPEN.2021.33090.

[3] E. Yavuz-Guzel, A. Atasoy, İ.E. Gören, N. Daglioglu, Impact of COVID- 19 pandemic on antidepressants consumptions by wastewater analysis in Turkey, Science of the Total Environment 838 (2022). https://doi.org/10.1016/j.scitotenv.2022.155916.

[4] A. Puga, M.M. Moreira, M.A. Sanromán, M.M. Pazos, C. Delerue-Matos, Antidepressants and COVID-19: Increased use, occurrence in water and effects

and consequences on aquatic environment. A review, Science of the Total Environment 953 (2024). https://doi.org/10.1016/j.scitotenv.2024.175993.

[5] N. Diaz-Camal, J.D. Cardoso-Vera, H. Islas-Flores, L.M. Gómez-Oliván, A. Mejía-García, Consumption and ocurrence of antidepressants (SSRIs) in pre- and post-COVID-19 pandemic, their environmental impact and innovative removal methods: A review, Science of the Total Environment 829 (2022). https://doi.org/10.1016/j.scitotenv.2022.154656.

[6] R.A. Mole, B.W. Brooks, Global scanning of selective serotonin reuptake inhibitors: occurrence, wastewater treatment and hazards in aquatic systems, Environmental Pollution 250 (2019) 1019–1031. https://doi.org/10.1016/J.ENVPOL.2019.04.118.

[7] T. Kosjek, E. Heath, Tools for evaluating selective serotonin re-uptake inhibitor residues as environmental contaminants, TrAC Trends in Analytical Chemistry 29 (2010) 832–847. https://doi.org/10.1016/J.TRAC.2010.04.012.

[8] R. Brauer, B. Alfageh, J.E. Blais, E.W. Chan, C.S.L. Chui, J.F. Hayes, K.K.C. Man, W.C.Y. Lau, V.K.C. Yan, M.Y. Beykloo, Z. Wang, L. Wei, I.C.K. Wong, Psychotropic medicine consumption in 65 countries and regions, 2008–19: a longitudinal study, Lancet Psychiatry 8 (2021) 1071–1082. https://doi.org/10.1016/S2215-0366(21)00292-3.

[9] V. Calisto, V.I. Esteves, Psychiatric pharmaceuticals in the environment, Chemosphere 77 (2009) 1257–1274. https://doi.org/10.1016/J.CHEMOSPHERE.2009.09.021.

[10] M.M. Schultz, E.T. Furlong, D.W. Kolpin, S.L. Werner, H.L. Schoenfuss, L.B. Barber, V.S. Blazer, D.O. Norris, A.M. Vajda, Antidepressant Pharmaceuticals in Two U.S. Effluent-Impacted Streams: Occurrence and Fate in Water and Sediment, and Selective Uptake in Fish Neural Tissue, Environ Sci Technol 44 (2010) 1918–1925. https://doi.org/10.1021/ES9022706.

[11] P. Nagarnaik, A. Batt, B. Boulanger, Source characterization of nervous system active pharmaceutical ingredients in healthcare facility wastewaters, J Environ Manage 92 (2011) 872–877. https://doi.org/10.1016/J.JENVMAN.2010.10.058.

[12] K.H. Langford, K. V. Thomas, Determination of pharmaceutical compounds in hospital effluents and their contribution to wastewater treatment works, Environ Int 35 (2009) 766–770. https://doi.org/10.1016/J.ENVINT.2009.02.007.

[13] J. Fick, H. Söderström, R.H. Lindberg, C. Phan, M. Tysklind, D.G.J. Larsson, Contamination of surface, ground, and drinking water from pharmaceutical production, Environ Toxicol Chem 28 (2009) 2522–2527. https://doi.org/10.1897/09-073.1.

[14] R.R. Singh, L.F. Angeles, D.M. Butryn, J.W. Metch, E. Garner, P.J. Vikesland, D.S. Aga, Towards a harmonized method for the global reconnaissance of multi-class antimicrobials and other pharmaceuticals in wastewater and receiving surface waters, Environ Int 124 (2019) 361–369. https://doi.org/10.1016/J.ENVINT.2019.01.025.

[15] W. Wang, J. Zhang, M. Hu, X. Liu, T. Sun, H. Zhang, Antidepressants in wastewater treatment plants: Occurrence, transformation and acute toxicity evaluation, Science of The Total Environment 903 (2023) 166120. https://doi.org/10.1016/J.SCITOTENV.2023.166120.

[16] D.W. Kolpin, E.T. Furlong, M.T. Meyer, E.M. Thurman, S.D. Zaugg, L.B. Barber, H.T. Buxton, Pharmaceuticals, Hormones, and Other Organic Wastewater Contaminants in U.S. Streams, 1999−2000: A National Reconnaissance, Environ Sci Technol 36 (2002) 1202–1211. https://doi.org/10.1021/ES011055J.

[17] C.D. Metcalfe, X.S. Miao, B.G. Koenig, J. Struger, Distribution of acidic and neutral drugs in surface waters near sewage treatment plants in the lower Great Lakes, Canada, Environ Toxicol Chem 22 (2003) 2881–2889. https://doi.org/10.1897/02-627.

[18] S. Mompelat, B. Le Bot, O. Thomas, Occurrence and fate of pharmaceutical products and by-products, from resource to drinking water, Environ Int 35 (2009) 803–814. https://doi.org/10.1016/J.ENVINT.2008.10.008.

[19] M.J. Benotti, R.A. Trenholm, B.J. Vanderford, J.C. Holady, B.D. Stanford, S.A. Snyder, Pharmaceuticals and Endocrine Disrupting Compounds in U.S. Drinking Water, Environ Sci Technol 43 (2008) 597–603. https://doi.org/10.1021/ES801845A.

[20] K. Demeestere, M. Petrović, M. Gros, J. Dewulf, H. Van Langenhove, D. Barceló, Trace analysis of antidepressants in environmental waters by molecularly imprinted polymer-based solid-phase extraction followed by ultra-performance liquid chromatography coupled to triple quadrupole mass spectrometry, Analytical and Bioanalytical Chemistry 2009 396:2 396 (2009) 825–837. https://doi.org/10.1007/S00216-009-3270-2.

[21] V.K.H. Barclay, N.L. Tyrefors, I.M. Johansson, C.E. Pettersson, Trace analysis of fluoxetine and its metabolite norfluoxetine. Part I: Development of a chiral liquid chromatography–tandem mass spectrometry method for wastewater samples, J Chromatogr A 1218 (2011) 5587–5596. https://doi.org/10.1016/J.CHROMA.2011.06.024.

[22] C. Miège, J.M. Choubert, L. Ribeiro, M. Eusèbe, M. Coquery, Fate of pharmaceuticals and personal care products in wastewater treatment plants – Conception of a database and first results, Environmental Pollution 157 (2009) 1721–1726. https://doi.org/10.1016/J.ENVPOL.2008.11.045.

[23] D. Buntner, S. Zabczynski, K. Miksch, B. Roig, Chapter 5. Performance of conventional treatment processes of the most resistant PPs, (2010) 87–114. https://doi.org/10.34894/VQ1DJA.

[24] P.H. Roberts, K. V. Thomas, The occurrence of selected pharmaceuticals in wastewater effluent and surface waters of the lower Tyne catchment, Science of

The Total Environment 356 (2006) 143–153. https://doi.org/10.1016/J.SCITOTENV.2005.04.031.

[25] L.J.G. Silva, C.M. Lino, L. Meisel, D. Barceló, A. Pena, Ecopharmacovigilance, Handbook of Environmental Chemistry 20 (2011) 213–241. https://doi.org/10.1007/698_2011_128.

[26] A. Lajeunesse, S.A. Smyth, K. Barclay, S. Sauvé, C. Gagnon, Distribution of antidepressant residues in wastewater and biosolids following different treatment processes by municipal wastewater treatment plants in Canada, Water Res 46 (2012) 5600–5612. https://doi.org/10.1016/j.watres.2012.07.042.

[27] A. Lajeunesse, M. Blais, B. Barbeau, S. Sauvé, C. Gagnon, Ozone oxidation of antidepressants in wastewater -Treatment evaluation and characterization of new by-products by LC-QToFMS, Chem Cent J 7 (2013) 1–11. https://doi.org/10.1186/1752-153X-7-15/FIGURES/7.

[28] J.W. Kwon, K.L. Armbrust, Aqueous Solubility, n-Octanol–Water Partition Coefficient, and Sorption of Five Selective Serotonin Reuptake Inhibitors to Sediments and Soils, Bulletin of Environmental Contamination and Toxicology 2008 81:2 81 (2008) 128–135. https://doi.org/10.1007/S00128-008-9401-1.

[29] C.D. Metcalfe, S. Chu, C. Judt, H. Li, K.D. Oakes, M.R. Servos, D.M. Andrews, Antidepressants and their metabolites in municipal wastewater, and downstream exposure in an urban watershed, Environ Toxicol Chem 29 (2010) 79–89. https://doi.org/10.1002/ETC.27.

[30] S. Mompelat, B. Le Bot, O. Thomas, Occurrence and fate of pharmaceutical products and by-products, from resource to drinking water, Environ Int 35 (2009) 803–814. https://doi.org/10.1016/J.ENVINT.2008.10.008.

[31] L.P. de Souza, F.O. Sanches-Neto, G.M.Y. Junior, B. Ramos, A.M. Lastre-Acosta, V.H. Carvalho-Silva, A.C.S.C. Teixeira, Photochemical environmental persistence of venlafaxine in an urban water reservoir: A combined experimental

and computational investigation, Process Safety and Environmental Protection 166 (2022) 478–490. https://doi.org/10.1016/J.PSEP.2022.08.049.

[32] L.J.G. Silva, C.M. Lino, L. Meisel, D. Barceló, A. Pena, Ecopharmacovigilance, Handbook of Environmental Chemistry 20 (2011) 213–241. https://doi.org/10.1007/698_2011_128.

[33] L.H.M.L.M. Santos, A.N. Araújo, A. Fachini, A. Pena, C. Delerue-Matos, M.C.B.S.M. Montenegro, Ecotoxicological aspects related to the presence of pharmaceuticals in the aquatic environment, J Hazard Mater 175 (2010) 45–95. https://doi.org/10.1016/J.JHAZMAT.2009.10.100.

[34] P. Sehonova, Z. Svobodova, P. Dolezelova, P. Vosmerova, C. Faggio, Effects of waterborne antidepressants on non-target animals living in the aquatic environment: A review, Science of The Total Environment 631–632 (2018) 789–794. https://doi.org/10.1016/J.SCITOTENV.2018.03.076.

[35] A.M. Christensen, S. Faaborg-Andersen, F. Ingerslev, A. Baun, Mixture and single-substance toxicity of selective serotonin reuptake inhibitors toward algae and crustaceans, Environ Toxicol Chem 26 (2007) 85–91. https://doi.org/10.1897/06-219R.1.

[36] C.G. Daughton, I.S. Ruhoy, Green pharmacy and pharmEcovigilance: prescribing and the planet, Expert Rev Clin Pharmacol 4 (2011) 211–232. https://doi.org/10.1586/ECP.11.6.

[37] E.S. McCallum, E. Krutzelmann, T. Brodin, J. Fick, A. Sundelin, S. Balshine, Exposure to wastewater effluent affects fish behaviour and tissue-specific uptake of pharmaceuticals, Science of The Total Environment 605–606 (2017) 578–588. https://doi.org/10.1016/J.SCITOTENV.2017.06.073.

[38] P. Sehonova, N. Hodkovicova, M. Urbanova, S. Örn, J. Blahova, Z. Svobodova, M. Faldyna, P. Chloupek, K. Briedikova, G. Carlsson, Effects of antidepressants with different modes of action on early life stages of fish and amphibians,

Environmental Pollution 254 (2019). https://doi.org/10.1016/j.envpol.2019.112999.

[39] D. Correia, I. Domingues, M. Faria, M. Oliveira, Effects of fluoxetine on fish: What do we know and where should we focus our efforts in the future?, Science of The Total Environment 857 (2023) 159486. https://doi.org/10.1016/J.SCITOTENV.2022.159486.

[40] M. Mantovani, S. Rossi, E. Ficara, E. Collina, F. Marazzi, M. Lasagni, V. Mezzanotte, Removal of pharmaceutical compounds from the liquid phase of anaerobic sludge in a pilot-scale high-rate algae-bacteria pond, Science of The Total Environment 908 (2024) 167881. https://doi.org/10.1016/J.SCITOTENV.2023.167881.

[41] Z. Xie, X. Wang, Y. Gan, H. Cheng, S. Fan, X. Li, J. Tang, Ecotoxicological effects of the antidepressant fluoxetine and its removal by the typical freshwater microalgae Chlorella pyrenoidosa, Ecotoxicol Environ Saf 244 (2022) 114045. https://doi.org/10.1016/J.ECOENV.2022.114045.

[42] Pratishtha Khurana, R.K. Das, S. Kaur Brar, From prescription to pollution: environmental behavior and breakdown of fluoxetine, Environ Sci (Camb) (2025). https://doi.org/10.1039/D5EW00636H.

[43] T. Palma, J. Valentine, V. Gomes, M. Faleiro, M. Costa, Batch Studies on the Biodegradation Potential of Paracetamol, Fluoxetine and 17α-Ethinylestradiol by the Micrococcus yunnanensis Strain TJPT4 Recovered from Marine Organisms, Water (Switzerland) 14 (2022) 3365. https://doi.org/10.3390/W14213365/S1.

[44] M.F. Khan, C.D. Murphy, Bacterial degradation of the anti-depressant drug fluoxetine produces trifluoroacetic acid and fluoride ion, Applied Microbiology and Biotechnology 2021 105:24 105 (2021) 9359–9369. https://doi.org/10.1007/S00253-021-11675-3.

[45] A.I. Rodarte-Morales, G. Feijoo, M.T. Moreira, J.M. Lema, Degradation of selected pharmaceutical and personal care products (PPCPs) by white-rot fungi, World Journal of Microbiology and Biotechnology 2011 27:8 27 (2011) 1839–1846. https://doi.org/10.1007/S11274-010-0642-X.

[46] A.D.M. Silva, J. Sousa, M. Hultberg, S.A. Figueiredo, O.M. Freitas, C. Delerue-Matos, Fluoxetine Removal from Aqueous Solutions Using a Lignocellulosic Substrate Colonized by the White-Rot Fungus Pleurotus ostreatus, Int J Environ Res Public Health 19 (2022) 2672. https://doi.org/10.3390/IJERPH19052672/S1.

[47] R.C. Racovita, M.D. Ciuca, R.C. Racovita, M.D. Ciuca, Wastewater Treatment Approaches for the Removal of Antidepressant Residues, Wastewater Treatment and Sludge Management Systems - The Gutter-to-Good Approaches (2024). https://doi.org/10.5772/INTECHOPEN.1004333.

[48] C. Pan, F. Zhu, M. Wu, L. Jiang, X. Zhao, M. Yang, Degradation and toxicity of the antidepressant fluoxetine in an aqueous system by UV irradiation, Chemosphere 287 (2022) 132434. https://doi.org/10.1016/J.CHEMOSPHERE.2021.132434.

[49] K. Köse, D. Yalçın Kehribar, V. Goodarzi, L. Uzun, Strategies for the detection, removal and elimination of antidepressants, Int J Environ Anal Chem 104 (2024) 323–354. https://doi.org/10.1080/03067319.2021.2019726.

[50] J.W. Choi, J.K. Bediako, Y. Zhao, S. Lin, A.K. Sarkar, M. Han, M.H. Song, C.W. Cho, Y.S. Yun, Adsorptive removal of cationic tricyclic antidepressants using cation-exchange resin, Environmental Science and Pollution Research 27 (2020) 24760–24771. https://doi.org/10.1007/S11356-019-06549-1/FIGURES/6.

[51] Y. Zhao, G. Yu, S. Chen, S. Zhang, B. Wang, J. Huang, S. Deng, Y. Wang, Ozonation of antidepressant fluoxetine and its metabolite product norfluoxetine: Kinetics, intermediates and toxicity, Chemical Engineering Journal 316 (2017) 951–963. https://doi.org/10.1016/J.CEJ.2017.02.032.

[52] D. Fotiou, C. Lykos, I. Konstantinou, Photocatalytic removal of the antidepressant fluoxetine from aqueous media using TiO2 P25 and g-C3N4 catalysts, J Environ Chem Eng 12 (2024) 111677. https://doi.org/10.1016/J.JECE.2023.111677.

[53] A. Aghaeinejad-Meybodi, A. Ebadi, S. Shafiei, A.R. Khataee, M. Rostampour, Modeling and optimization of antidepressant drug Fluoxetine removal in aqueous media by ozone/H2O2 process: Comparison of central composite design and artificial neural network approaches, J Taiwan Inst Chem Eng 48 (2015) 40–48. https://doi.org/10.1016/J.JTICE.2014.10.022.

[54] Y. Zhao, G. Yu, S. Chen, S. Zhang, B. Wang, J. Huang, S. Deng, Y. Wang, Ozonation of antidepressant fluoxetine and its metabolite product norfluoxetine: Kinetics, intermediates and toxicity, Chemical Engineering Journal 316 (2017) 951–963. https://doi.org/10.1016/J.CEJ.2017.02.032.

[55] C. Salazar, C. Ridruejo, E. Brillas, J. Yáñez, H.D. Mansilla, I. Sirés, Abatement of the fluorinated antidepressant fluoxetine (Prozac) and its reaction by-products by electrochemical advanced methods, Appl Catal B 203 (2017) 189–198. https://doi.org/10.1016/J.APCATB.2016.10.026.

[56] Z. Ye, J.A. Padilla, E. Xuriguera, J.L. Beltran, F. Alcaide, E. Brillas, I. Sirés, A Highly Stable Metal–Organic Framework-Engineered FeS2/C Nanocatalyst for Heterogeneous Electro-Fenton Treatment: Validation in Wastewater at Mild pH, Environ Sci Technol 54 (2020) 4664–4674. https://doi.org/10.1021/ACS.EST.9B07604.

[57] T. Dalbosco, J.S. Cadore, A. Pezzini, N.M.G. Bandeira, G.O.M. Giubel, T. Lazzari, L.D. Barbizan, D.T. Novello, V.B. Brião, Removal of fluoxetine from water by nanofiltration and reverse osmosis, Revista Ambiente & Água 18 (2023) e2885. https://doi.org/10.4136/AMBI-AGUA.2885.

[58] G. Jaria, V. Calisto, M.V. Gil, M. Otero, V.I. Esteves, Removal of fluoxetine from water by adsorbent materials produced from paper mill sludge, J Colloid Interface Sci 448 (2015) 32–40. https://doi.org/10.1016/J.JCIS.2015.02.002.

[59] M.J. Fernandes, M.M. Moreira, P. Paíga, D. Dias, M. Bernardo, M. Carvalho, N. Lapa, I. Fonseca, S. Morais, S. Figueiredo, C. Delerue-Matos, Evaluation of the adsorption potential of biochars prepared from forest and agri-food wastes for the removal of fluoxetine, Bioresour Technol 292 (2019) 121973. https://doi.org/10.1016/J.BIORTECH.2019.121973.

[60] S. Escudero-Curiel, M. Pazos, A. Sanromán, Sustainable regeneration of a honeycomb carbon aerogel used as a high-capacity adsorbent for Fluoxetine removal, J Mol Liq 357 (2022) 119079. https://doi.org/10.1016/J.MOLLIQ.2022.119079.

[61] B. Silva, M. Martins, M. Rosca, V. Rocha, A. Lago, I.C. Neves, T. Tavares, Waste-based biosorbents as cost-effective alternatives to commercial adsorbents for the retention of fluoxetine from water, Sep Purif Technol 235 (2020) 116139. https://doi.org/10.1016/J.SEPPUR.2019.116139.

[62] A. Camiré, B. Chabot, A. Lajeunesse, Sorption Capacities of a Lignin-Based Electrospun Nanofibrous Material for Pharmaceutical Residues Remediation in Water, Sorption in 2020s (2019). https://doi.org/10.5772/INTECHOPEN.88621.

[63] J. Narayanan, J.G. Hernández, I.I. Padilla-Martínez, P. Thangarasu, S.E. Santos Garay, C.B. Palacios Cabrera, A.J. Santiago Cuevas, Geometry influenced adsorption of fluoxetine over the surface of RuFeO3 and CeFeO3 nanoparticles: Kinetics and thermodynamic studies, Ceram Int 47 (2021) 20544–20561. https://doi.org/10.1016/J.CERAMINT.2021.04.064.

[64] C. Piccirillo, I.S. Moreira, R.M. Novais, A.J.S. Fernandes, R.C. Pullar, P.M.L. Castro, Biphasic apatite-carbon materials derived from pyrolysed fish bones for effective adsorption of persistent pollutants and heavy metals, J Environ Chem Eng 5 (2017) 4884–4894. https://doi.org/10.1016/J.JECE.2017.09.010.

[65] A. Camiré, J. Espinasse, B. Chabot, A. Lajeunesse, Development of electrospun lignin nanofibers for the adsorption of pharmaceutical contaminants in wastewater,

Environmental Science and Pollution Research 27 (2020) 3560–3573. https://doi.org/10.1007/s11356-018-3333-z.

[66] S. Escudero-Curiel, U. Penelas, M.Á. Sanromán, M. Pazos, An approach towards Zero-Waste wastewater technology: Fluoxetine adsorption on biochar and removal by the sulfate radical, Chemosphere 268 (2021) 129318. https://doi.org/10.1016/J.CHEMOSPHERE.2020.129318.

[67] H.H. Farghal, M. Nebsen, M.M.H. El-Sayed, Eco-friendly Biopolymer/Activated Charcoal Magnetic Nanocomposites with Enhanced Stability and Adsorption Properties for Water Treatment Applications, J Polym Environ 31 (2023) 5338–5354. https://doi.org/10.1007/S10924-023-02959-Y/METRICS.

[68] S. Escudero-Curiel, M. Pazos, A. Sanromán, Facile one-step synthesis of a versatile nitrogen-doped hydrochar from olive oil production waste, “alperujo”, for removing pharmaceuticals from wastewater, Environmental Pollution 330 (2023) 121751. https://doi.org/10.1016/J.ENVPOL.2023.121751.

[69] Z. Qian, X. Li, G. Yan, X. Chen, M.S. Sajab, G. Ding, W.N.L. Wan Jusoh, Sodium Alginate/Carboxymethyl Chitosan Hydrogel Microbeads for Antibiotic Adsorption in Single and Binary Systems, Gels 2025, Vol. 11, Page 646 11 (2025) 646. https://doi.org/10.3390/GELS11080646.

[70] W.J. Weber, J.H. Edward Smith, Simulation and design models for adsorption processes, 1987.

[71] M.A. Hubbe, Insisting upon Meaningful Results from Adsorption Experiments, Separation and Purification Reviews 51 (2022) 212–225. https://doi.org/10.1080/15422119.2021.1888299.

[72] B.S. Rathi, P.S. Kumar, Application of adsorption process for effective removal of emerging contaminants from water and wastewater, Environmental Pollution 280 (2021) 116995. https://doi.org/10.1016/J.ENVPOL.2021.116995.

[73] A. Puga, M.M. Moreira, M. Pazos, S.A. Figueiredo, M.Á. Sanromán, C. Delerue-Matos, E. Rosales, Continuous adsorption studies of pharmaceuticals in multicomponent mixtures by agroforestry biochar, J Environ Chem Eng 10 (2022) 106977. https://doi.org/10.1016/J.JECE.2021.106977.

[74] H. Patel, Comparison of batch and fixed bed column adsorption: a critical review, International Journal of Environmental Science and Technology (2021). https://doi.org/10.1007/s13762-021-03492-y.

[75] W.J. Weber, M. Asce, Evolution of A Technology 3, J. Environ. Eng 110 (1984) 899–917.

[76] H.N. Tran, E.C. Lima, R.S. Juang, J.C. Bollinger, H.P. Chao, Thermodynamic parameters of liquid–phase adsorption process calculated from different equilibrium constants related to adsorption isotherms: A comparison study, J Environ Chem Eng 9 (2021) 106674. https://doi.org/10.1016/J.JECE.2021.106674.

[77] N. Ayawei, N. Ebelegi, D. Wankasi, Modelling and Interpretation of Adsorption Isotherms, (2017). https://doi.org/10.1155/2017/3039817.

[78] I. Langmuir, The Constitution and Fundamental Properties of Solids and Liquids. PART I. SOLIDS., J Am Chem Soc 38 (2002) 2221–2295. https://doi.org/10.1021/JA02268A002.

[79] H.M.F. Freundlich, Freun Over the adsorption in solution, J. Phys. Chem 57 (1906) 1100–1107.

[80] H. Qiu, L. Lv, B.C. Pan, Q.J. Zhang, W.M. Zhang, Q.X. Zhang, Critical review in adsorption kinetic models, Journal of Zhejiang University: Science A 10 (2009) 716–724. https://doi.org/10.1631/jzus.A0820524.

[81] H.N. Tran, S.J. You, A. Hosseini-Bandegharaei, H.P. Chao, Mistakes and inconsistencies regarding adsorption of contaminants from aqueous solutions: A

critical review, Water Res 120 (2017) 88–116. https://doi.org/10.1016/j.watres.2017.04.014.

[82] J. Wang, X. Guo, Rethinking of the intraparticle diffusion adsorption kinetics model: Interpretation, solving methods and applications, Chemosphere 309 (2022). https://doi.org/10.1016/j.chemosphere.2022.136732.

[83] X. Zhou, X. Zhou, THE UNIT PROBLEM IN THE THERMODYNAMIC CALCULATION OF ADSORPTION USING THE LANGMUIR EQUATION, Chem Eng Commun 201 (2014) 1459–1467. https://doi.org/10.1080/00986445.2013.818541.

[84] X. Zhou, X. Yu, J. Hao, H. Liu, Correction to the thermodynamic calculation using the Langmuir isotherm model by Saeed et al. (2022), J Hazard Mater 435 (2022). https://doi.org/10.1016/j.jhazmat.2022.129014.

[85] H.C. Thomas, Heterogeneous Ion Exchange in a Flowing System, J Am Chem Soc 66 (2002) 1664–1666. https://doi.org/10.1021/JA01238A017.

[86] Y.H. Yoon, J.H. Nelson, Application of Gas Adsorption Kinetics I. A Theoretical Model for Respirator Cartridge Service Life, Am Ind Hyg Assoc J 45 (1984) 509–516. https://doi.org/10.1080/15298668491400197.

[87] P. Patel, P. Thareja, Hydrogels differentiated by length scales: A review of biopolymer-based hydrogel preparation methods, characterization techniques, and targeted applications, Eur Polym J 163 (2022) 110935. https://doi.org/10.1016/J.EURPOLYMJ.2021.110935.

[88] Z. Li, L. Yang, H. Cao, Y. Chang, K. Tang, Z. Cao, J. Chang, Y. Cao, W. Wang, M. Gao, C. Liu, D. Liu, H. Zhao, Y. Zhang, M. Li, Carbon materials derived from chitosan/cellulose cryogel-supported zeolite imidazole frameworks for potential supercapacitor application, Carbohydr Polym 175 (2017) 223–230. https://doi.org/10.1016/j.carbpol.2017.07.089.

[89] Z. Shariatinia, Carboxymethyl chitosan: Properties and biomedical applications, Int J Biol Macromol 120 (2018) 1406–1419. https://doi.org/10.1016/J.IJBIOMAC.2018.09.131.

[90] V. Zargar, M. Asghari, A. Dashti, A Review on Chitin and Chitosan Polymers: Structure, Chemistry, Solubility, Derivatives, and Applications, ChemBioEng Reviews 2 (2015) 204–226. https://doi.org/10.1002/CBEN.201400025;WGROUP:STRING:PUBLICATION.

[91] M. Kaya, Y.S. Cakmak, T. Baran, M. Asan-Ozusaglam, A. Mentes, K.O. Tozak, New chitin, chitosan, and O-carboxymethyl chitosan sources from resting eggs of Daphnia longispina (Crustacea); with physicochemical characterization, and antimicrobial and antioxidant activities, Biotechnology and Bioprocess Engineering 19 (2014) 58–69. https://doi.org/10.1007/s12257-013-0488-9.

[92] A. Anitha, V. V. Divya Rani, R. Krishna, V. Sreeja, N. Selvamurugan, S. V. Nair, H. Tamura, R. Jayakumar, Synthesis, characterization, cytotoxicity and antibacterial studies of chitosan, O-carboxymethyl and N,O-carboxymethyl chitosan nanoparticles, Carbohydr Polym 78 (2009) 672–677. https://doi.org/10.1016/j.carbpol.2009.05.028.

[93] P. Mohammadzadeh Pakdel, S.J. Peighambardoust, Review on recent progress in chitosan-based hydrogels for wastewater treatment application, Carbohydr Polym 201 (2018) 264–279. https://doi.org/10.1016/j.carbpol.2018.08.070.

[94] B. Asadi, H. Mirzadeh, N. Olov, A. Samadikuchaksaraei, R. Kheirbakhsh, R. Moradi, S. Amanpour, S. Bagheri-Khoulenjani, Carboxymethyl chitosan/gelatin/hydroxyapatite biomimetic cryogels for bone regeneration, Bioinspired, Biomimetic and Nanobiomaterials 12 (2023) 1–11. https://doi.org/10.1680/JBIBN.22.00020.

[95] H. Karimi-Maleh, A. Ayati, R. Davoodi, B. Tanhaei, F. Karimi, S. Malekmohammadi, Y. Orooji, L. Fu, M. Sillanpää, Recent advances in using of

chitosan-based adsorbents for removal of pharmaceutical contaminants: A review, J Clean Prod 291 (2021). https://doi.org/10.1016/J.JCLEPRO.2021.125880.

[96] D.K. Kowanga, W.N. Nyairo, A review on decontamination of aqueous systems using chitosan-derived adsorbents, Discover Environment 2025 3:1 3 (2025) 237-. https://doi.org/10.1007/S44274-025-00435-Z.

[97] H. Patel, Review on solvent desorption study from exhausted adsorbent, Journal of Saudi Chemical Society 25 (2021) 101302. https://doi.org/10.1016/J.JSCS.2021.101302.

[98] F. Alcalde-Garcia, S. Prasher, S. Kaliaguine, J.R. Tavares, M.-J. Dumont, Desorption Strategies and Reusability of Biopolymeric Adsorbents and Semisynthetic Derivatives in Hydrogel and Hydrogel Composites Used in Adsorption Processes, ACS Engineering Au 3 (2023) 443–460. https://doi.org/10.1021/ACSENGINEERINGAU.3C00022.

[99] N. Wang, W. Xiao, B. Niu, W. Duan, L. Zhou, Y. Zheng, Highly efficient adsorption of fluoroquinolone antibiotics using chitosan derived granular hydrogel with 3D structure, J Mol Liq 281 (2019) 307–314. https://doi.org/10.1016/J.MOLLIQ.2019.02.061.

[100] W. Ma, J. Dai, X. Dai, Z. Da, Y. Yan, Core–shell molecularly imprinted polymers based on magnetic chitosan microspheres for chloramphenicol selective adsorption, Monatshefte Für Chemie - Chemical Monthly 2014 146:3 146 (2014) 465–474. https://doi.org/10.1007/S00706-014-1351-1.

[101] J. Ma, Y. Lei, M.A. Khan, F. Wang, Y. Chu, W. Lei, M. Xia, S. Zhu, Adsorption properties, kinetics & thermodynamics of tetracycline on carboxymethyl-chitosan reformed montmorillonite, Int J Biol Macromol 124 (2019) 557–567. https://doi.org/10.1016/J.IJBIOMAC.2018.11.235.

[102] Y. Liu, R. Liu, M. Li, F. Yu, C. He, Removal of pharmaceuticals by novel magnetic genipin-crosslinked chitosan/graphene oxide-SO3H composite, Carbohydr Polym 220 (2019) 141–148. https://doi.org/10.1016/J.CARBPOL.2019.05.060.

[103] Y. Privar, D. Shashura, A. Pestov, E. Modin, A. Baklykov, D. Marinin, S. Bratskaya, Metal-chelate sorbents based on carboxyalkylchitosans: Ciprofloxacin uptake by Cu (II) and A l(III)-chelated cryogels of N-(2-carboxyethyl) chitosan, Int J Biol Macromol 131 (2019) 806–811. https://doi.org/10.1016/J.IJBIOMAC.2019.03.122.

[104] T.O. Carvalho, A.E.B. Matias, L.R. Braga, S.M. Evangelista, A.G.S. Prado, Calorimetric studies of removal of nonsteroidal anti-inflammatory drugs diclofenac and dipyrone from water, J Therm Anal Calorim 106 (2011) 475–481. https://doi.org/10.1007/S10973-010-1243-5.

[105] A.K. dos S. Pereira, D.T. Reis, K.M. Barbosa, G.N. Scheidt, L.S. da Costa, L.S.S. Santos, Antibacterial effects and ibuprofen release potential using chitosan microspheres loaded with silver nanoparticles, Carbohydr Res 488 (2020) 107891. https://doi.org/10.1016/J.CARRES.2019.107891.

[106] G.R.N. Nkana, A. Lajeunesse, B. Chabot, P. Nguyen-Tri, Design of porous spherical biomaterials from carboxymethyl chitosan for removal of fluoxetine in aqueous medium, J Environ Chem Eng 12 (2024) 112228. https://doi.org/10.1016/J.JECE.2024.112228.

[107] G.R.N. Nkana, B. Chabot, P. Nguyen-Tri, Adsorption of fluoxetine in aqueous environments: Development of macroporous cryogels based on sodium poly(acrylate) and carboxymethyl chitosan, React Funct Polym 205 (2024). https://doi.org/10.1016/j.reactfunctpolym.2024.106069.

[108] X. qi Liu, X. xin Zhao, Y. Liu, T. an Zhang, Review on preparation and adsorption properties of chitosan and chitosan composites, Polymer Bulletin 2021 79:4 79 (2021) 2633–2665. https://doi.org/10.1007/S00289-021-03626-9.

[109] T. Ahamad, M. Naushad, T. Al-Shahrani, N. Al-hokbany, S.M. Alshehri, Preparation of chitosan based magnetic nanocomposite for tetracycline adsorption: Kinetic and thermodynamic studies, Int J Biol Macromol 147 (2020) 258–267. https://doi.org/10.1016/J.IJBIOMAC.2020.01.025.

[110] A. Benettayeb, S. Ghosh, M. Usman, F.Z. Seihoub, I. Sohoo, C.H. Chia, M. Sillanpää, Some Well-Known Alginate and Chitosan Modifications Used in Adsorption: A Review, Water 2022, Vol. 14, Page 1353 14 (2022) 1353. https://doi.org/10.3390/W14091353.

[111] D.C. da Silva Alves, B. Healy, L.A. de A. Pinto, T.R.S. Cadaval, C.B. Breslin, Recent Developments in Chitosan-Based Adsorbents for the Removal of Pollutants from Aqueous Environments, Molecules 2021, Vol. 26, Page 594 26 (2021) 594. https://doi.org/10.3390/MOLECULES26030594.

[112] N. Rahman, M. Nasir, Effective removal of acetaminophen from aqueous solution using Ca (II)-doped chitosan/β-cyclodextrin composite, J Mol Liq 301 (2020) 112454. https://doi.org/10.1016/J.MOLLIQ.2020.112454.

[113] A.G.B. Pereira, F.H.A. Rodrigues, A.T. Paulino, A.F. Martins, A.R. Fajardo, Recent advances on composite hydrogels designed for the remediation of dye-contaminated water and wastewater: A review, J Clean Prod 284 (2021). https://doi.org/10.1016/j.jclepro.2020.124703.

[114] A.S. Hoffman, Hydrogels for biomedical applications, Adv Drug Deliv Rev 64 (2012) 18–23. https://doi.org/10.1016/j.addr.2012.09.010.

[115] F. Ullah, M.B.H. Othman, F. Javed, Z. Ahmad, H.M. Akil, Classification, processing and application of hydrogels: A review, Materials Science and Engineering: C 57 (2015) 414–433. https://doi.org/10.1016/J.MSEC.2015.07.053.

[116] W. Luo, Z. Bai, Y. Zhu, Fast removal of Co(ii) from aqueous solution using porous carboxymethyl chitosan beads and its adsorption mechanism, RSC Adv 8 (2018) 13370–13387. https://doi.org/10.1039/c7ra13064c.

[117] M. V. Badiger, M.E. McNeill, N.B. Graham, Porogens in the preparation of microporous hydrogels based on poly(ethylene oxides), Biomaterials 14 (1993) 1059–1063. https://doi.org/10.1016/0142-9612(93)90206-H.

[118] M. Khan, I.M.C. Lo, A holistic review of hydrogel applications in the adsorptive removal of aqueous pollutants: Recent progress, challenges, and perspectives, Water Res 106 (2016) 259–271. https://doi.org/10.1016/j.watres.2016.10.008.

[119] W.E. Hennink, C.F. van Nostrum, Novel crosslinking methods to design hydrogels, Adv Drug Deliv Rev 64 (2012) 223–236. https://doi.org/10.1016/J.ADDR.2012.09.009.

[120] A. Oryan, A. Kamali, A. Moshiri, H. Baharvand, H. Daemi, Chemical crosslinking of biopolymeric scaffolds: Current knowledge and future directions of crosslinked engineered bone scaffolds, Int J Biol Macromol 107 (2018) 678–688. https://doi.org/10.1016/J.IJBIOMAC.2017.08.184.

[121] M.M. Bhuyan, J.H. Jeong, Preparation of Hydrogel by Crosslinking and Multi-Dimensional Applications, Gels 2025, Vol. 11, Page 896 11 (2025) 896. https://doi.org/10.3390/GELS11110896.

[122] A. Fiamingo, S.P. Campana-Filho, Structure, morphology and properties of genipin-crosslinked carboxymethylchitosan porous membranes, Carbohydr Polym 143 (2016) 155–163. https://doi.org/10.1016/j.carbpol.2016.02.016.

[123] F. Yin, J. Liu, Research and application progress of Gardenia jasminoides, Chin Herb Med 10 (2018) 362–370. https://doi.org/10.1016/j.chmed.2018.09.001.

[124] R. Ahmed, N. ul ain Hira, M. Wang, S. Iqbal, J. Yi, Y. Hemar, Genipin, a natural blue colorant precursor: Source, extraction, properties, and applications, Food Chem 434 (2024) 137498. https://doi.org/10.1016/J.FOODCHEM.2023.137498.

[125] W. Winotapun, P. Opanasopit, T. Ngawhirunpat, T. Rojanarata, One-enzyme catalyzed simultaneous plant cell disruption and conversion of released glycoside to aglycone combined with in situ product separation as green one-pot production

of genipin from gardenia fruit, Enzyme Microb Technol 53 (2013) 92–96. https://doi.org/10.1016/J.ENZMICTEC.2013.05.001.

[126] H. Chen, X. Tan, M. Hu, J. Xie, X. Han, Y. Yu, H. Zhu, H. Wang, Y. Zhang, Genipin-mediated subunit-subunit crosslinking of ferritin nanocages: Structure, properties, and its application for food bioactive compound sealing, Food Chem 411 (2023) 135437. https://doi.org/10.1016/J.FOODCHEM.2023.135437.

[127] S. Ghosh, T. Sarkar, A. Das, R. Chakraborty, Natural colorants from plant pigments and their encapsulation: An emerging window for the food industry, LWT 153 (2022) 112527. https://doi.org/10.1016/J.LWT.2021.112527.

[128] I.A. Neri-Numa, M.G. Pessoa, B.N. Paulino, G.M. Pastore, Genipin: A natural blue pigment for food and health purposes, Trends Food Sci Technol 67 (2017) 271–279. https://doi.org/10.1016/J.TIFS.2017.06.018.

[129] G. Náthia-Neves, R. Vardanega, M.A.A. Meireles, Extraction of natural blue colorant from Genipa americana L. using green technologies: Techno-economic evaluation, Food and Bioproducts Processing 114 (2019) 132–143. https://doi.org/10.1016/J.FBP.2018.12.004.

[130] F. Yin, J. Liu, Research and application progress of Gardenia jasminoides, Chin Herb Med 10 (2018) 362–370. https://doi.org/10.1016/J.CHMED.2018.09.001.

[131] A.M. Ramos-De-La-Peña, C.M.G.C. Renard, L. Wicker, J.C. Montañez, L.A. García-Cerda, J.C. Contreras-Esquivel, Environmental friendly cold-mechanical/sonic enzymatic assisted extraction of genipin from genipap (Genipa americana), Ultrason Sonochem 21 (2014) 43–49. https://doi.org/10.1016/J.ULTSONCH.2013.06.008.

[132] A.S. Bellé, C.R. Hackenhaar, L.S. Spolidoro, E. Rodrigues, M.P. Klein, P.F. Hertz, Efficient enzyme-assisted extraction of genipin from genipap (Genipa americana L.) and its application as a crosslinker for chitosan gels, Food Chem 246 (2018) 266–274. https://doi.org/10.1016/J.FOODCHEM.2017.11.028.

[133] W. Xu, Q. Lou, L. Hao, K. Hu, M. Cao, Y. Liu, R. Han, C. He, J. Song, O-methyltransferases catalyze the last step of geniposide biosynthesis in Gardenia jasminoides, Ind Crops Prod 177 (2022) 114438. https://doi.org/10.1016/J.INDCROP.2021.114438.

[134] J. Tian, S. Qin, J. Han, J. Meng, A. Liang, A review of the ethnopharmacology, phytochemistry, pharmacology and toxicology of Fructus Gardeniae (Zhi-zi), J Ethnopharmacol 289 (2022) 114984. https://doi.org/10.1016/J.JEP.2022.114984.

[135] Y.H. Lin, H.F. Liang, C.K. Chung, M.C. Chen, H.W. Sung, Physically crosslinked alginate/N,O-carboxymethyl chitosan hydrogels with calcium for oral delivery of protein drugs, Biomaterials 26 (2005) 2105–2113. https://doi.org/10.1016/J.BIOMATERIALS.2004.06.011.

[136] Y. Luo, Z. Teng, X. Wang, Q. Wang, Development of carboxymethyl chitosan hydrogel beads in alcohol-aqueous binary solvent for nutrient delivery applications, Food Hydrocoll 31 (2013) 332–339. https://doi.org/10.1016/j.foodhyd.2012.11.011.

[137] H. Zhang, F. Zhang, J. Wu, Physically crosslinked hydrogels from polysaccharides prepared by freeze-thaw technique, React Funct Polym 73 (2013) 923–928. https://doi.org/10.1016/j.reactfunctpolym.2012.12.014.

[138] V. Manojlovic, N. Rajic, J. Djonlagic, B. Obradovic, V. Nedovic, B. Bugarski, Application of Electrostatic Extrusion – Flavour Encapsulation and Controlled Release, Sensors 8 (2008) 1488–1496. www.mdpi.org/sensors.

[139] B. Bugarski, Q. Li, M.F.A. Goosen, D. Poncelet, R.J. Neufeld, G. Vunjak, Electrostatic droplet generation: Mechanism of polymer droplet formation, AIChE Journal 40 (1994) 1026–1031. https://doi.org/10.1002/AIC.690400613.

[140] N.F. Alharby, R.S. Almutairi, N.A. Mohamed, Adsorption Behavior of Methylene Blue Dye by Novel CrossLinked O-CM-Chitosan Hydrogel in Aqueous Solution:

Kinetics, Isotherm and Thermodynamics, Polymers 2021, Vol. 13, Page 3659 13 (2021) 3659. https://doi.org/10.3390/POLYM13213659.

[141] K. yan Zhang, D. Li, Y. Wang, L. jun Wang, Carboxymethyl chitosan/polyvinyl alcohol double network hydrogels prepared by freeze-thawing and calcium chloride cross-linking for efficient dye adsorption, Int J Biol Macromol 253 (2023) 126897. https://doi.org/10.1016/J.IJBIOMAC.2023.126897.

[142] C. Lei, Q. Xiao, S. Zhou, W. Zu, J. Li, J. Zeng, L. Yan, Y. Huang, B. Wang, Synthesis and characterization of magnetic carboxymethyl chitosan-poly(acrylic acid-itaconic acid) hydrogel for the efficient adsorption of malachite green, J Appl Polym Sci 139 (2022) 52347. https://doi.org/10.1002/APP.52347;WGROUP:STRING:PUBLICATION.

[143] Z. Zhang, N. Abidi, L. Lucia, Smart superabsorbent alginate/carboxymethyl chitosan composite hydrogel beads as efficient biosorbents for methylene blue dye removal, J Mater Sci Technol 159 (2023) 81–90. https://doi.org/10.1016/J.JMST.2023.02.045.

[144] H. Zhu, S. Chen, H. Duan, J. He, Y. Luo, Removal of anionic and cationic dyes using porous chitosan/carboxymethyl cellulose-PEG hydrogels: Optimization, adsorption kinetics, isotherm and thermodynamics studies, Int J Biol Macromol 231 (2023) 123213. https://doi.org/10.1016/J.IJBIOMAC.2023.123213.

[145] D. Han, H. Zhao, L. Gao, Z. Qin, J. Ma, Y. Han, T. Jiao, Preparation of carboxymethyl chitosan/phytic acid composite hydrogels for rapid dye adsorption in wastewater treatment, Colloids Surf A Physicochem Eng Asp 628 (2021) 127355. https://doi.org/10.1016/J.COLSURFA.2021.127355.

[146] Z. Qian, X. Li, G. Yan, X. Chen, M.S. Sajab, G. Ding, W.N.L. Wan Jusoh, Sodium Alginate/Carboxymethyl Chitosan Hydrogel Microbeads for Antibiotic Adsorption in Single and Binary Systems, Gels 2025, Vol. 11, Page 646 11 (2025) 646. https://doi.org/10.3390/GELS11080646.

[147] A. Izadpanah, S. Nemati, S. Nojavan, A comprehensive review on synthesis and applications of cryogel-based sorbents in solid-phase extraction techniques, TrAC - Trends in Analytical Chemistry 180 (2024). https://doi.org/10.1016/j.trac.2024.117899.

[148] V.I. Lozinsky, Cryostructuring of Polymeric Systems. 50. Cryogels and Cryotropic Gel-Formation: Terms and Definitions, Gels 2018, Vol. 4, Page 77 4 (2018) 77. https://doi.org/10.3390/GELS4030077.

[149] A. Baimenov, D.A. Berillo, S.G. Poulopoulos, V.J. Inglezakis, A review of cryogels synthesis, characterization and applications on the removal of heavy metals from aqueous solutions, Adv Colloid Interface Sci 276 (2020). https://doi.org/10.1016/j.cis.2019.102088.

[150] R.M.P. Karlsson, P.T. Larsson, T. Pettersson, L. Wågberg, Swelling of Cellulose-Based Fibrillar and Polymeric Networks Driven by Ion-Induced Osmotic Pressure, Langmuir 36 (2020) 12261–12271. https://doi.org/10.1021/acs.langmuir.0c02051.

[151] V.M. Gun'ko, I.N. Savina, S. V. Mikhalovsky, Cryogels: Morphological, structural and adsorption characterisation, Adv Colloid Interface Sci 187–188 (2013) 1–46. https://doi.org/10.1016/j.cis.2012.11.001.

[152] G. Doser, E. Su, O. Okay, Effects of cryogenic condition and chemistry on the properties of synthetic and biopolymer cryogels, React Funct Polym 190 (2023) 105635. https://doi.org/10.1016/J.REACTFUNCTPOLYM.2023.105635.

[153] O.E. Zaborina, R.G. Gasanov, A.S. Peregudov, V.I. Lozinsky, Cryostructuring of polymeric systems. 38. the causes of the covalently-crosslinked cryogels formation upon the homopolymerization of N,N-dimethylacrylamide in moderately-frozen aqueous media, Eur Polym J 61 (2014) 226–239. https://doi.org/10.1016/j.eurpolymj.2014.10.006.

[154] S.A. El-Kholy, Environmentally Benign Freeze-dried Biopolymer-Based Cryogels for Textile Wastewater Treatments: A review, Int J Biol Macromol 276 (2024) 133931. https://doi.org/10.1016/J.IJBIOMAC.2024.133931.

[155] P. Wu, R.H. He, Y. Fang, K. Chen, M. Wu, W. Zhang, J. Lv, Y. Zhao, The study of double-network carboxymethyl chitosan/sodium alginate based cryogels for rapid hemostasis in noncompressible hemorrhage, Int J Biol Macromol 266 (2024) 131399. https://doi.org/10.1016/J.IJBIOMAC.2024.131399.

[156] Y. Privar, D. Shashura, A. Pestov, E. Modin, A. Baklykov, D. Marinin, S. Bratskaya, Metal-chelate sorbents based on carboxyalkylchitosans: Ciprofloxacin uptake by Cu(II) and Al(III)-chelated cryogels of N-(2-carboxyethyl)chitosan, Int J Biol Macromol 131 (2019) 806–811. https://doi.org/10.1016/J.IJBIOMAC.2019.03.122.

[157] M.V. Dumitru, T. Sandu, A. Miron, A. Zaharia, I.C. Radu, A.M. Gavrilă, A. Sârbu, H. Iovu, A.L. Chiriac, T.V. Iordache, Hybrid Cryogels with Superabsorbent Properties as Promising Materials for Penicillin G Retention, Gels 9 (2023) 443. https://doi.org/10.3390/GELS9060443/S1.

[158] M. Jalilzadeh, S. Şenel, Removal of Cu(II) ions from water by ion-imprinted magnetic and non-magnetic cryogels: A comparison of their selective Cu(II) removal performances, Journal of Water Process Engineering 13 (2016) 143–152. https://doi.org/10.1016/J.JWPE.2016.08.010.

[159] V.M. Gun'ko, I.N. Savina, S. V. Mikhalovsky, Cryogels: Morphological, structural and adsorption characterisation, Adv Colloid Interface Sci 187–188 (2013) 1–46. https://doi.org/10.1016/J.CIS.2012.11.001.

[160] R. Kecili, C.M. Hussain, Mechanism of Adsorption on Nanomaterials, Nanomaterials in Chromatography: Current Trends in Chromatographic Research Technology and Techniques (2018) 89–115. https://doi.org/10.1016/B978-0-12-812792-6.00004-2.

[161] R. Dobritoiu, S. Patachia, A study of dyes sorption on biobased cryogels, Appl Surf Sci 285 (2013) 56–64. https://doi.org/10.1016/J.APSUSC.2013.07.164.

[162] T. Sandu, A.L. Chiriac, A. Zaharia, T.V. Iordache, A. Sarbu, New Trends in Preparation and Use of Hydrogels for Water Treatment, Gels 11 (2025). https://doi.org/10.3390/gels11040238.

Chapitre 3 - Matériels et méthodes

3.1 Matériaux

La carboxyméthylation est la voie de modification chimique du chitosane. Le chitosane qui a été utilisé est de poids moléculaire moyen (50 000 – 190 000) et de degré de désacétylation ≥ 75% fournit par Sigma Aldrich. L'hydroxyde de sodium (NaOH, 98 %), l'acide monochloroacétique ($C_2H_3ClO_2$, ≥ 99 %) sont les réactifs qui ont été utilisés pour cette réaction et l'isopropanol (C_3H_8O, 99.9 %) est le solvant organique utilisé. Le carboxyméthylchitosane de sodium (NaCMCs) synthétisé a été le polymère de base des hydrogels sphériques poreux et le polyéthylène glycol (PEG 2000) a été utilisé comme porogène. L'acide acrylique, 99% a été combiné au NaCMCs pour fabriquer les cryogels monolithes. Les couples initiateurs utilisés sont le potassium persulfate (KPS, ≥ 99 %)/métabisulfite de sodium (SMS, ≥ 99 %) et peroxydisulfate d'ammonium (APS, ≥ 98 %) /N, N, N', N'-tétraméthylènediamine (TEMED). Le chlorure de calcium ($CaCl_2$, ≥ 93 %) a été utilisé comme agent de réticulation physique et le N, N-méthylènebis(acrylamide), ≥ 99 % ainsi que la génipine, ≥ 98 % sont les agents de réticulation chimique. Le chlorhydrate de fluoxétine, ≥ 98 %, le chlorhydrate de N-Desméthylcitalopram, ≥ 98 % et le chlorhydrate de venlafaxine, ≥ 98 % ont été utilisé comme contaminants modèles pour les tests d'adsorption. L'acétonitrile (CH_3CN, ≥ 99 %) et l'acide phosphorique (H_3PO_4, 85 %) ont été utilisés pour préparer la phase mobile pour l'analyse des échantillons. Le méthanol (CH_3OH, ≥ 99 %) et l'eau déminéralisée ont été utilisés pour préparer les solutions d'antidépresseurs.

3.2 Méthodologie

La méthodologie mise en œuvre dans cette thèse est schématisée à la figure 3.1. Sa description détaillée est, quant à elle, disponible dans les articles scientifiques des chapitres 4 à 7.

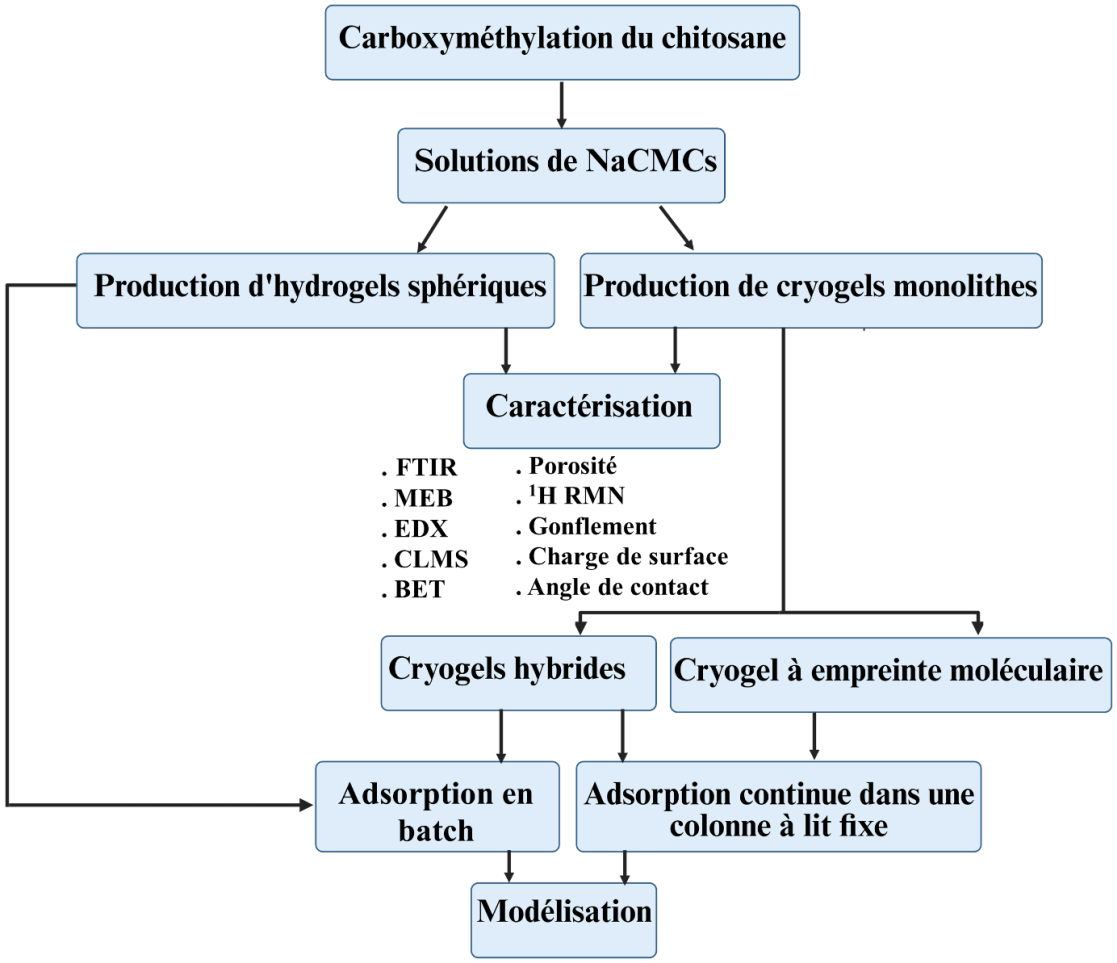

Figure 3.1 Schéma récapitulatif de la méthodologie mise en œuvre dans cette thèse

L'article 1 porte sur la modification chimique du chitosane par la réaction de carboxyméthylation et la fabrication d'hydrogels sphériques par la méthode d'extrusion électrostatique et gélification. Une analyse complète de l'adsorption en cuvée de la fluoxétine (isothermes, cinétique, thermodynamique) et la régénération des hydrogels par lavage avec un solvant organique sont également présentées dans cette étude.

L'article 2 porte sur la fabrication des cryogels hybride macroporeux à partir de poly(acrylate) de sodium et de chitosane carboxyméthylé par la technique de cryopolymérisation. Il présente également les investigations et analyses de l'adsorption de la fluoxétine en cuvée (isothermes, cinétique, thermodynamique) ainsi que des expériences de désorption.

L’article 3 traite de l’élaboration d’un cryogel hybride à partir de poly(acrylate) de sodium et de chitosane carboxyméthylé. Il présente également une étude de l’adsorption de la fluoxétine en mode continu dans une colonne à lit fixe ainsi que la modélisation des courbes de percée. Une étude préliminaire de l’adsorption compétitive de trois antidépresseurs est également évoquée dans cette étude ainsi que la régénération et la réutilisation du cryogels.

Enfin, l’article 4 présente la fabrication d’un cryogel hybride à empreinte moléculaire et d’un cryogel non imprimé à partir d’acrylate de sodium et de chitosane carboxyméthylée. L’étude de l’adsorption continue de la fluoxétine sur ces deux matériaux et l’investigation de la sélectivité par des tests préliminaires d’adsorption compétitive avec le citalopram sont également présentées dans cette étude.

Chapitre 4 - Article 1

4.1 Avant-propos

Le titre du premier article scientifique est: « Design of porous spherical biomaterials from carboxymethyl chitosan for removal of fluoxetine in aqueous medium » Il a été publié dans la revue scientifique Journal of Environmental Chemical Engineering en 2023.

Les auteurs et leurs coordonnées correspondantes sont, dans l'ordre:

Gilbert Romeo Nkana Nkana : Étudiant au Doctorat en sciences et génie des matériaux lignocellulosiques, Institut d'Innovations en Écomatériaux, Écoproduits et Écoénergies à base de biomasse (I2E3), Université du Québec à Trois-Rivières, 3351 Boulevard des Forges, CP.500, Trois-Rivières, Québec, Canada, G9A 5H7
Courriel : Gilbert.Nkana@uqtr.ca

Phuong Nguyen-Tri, Ph.D. : Directeur de thèse
Professeur au Département de biochimie, chimie, physique et sciences forensiques et chercheuse à l'Institut de recherche sur l'hydrogène, Université du Québec à Trois-Rivières, 3351 Boulevard des Forges, C.P. 500, Trois-Rivières, Québec, Canada, G9A 5H7.
Courriel: Phuong.Nguyen-Tri@uqtr.ca

André Lajeunesse, Ph.D. : Co-chercheur
Chimiste, Station d'épuration Jean-R. Marcotte, 12001 boul. Maurice-Duplessis, Montréal, QC H1C 1V3, Canada

Bruno Chabot, Ph.D. Co-Directeur de thèse et auteur pour la correspondance Institut d'Innovation en Écomatériaux, Écoproduits et Écoénergies à basse de biomasse, Université du Québec à Trois-Rivières, 3351 Boulevard des Forges, C.P. 500, Trois-Rivières, Québec, Canada, G9A 5H7
Courriel: bruno.Chabot@uqtr.ca

Contribution des auteurs: Gilbert Nkana est l'auteur principal de cet article. Il a effectué toutes les expériences scientifiques et les développements associés. M. Nguyen-Tri est directeur de recherche. M. Lajeunesse était initialement directeur de recherche et travaille maintenant comme chercheur à la station d'épuration des eaux usées de la ville de

Montréal, et M. Chabot est co-directeur de cette recherche. Le directeur et le co-directeur ont participé à la révision et à la correction du manuscrit.

4.2 Résumé

Des hydrogels poreux ont été développés par modification chimique du chitosane, suivie d'une extrusion électrostatique des solutions polymères et d'une stabilisation des gels par $CaCl_2$ et génipine. La caractérisation des polymères et des hydrogels a été réalisée à l'aide de la spectroscopie FTIR, de la RMN 1H, de la spectroscopie EDX, de l'analyse BET et MEB. Le potentiel zêta et le gonflement ont également été étudiés. La concentration résiduelle en FLX a été déterminée par analyse HPLC. Le mécanisme de diffusion de l'eau distillée à pH 8,5 dans la structure des gels correspond à un mécanisme de diffusion de Fick et contrôle le gonflement des billes. L'effet des paramètres (température, pH, concentration initiale et temps de contact) a été étudié lors des tests d'adsorption par lots de FLX. Le modèle cinétique pseudo-premier ordre correspondait le mieux aux données expérimentales, tandis que l'étude du modèle de diffusion intraparticulaire sectionnelle a montré que les intervalles de temps $0 \leq t \leq 60$ min et 60 min $\leq t \leq 180$ min présentaient les meilleurs paramètres statistiques. L'isotherme de Langmuir a fourni le meilleur ajustement avec $R^2 > 0,99$ par rapport au modèle de Freundlich. q_{max} et K_L ont diminué avec l'augmentation de la température, suggérant une physisorption de la fluoxétine sur les sites actifs. La capacité d'adsorption maximale était comprise entre 90 et 113 $mg.g^{-1}$ pour tous les adsorbants testés. Le facteur de séparation $R_L < 1$ et l'énergie de Gibbs ont révélé un processus d'adsorption favorable. L'étude thermodynamique a suggéré que l'adsorption était exothermique et que les molécules FLX pouvaient être disposées de manière aléatoire à l'interface solution/adsorbant. Les échantillons PHB4 et PHB5 ont montré une meilleure capacité d'élimination du FLX, même après cinq cycles d'adsorption/désorption.

4.3 Abstract

Porous hydrogels have been developed by chemical modification of chitosan, followed by electrostatic extrusion of the polymer solutions and stabilization of the gels by $CaCl_2$ and

genipin. The characterization of the polymers and hydrogels was completed by carrying out FTIR spectroscopy, ^{1}H NMR, BET, SEM and EDX spectroscopy. The Zeta potential and swelling were also studied. The residual FLX concentration was determined by HPLC analysis. The diffusion mechanism of distilled water at pH 8.5 in the structure of the gels corresponds to a Fickian diffusion mechanism and controls the swelling of the beads. The effect of the parameters (temperature, pH, initial concentration and contact time) was investigated during the FLX batch adsorption tests. The pseudo-first-order kinetic model best fitted the experimental data, while study of the sectional intraparticle diffusion model showed that the time intervals $0 \leq t \leq 60$ min and 60 min $\leq t \leq 180$ min had the best statistical parameters. The Langmuir isotherm provided the best fit with $R^2 > 0.99$ compared to the Freundlich model. q_{max} and K_L decreased with increasing temperature suggesting physisorption of Fluoxetine on the active sites. The maximum adsorption capacity was between 90 and 113 mg.g^{-1} for all adsorbents tested. The separation factor $R_L < 1$ and Gibbs energy revealed a favorable adsorption process. The thermodynamic study suggested that the adsorption was exothermic and FLX molecules could be randomly laid at the solution/adsorbent interface. Samples PHB4 and PHB5 showed better FLX removal capacity even after five adsorption/desorption cycles.

4.4 Introduction

The development of more sensitive analytical methods has made it possible to identify and distinguish the presence of many emerging contaminants in the effluent of wastewater treatment plants (WWTP) and in many environmental matrices (surface water, groundwater, sediments) [1–3]. These are pharmaceuticals and personal care products, which are closely monitored [4]. Among them, residues of bioactive molecules belonging to the family of antidepressants classified as selective inhibitors of serotonin reuptake stand out. Fluoxetine (FLX), marketed as PROZAC, is one of the residues identified in the environment [5,6]. This drug is widely prescribed worldwide as it is intended for the treatment of mental health disorders and is associated with various pharmacological approaches in many countries [7].

4.5 Materials and methods

4.5.1 Materials

A low molecular weight chitosan (CS) (MW 50,000 – 190,000 g/mol, deacetylation degree ≥ 75%), Chloroacetic acid ($C_2H_3ClO_2$) ACS Reagent ≥ 99.0%, Sodium hydroxide (NaOH) Bioxtra ≥ 98%, Polyethylene glycol (PEG) 2000, Calcium Chloride anhydrous ($CaCl_2$) ≥ 93.0%, Genipin ≥ 98% (HPLC), Deuterium oxide (D_2O) deuteration degree min 99.9% for NMR spectroscopy, Acetic acid-d4 ($C_2H_4O_2$) ≥ 99.5%, and Isopropyl alcohol (C_3H_8O) were supplied by Sigma-Aldrich. Hydrochloric acid (HCl) 37% was supplied by Acros organic. Ethyl alcohol anhydrous (C_2H_5OH) was purchased from Commercial Alcohol Greenfield Global (Brampton, ON, Canada). Fluoxetine hydrochloride (FLX) from Sigma-Aldrich (Oakville, ON, Canada) was used for the adsorption batch test as a model contaminant.

4.5.2 Methods

The Carboxymethyl chitosan derivatives (O-CMCs and N,O-CMCs) were synthesized based on the method of Medeiros Borsagli [28] with some modifications. This was carried out in two steps, the first of which was the alkalinization of chitosan (3 g) in a solution containing 8.16 g of NaOH dissolved in 50 mL of a distilled water/Isopropanol mixture (1:4 v/v) which was kept under stirring for 1h. For this step, the temperature of -20 °C was set for the synthesis of O-CMCs and 30 °C for N,O-CMCs. The second step is the carboxymethylation where a solution containing 14.4 g of monochloroacetic acid dissolved in Isopropanol (1:1 w/w) was added gradually over 30 min with constant stirring. Subsequently, the temperature was adjusted to 30 °C for O-CMCs and 60 °C for N,O-CMCs. The suspensions were kept under stirring for 4h and the reaction was stopped by adding 200 mL of 70 % ethanol. The suspensions were filtered and the recovered products washed with increasing grades of ethanol (70 % - 100 %) and then dried under vacuum for 72 h.

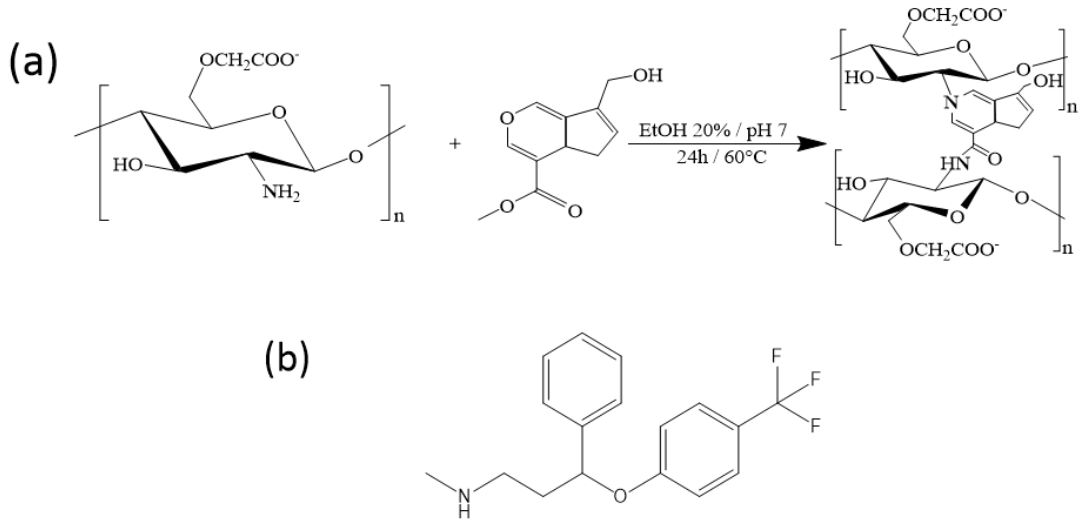

Scheme 1. Crosslinking reaction between carboxymethyl chitosan and Genipin (a) and Chemical structure of Fluoxetine (b).

Aqueous solutions of O-CMCs and N,O-CMCs (0.03 g/mL) were prepared and PEG 2000 was added to each solution to obtain the ratios of PEG/O-CMCs (0:3, 1:3, 2:3, 3:3) denoted PHB1, PHB2, PHB3, PHB4 and PEG/N,O-CMCs (0:3) denoted PHB5, respectively. The suspensions were stirred for 2h and subjected to electrostatic extrusion at a flow rate of 0.5 mL/h (KD Scientific syringe pump, USA) and an applied voltage of 7.5 kV using a high voltage generator (Gamma High Voltage Research, Ormond Beach, FL 32174). The suspensions were dropped into a $CaCl_2$ bath (0.03 g/L) prepared with 70 % ethanol (Figure 4.1).

The resulting beads were recovered and cross-linked for 24 h, 60 °C and pH: 7 in a genipin bath (1 $mmol.L^{-1}$) prepared with 40 % ethanol (scheme 1a). Genipin is a natural water-soluble cross-linking agent and was used as a substitute to toxic glutaraldehyde or epichlorohydrin which are both widely used for such applications. The cross-linked beads were recovered and washed extensively with 20 % ethanol, freeze-dried and stored in a desiccator and tested for FLX adsorption in aqueous solution.

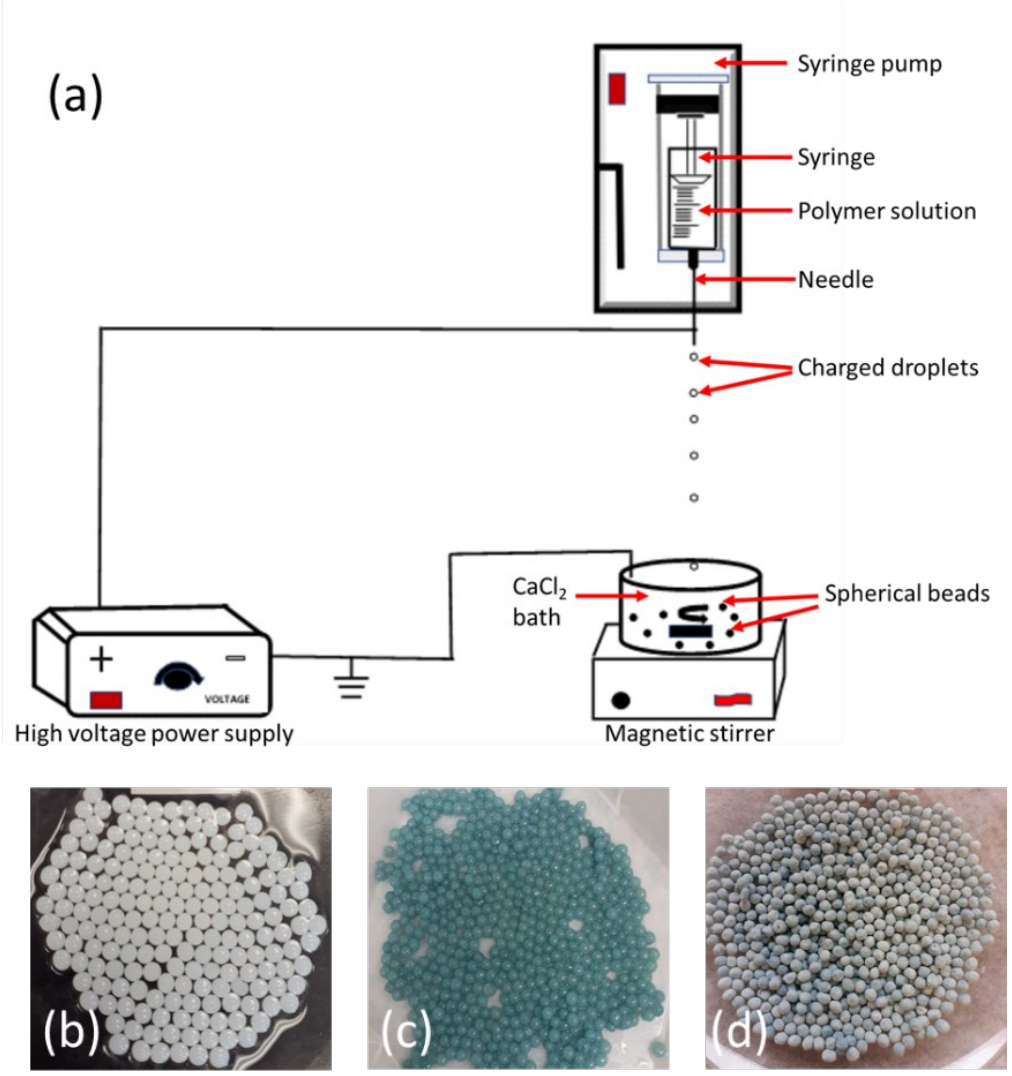

Figure 4.1 Electrostatic extrusion experimental device (a). Fresh beads (b), Cross-linked beads by genipin (c), and Freeze-dried beads (d).

4.5.3 Characterization of Chitosan, Carboxymethyl chitosan and carboxymethyl chitosan hydrogel beads

Fourier transform infrared spectroscopy (FTIR Thermo iS10) and proton nuclear magnetic resonance spectroscopy (NMR Bruker 400 MHz Neo Advance) were applied to confirm the chemical modifications of chitosan. Conductometric titration of the samples was carried out in triplicates using a Metrohm Brinkmann 765 Dosimat automatic titrator equipped with a Thermo Orion model 150A+ conductivity meter. It was used to evaluate the degree of deacetylation (*% DD*), degree of substitution (*DS*) and percentage of free

amine group (*% FA*). The titration curves were plotted to graphically determine volumes V_1, V_2 and V_3 which allowed them to be calculated from equations 4.1, 4.2 and 4.3 (see Fig. S1 in Supplementary material).

$$\%DD = [NaOH]\,(V_2 - V_1) \times 161 / W_{CS} \quad \text{Equation 4.1}$$

$$DS = (V_2 - V_1) \times DD \,/\, (V_3 - V_2) \quad \text{Equation 4.2}$$

$$\%FA = (V_3 - V_2)\,[NaOH] \times 240.07 / W \quad \text{Equation 4.3}$$

Where V_1 (mL), the first inflection point represents the volume of NaOH solution needed to consume the excess H_3O^+ ion in the solution, V_2 (mL), the second inflection point where (V_2 - V_1) is the volume of NaOH solution needed to deprotonate the carboxymethyl groups in the titration of carboxymethyl chitosan derivatives and the $-NH_3^+$ ions in the case of chitosan. V_3 (mL) is the third inflection point, where (V_3 - V_2) is the volume of NaOH solution required to deprotonate the $-NH_3^+$ ions. [NaOH] is the molarity of the NaOH solution in ($mol.L^{-1}$), W_{CS} and W are the mass of chitosan and carboxymethyl chitosan samples in (mg), 161 is the molar mass of the monomer D-Glucosamine and 240.07 is the average molecular mass of the saccharide units of the carboxymethyl chitosan molecules. The Zeta potential measurements were carried out using a Zetasizer Nano (Malvern Instruments, model Zen 3600). The thermal properties of materials were investigated using differential scanning calorimetry. The swelling behavior of the bead materials was studied by placing 0.1 g of freeze-dried beads in 50 mL of deionized water at pH 8.5, maintained at 25 ± 1°C. The beads were allowed to swell for various time from 30 to 300 min. After each predetermined swelling time, the beads were recovered by filtration, the excess of moisture was blotted off, and they were weighed on an analytical balance. The degree of swelling (*% SW*) was calculated using equation 4.4

$$\%SW = (W_2 - W_1)/W_1 \times 100 \quad \text{Equation 4.4}$$

where W_1 (g) is the mass of freeze-dried beads and W_2 (g) is the mass of swollen beads, respectively. The surface morphology was studied by scanning electron microscopy

(Hitachi SU1510 Scanning Electron Microscope). The specific surface area of bead materials was determined using a Micromeritics TriStar II 3020 BET instrument.

4.5.4 Adsorption of FLX onto carboxymethyl chitosan hydrogel beads

FLX adsorption tests on materials samples (PHB1, PHB2, PHB3, PHB4, and PHB5) were carried out in batch mode. The effect of different pH (7, 7.5, 8, 8.5) and different temperatures (30, 40, 50, 60 °C) on FLX removal efficiency was investigated by contacting 25 mg of beads with 50 mL of 50 ppm FLX solution. The suspensions were shaken at 150 rpm for 180 min using an orbital shaker (ORBIT Environ-Shaker, Lab-line). For the study of adsorption kinetics, the temperature was set at 30 °C, the pH: 8.5 and 50 ppm FLX initial concentration. The study was completed in a time range of 0 to 180 min. The adsorption isotherm study was carried out at different FLX initial concentration (10 to 100 ppm), for 180 min, pH: 8.5. The residual FLX concentration was determined following the methodology described by Camiré et al [29]. A HPLC system equipped with a DAD iodine bar detector (Shimadzu i-Series Plus) and a C18 reverse phase column (XB-C18, 100Å, 150 x 3 mm, particle size 2.6 µm, Phenomenex, Kinetex) was required. The adsorption capacity of FLX was determined by equations 4.5 and 4.6.

$$\%R = (C_0 - C_t) / C_0 \times 100$$ Equation 4.5

$$q_e = \left(C_0 - C_e\right) \times V \Big/ m$$ Equation 4.6

Where *% R* is the removal efficiency, q_e is the amount of FLX adsorbed by the beads at equilibrium ($mg.g^{-1}$). C_0 is the initial concentration of FLX (ppm), *V* (mL) and *m* (g).

The goodness of fit of the isotherm models to the experimental data was validated using several error functions such as R^2, R^2_{Adj}, and the root mean square error (*RMSE*). OriginPro 2023 software (OriginLab Corporation, Northampton, USA) was used for the nonlinear optimization of the isothermal models, thus making it possible to obtain the parameters of each model. Adsorption tests were carried out in triplicate.

$$R^2 = \sum (q_{mean} - q_{cal})^2 \Big/ \sum (q_{cal} - q_{mean})^2 + \sum (q_{cal} - q_{\exp})^2$$ Equation 4.7

$$R^2_{Adj} = 1 - (1 - R^2)(N_{\exp} - 1) \Big/ (N_{\exp} - N_{par} - 1)$$ Equation 4.8

$$RMSE = \sqrt{1/N_{\exp} \sum (q_{\exp} - q_{cal})^2}$$ Equation 4.9

q_{exp} ($mg.L^{-1}$): experimental adsorption capacity; q_{mean} ($mg.L^{-1}$): average value of experimental adsorption capacity; q_{cal} ($mg.L^{-1}$): calculated adsorption capacity; N_{exp}: number of data points; N_{par}: number of parameters [30].

FLX is extracted from the body through urine and excreta in the native form or as a secondary metabolite, the most identified being norfluoxetine. They are found through domestic sewage in municipal wastewater that is continuously discharged to WWTPs. Anthropogenic activity is also responsible for their presence in various environmental matrices [3,8,9]. The large flow of wastewater that reaches WWTPs and the inefficiency of conventional treatments do not allow effective removal of these contaminants that are released into nature at the end of each treatment cycle. Detected at concentrations ranging from $\mu g.L^{-1}$ to $mg.L^{-1}$ in the environment, they affect many aquatic species living in receiving environments through their toxicity, their ability to diffuse beyond biological membranes and their potential to bioaccumulate in tissues. They affect the reproduction, growth, behavior and survival of many aquatic species [9–11] . These pollutants constitute a real danger to aquatic biodiversity, hence the urgency of limiting their entry into the environment.

This has motivated the development of technologies that have improved the removal rates of its pharmaceutical residues in WWTPs [12–14]. Advanced oxidation, photodegradation, ozonation and electrochemical degradation processes developed over the past decade have proven effective as alternative tertiary treatment processes for pharmaceutical residues in wastewater [9,15,16]. However, these wastewater treatment methods have limits. They generate more toxic by-products, produce greenhouse gases, consume a lot of energy and are more expensive to operate. An alternative, such as adsorption, which is a greener approach and less expensive to implement, has been

developed by researchers. Several new adsorbent materials have been developed from biopolymers, in particular hydrogels, which have shown enormous potential for purifying contaminated water [17–23]. Biopolymers in general and chitosan in particular are promising alternatives that are good candidates for the development of biodegradable and biocompatible adsorbents. They have highly reactive chemical functions that can be chemically modified to improve the selectivity and specificity of adsorbents [24,25]. Chitosan has received much more attention in the last decade because this biopolymer has exceptional properties and is readily available as it is derived from the partial deacetylation of chitin, the second most abundant natural polymer after cellulose [24,26].

The preparation of hydrogels from hydrophilic biopolymers and their composites has been widely studied for the adsorption of metal ions and organic molecules such as dyes and pharmaceuticals [17–23]. The swelling properties of the hydrogels, their sensitivity to different types of physicochemical stimuli and their excellent mechanical stability make them prime candidates for wastewater treatment applications compared with traditional materials. The study of solute adsorption by hydrogels in some works has been carried out under conditions where the hydrogels have previously reached swelling equilibrium before being brought into contact with the analytes. Adsorption begins after the beads have reached thermodynamic equilibrium with the solution [27]. To our knowledge, no study has reported the evaluation of Fluoxetine adsorption on carboxymethyl chitosan porous hydrogels during the swelling of the gels. The aim of this study was to investigate the efficiency and adsorption capacity of Fluoxetine by porous hydrogels developed from the biopolymer carboxymethyl chitosan during the swelling process.

4.6 Results and discussions

4.6.1 Characterization of chitosan, carboxymethyl chitosan derivatives and carboxymethyl chitosan hydrogel beads

The aim of the polymer characterization is to confirm the chemical modifications on raw chitosan. For this purpose, numerous analyses were carried out, including FTIR spectroscopy, ^{1}H NMR, conductometric titration, Zeta potential analysis, BET, Energy-dispersive X-ray spectroscopy (EDX) and swelling behavior.

Figure 4.2 presents the FTIR spectra of raw chitosan, O-CMCs, N,O-CMCs, PHB1, PHB2, PHB3, PHB4, PHB5, PEG 2000 and genipin, respectively. They confirm the substitution of carboxymethyl group on raw chitosan and effective crosslinking by genipin.

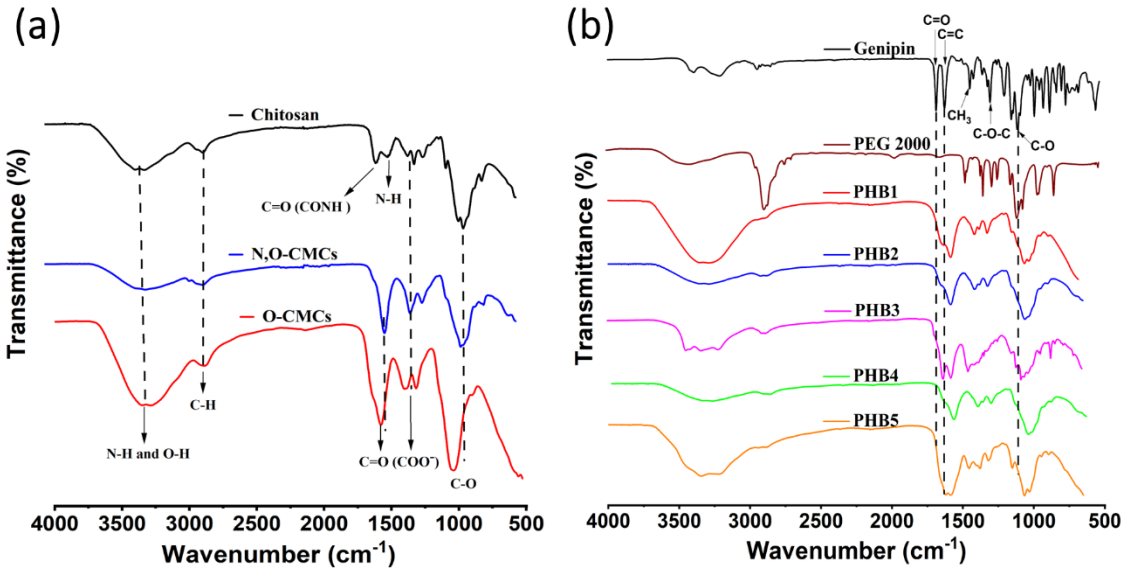

Figure 4.2 FTIR spectra of Chitosan, N,O-CMCs and O-CMCs (a), Genipin, PEG 2000, PEG/O-CMCS 0:3 (PHB1), PEG/O-CMCS 1:3 (PHB2), PEG/O-CMCS 2:3 (PHB3), PEG/O-CMCS 3:3 (PHB4) and PEG/N,O-CMCS 0:3 PHB5 (b)

The IR spectrum of chitosan (Figure 4.2a) reveals characteristic absorption bands of this polysaccharide as reported in studies by [28,31]. These are the absorption bands at 3359 cm^{-1} attributed to N-H and O-H elongations and intermolecular hydrogen bonds associated with polymers. The absorption band at 2874 cm^{-1} is attributed to C-H elongation while the absorption bands identified at 1648 cm^{-1} and 1562 cm^{-1} correspond to C=O elongation of amide II and N-H plane deformation of amine I respectively. The absorption bands at 1420 cm^{-1} and 1375 cm^{-1} correspond to the antisymmetric and symmetric -CH_3 deformations respectively and that at 1314 cm^{-1} corresponds to the C-N elongation of amide III. The band at 1150 cm^{-1} was assigned to antisymmetric C-O-C elongation and that at 1060 cm^{-1} to symmetric C-O elongation and the band at 1026 cm^{-1} was assigned to the elongation of the primary hydroxyl groups. The FTIR spectra of N,O-CMCs and O-CMCs (Figure 4.2a) show the structural changes made on raw chitosan. The chemical modifications were

confirmed by the appearance of new absorption bands at 1587 cm^{-1} (intense) and 1403 cm^{-1} (average) for N,O-CMCs as well as those at 1587 cm^{-1} (intense) and 1400 cm^{-1} (average) for O-CMCs. They were attributed to symmetric and antisymmetric -COO^- elongations confirming the substitution of deprotonated carboxymethyl groups (-CH_2COO^-) on the free hydroxyl and amine groups of chitosan [28]. Moreover, in the N,O-CMCs spectrum, a broad band between 3500 - 3100 cm^{-1} was observed compared to that of chitosan which could reveal a more hydrophilic character of this derivative. This may assign free amine groups and hydroxyl groups of the monomer units were reacted together. The disappearance of the absorption bands of chitosan at 1060 cm^{-1} and 1026 cm^{-1} and the appearance of new intense bands at 1044 cm^{-1} and 1038 cm^{-1} on the IR spectra of N,O-CMCs and O-CMCs respectively was attributed to the C-O elongation of the primary hydroxyl groups. This confirms an O-substitution of carboxymethyl groups on the C_6 carbon of the monomer units.

The appearance of the blue pigment on the beads after immersion in the genipin bath (Figure 4.1c) is an indication of cross-linking of the polymer chains by genipin. It is attributed to the reaction of genipin on the free amine groups present in the backbone of O-CMCs and N,O-CMCs derivatives [32–34]. FTIR analysis of genipin and cross-linked beads are shown in Fig. 2b. The IR spectrum of genipin reveals characteristic bands at 1680 cm^{-1} and 1620 cm^{-1}. They are attributed to the C=O elongation of the ester group and C=C elongation of the heterocycle respectively. The absorption band at 1442 cm^{-1} is attributed to the CH_3 antisymmetric deformation of the ester group, the one at 1300 cm^{-1} corresponds to the C-O-C elongation. The absorption bands at 1104 cm^{-1} and at 990 cm^{-1} are attributed to C-O elongation and out-of-plane C-H deformation. The cross-linking of the beads is accompanied by a shift of the band at 1680 cm^{-1} from the carbonyl belonging to the ester group of genipin to 1631 cm^{-1} in the spectra of hydrogel beads. This new band corresponds to a C=O elongation linked to the formation of amide group II following the nucleophilic substitution reaction between the ester group of genipin and the free amine groups present in the structure of the derivative. The shift of the band at 1587 cm^{-1} observed in the FTIR spectra of O-CMCs and N,O-CMCs towards 1578 cm^{-1} could be explained by the substitution of the amine groups of the polymers on the olefinic carbon of genipin and the formation of an amine heterocycle [210]. The intense absorption band

at 1100 cm^{-1} characteristic of PEG (Figure 4.2b) is attributed to the elongation of the C-O bonds of the ether groups. This absorption band is not observed on the infrared spectra of the hydrogels. This suggests that washing the beads with distilled water eliminated the PEG, which is highly soluble in water [35].

The ^{1}H NMR analysis of chitosan, N,O-CMCs and O-CMCs was done to confirm the information obtained from the FTIR spectroscopic analysis. The ^{1}H-NMR spectra of the samples (Figure S2) agree with data reported in the literature [36–39]. The spectra of chitosan derivatives revealed characteristic peaks confirming the substitution of carboxyl groups on the hydroxyl and amine groups of chitosan. The ^{1}H NMR spectrum of Chitosan shows a signal at $\delta = 1.9$ ppm attributed to the methyl protons belonging to the acetamide group ($-NHCOCH_3$) of the N-acetylglucosamine unit as shown in Figure S2a. The peak at $\delta = 2.9$ ppm corresponds to the proton bound to the C_2 carbon of the glucosamine unit. The signal overlap between $\delta = 3.3$ ppm and $\delta = 4$ ppm is attributed to protons bound to the C_3, C_4, C_5, and C_6 carbons of the pyranose ring. The signal at $\delta = 4.4$ ppm corresponds to the proton bound to carbon C_1 of the pyranose ring. The spectra observed in Figure S2b and S2c show proton signals attributed to the characteristic signals identified on the chitosan spectrum. Figure S2b, presents two new signals at $\delta = 3.2$ ppm and at $\delta = 4.05$ ppm. They are attributed to the protons of the carboxymethyl group ($-CH_2COO^-$) indicating that substitution occurred on the free amine groups bound to the C_2 carbon and on the hydroxyl groups bound to the C_6 carbon, respectively. This helps to confirm the synthesis of the N,O-CMCs derivative. Figure S2c shows a strong signal at $\delta = 4.05$ ppm and a weak signal at $\delta = 3.2$ ppm which allow us to conclude that the substitution reaction was directed preferentially on the hydroxyl groups bound to the C_6 carbon and that a very small fraction of free amine groups was involved during the reaction. The majority of the O-CMCs derivative is thus obtained.

Conductometric titration was carried out by dissolving 0.15 g of each sample in 100 mL of 0.05 M HCl solution for 4h. The pH of each polymer solution was adjusted at 2 and a 0.1 M NaOH solution was added automatically with an increment of 0.5 mL, 40 s stabilization time at room temperature under constant stirring. The conductometric titration data are presented in Figure S1a, S1b and S1c. The *DD*, *DS* and *FA* values (from

equations 4.1, 2 and 3) are reported in Table S1. The *DD* of chitosan is approximately 81% and agrees well with the supplier's information (*DD* ≥ 75%). *DS* values for N,O-CMCs and O-CMCs are 1.78 and 1.12, respectively. The evaluation of the number of free amine groups reveals that almost 95 % of the amine groups remained unreacted during the synthesis of O-CMCs while for N,O-CMCs, almost 46 % of the amine groups remained free. From these results, it can be concluded that only a fraction of the amine group (5 %) reacted during the synthesis of O-CMCs which could justify the low intensity of the corresponding peaks observed on the ^{1}H NMR spectra of this polymer.

Determination of the Zeta potential was investigated by first preparing O-CMCs and N,O-CMCs solutions at different pH: 2 to 9. A 1mL sample of each solution was analyzed by a ZetasizerNano instrument previously calibrated with a standard solution of Zp = ± 42 mV. The Zp = f(pH) curve (Figure 4.3) was used to determine the isoelectric point (IEP) of each polymer. The study of Zeta potential as a function of pH gave positive Zp values in the range $2 \leq pH < 4$ for O-CMCs and $2 \leq pH < 5.3$ for N,O-CMCs. On the other hand, it is negative in the range $4 < pH \leq 9$ and $5.3 < pH \leq 9$ for O,CMCs and N,O-CMCs respectively. These values can be explained by the protonation of the free amine groups initially, then as the pH of the medium becomes alkaline, these functional groups are deprotonated, as are the carboxyl groups. The isoelectric point corresponds to the pH at which the polymers are considered to be a zwitterion (NH_3^+/COO^-). They were determined at pH = 4 and pH = 5.3 for O-CMCs and N,O-CMCs respectively. It is therefore assumed that the beads made from these precursors could interact with FLX in aqueous solution thanks to attractive electrostatic interactions when the pH of the medium is higher than the IEP and lower than the pKa = 9.8 of FLX (scheme. 1b) [9], which would be ionised.

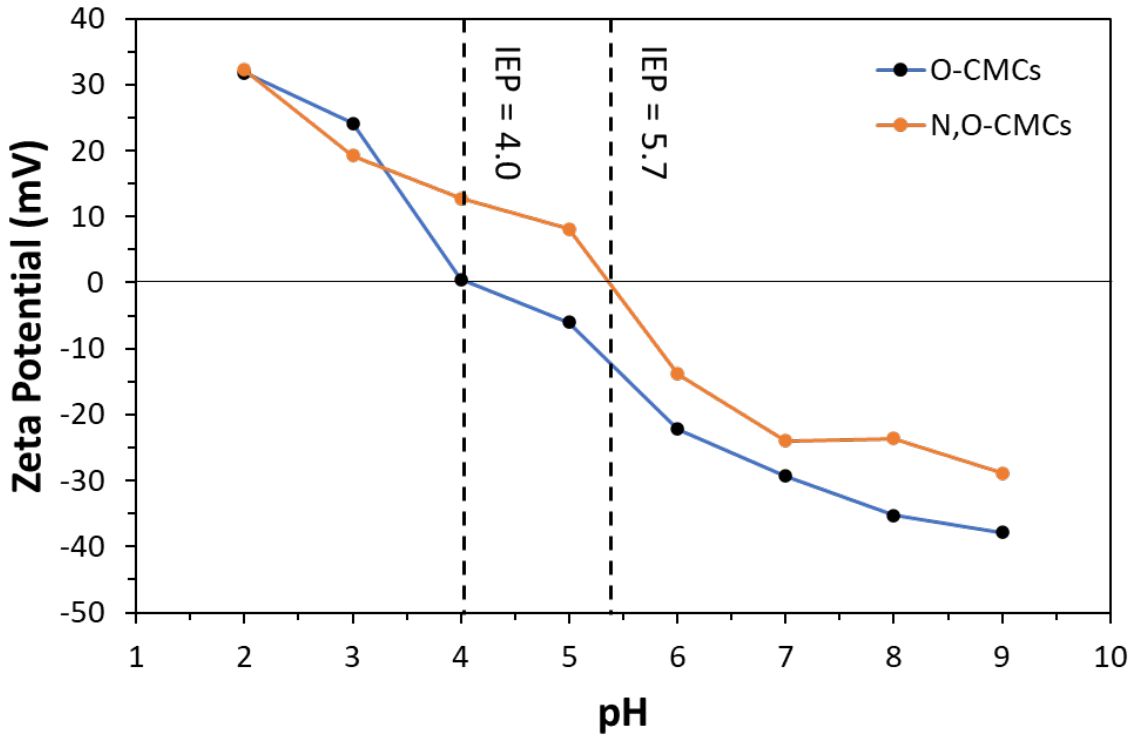

Figure 4.3 Effect of pH on the Zeta-potential of O-CMCs and N,O-CMCs

Figure 4.4 presents SEM images of bead surfaces and their respective cross sections to study the external surface morphology and internal structure (pores) of each material (PHB1 to PHB5). Figures. 4a-e show that hydrogel beads are approximately 2 mm in diameter with good sphericity. They also mostly show a smooth surface, except for PHB1 (Figure 4.4a) which has a rougher surface morphology. Due to the low magnification used for SEM, it was not possible to clearly determine if a porous surface was developed on the external side of bead materials, except for PHB1. Since those images were taken on freeze-dried beads, it is expected that they will exhibit some swelling characteristics when dispersed in aqueous media providing access to the internal structure of the beads. This topic will be discussed later but prior to that, an analysis of the internal structure of the bead materials is provided. Figures 4.4f-j (PHB1 to PHB5) show SEM micrographs of freeze-dried bead cross-sections at a higher magnification. A porous structure network of interconnected macropores with a variable pore size distribution is clearly observed for those samples. PHB3 and PHB4 cross-sectional images (Figures 4.4h and 4.4i) show higher porosity than PHB1 and PHB2 cross-sectional samples (Figures 4.4f and 4.4g).

This could be attributed to the use of higher amount of PEG 2000 (pore-forming agent) during the preparation of the extrusion solutions of those two materials, compared to the levels used for PHB1 and PHB2. It is assumed that the PEG-2000 was removed during the washing of the beads and the empty spaces left by its removal would constitute the pores observed in the images. Similar observations have been reported in the work of [40]. On the other hand, although no PEG-2000 was added during the preparation of the PHB1 and PHB5 samples, their SEM images show more apparent pores in the PHB5 than in the PHB1 cross-sectional images. This could be caused by the freeze-drying process of the hydrogel beads, which would allow a rapid sublimation of the water and prevent shrinkage of the beads, thus leaving cavities in the beads. Similar observations were made by [41]. The porous internal structure of bead materials is confirmed by the specific surface area reported in Table 4.1

Table 4.1 Effect of PEG/O-CMCs and PEG/N,O-CMCs ratios on specific sur-face area of freeze-dried beads

Sample		PEG:CMCs ratio	Specific surface area (m^2/g)
PHB1	O-CMCs	0:3	19.84
PHB2	O-CMCs	1:3	29.81
PHB3	O-CMCs	2:3	37.50
PHB4	O-CMCs	3:3	38.69
PHB5	N,O-CMCs	0:3	25.93

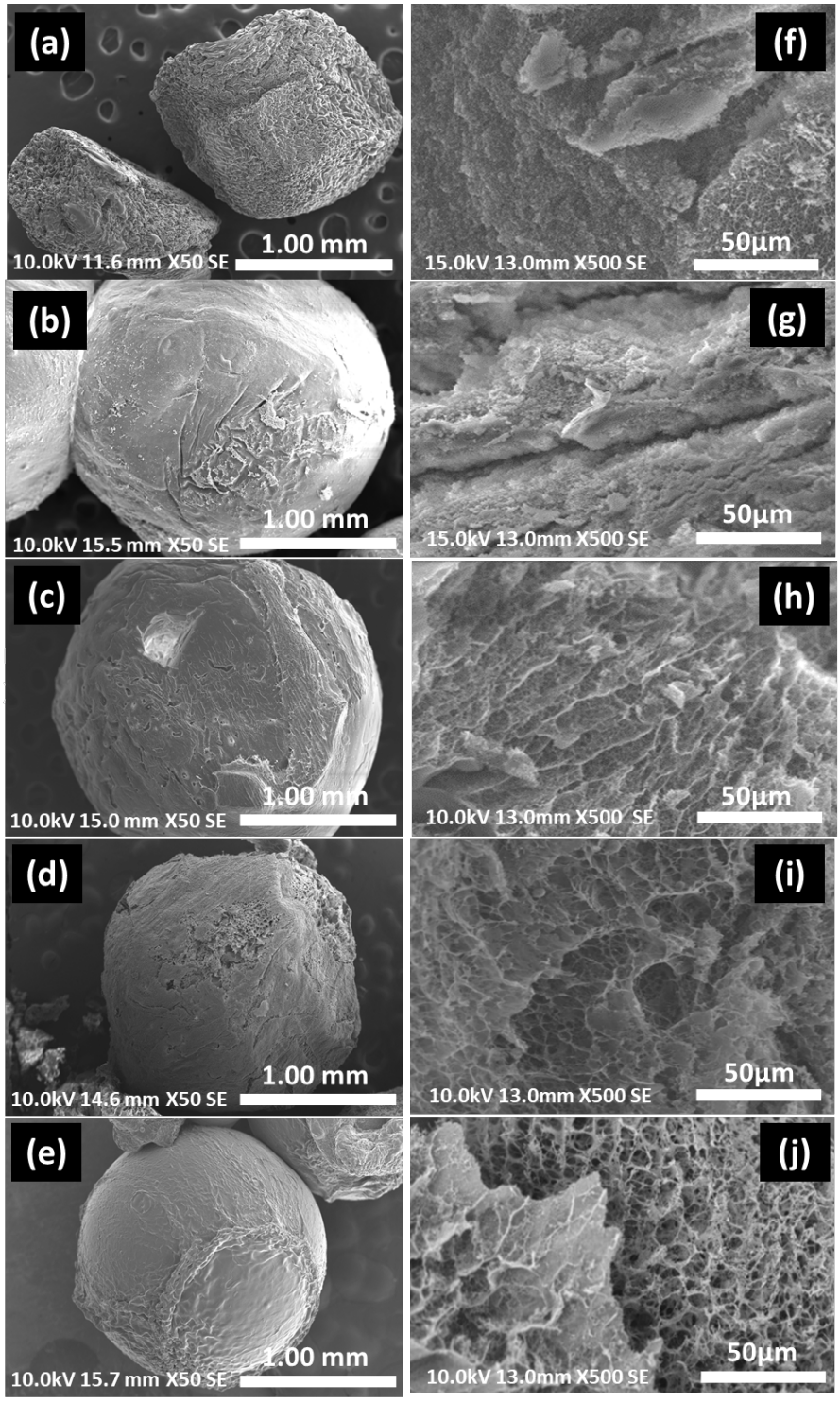

Figure 4.4 **SEM micrographs of PEG/O-CMCS 0:3 (PHB1), PEG/O-CMCS 1:3 (PHB2), PEG/O-CMCS 2:3 (PHB3), PEG/O-CMCS 3:3 (PHB4) and PEG/N,O-CMCS 0:3 PHB5 samples, external morphology of beads (a-e), and cross-sections showing their respective in-ternal structure (f-j)**

Swelling behavior was carried out to examine their water-absorption rate under a controlled environment. Figure 4.5 shows the water absorption rate curve of hydrogel beads (PHB1 to PHB5). The swelling of the beads in water at pH=8.5 occurs due to the total dissociation of the carboxyl groups present on the polymer chains in the gel network. This creates an osmotic pressure difference at the interface between the gel structure and the water around the gels.

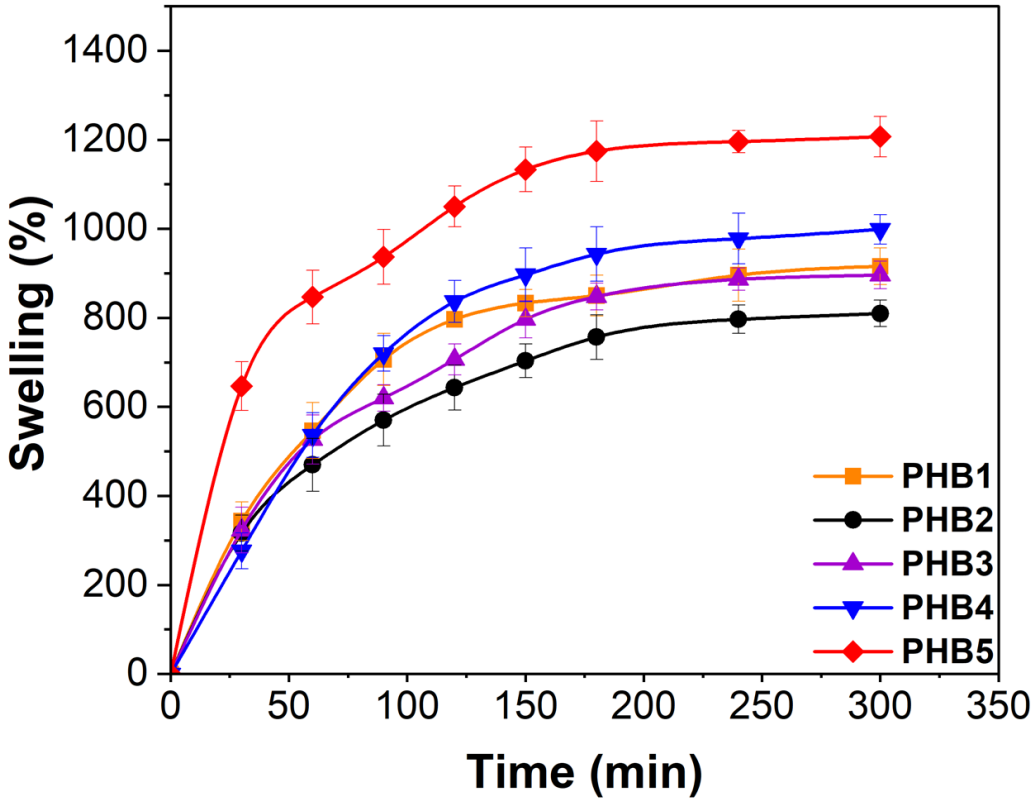

Figure 4.5 Swelling kinetics of hydrogel beads: PHB1, PHB2, PHB3, PHB4, and PHB5 in deionized water at pH: 8.5, temperature: 25 ± 1 °C (n =3, mean ± standard error)

The swelling profile of the hydrogels tested reveals that the swelling of the beads can be associated with the diffusion of water through the pore network in the gel structure between 0 -180 min and the relaxation of the polymer chains as a result of the repulsion between the deprotonated carboxyl groups on the polymer repeat units between 180 - 300 min. On the other hand, the ionic density in the polymer network linked to the ionisation of the carboxyl groups is greater in PHB5 made with N,O-CMCs than in other hydrogels

made with O-CMCs. This could explain the higher swelling rates of this sample compared to the others due to the increase in osmotic pressure [42]. In view of the above, it can be said that the cross-linking density of the polymer chains in the gel structures is not high enough to restrict the mobility of the polymer chains but sufficient to guarantee the stability of the structures. Equation 4.10 allows us to determine the nature of solvent diffusion in the polymer network according to the values of the diffusion exponent *n*. M_t and M_α correspond to the amount of solvent that has diffused into the gel structure at time t and equilibrium respectively and k is the constant specific to the type of polymer network ($min^{1/n}$). Linearization of this equation gives Ln *F* vs Ln t (equation 4.11) where n is the slope and Ln k the y-intercept. For $n \leq 0.5$, the solvent diffusion mechanism in the gel structure is of the Fickian type: diffusion controls the swelling process. For $0.5 < n < 1$, solvent diffusion and polymer chain relaxation control the swelling process. The solvent diffusion mechanism is non-Fickian [43].

$$F = M_t / M_\alpha = kt^n \qquad \text{Equation 4.10}$$

$$Ln\,F = Ln\,k + n\,Ln\,t \qquad \text{Equation 4.11}$$

The values of the parameters of equation 4.11 are listed in Table 4.2. It can be seen that the values of the diffusion exponent n obtained lead to the conclusion that there is a Fickian diffusion mechanism for water in the porous hydrogels produced and that the bead swelling process is controlled by water.

Table 4.2 Parameters of swelling and diffusion of porous hydrogels in distilled water at pH 8.5

Samples	*n*	*k* ($min^{1/n}$)	R^2
PHB1	0.358	0.143	0.921
PHB2	0.350	0.148	0.969
PHB3	0.378	0.077	0.955
PHB4	0.463	0.083	0.908
PHB5	0.253	0.254	0.950

4.6.2 Effect of temperature and pH on Fluoxetine removal efficiency

Figure 4.6a presents the effect of temperature (from 30 to 60 °C) under the following experimental conditions; initial concentration: 50 ppm; agitation speed: 150 rpm; adsorbent dose: 0.5 mg/mL; pH: 8.5; contact time: 180 min. Figure 4.6b shows the effect of pH (from 7 to 8.5) under the following experimental conditions initial concentration: 50 ppm; agitation speed: 150 rpm; adsorbent dose: 0.5 mg/mL; temperature: 30 °C; contact time: 180 min. It can be seen that increasing temperature led to a significant decrease in FLX removal efficiency for all the adsorbents tested.

The maximum values were observed at a temperature of 30 °C and were greater than 70 % under the fixed experimental conditions, suggesting that addition of energy in the form of heat to the medium was detrimental to the adsorption of Fluoxetine on the active sites process. On the other hand, increasing the pH from 7 to 8.5 favored the elimination of FLX for all the adsorbents tested. The best elimination efficiency was observed at pH: 8.5 and was greater than 70 % for all the adsorbents tested at a temperature of 30 °C. This could be justified by the increase in negatively charged sites on the surface of the adsorbents, favoring electrostatic interactions with FLX. This can be confirmed by the negative charge of the precursor polymers of the adsorbents tested (O-CMCs and N,O-CMCs) under the pH conditions studied for the adsorption tests, as shown in Figure 4.3. These weak interactions would be linked to the $-CH_2COO^-$ groups and to the ionized FLX in solution, which is positively charged when the $pH_{solution} < pKa_{FLX}$: 9.8 [9]. The optimum conditions for the temperature and pH parameters were set at 30°C and 8.5 respectively to complete the subsequent adsorption tests.

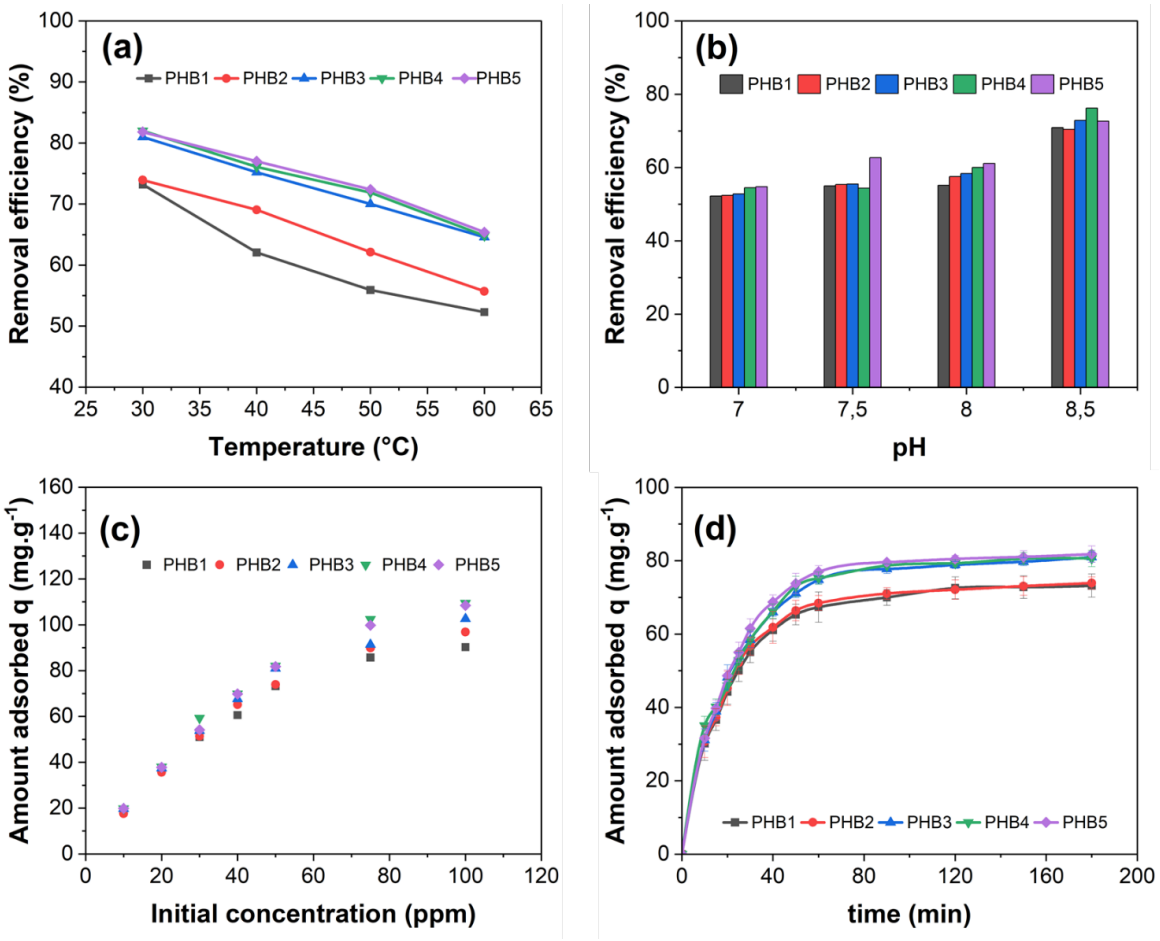

Figure 4.6 **Effect of different parameters on the Fluoxetine adsorption by hydrogel beads (PEG/O-CMCs 0:3 (PHB1), PEG/O-CMCs 1:3 (PHB2), PEG/O-CMCs 2:3 (PHB3), PEG/O-CMCs 3:3 (PHB4), PEG/N,O-CMCs 0:3 PHB5): (a) Temperature at initial concentration: 50ppm; agitation speed: 150 rpm; adsorbent dose: 0.5 mg.mL^{-1}; pH: 8.5; contact time: 180 min, (b) pH at initial concentration: 50 ppm; agitation speed: 150 rpm; adsorbent dose: 0.5 mg.mL^{-1}; temperature: 30 °C; contact time: 180 min, (c) Initial concentration: temperature: 30 °C; pH: 8.5; contact time: 180 min; agitation speed: 150 rpm; adsorbent dose: 0.5 mg.mL^{-1}, (d) Contact time at Initial concentration: 50 ppm; temperature: 30 °C; pH: 8.5; agitation speed: 150 rpm; adsorbent dose: 0.5 mg.mL^{-1}**

4.6.3 Effect of initial concentration on Fluoxetine adsorption efficiency and contact time

The effect of initial concentration in the range 10 to 100 ppm and contact time in the range 0 to 180 min under the respective experimental conditions (Initial concentration: temperature: 30 °C; pH: 8.5; contact time: 180 min; agitation speed: 150 rpm; adsorbent

dose: 0.5 mg.mL^{-1}) and (Contact time at Initial concentration: 50 ppm; temperature: 30 °C; pH: 8.5; agitation speed: 150 rpm; adsorbent dose: 0.5 mg.mL^{-1}) was investigated. The results are presented in Figure 4.6c and 4.6d. It can be seen that the FLX removal efficiency increases as the initial FLX concentration increases. This could be explained by the fact that increasing the initial FLX concentration would allow the boundary layer responsible for mass transfer resistance at the solution/adsorbent interface to be overcome. In addition, increasing concentration favors a concentration gradient which would also help to improve mass transfer rate due to the high mobility of FLX towards the surface of the beads. This high mobility of FLX is thought to be due to the driving force of intraparticle diffusion attributed to the concentration gradient. The higher the initial concentration of FLX, the greater the driving force of intraparticle diffusion, resulting in high diffusion rates [44].

On the other hand, FLX adsorption increases gradually in the first hour of contact (Figure 4.6d) and is not really spontaneous from the first few minutes, demonstrating that the mass transfer process took place in stages. This could be explained firstly by the resistance of the boundary layer to FLX transfer during film diffusion which results in slow film diffusion [45] and secondly by the swelling kinetics in distilled water which show that the diffusion of water molecules from the surface to the interior of the porous structure of the beads was not optimal from the first minutes of contact, providing evidence that a large proportion of the hydrophilic groups on the surface of the polymer chains were not in contact with water. This would indirectly support lower adsorption rates in the first minutes of contact of the hydrogel beads with the FLX solution. Similar behavior was observed in fast removal of Co (II) from aqueous solution using porous carboxymethyl chitosan beads [46]. After one hour's contact between the beads and the FLX solution, we observed that the amount of FLX adsorbed was between 67 and 77 mg.g^{-1} for all the hydrogel beads tested. This could be explained by excellent intraparticle diffusion both on the surface of macropores and on the walls of smaller pores, and rapid adsorption on vacant active sites. After 120 min of contact, we observed a slight increase in the quantity of FLX adsorbed up to 180 min, which could suggest that the porous structure having been saturated, the FLX had diffused towards the smaller pore sizes. The decrease in the adsorption capacity of the beads could be due to resistance to diffusion to even smaller

pore sizes, the equilibrium of water absorption in the beads and saturation of the vacant active sorption sites.

The results of the investigation of the effect of the experimental parameters temperature, pH, initial concentration and contact time on the capacity to eliminate FLX in aqueous solution show that the adsorbents PHB4 and PHB5 are the best candidates for the adsorption of FLX because they have the best elimination yield and excellent adsorption capacity under the experimental conditions tested. This could be explained by the presence of a large number of active sites on the PHB5 sample, as demonstrated by the degree of substitution of deprotonated carboxyl groups on its precursor polymer (N,O-CMCs), and the specific surface area of the PHB4 sample, as revealed by BET analysis, which would be linked to the addition of a higher ratio of PEG 2000 during their design.

4.6.4 Adsorption kinetics

The adsorption kinetics was studied using pseudo-first order (PFO), pseudo-second order (PSO), and intraparticle diffusion kinetic models (IPD). Their respective models are determined by equations 4.12, 4.13, 4.14 and 4.15. Figures 4.7a, and 4.7b show non-linear PFO and PSO curve fitting for adsorbent materials and the calculated kinetic parameters are listed in Table 4.3 and 4.4, respectively.

$$q_t = q_e(1 - e^{-k_1 t}) \qquad \text{Equation 4.12}$$

$$q_t = k_2 q_e^2 t / 1 + k_2 q_e t \qquad \text{Equation 4.13}$$

k_1 (min^{-1}): pseudo-first-order rate constant t (min): the contact time, k_2 ($g.mg^{-1}$ min^{-1}): pseudo-second order rate constant.

$$q_t = k_1 t^{1/2} \quad 0 \le t \le t_1$$ Equation 4.14

$$q_t - q_{t=t_1} = k_2 (t - t_1)^{1/2} \quad t_1 < t \le t_2$$ Equation 4.15

k_1 (mg.g $^{-1}$. min$^{-1/2}$) : intraparticle diffusion constant, k_2 (mg.g $^{-1}$. min$^{-1/2}$) : intraparticle diffusion constant.

The fitting parameters reported in Table 4.3 reveals that both PFO and PSO models have high determination coefficients ($R^2 > 0.99$) for all the adsorbent samples tested. Values of R^2_{Adj} are also very closed to R^2 indicating that the variations observed are similar for both models. The low *RMSE* values are also in agreement with the findings. The slight deviation between $q_{e.exp}$ and $q_{e.cal}$ of the PFO model compared to that of the PSO model indicates that the PFO slightly best fitted the experimental data.

Both PFO and PSO are empirical adsorption kinetics models that lack theoretical basis. However, they are extensively used to fit adsorption data for various types of adsorbent materials. High fitting correlations are very often reported in the literature describing some relationship to physisorption for PFO and chemisorption to PSO. In our case, since PFO and PSO fits were very similar, it is difficult to establish if the main adsorption mechanism involved is based on physisorption or chemisorption. Moreover, several authors are raising concerns about the validity of the chemisorption mechanism implying the formation of a chemical bond such as a covalent attachment between the adsorbate and the adsorbent [45,47,48]. Some authors point out that the adsorption mechanism cannot be attributed simply by fitting the PFO and PSO kinetic models. The physico-chemical parameters specific to the adsorbent and adsorbate, activation energy and thermodynamic data must be taken into account to determine the nature of the adsorption process. On the other hand, the IPD intraparticle diffusion model is probably involved in the mechanism driving the adsorption process [49]. Finally, both PFO and PSO models do not take mass transfer into consideration. This issue may be important in our case since our adsorbent materials are porous hydrogels spheres with internal pores reachable by the fluid and the contaminant. The mass transfer of the contaminants to adsorbents includes external/internal diffusion and adsorption onto active sites.

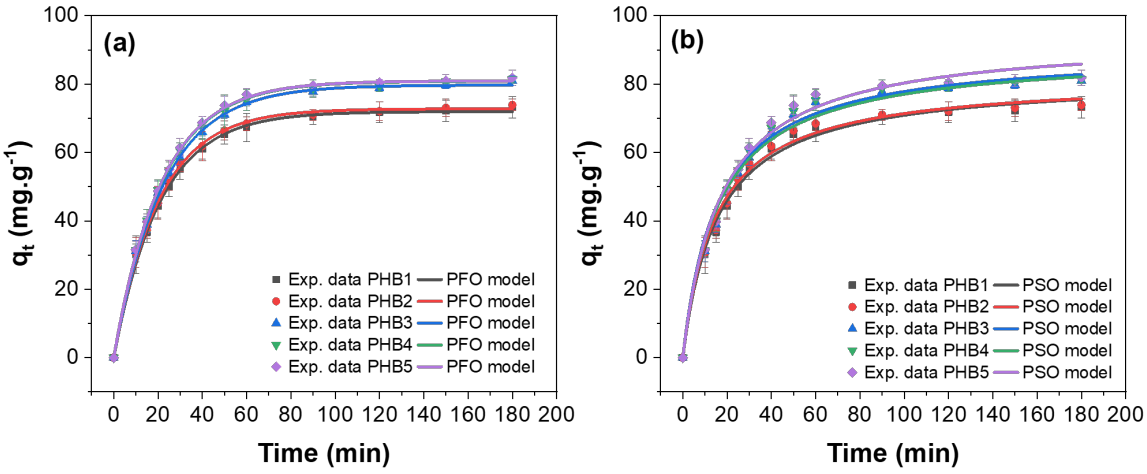

Figure 4.7 Kinetic curves fittings for PEG/O-CMCs 0:3 (PHB1), PEG/O-CMCs 1:3 (PHB2), PEG/O-CMCs 2:3 (PHB3), PEG/O-CMCs 3:3 (PHB4), PEG/N,O-CMCs 0:3 (PHB5) samples (25 mg), T = 30 °C, pH = 8.5, 150 rpm, (a) pseudo-first order (PFO), (b) pseudo-second order (PSO)

To understand the mechanism and enhance the adsorption performance of FLX for adsorbent materials, it is important to determine the rate-limiting step involved during the process. Modified forms of the intraparticle diffusion (IPD) model (Weber and Morris kinetics model) were used to fit experimental data [44]. To find the optimal statistical adsorption kinetics parameters, ten different divisions (10, 15, 20, 25, 30, 40, 50, 60, 90, 120 min) of the kinetics data groups based on the adsorption time range studied were tested. Figure 4.8 presents the non-linear IPD fits for adsorbent materials (PHB1, PHB2, PHB3, PHB4 and PHB5) at the optimal time division (60 min) and Table 4.4 presents the corresponding fitting parameters. Fitting results for other time divisions studied are presented in Table S2. Fig. S3 presents a representative example of time division selection for PHB1 adsorbent. Results show that the subdivision of the kinetic data having obtained the best statistical parameters corresponds to time intervals $0 \leq t \leq 60$ min and 60 min $\leq t \leq 180$ min for all adsorbents tested. It is observed that the intraparticle diffusion rate constant k_1 is higher in the first hour of FLX adsorption ($0 \leq t \leq 60$ min) for each adsorbent tested and the intraparticle diffusion rate constant k_2 is very lower than k_1. The major difference between k_1 and k_2 could be a consequence of the stages in the adsorption process on the surface and inside the adsorbents. The k_1 values are much higher because sorption on the surface of the macropores would be due to the maximum availability of active sites in the macropores, which would favor higher diffusion rates given the

electrostatic interactions between the hydrogel beads and the FLX. When these active sites have been saturated, the FLX diffuses into the smaller pore sizes and is adsorbed. The k_2 values would be due either to a resistance to diffusion into the smaller pore sizes or to a diffusion equilibrium created by the decrease in the concentration of FLX in solution. Similar observations have been made in the adsorption of organic compounds by activated carbons [50].

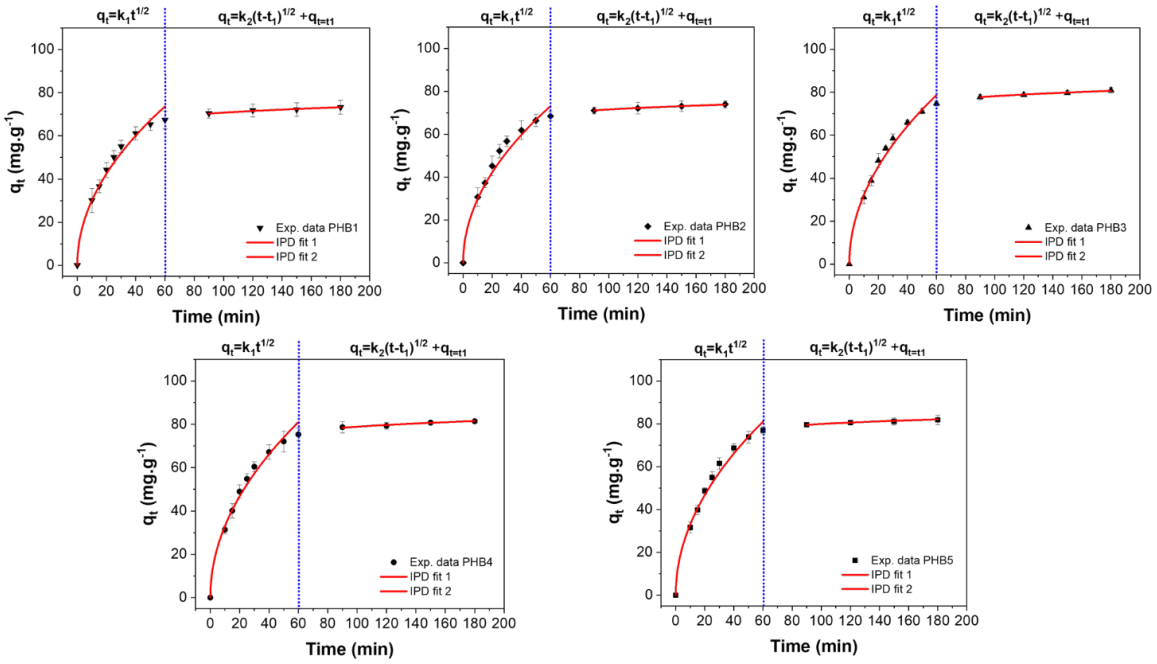

Figure 4.8 **IPD Kinetic curves fittings at optimal time division (60 min) for PEG/O-CMCs 0:3 (PHB1), PEG/O-CMCs 1:3 (PHB2), PEG/O-CMCs 2:3 (PHB3), PEG/O-CMCs 3:3 (PHB4), PEG/N,O-CMCs 0:3 (PHB5). Samples (25 mg), T = 30 °C, pH = 8.5, 150 rpm**

Table 4.3 Kinetic parameters for PFO and PSO models obtained by using the non-linear method

Kinetic Models	Parameters	PHB1	PHB2	PHB3	PHB4	PHB5
PFO	$q_{e\ exp}$ (mg.g^{-1})	73.21	73.92	80.99	81.41	81.81
	$q_{e\ cal}$ (mg.g^{-1})	71.97 (0.30)*	72.78 (0.35)	79.70 (0.27)	80.86 (0.17)	80.91 (0.15)
	K_1(min^{-1})	0.048 (0.001)	0.049 (0.001)	0.045 (0.001)	0.046 (0.001)	0.047 (0.001)
	R^2	0.9998	0.9995	0.9995	0.9997	0.9998
	R^2_{Adj}	0.9998	0.9995	0.9995	0.9997	0.9998
	RMSE	0.2187	0.3563	0.4763	0.4277	0.3567
PSO	$q_{e\ cal}$ (mg.g^{-1})	82.10 (1.53)	81.95 (1.46)	90.02 (1.60)	89.48 (0.74)	94.06 (1.66)
	K_2 x 10^{-4} (g.mg^{-1}.min^{-1})	7.71 (0.72)	8.26 (0.86)	7.10 (0.71)	6.93 (0.48)	6.21 (0.70)
	R^2	0.9978	0.9971	0.9943	0.9983	0.9953
	R^2_{Adj}	0.9977	0.9968	0.9938	0.9982	0.9948
	RMSE	0.6669	0.9043	1.6598	0.9780	1.6437

* Standard error in parentheses

Table 4.4 Kinetic parameters using modified forms of IPD models obtained by using the non-linear method at optimal time division (60 min)

Kinetic Models	Parameters	PHB1	PHB2	PHB3	PHB4	PHB5
IPD1	K_1 (mg.g^{-1}.min$^{-1/2}$)	9.508 (0.159)*	9.440 (0.214)	10.167 (0.149)	10.462 (0.188)	10.463 (0.166)
	R^2	0.9962	0.9923	0.9923	0.9950	0.9949
	R^2_{Adj}	0.9962	0.9923	0.9923	0.9950	0.9949
	RMSE	0.7882	1.2619	1.8626	1.0074	1.2860
IPD2	K_2 (mg.g^{-1}.min$^{-1/2}$)	0.539 (0.013)	0.489 (0.006)	0.538 (0.010)	0.565 (0.007)	0.466 (0.010)
	R^2	0.9675	0.9945	0.9759	0.9482	0.9517
	R^2_{Adj}	0.9675	0.9945	0.9759	0.9482	0.9517
	RMSE	0.0810	0.0546	0.1647	0.1922	0.1851

* Standard error in parentheses

4.6.5 Adsorption isotherm

The adsorption equilibrium study was completed by varying the initial concentration (10, 20, 30, 40, 50, 75 and 100 ppm) and temperature (30, 40, 50, 60 °C). The experimental parameters were set as follows: pH = 8.5, 180 min, 25 mg of beads, and 50 mL.

Numerous adsorption isotherm models have been studied in the literature to describe the relationship between the concentration of analytes in solution and the adsorbent under specific experimental conditions. The Langmuir and Freundlich models are the most widely used. They are classified as two-parameter empirical models. Their study makes it possible to identify the zone where the experimental equilibrium data are located. These models are based on assumptions that allow prediction of the nature of adsorption mechanisms. The Langmuir model (equation 4.16) assumes that adsorption of the adsorbate takes place on active sites of the same nature, with uniform adsorption energy. There is no interaction between the adsorbates and adsorption is monolayer on a homogeneous surface. The Freundlich model (equation 4.17) assumes multilayer adsorption on a heterogeneous surface with interactions between the adsorbates [30].

$$q_e = q_{\max} K_L C_e / 1 + K_L C_e \qquad \text{Equation 4.16}$$

$$q_e = K_F C_e^{1/n_F} \qquad \text{Equation 4.17}$$

K_L (L.mg^{-1}): Langmuir isotherm constant, q_{max} (mg.g^{-1}): maximum monolayer adsorption capacity, K_F (mg.g^{-1}): Freundlich isotherm constant n_F the heterogeneity factor in the Freundlich model. The linear and non-linear forms of the Langmuir and Freundlich models have been widely evaluated in the literature, but many studies have reported that the linearization process generates biases that render the parameters obtained invalid. This has contributed to the recommendation of the use of non-linear as a suitable approach for determining the specific constants of each adsorption isotherm model. Furthermore, in our specific case, the linear models do not fit the specific curves followed by the experimental adsorption data, which led us to carry out an analysis using the non-linear regression method. Figures 4.9 and 4.10 show the Langmuir and Freundlich non-linear fits of

experimental data for the sorbent materials at different temperatures. The fitting coefficients and statistical parameters for both models are listed in Table 4.5. It can be seen that the highest maximum monolayer adsorption capacity (q_{max}) was observed at a temperature of 30°C for all the adsorbents tested and ranged from 90.6 - 112.6 $mg.g^{-1}$. On the other hand, for each adsorbent tested, we observed that the q_{max} capacity and the Langmuir constant K_L decreased with increasing temperature. This is also observed for the Freundlich constant, which would suggest that this is an exothermic adsorption process that is assigned to physisorption [49]. We also note that q_{max} is better for the PHB4 and PHB5 adsorbents with values between 97.8 - 112.6 $mg.g^{-1}$ for PHB4 and 100.1 – 109.3 $mg.g^{-1}$ for PHB5 respectively. This could be justified by the greater substitution as revealed by the *DS* of the N,O-CMCs polymer precursor of the PHB5 adsorbents of the - CH_2COO^- groups which would have an electrostatic interaction with Fluoxetine and the greater specific surface area of the PHB4 adsorbents.

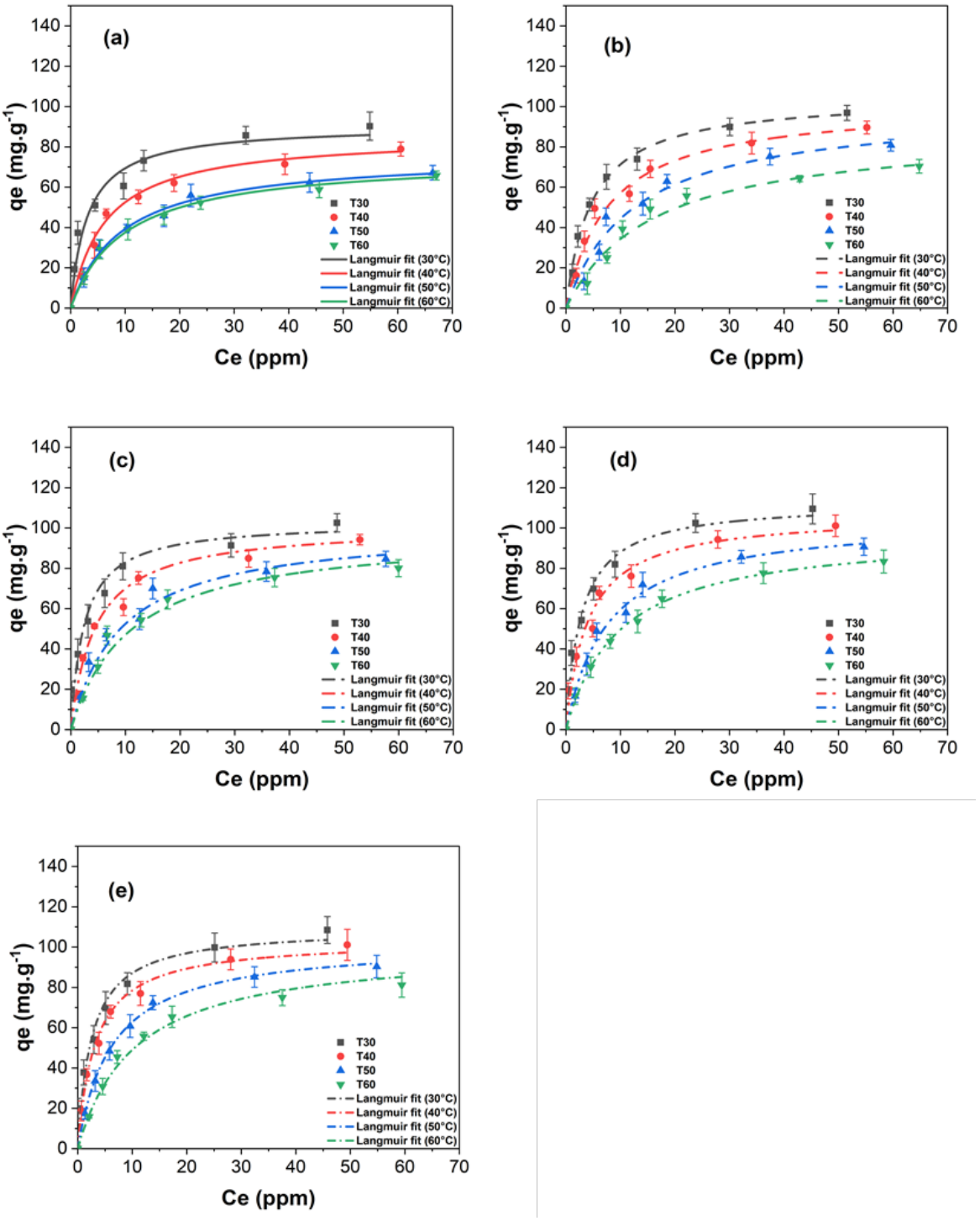

Figure 4.9 **Non-linear fit of the Langmuir isotherm model of FLX at various temperatures, pH = 8.5, 150 rpm and 25 mg of each adsorbents: a) PEG/O-CMCs 0:3 (PHB1), b) PEG/O-CMCs 1:3 (PHB2), c) PEG/O-CMCs 2:3 (PHB3), d) PEG/O-CMCs 3:3 (PHB4), and PEG/N,O-CMCs 0:3 PHB5**

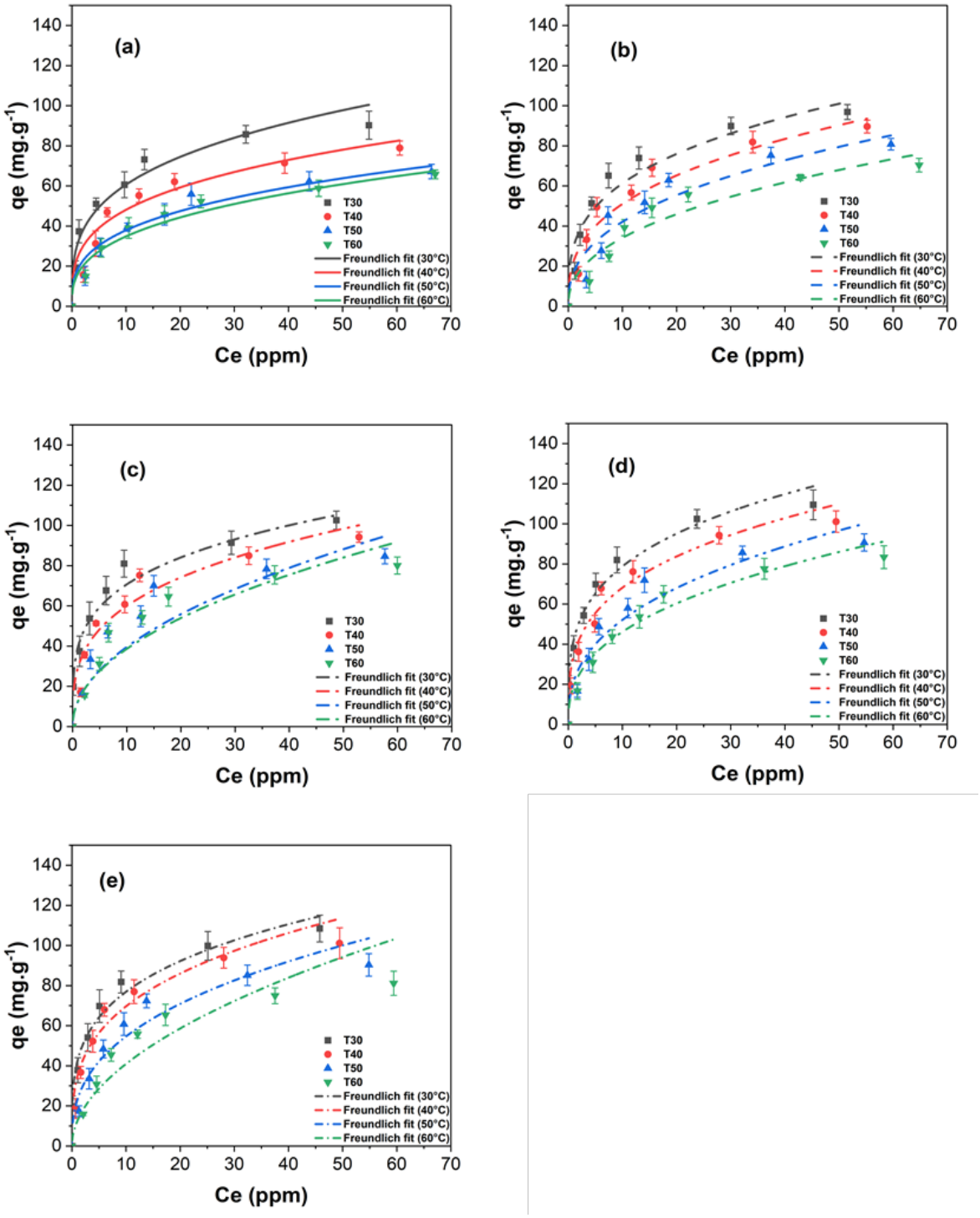

Figure 4.10 **Non-linear fit of the Freundlich isotherm model of FLX at various temperatures, pH=8.5, 150 rpm and 25 mg of each adsorbents: a) PEG/O-CMCs 0:3 (PHB1), b) PEG/O-CMCs 1:3 (PHB2), c) PEG/O-CMCs 2:3 (PHB3), d) PEG/O-CMCs 3:3 (PHB4), and PEG/N,O-CMCs 0:3 (PHB5)**

Table 4.5 Adsorption isotherms parameters for removal of FLX on porous hydrogel beads by using non-linear method

Samples		Langmuir					Freundlich				
	T (K)	q_{max} (mg/g)	K_L (L/mg)	R^2	R^2_{Adj}	*RMSE*	K_F $(mg/g)/(mg/L)^{1/n}$	*1/n*	R^2	R^2_{Adj}	*RMSE*
PHB1	303	90.656 (4.765)	0.326 (0.059)	0.9923	0.9910	1.099	30.634 (3.196)	0.296 (0.036)	0.9438	0.9325	1.533
	313	85.829 (3.989)	0.157 (0.022)	0.9946	0.9938	1.000	24.064 (4.098)	0.300 (0.053)	0.8753	0.8503	2.186
	323	76.213 (1.883)	0.106 (0.007)	0.9985	0.9985	0.399	18.004 (2.153)	0.323 (0.036)	0.9459	0.9350	1.105
	333	74.529 (1.410)	0.101 (0.007)	0.9989	0.9989	0.407	15.676 (2.568)	0.347 (0.043)	0.9561	0.9473	1.343
PHB2	303	104.838 (1.986)	0.212 (0.014)	0.9988	0.9987	0.502	29.962 (4.266)	0.310 (0.043)	0.9297	0.9156	2.002
	313	101.577 (4.459)	0.129 (0.018)	0.9954	0.9946	0.989	22.536 (4.235)	0.355 (0054)	0.9223	0.9067	2.109
	323	99.377 (6.522)	0.080 (0.016)	0.9920	0.9906	1.295	16.976 (4.488)	0.395 (0.074)	0.8904	0.8685	2.414
	333	88.449 (4.799)	0.063 (0.063)	0.9960	0.9952	1.042	12.735 (3.152)	0.428 (0.067)	0.9284	0.9141	1.962
PHB3	303	103.022 (7.067)	0.413 (0.150)	0.9838	0.9811	1.588	39.709 (3.043)	0.250 (0.023)	0.9787	0.9745	0.979
	313	101.126 (5.141)	0.225 (0.028)	0.9906	0.9890	1.901	29.515 (3.881)	0.307 (0.049)	0.8733	0.8480	4.351
	323	100.547 (5.045)	0.109 (0.008)	0.9914	0.9900	1.214	12.577 (1.133)	0.497 (0.041)	0.9157	0.8988	3.523
	333	97.927 (5.200)	0.092 (0.010)	0.9930	0.9919	1.055	12.696 (2.451)	0.483 (0.060)	0.8949	0.8948	3.088
PHB4	303	112.668 (8.779)	0.357 (0.098)	0.9843	0.9817	1.655	42.155 (2.315)	0.272 (0.019)	0.9829	0.9795	0.888
	313	106.801 (6.701)	0.251 (0.052)	0.9908	0.9892	1.407	34.398 (3.945)	0.297 (0.040)	0.9379	0.9255	1.834
	323	105.278 (3.363)	0.130 (0.013)	0.9976	0.9972	0.703	21.510 (4.222)	0.384 (0.058)	0.9297	0.9156	2.180
	333	97.883 (2.388)	0.103 (0.007)	0.9990	0.9989	0.342	18.952 (2.746)	0.386 (0.045)	0.9480	0.9376	1.284
PHB5	303	109.336 (8.391)	0.391 (0.096)	0.9847	0.9821	1.657	42.037 (2.790)	0.262 (0.022)	0.9824	0.9788	0.915
	313	103.536 (2.781)	0.313 (0.025)	0.9983	0.9980	0.546	34.530 (3.721)	0.305 (0.041)	0.9223	0.9069	1.818
	323	102.426 (1.674)	0.158 (0.008)	0.9994	0.9993	0.392	23.000 (4.245)	0.376 (0.060)	0.9118	0.8942	2.314
	333	100.186 (4.635)	0.095 (0.008)	0.9953	0.9945	0.852	12.424 (2.093)	0.518 (0.063)	0.9070	0.8884	3.730

* Standard error in parentheses

The analysis of the statistical parameters obtained following the non-linear optimization of the experimental data to the Langmuir and Freundlich isotherms shows that the coefficient of determination (R^2) of the Langmuir model is greater than that of the Freundlich model. In addition, the *RMSE* values of the Langmuir isotherm are smaller than those of the Freundlich isotherm, with the exception of the values obtained for samples PHB3, PHB4 and PHB5 at 30°C. Nevertheless, there is a small difference between the *RMSE* values at this temperature for these three adsorbents, with higher R^2_{Adj} values for the Langmuir model than for the Freundlich model. These observations, based on the error functions evaluated, suggest that the non-linear Langmuir model is the one that best fits the experimental data for FLX adsorption by the adsorbents tested.

As the experimental data is best described by the Langmuir model, it is appropriate to determine the separation factor R_L. This is a dimensionless quantity that depends in particular on the Langmuir constant K_L and the initial concentration of adsorbate in solution C_0 (equation 4.18).

$$R_L = 1 / (1 + K_L C_0)$$

Equation 4.18

This parameter is used to analyze the feasibility of the adsorption process. Adsorption is favorable if $0 < R_L < 1$, unfavorable if $R_L > 1$, linear if $R_L = 1$ and irreversible if $R_L = 0$ [45]. The results of calculating the separation factor R_L are shown in Table 4.6.

Table 4.6 Separation factor evaluated at different temperatures from the Langmuir constant and the initial concentration of Fluoxetine in solution (50ppm)

T(K)	PHB1		PHB2		PHB3		PHB4		PHB5	
	K_L (L/mg)	R_L	K_L (L/mg)	R_L	K_L (L/mg)	R_L	K_L (L/mg)	R_L	K_L (L/mg)	R_L
303	0.326	0.058	0.212	0.086	0.413	0.046	0.357	0.053	0.391	0.048
313	0.157	0.113	0.129	0.134	0.225	0.082	0.251	0.074	0.313	0.060
323	0.106	0.159	0.080	0.200	0.109	0.155	0.130	0.133	0.158	0.112
333	0.101	0.165	0.063	0.241	0.092	0.179	0.103	0.163	0.095	0.174

These are less than 1 ($0 < R_L < 1$) at all the temperatures tested and for all the adsorbents, revealing that the FLX adsorption process is favorable, which can be confirmed using the

Gibbs energy. This would indicate a good affinity between the surface of the hydrogel beads tested and FLX under the experimental conditions set during the adsorption tests.

4.6.6 Adsorption thermodynamics of the Fluoxetine

In order to better understand the adsorption process, it is essential to establish the adsorption mechanisms involved in the process. The study of adsorption isotherms is far from exhaustive for describing the adsorption process with the information it provides. It is necessary to supplement this study with an analysis of the thermodynamic parameters, which are highly revealing of the nature of the mechanisms involved in adsorption of the adsorbents. The thermodynamic parameters can be calculated according to the laws of thermodynamics using the following equations.

$$\Delta G^0 = -RT\,Ln(Kc) \qquad \text{Equation 4.19}$$

$$\Delta G^0 = \Delta H^0 - T\,\Delta S^0 \qquad \text{Equation 4.20}$$

$$Ln(Kc) = -\Delta H^0/RT + \Delta S^0/R \qquad \text{Equation 4.21}$$

R is the perfect gas constant (8.3144 J/mol.K), T is the temperature in Kelvin (K), $\Delta G°$ (kJ.mol^{-1}) is the Gibbs energy calculated from equation 4.19. The enthalpy $\Delta H°$ (kJ.mol^{-1}) and entropy ΔS° (J.mol^{-1}.K^{-1}) are determined from the Van't Hoff equation 4.21 by plotting Ln K_C versus 1/T where $\Delta H°/R$ is the slope and $\Delta S°/R$ is the y-intercept [51].

Dimensionless Kc is the thermodynamic equilibrium constant. Several studies in literature have shown that the determination of thermodynamic parameters depends on the value of K_C, which can be calculated from either the Langmuir constant K_L, the Freundlich constant K_F, the partition coefficient K_P and the distribution coefficient K_d [52,53]. The Langmuir model best describes our adsorption data, so the Langmuir constant K_L is appropriate for calculating the thermodynamic equilibrium constant K_C. For this purpose, S.K. Milonjić's calculation method [52] was applied to obtain dimensionless values of K_C in accordance with the International Union of Pure and Applied Chemistry (IUPAC) assumption. According to S.K. Milonjić, dimensionless K_C is obtained from K_L (L/mg) by multiplying

it by a factor of 10^6 which is the density of the solution with the assumption of the density of pure water equal to 1 g/mL [52].

$$K_C = 10^6 K_L \quad \text{Equation 4.22}$$

$$\Delta G^0 = -RT\,Ln(10^6 K_L) \quad \text{Equation 4.23}$$

$$Ln(10^6 K_L) = -\Delta G^0 / RT + \Delta S^0 / R \quad \text{Equation 4.24}$$

The results of the calculation of the thermodynamic parameters are presented in Table 4.7. It can be seen that the Gibbs energy is negative ($\Delta G° < 0$) at all temperatures tested and for the entire range of adsorbents tested. This indicates that the adsorption process is favorable and spontaneous.

Table 4.7 Thermodynamic parameters for adsorption of FLX

Samples	*T(K)*	K_L *(L/mg)*	*Kc*	*ΔG°* *(kJ/mol)*	*ΔH°* *(kJ/mol)*	*ΔS°* *(J/mol.K)*
PHB1	303	0.326	326 000	-31.97	-33.12	-5.04
	313	0.157	157 000	-31.13		
	323	0.106	106 000	-31.07		
	333	0.101	101 000	-31.90		
PHB2	303	0.212	212 000	-30.90	-32.00	-3.71
	313	0.129	129 000	-30.62		
	323	0.108	108 000	-31.12		
	333	0.063	63 000	-30.60		
PHB3	303	0.413	413 000	-32.60	-44.07	-38.4
	313	0.225	225 000	-32.07		
	323	0.109	109 000	-31.15		
	333	0.092	92 000	-31.64		
PHB4	303	0.357	357 000	-32.20	-37.08	-15.88
	313	0.251	251 000	-32.35		
	323	0.130	130 000	-31.62		
	333	0.102	102 000	-31.93		
PHB5	303	0.355	355 000	-32.20	-38.37	-19.20
	313	0.313	313 000	-32.93		
	323	0.159	159 000	-32.16		
	333	0.096	96 000	-31.76		

The negative enthalpy ($\Delta H° < 0$) suggests that the FLX adsorption process on our adsorbent materials is exothermic, which could justify the decrease in adsorption capacity

with increasing temperature, which is a specific characteristic of physisorption [49]. FLX adsorption is due to weak chemical bonds, mainly of the electrostatic interaction type, between the negatively charged ($-CH_2COO^-$) groups on the surface of the hydrogel beads and the positively charged FLX in solution, under experimental conditions where pH = 8.5 is lower than the pKa = 9.8 of FLX. Other weak interactions could also contribute to the adsorption of FLX, in particular hydrogen bonds and Van der Waals type bonds as well as hydrophobic interactions between FLX molecules due to their lipophilic nature (log p = 4.05) [9] and potentially Π interactions attributed to the electron density provided by the genipin.

Analysis of the entropy provides information on the organization of the adsorbate at the solution/adsorbent interface during adsorption [49]. The entropy values are negative ($\Delta S° < 0$) which suggests that the organization of the FLX at the solution/adsorbent interface during the adsorption process is much more ordered and therefore less random.

4.6.7 Schematic showing adsorption mechanism of the Fluoxetine by hydrogels tested under optimal conditions

The chemical quantification of the elements was carried out by Energy-dispersive X-ray spectroscopy (EDX) Oxford instrument X-Max 20 mm^2. EDX spectrum of samples reveal the presence of calcium in the freeze-dried hydrogels Figures 4.11a-e. This calcium comes from the $CaCl_2$ used to stabilise the structure of the gels three-dimensional network. The presence of calcium in the gels is thought to be due to a concentration gradient and the flow of water contained in the 70% ethanol through the network formed by the macromolecular chains, which binds to the hydrophilic groups. This encourages calcium ions to access the carboxyl groups on the polymer chains that are likely to interact with the FLX thanks to attractive electrostatic interactions. It could be assumed that washing the beads after processing would have removed only the calcium ions on the surface of the beads and those present in the interstices of the polymer network. Thus, the calcium ions identified in the EDX spectra would be those that interacted with the carboxyl groups and remained in the hydrogel structure even after washing.

The small difference observed between the adsorption capacity of PHB5 compared with the other beads could be explained by the greater presence of calcium ions in the polymer network, which interact with the active FLX adsorption sites, having a negative effect on the availability of carboxyl sites and lowering the capacity of this sample to bind FLX by attractive electrostatic interactions although it was prepared with N,O-CMCs. On the other hand, although the relaxation of polymer chains during bead swelling has created spaces through which solution diffuses, FLX would encounter diffusion resistance in small pore sizes, limiting their access to the active sites beyond these pores.

Following adsorption tests carried out under optimal adsorption conditions (temperature 30°C, pH 8.5, hydrogel mass 25 mg, solution volume 50 mL, FLX concentration 50 ppm, stirring speed 150 rpm and contact time 180 min) and given the negative effect of Ca^{2+} ions on the availability of carboxylate sites, the proposed Fig. 4.11f would be appropriate for describing the interactions that promote FLX adsorption on the porous hydrogels tested in this study.

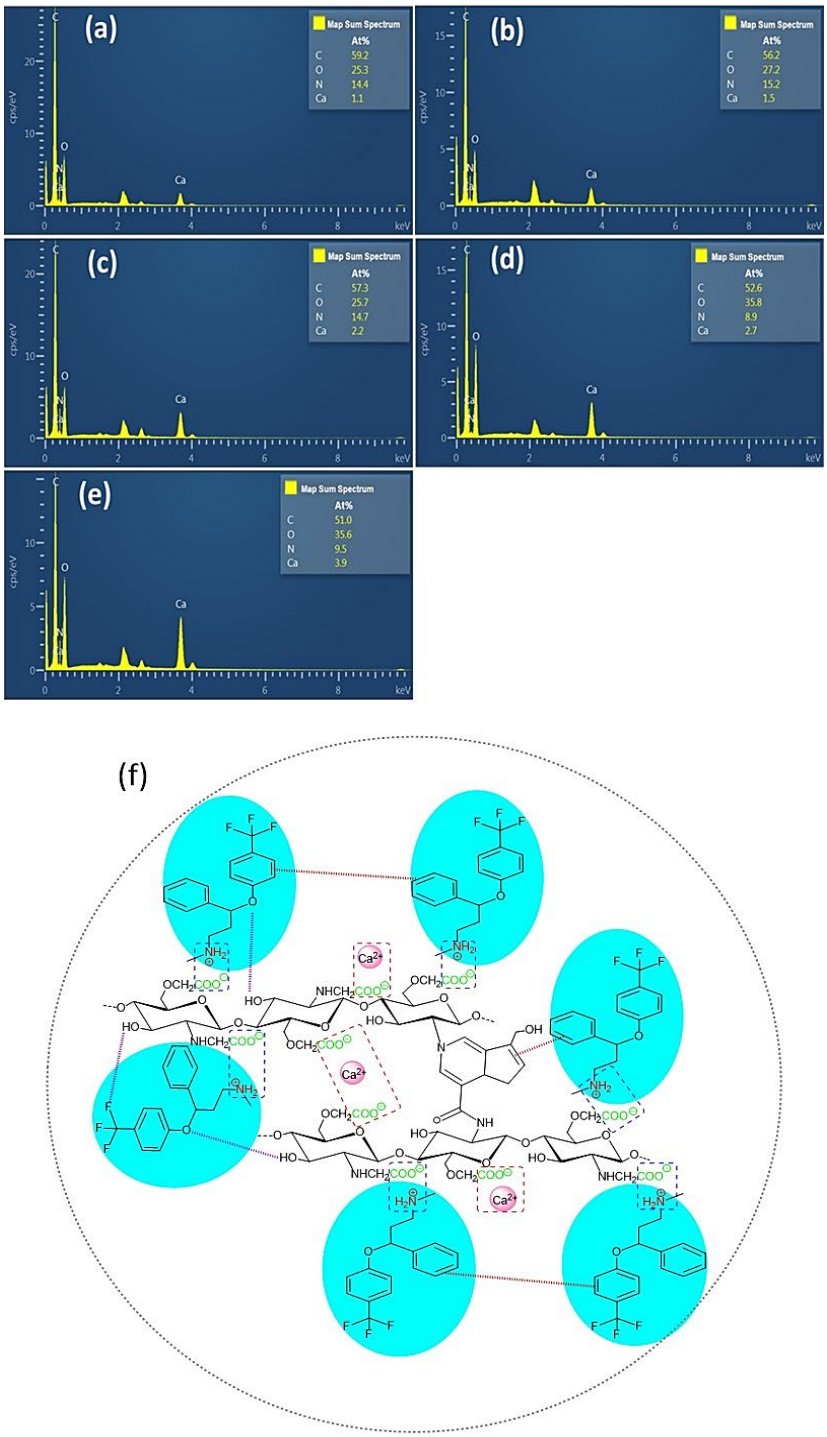

Figure 4.11 **EDS analysis of calcium loaded in the hydrogel beads: a) PHB1, b) PHB2, c) PHB3, d) PHB4, e) PHB5, and f) possible interactions between carboxymethyl chitosan hydrogels and Fluoxetine under optimal adsorption conditions**

4.6.8 Reusability

The regenerative capacity of the adsorbent is a key factor that could significantly reduce their operating costs. To investigate the reusability of the bead materials, desorption experiments were carried out with PHB4 and PHB5 samples by immersing them in ethanol and methanol at pH = 2 to 6, for 24h at 30°C under low magnetic stirring. After desorption, the beads were washed extensively with 1N NaOH solution and then lyophilized. Five adsorption/desorption cycles were performed.

The data of desorption tests presented in Table 4.8 show that methanol at pH = 2 is the best desorption solvent for FLX. Figure 4.12 shows that the adsorption capacity decreases with the number of adsorption/desorption cycles but remains above 65 % after 5 cycles. However, deformation of the beads and loss of mass was observed after each regeneration test.

Table 4.8 Fluoxetine recovered (%)

		pH				
Sample	**Solvent**	2	3	4	5	6
PHB4	Ethanol 100 % Methanol 100 %	59.71 96.05	59.22 94.87	6.80 11.10	0.40 1.80	0.20 0.70
PHB5	Ethanol 100 % Methanol 100 %	78.70 97.46	78.02 96.87	72.35 84.89	53.29 65.00	3.52 14.17

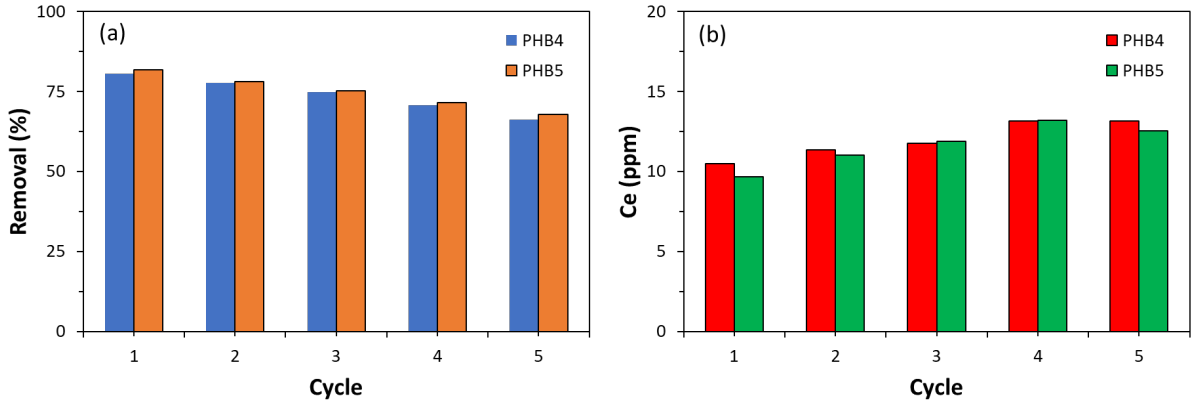

Figure 4.12 Adsorption cycles of FLX (50 ppm) by PEG/O-CMCs 3:3 (PHB4) and PEG/N,OCMCs 0:3 (PHB5) (25 mg of beads, 180 min contact time at 30 °C) (a) and desorption cycles of PHB4 and PHB5 samples on Methanol 100%, pH = 2, 24 h and 30 °C (b)

4.6.9 Comparison with other sorbents developed in the literature

The q_{ecal} values of the PHB4 and PHB5 adsorbents were compared to the adsorption results of other biobased adsorbent materials identified in the literature (Table 4.9).

Table 4.9 Comparison of different existing adsorbents used for FLX removal

	qmax ***(mg.g^{-1})***	**pH**	**Initial concentration *(ppm)***	**Temperature *°C***	**References**
Commercial adsorbents					
Activated carbon PBFG4	96.2	-	10	25	[54]
Granular activated carbon (GAC)	233.5	9	5	25	[55]
Biosorbents					
PS800-10KOH	120.4	-	10	25	[54]
PS800-10NaOH	191.6	-	10	25	[54]
PS800-10$ZnCl_2$	136.6	-	10	25	[54]
Nanocomposite XCM	90.9	7.35	25	28	[56]
Nanocomposite PCM	114.9	7.35	25	28	[56]
Nanofiber AL:PVA 50:50	29	-	50	-	[29]
PHB4 (PEG/ O-CMCs, 3:3)	112.6	8.5	50	30	This work
PHB5(PEG/N,O-CMCs 0:3)	109.3	8.5	50	30	This work

We observed that our adsorbents are viable and could be more attractive than other bio-materials tested for the removal of FLX in aqueous solution. They could be a promising

alternative given their adsorption capacity, their easy regeneration from an easily recyclable solvent, which could minimize the cost of use.

4.7 Conclusions

In this work, porous hydrogel beads were designed by the electrostatic extrusion method from chitosan modified by carboxymethylation and stabilized by $CaCl_2$ and genipin. Characterization of the materials confirmed the substitution of $-CH_2COO^-$ groups on the polymer chains, the presence of interconnected pore networks on the surface of the beads and a specific surface area that improved as a function of the PEG 2000/polymer ratio. The swelling study has been completed, and it was determined that the profiles obtained corresponded to the diffusion of water into the gel structure and the relaxation of the polymer chains. Solvent diffusion is of the Fickian type and controls the swelling process. The effect of the parameters (temperature, pH, contact time and initial concentration) has been investigated during the FLX adsorption tests.

The results revealed that the pH: 8.5 of the FLX solution was ideal for optimal adsorption of FLX, increasing the temperature resulted in a decrease in the removal efficiency showing that the adsorption process was exothermic. Increasing concentration improved sorption rates because the resistance of the boundary layer to mass transfer was overcome by the driving force attributed to the concentration gradient at the solution/adsorbent interface. The study of contact time showed that the adsorption process was not really spontaneous but took place in stages and that the slow external diffusion was due to the boundary layer's resistance to mass transfer in the first few minutes of contact.

The non-linear regression method was used to optimize the kinetic models and adsorption isotherms. Error functions were used to discuss the choice of models that best fit the experimental data. The study of adsorption kinetics revealed that the first-order kinetic model best described the kinetic data. The study of the sectional intraparticle diffusion model showed that the subdivisions with the best statistical parameters for all adsorbents were $0 \leq t \leq 60$ min and 60 min $\leq t \leq 180$ min. The intraparticle diffusion constant K_1 of the first section is very large compared to that of the second section K_2 suggesting sorption by electrostatic interactions at the macropore surface in the first section and diffusion

equilibrium in the second. Analysis of the adsorption isotherms showed that the maximum monolayer adsorption capacity of the adsorbents was between 90.6 and 112.9 $mg.g^{-1}$ when the temperature was 30°C. q_{max} and K_L decreased with increasing temperature, suggesting that the FLX adsorption mechanism is physisorption. The Langmuir model was in good agreement with the experimental adsorption data.

The thermodynamic analysis of the adsorption of FLX on our adsorbent materials reveals that the adsorption process is favorable at all the temperatures tested, since $0 < R_L < 1$ and $\Delta G° < 0$. The enthalpy is negative, which indicates that the adsorption process is exothermic, and the negative entropy indicates that the arrangement of the adsorbates is less random at the adsorbent solution interface. Regeneration tests showed that even after five adsorption/desorption cycles, the PHB4 and PHB5 adsorbents had a FLX adsorption capacity of more than 65%. It would be wise in our future work to investigate the possibility of substituting other reactive functions on the free amine groups of the O-CMCs and N,OCMCs polymers in order to optimize the interactions with FLX to increase the adsorption capacity of the beads.

4.8 Acknowledgments

The authors would like to thank the natural sciences and engineering research council of Canada (NSERC) for financial support and the University of Quebec at Trois-Rivières for providing the space, materials and equipment to complete this research work.

Declaration of Competing Interest

The authors have no financial or non-financial interests to disclose.

4.9 References

[1] C. Castillo-Zacarías, M.E. Barocio, E. Hidalgo-Vázquez, J.E. Sosa-Hernández, L. Parra-Arroyo, I.Y. López-Pacheco, D. Barceló, H.N.M. Iqbal, R. Parra-Saldívar, Antidepressant drugs as emerging contaminants: Occurrence in urban and non-urban waters and analytical methods for their detection, Science of the Total Environment 757 (2021). https://doi.org/10.1016/j.scitotenv.2020.143722.

[2] M.P. Schlüsener, P. Hardenbicker, E. Nilson, M. Schulz, C. Viergutz, T.A. Ternes, Occurrence of venlafaxine, other antidepressants and selected metabolites in the Rhine catchment in the face of climate change, Environmental Pollution 196 (2015) 247–256. https://doi.org/10.1016/j.envpol.2014.09.019.

[3] A. Singh, D. Saidulu, A.K. Gupta, V. Kubsad, Occurrence and fate of antidepressants in the aquatic environment: Insights into toxicological effects on the aquatic life, analytical methods, and removal techniques, J Environ Chem Eng 10 (2022) 109012. https://doi.org/10.1016/J.JECE.2022.109012.

[4] E.M. Melchor-Martínez, M.G. Jiménez-Rodríguez, M. Martínez-Ruiz, S.A. Peña-Benavides, H.M.N. Iqbal, R. Parra-Saldívar, J.E. Sosa- Hernández, Antidepressants surveillance in wastewater: Overview extraction and detection, Case Studies in Chemical and Environmental Engineering 3 (2021) 100074. https://doi.org/10.1016/j.cscee.2020.100074.

[5] M. Pelli, V.P. Connaughton, Chronic exposure to environmentally-relevant concentrations of fluoxetine (Prozac) decreases survival, increases abnormal behaviors, and delays predator escape responses in guppies, Chemosphere 139 (2015) 202–209. https://doi.org/10.1016/J.CHEMOSPHERE.2015.06.033.

[6] A. Singh, D. Saidulu, A.K. Gupta, V. Kubsad, Occurrence and fate of antidepressants in the aquatic environment: Insights into toxicological effects on the aquatic life, analytical methods, and removal techniques, J Environ Chem Eng 10 (2022) 109012. https://doi.org/10.1016/J.JECE.2022.109012.

[7] C.G. Davey, A.M. Chanen, S.E. Hetrick, S.M. Cotton, A. Ratheesh, G.P. Amminger, J. Koutsogiannis, M. Phelan, E. Mullen, B.J. Harrison, S. Rice, A.G. Parker, O.M. Dean, A. Weller, M. Kerr, A.L. Quinn, L. Catania, N. Kazantzis, P.D. McGorry, M. Berk, The addition of fluoxe-tine to cognitive behavioural therapy for youth depression (YoDA-C): a randomised, double-blind, placebo-controlled, multicentre clinical trial, Lancet Psychiatry 6 (2019) 735–744. https://doi.org/10.1016/S2215-0366(19)30215-9.

[8] A. Lajeunesse, S.A. Smyth, K. Barclay, S. Sauvé, C. Gagnon, Distribution of antidepressant residues in wastewater and biosolids following different treatment processes by municipal wastewater treatment plants in Canada, Water Res 46 (2012) 5600–5612. https://doi.org/10.1016/J.WATRES.2012.07.042.

[9] N. Diaz-Camal, J.D. Cardoso-Vera, H. Islas-Flores, L.M. Gómez-Oliván, A. Mejía-García, Consumption and occurrence of antidepressants (SSRIs) in pre- and post-COVID-19 pandemic, their environmental impact and innovative removal methods: A review, Science of the Total Environment 829 (2022). https://doi.org/10.1016/j.scitotenv.2022.154656.

[10] P. Sehonova, Z. Svobodova, P. Dolezelova, P. Vosmerova, C. Faggio, Effects of waterborne antidepressants on non-target animals living in the aquatic environment: A review, Science of The Total Environment 631–632 (2018) 789–794. https://doi.org/10.1016/J.SCITOTENV.2018.03.076.

[11] B. Campos, C. Rivetti, T. Kress, C. Barata, H. Dircksen, Depressing Antidepressant: Fluoxetine Affects Serotonin Neurons Causing Adverse Reproductive Responses in Daphnia magna, Envi-ron Sci Technol 50 (2016) 6000–6007. https://doi.org/10.1021/ACS.EST.6B00826/SUPPL_FILE/ES6B00826_SI_001.PDF.

[12] J. Hollman, J.A. Dominic, G. Achari, Degradation of pharmaceutical mixtures in aqueous solutions using UV/peracetic acid process: Kinetics, degradation pathways and comparison with UV/H2O2, Chemosphere 248 (2020) 125911. https://doi.org/10.1016/J.CHEMOSPHERE.2020.125911.

[13] R.A. Osawaa, B.T. Barrocas, O.C. Monteiro, M.C. Oliveira, M.H. Florêncio, Visible light photocatalytic degradation of amitriptyline using cobalt doped titanate nanowires: Kinetics and characterization of transformation products, J Environ Chem Eng 8 (2020) 103585. https://doi.org/10.1016/J.JECE.2019.103585.

[14] S. Kharel, M. Stapf, U. Miehe, M. Ekblad, M. Cimbritz, P. Falås, J. Nilsson, R. Sehlén, K. Bester, Ozone dose dependent formation and removal of ozonation products of pharmaceuticals in pilot and full-scale municipal wastewater treatment plants, Science of The Total Environment 731 (2020) 139064. https://doi.org/10.1016/J.SCITOTENV.2020.139064.

[15] C. Pan, F. Zhu, M. Wu, L. Jiang, X. Zhao, M. Yang, Degradation and toxicity of the antidepressant fluoxetine in an aqueous system by UV irradiation, Chemosphere 287 (2022) 132434. https://doi.org/10.1016/J.CHEMOSPHERE.2021.132434.

[16] F. Akbari Beni, A. Gholami, A. Ayati, M. Niknam Shahrak, M. Sillanpää, UV-switchable phosphotungstic acid sandwiched between ZIF-8 and Au nanoparticles to improve simultaneous adsorption and UV light photocatalysis toward tetracycline degradation, Microporous and Mesoporous Materials 303 (2020) 110275. https://doi.org/10.1016/J.MICROMESO.2020.110275.

[17] Y. Lu, Z. Wang, X. kun Ouyang, C. Ji, Y. Liu, F. Huang, L.Y. Yang, Fabrication of cross-linked chitosan beads grafted by polyethylenimine for efficient adsorption of diclofenac sodium from water, Int J Biol Macromol 145 (2020) 1180–1188. https://doi.org/10.1016/j.ijbiomac.2019.10.044.

[18] M. Pooresmaeil, H. Namazi, Positively charged covalent organic framework modified magnetic chitosan as a smart device for efficient diclofenac sodium removal from water, Chemical Engineering Journal 452 (2023). https://doi.org/10.1016/j.cej.2022.139557.

[19] A. Nezhadali, S.E. Koushali, F. Divsar, Synthesis of polypyrrole - Chitosan magnetic nanocomposite for the removal of carbamazepine from wastewater: Adsorption isotherm and kinetic study, J Environ Chem Eng 9 (2021). https://doi.org/10.1016/j.jece.2021.105648.

[20] A.A. Wani, A.M. Khan, Y.K. Manea, M. Singh, Facile synthesis of layered superparamagnetic Fe3O4-MoS2 nanosheets on chitosan for efficient removal of

chromium and ciprofloxacin from aqueous solutions, Journal of Water Process Engineering 51 (2023). https://doi.org/10.1016/j.jwpe.2022.103340.

[21] E.W.E.S. Shahrin, N.A.H. Narudin, N.N.M. Shahri, M. Nur, J.W. Lim, M.R. Bilad, A.H. Mahadi, J. Hobley, A. Usman, A comparative study of adsorption behavior of rifampicin, streptomycin, and ibuprofen contaminants from aqueous solutions onto chitosan: Dynamic interactions, kinetics, diffusions, and mechanisms, Emerg Contam 9 (2023). https://doi.org/10.1016/j.emcon.2022.100199.

[22] A.G.B. Pereira, F.H.A. Rodrigues, A.T. Paulino, A.F. Martins, A.R. Fajardo, Recent advances on composite hydrogels designed for the remediation of dye-contaminated water and wastewater: A review, J Clean Prod 284 (2021). https://doi.org/10.1016/j.jclepro.2020.124703.

[23] L. Weerasundara, B. Gabriele, A. Figoli, Y.S. Ok, J. Bundschuh, Hydrogels: Novel materials for contaminant removal in water—A review, Crit Rev Environ Sci Technol 51 (2021) 1970–2014. https://doi.org/10.1080/10643389.2020.1776055.

[24] H. Karimi-Maleh, A. Ayati, R. Davoodi, B. Tanhaei, F. Karimi, S. Malekmohammadi, Y. Orooji, L. Fu, M. Sillanpää, Recent advances in using of chitosan-based adsorbents for removal of phar-maceutical contaminants: A review, J Clean Prod 291 (2021). https://doi.org/10.1016/J.JCLEPRO.2021.125880.

[25] S.A. Qamar, M. Ashiq, M. Jahangeer, A. Riasat, M. Bilal, Chitosan-based hybrid materials as adsorbents for textile dyes–A review, Case Studies in Chemical and Environmental Engineering 2 (2020) 100021. https://doi.org/10.1016/J.CSCEE.2020.100021.

[26] B. Tanhaei, A. Ayati, M. Lahtinen, M. Sillanpää, Preparation and characterization of a novel chitosan/Al2O3/magnetite nanoparticles composite adsorbent for kinetic, thermodynamic and isotherm studies of Methyl Orange adsorption,

Chemical Engineering Journal 259 (2015) 1–10. https://doi.org/10.1016/J.CEJ.2014.07.109.

[27] D.R. Kioussis, P. Kofinas, Characterization of anion diffusion in polymer hydrogels used for wastewater remediation, Polymer (Guildf) 46 (2005) 9342–9347. https://doi.org/10.1016/j.polymer.2005.07.045.

[28] F.G.L. Medeiros Borsagli, A.A.P. Mansur, P. Chagas, L.C.A. Oliveira, H.S. Mansur, O-carboxymethyl functionalization of chitosan: Complexation and adsorption of Cd (II) and Cr (VI) as heavy metal pollutant ions, React Funct Polym 97 (2015) 37–47. https://doi.org/10.1016/j.reactfunctpolym.2015.10.005.

[29] A. Camiré, J. Espinasse, B. Chabot, A. Lajeunesse, Development of electrospun lignin nanofibers for the adsorption of pharmaceutical contaminants in wastewater, Environmental Science and Pollution Research 27 (2020) 3560–3573. https://doi.org/10.1007/s11356-018-3333-z.

[30] J. Wang, X. Guo, Adsorption isotherm models: Classification, physical meaning, application and solving method, Chemosphere 258 (2020). https://doi.org/10.1016/j.chemosphere.2020.127279.

[31] A. Fiamingo, S.P. Campana-Filho, Structure, morphology and properties of genipin-crosslinked carboxymethylchitosan porous membranes, Carbohydr Polym 143 (2016) 155–163. https://doi.org/10.1016/j.carbpol.2016.02.016.

[32] G.Q. Huang, X.N. Han, J.X. Xiao, L.Y. Cheng, Effects of coacervation acidity on the genipin crosslinking action and intestine-targeted delivery potency of the O-carboxymethyl chitosan–gum arabic coacervates, International Journal of Polymeric Materials and Polymeric Biomaterials 66 (2017) 89–96. https://doi.org/10.1080/00914037.2016.1190924.

[33] S.F. Hisham, S.H. Kasim, S. Abu Bakar, S.N. Mohd Sabri, A. Mastor, A.Y. Abdul Manaf, N. Abu, K. Noorsal, A.H. Abdul Rashid, Cross-Linked Effects by Genipin

on Physicochemical Properties of Chitosan Film, Adv Mat Res 1133 (2016) 108–112. https://doi.org/10.4028/www.scientific.net/amr.1133.108.

[34] F.L. Mi, S.S. Shyu, C.K. Peng, Characterization of ring-opening polymerization of genipin and pH-dependent cross-linking reactions between chitosan and genipin, J Polym Sci A Polym Chem 43 (2005) 1985–2000. https://doi.org/10.1002/pola.20669.

[35] S. Li, X. Liu, T. Zou, W. Xiao, Removal of cationic dye from aqueous solution by a macroporous hydrophobically modified poly(acrylic acid-acrylamide) hydrogel with enhanced swelling and adsorption properties, Clean (Weinh) 38 (2010) 378–386. https://doi.org/10.1002/clen.200900220.

[36] M. Zheng, B. Han, Y. Yang, W. Liu, Synthesis, characterization and biological safety of O-carboxymethyl chitosan used to treat Sarcoma 180 tumor, Carbohydr Polym 86 (2011) 231–238. https://doi.org/10.1016/j.carbpol.2011.04.038.

[37] M. Lavertu, Z. Xia, A.N. Serreqi, M. Berrada, A. Rodrigues, D. Wang, M.D. Buschmann, A. Gupta, A validated 1H NMR method for the determination of the degree of deacetylation of chitosan, J Pharm Biomed Anal 32 (2003) 1149–1158. https://doi.org/10.1016/S0731-7085(03)00155-9.

[38] M. Kaya, Y.S. Cakmak, T. Baran, M. Asan-Ozusaglam, A. Mentes, K.O. Tozak, New chitin, chitosan, and O-carboxymethyl chitosan sources from resting eggs of Daphnia longispina (Crus-tacea); with physicochemical characterization, and antimicrobial and antioxidant activities, Bio-technology and Bioprocess Engineering 19 (2014) 58–69. https://doi.org/10.1007/s12257-013-0488-9.

[39] J. Du, Y. Lo Hsieh, Nanofibrous membranes from aqueous electrospinning of carboxymethyl chitosan, Nanotechnology 19 (2008). https://doi.org/10.1088/0957-4484/19/12/125707.

[40] W. Luo, Z. Bai, Y. Zhu, Fast removal of Co(ii) from aqueous solution using porous carboxyme-thyl chitosan beads and its adsorption mechanism, RSC Adv 8 (2018) 13370–13387. https://doi.org/10.1039/C7RA13064C.

[41] H. Farhadnejad, S.A. Mortazavi, M. Erfan, B. Darbasizadeh, H. Motasadizadeh, Y. Fatahi, Facile preparation and characterization of pH sensitive Mt/CMC nanocomposite hydrogel beads for propranolol controlled release, Int J Biol Macromol 111 (2018) 696–705. https://doi.org/10.1016/j.ijbiomac.2018.01.061.

[42] R.M.P. Karlsson, P.T. Larsson, T. Pettersson, L. Wågberg, Swelling of Cellulose-Based Fibrillar and Polymeric Networks Driven by Ion-Induced Osmotic Pressure, Langmuir 36 (2020) 12261–12271. https://doi.org/10.1021/acs.langmuir.0c02051.

[43] A. Zdravković, L. Nikolić, S. Ilić-Stojanović, V. Nikolić, S. Najman, Ž. Mitić, A. Ćirić, S. Petrović, The removal of heavy metal ions from aqueous solutions by hydrogels based on N-isopropylacrylamide and acrylic acid, Polymer Bulletin 75 (2018) 4797–4821. https://doi.org/10.1007/s00289-018-2295-0.

[44] J. Wang, X. Guo, Rethinking of the intraparticle diffusion adsorption kinetics model: Interpretation, solving methods and applications, Chemosphere 309 (2022). https://doi.org/10.1016/j.chemosphere.2022.136732.

[45] H.N. Tran, S.J. You, A. Hosseini-Bandegharaei, H.P. Chao, Mistakes and inconsistencies regarding adsorption of contaminants from aqueous solutions: A critical review, Water Res 120 (2017) 88–116. https://doi.org/10.1016/j.watres.2017.04.014.

[46] W. Luo, Z. Bai, Y. Zhu, Fast removal of Co(ii) from aqueous solution using porous carboxymethyl chitosan beads and its adsorption mechanism, RSC Adv 8 (2018) 13370–13387. https://doi.org/10.1039/c7ra13064c.

[47] M.A. Hubbe, Insisting upon Meaningful Results from Adsorption Experiments, Separation and Purification Reviews 51 (2022) 212–225. https://doi.org/10.1080/15422119.2021.1888299.

[48] M.A. Hubbe, S. Azizian, S. Douven, Implications of Apparent Pseudo-Second-Order Adsorption Kinetics onto Cellulosic Materials: A Review, n.d.

[49] H.N. Tran, S.J. You, H.P. Chao, Thermodynamic parameters of cadmium adsorption onto orange peel calculated from various methods: A comparison study, J Environ Chem Eng 4 (2016) 2671–2682. https://doi.org/10.1016/j.jece.2016.05.009.

[50] C. Valderrama, X. Gamisans, X. de las Heras, A. Farrán, J.L. Cortina, Sorption kinetics of polycyclic aromatic hydrocarbons removal using granular activated carbon: Intraparticle diffusion coefficients, J Hazard Mater 157 (2008) 386–396. https://doi.org/10.1016/j.jhazmat.2007.12.119.

[51] J. López-Luna, L.E. Ramírez-Montes, S. Martinez-Vargas, A.I. Martínez, O.F. Mijangos-Ricardez, · María, C.A. González-Chávez, R. Carrillo-González, · Fernando, A. Solís-Domínguez, C. Cuevas-Díaz, · Virgilio Vázquez-Hipólito, Linear and nonlinear kinetic and iso-therm adsorption models for arsenic removal by manganese ferrite nanoparticles, SN Appl Sci 1 (2019). https://doi.org/10.1007/s42452-019-0977-3.

[52] S.K. Milonjić, Comments on "Removal of uranium (VI) from aqueous solution by adsorption of hematite", by X. Shuibo, Z. Chun, Z. Xinghuo, Y. Jing, Z. Xiaojian, W. Jingsong., J Environ Radioact 100 (2009) 921–922. https://doi.org/10.1016/J.JENVRAD.2009.06.014.

[53] X. Zhou, X. Zhou, The Unit problem in the thermodynamic calculation of adsorption using the langmuir equation, Chem Eng Commun 201 (2014) 1459–1467. https://doi.org/10.1080/00986445.2013.818541.

[54] G. Jaria, V. Calisto, M.V. Gil, M. Otero, V.I. Esteves, Removal of fluoxetine from water by adsorbent materials produced from paper mill sludge, J Colloid Interface Sci 448 (2015) 32–40. https://doi.org/10.1016/J.JCIS.2015.02.002.

[55] B. Silva, M. Martins, M. Rosca, V. Rocha, A. Lago, I.C. Neves, T. Tavares, Waste-based biosorbents as cost-effective alternatives to commercial adsorbents for the retention of fluoxetine from water, Sep Purif Technol 235 (2020). https://doi.org/10.1016/j.seppur.2019.116139.

[56] H.H. Farghal, M. Nebsen, M.M.H. El-Sayed, Eco-friendly Biopolymer/Activated Charcoal Magnetic Nanocomposites with Enhanced Stability and Adsorption Properties for Water Treatment Applications, J Polym Environ 31 (2023) 5338–5354. https://doi.org/10.1007/s10924-023-02959-y.

Chapitre 5 - Article 2

5.1 Avant-propos

Le titre du deuxième article scientifique est: «Adsorption of fluoxetine in aqueous environments: Development of macroporous cryogels based on sodium poly(acrylate) and carboxymethyl chitosan». Il a été publié dans la revue scientifique Reactive and Functional Polymers en 2024.

Les auteurs et leurs coordonnées correspondantes sont, dans l'ordre:

Gilbert Romeo Nkana Nkana : Étudiant au Doctorat en sciences et génie des matériaux lignocellulosiques, Institut d'Innovations en Écomatériaux, Écoproduits et Écoénergies à base de biomasse (I2E3), Université du Québec à Trois-Rivières, 3351 Boulevard des Forges, CP.500, Trois-Rivières, Québec, Canada, G9A 5H7
Courriel : Gilbert.Nkana@uqtr.ca

Phuong Nguyen-Tri, Ph.D. : Directeur de thèse
Professeur au Département de biochimie, chimie, physique et sciences forensiques et chercheuse à l'Institut de recherche sur l'hydrogène, Université du Québec à Trois-Rivières, 3351 Boulevard des Forges, C.P. 500, Trois-Rivières, Québec, Canada, G9A 5H7.
Courriel: Phuong.Nguyen-Tri@uqtr.ca

Bruno Chabot, Ph.D. Co-Directeur de thèse et auteur pour la correspondance Institut d'Innovation en Écomatériaux, Écoproduits et Écoénergies à basse de biomasse, Université du Québec à Trois-Rivières, 3351 Boulevard des Forges, C.P. 500, Trois-Rivières, Québec, Canada, G9A 5H7
Courriel: bruno.Chabot@uqtr.ca

Contribution des auteurs: Gilbert Nkana est l'auteur principal de cet article. Il a mené toutes les expériences scientifiques et réalisé les développements associés. M. Nguyen-Tri est directeur de recherche et M. Chabot est co-directeur de cette recherche. Le directeur et le co-directeur ont participé à la révision et à la correction du manuscrit.

5.2 Résumé

Cette étude porte sur le développement de monolithes macroporeux à l'aide de la cryopolymérisation de solutions d'acrylate de sodium/carboxyméthylchitosane pour l'adsorption de la fluoxétine, un antidépresseur, dans des environnements aqueux. Les cryogels ont été caractérisés à l'aide de diverses techniques analytiques, et les effets du pH, de la température, de la concentration initiale et du temps de contact sur la capacité d'adsorption ont été étudiés. La charge de surface du cryogel était négative lorsque $pH_{solution} > pH_{PZC}$, et un pH de 8,5 s'est avéré optimal pour les taux de gonflement et l'efficacité d'élimination de la fluoxétine. Le cryogel $NaPA_4$-CMCs (0,5 $mg.mL^{-1}$) a présenté les meilleures performances d'adsorption, le modèle pseudo-premier ordre décrivant le mieux les données cinétiques expérimentales. Le modèle de diffusion intraparticulaire a révélé une diffusion rapide à travers les macropores et les mésopores. Le modèle de Langmuir s'est bien adapté aux données expérimentales d'équilibre d'adsorption, avec q_{max} = 80,6 ± 3,4 $mg.g^{-1}$. Le processus d'adsorption était favorable, exothermique et régi par la physisorption, impliquant des interactions électrostatiques, des liaisons hydrogène, des interactions π–π et des interactions hydrophobes. Le solvant binaire HCl (0,1 M)/méthanol 1:1 v/v s'est avéré efficace pour régénérer l'adsorbant, avec une efficacité d'adsorption supérieure à 60 % après trois cycles de réutilisation. L'étude souligne le potentiel de ces monolithes macroporeux pour l'élimination efficace des antidépresseurs des environnements aqueux.

5.3 Abstract

This study focuses on the development of macroporous monoliths using cryopolymerization of sodium acrylate/carboxymethyl chitosan solutions for the adsorption of the antidepressant fluoxetine in aqueous environments. The cryogels were characterized using various analytical techniques, and the effects of pH, temperature, initial concentration, and contact time on the adsorption capacity were investigated. The surface charge of the cryogel was negative when $pH_{solution} > pH_{PZC}$, and pH 8.5 was optimal for swelling rates and fluoxetine removal efficiency. The $NaPA_4$-CMCs cryogel (0.5 $mg.mL^{-1}$) showed the best adsorption performance, with the pseudo-first-order model

best describing the experimental kinetics data. The intraparticle diffusion model revealed rapid diffusion through macropores and mesopores. The Langmuir model fitted well to the experimental adsorption equilibrium data, with q_{max} = 80.6 ± 3.4 $mg.g^{-1}$. The adsorption process was favorable, exothermic, and governed by physisorption, involving electrostatic, hydrogen bonding, π–π, and hydrophobic interactions. The binary solvent HCl (0.1 M)/methanol 1:1 v/v was effective for regenerating the adsorbent, with adsorption efficiency greater than 60% after three cycles of reuse. The study highlights the potential of these macroporous monoliths for the effective removal of antidepressants from aqueous environments.

5.4 Introduction

The COVID-19 pandemic has intensified mental health disorders such as anxiety and depression among vulnerable people around the world [1,2]. This has led to an increase in the consumption of psychotropic drugs, such as antidepressants, which are prescribed to reduce or eliminate the effects of these pathologies on the body [3–5]. In 2021, the global sales market for antidepressants exceeded $15 billion [6]. Research indicates that the use and prescription of psychoactive drugs are likely to increase with the rising prevalence of mental illnesses in the coming year [4,7] s. There are various types of antidepressants available, but the most prescribed antidepressants are selective serotonin reuptake inhibitors (SSRIs), such as fluoxetine, a hydrophobic molecule with very low solubility in water (see Scheme 1) because of their effectiveness and safety [8]. The increase in the use of antidepressants highlights the need to consider their environmental impact once consumed. These artificial compounds undergo biotransformation after being taken up, and the biologically active remnants are released into the environment with almost no degradation [9,10]. Moreover, their strong affinity for soils and sediments enables them to persist in aquatic organisms, and their build-up in the biological membranes of aquatic species adversely affects unintended species in the receiving environments [11,12]. Research has shown that they have a negative impact on the growth, development, behavior, reproduction, movement, metabolism, and heart rate of multiple aquatic organisms [13,14],. This could lead to the disappearance of marine species and limit the availability of specific fish essential for human consumption.

Advanced, more efficient technologies using non-toxic, low-cost materials with exceptional potential for eliminating emerging contaminants have been developed by researchers [15,16]. Adsorption technologies using such materials have attracted considerable interest because they are more cost-effective and environmentally friendly. Although traditional adsorbents have shown several drawbacks, such as poor stability, availability and cost of synthetic precursors, and low reuse potential [17], the design of functionalized adsorbent materials and their composites from biopolymers is a viable alternative to enhance the effectiveness of this technology. The possibility of adjusting and/or modifying these biopolymers is a significant advantage that presents a challenge for improving the selectivity of adsorbents based on these precursor [18,19] s. This type of material has the advantages of being biocompatible, biodegradable, non-toxic, and inexpensive [20,21]. Several intelligent adsorbents based on polysaccharides (cellulose, chitin, chitosan, lignin, starch, alginate, hyaluronic acid, dextran, pectin, and their derivatives) have been developed for effective, economical, sustainable, and green wastewater treatment [22].

Polysaccharide hydrogels with remarkable properties (swelling, mechanical stability, sensitivity to various types of stimuli, etc.) have shown promising or even satisfactory results in the elimination of a wide range of emerging pollutants and are attracting increasing attention [23–25]. These materials consist of flexible polymer chains with highly reactive hydrophilic chemical functions [hydroxyl (-OH), carboxyl (-COOH), sulfonic acid (-SO_3H), and amine (-NH_2) groups), which form a stable three-dimensional network following physical, chemical, or physical and chemical cross-linking [19,26]. The formation of a porous structure in a hydrogel matrix can be achieved using techniques such as freeze-drying, porogenation, phase separation, and microemulsion [27,28]. In addition, controlling the degree of cross-linking and porosity influences the sorption efficiency, swelling, and mechanical stability of hydrogels [29]. The drawbacks of using polysaccharide hydrogels to purify contaminated water include low diffusion rates, which are caused by the reduced active surface area due to porosity, and the utilization of active sites for cross-linking polymer chains, which limits the number of available adsorption sites. Hydrogels with advanced properties, called cryogels, have been developed to overcome these limitations and are distinguished by their manufacturing methods [30,31].

Owing to their properties and the added value conferred by the manufacturing method, these hydrogels have applications in several fields (water purification, catalysis, biosensors, tissue engineering, medicine, and supercapacitors, etc.) [32–34].

Cryogels can be obtained using the cryotopic gelation method, which is an approach that has attracted a great deal of interest [30,31] t. In this method, the monomer is cryopolymerized in the presence of an initiator and cross-linking agent at temperatures below the freezing point [31,35]. The formed ice crystals constitute porogens that create a superporous matrix. [20,30] This positively affects the diffusion rate, essential for achieving better kinetics and excellent sorption performance. Cryogels are made from functional monomers; the most commonly used functional monomers were 2-acrylamido-2-methyl-1-propansulfonic acid, acrylic acid, maleamic acid, methacrylic acid, (3-acrylamidopropyl) trimethylammonium chloride, 2-(dimethylamino) ethyl methacrylate, allylamine, vinylamine, 4-vinyl pyridine, and 3-vinyl pyridine [31,36]. These materials can be used to obtain anionic, cationic, and amphoteric cryogels [37,38]. The use of natural polyelectrolytes in the design of composite cryogels has gained attention. This approach has shown promise in enhancing the physical, chemical, and mechanical properties of these materials, as well as their longevity, biocompatibility, biodegradability, and effectiveness in water-decontamination applications [31,34]. They have the advantage of being functionalized and have a faster reactivity than conventional hydrogels, which is attributed to their permeability [31]. This highly developed interconnected macroporosity facilitates the flow of water and pollutants through the network [20,39]. Although cryogels have shown great potential for removing metal ions and toxic dyes in numerous studies [40,41], to the best of our knowledge, no study has reported the design of a poly (acrylic acid)/carboxymethyl chitosan composite cryogel or the use of this composite for the purification of water contaminated by pharmaceutical molecules, particularly antidepressants. Carboxymethyl chitosan was chosen as the biopolymer because, in addition to the exceptional properties associated with the precursor polymer (chitosan) from which it was derived, it is sensitive to pH variation and is a chelating agent for Ca^{2+} ions, which forms a physical network. This material has the ability to swell in water depending on the pH of the medium [25]. In addition, our previous work demonstrated

the ability of hydrogels based on this polysaccharide to bind fluoxetine under specific experimental conditions [19].

This study explores this avenue by synthesizing a polyelectrolyte from chitosan using a carboxymethylation reaction. This multifunctional derivative was combined with an acrylic acid monomer, and the suspension underwent cryotopic gelation after adding a crosslinker and initiator solution. The obtained three-dimensional monolith was characterized and tested to eliminate the target antidepressant fluoxetine.

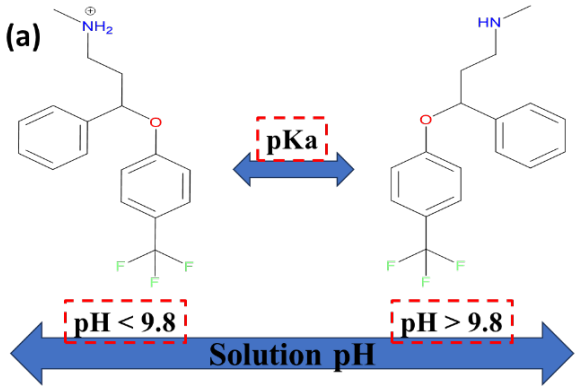

(b)

Chemical	Fluoxetine (FLX)
Molecular formula	$C_{17}H_{18}F_3NO$
Molecular weight	309.32 $g.mol^{-1}$
pKa	9.8
Solubility	14 $g.L^{-1}$
log K_{OW}	4.17
λ_{max}	226 nm
Therapeutic group	Antidepressant

Scheme 1 **a) Effect of solution pH on fluoxetine solubilization, b) physico-chemical characteristics of the fluoxetine [42].**

5.5 Materials and methods

5.5.1 Materials

A low molecular weight chitosan (CS) (MW 50,000 – 190,000 g/mol, deacetylation degree ≥ 75 %) from shrimp shells, Chloroacetic acid ($C_2H_3ClO_2$) ACS Reagent ≥ 99.0 %, Sodium hydroxide (NaOH) Bioxtra ≥ 98 %, Calcium Chloride anhydrous ($CaCl_2$) ≥ 93.0 %, Genipin ≥ 98% (HPLC), Deuterium oxide (D_2O) deuteration degree min 99.9 % for NMR spectroscopy, Acetic acid-d4 ($C_2H_4O_2$) ≥ 99.5 %, Acrylic acid anhydrous, containing 200 ppm MEHQ as inhibitor 99 % (AAc), N,N-Methylenebis (acrylamide) 99.0 % (MBA), Sodium metabisulfite ≥ 99.0% (SMS), Potassium persulfate ACS reagent ≥ 99.0 % (KPS) Isopropyl alcohol (C_3H_8O) and Fluoxetine hydrochloride (FLX), pharmaceutical Secondary standard used for the adsorption batch test as a model contaminant were supplied by Sigma-Aldrich. Hydrochloric acid (HCl), 37 %, was

provided by Acros Organic, and anhydrous ethyl alcohol (C_2H_5OH) was purchased from Commercial Alcohol Greenfield Global (Brampton, ON, Canada). Distilled water was used to prepare most of the solutions.

5.5.2 Methods

5.5.2.1 Design of cryogel materials by radical polymerization

The synthesis of carboxymethyl chitosan (CMCs) was accomplished by expanding our previous research and adjusting several parameters [19]. NaOH (10 g) was dissolved in 50 mL of a binary solvent (water/isopropanol 1:3 v/v) in a 500 mL flask. Chitosan (5 g) was added to the NaOH solution and stirred for 30 min at 350 rpm. The mixture was placed in a freezer at -18°C for 90 min. The mixture was then returned to room temperature. The carboxymethylation step was completed by adding a solution of monochloroacetic acid (15 g dissolved in 10 mL isopropanol) dropwise over 30 min. The suspension was kept under stirring for 150 min at 50°C. The reaction was stopped by adding 200 mL of 70 % ethanol. The suspension was filtered, and the product was washed extensively with increasing grades of ethanol (70 – 100 %) to remove unreacted reagents. The obtained polymer was dried under vacuum for 72 h. To purify the obtained derivative, it was dissolved in 200 mL demineralized water for 5 h, and the polymer solution was centrifuged for 15 min at 13,000 rpm. The impurity-free solution was recovered, and the polymer was recrystallized by adding 100% ethanol. The obtained CMCs were recovered by Büchner filtration and dried under vacuum for 24 h.

The synthesis mechanism of the interpenetrated polymer networks (IPN) of sodium polyacrylate-co-carboxymethyl chitosan (NaPA-CMCs) crosslinked by N,N᾽-methylene-bis-acrylamide, and genipin is shown in Scheme 2.

Different solutions of AAc at concentrations of 50 %, 40 %, 30 %, and 20 % w/v were prepared from a commercial solution of 99 % AAc by dilution in distilled water. 0.76 mL of each solution was placed in 50 mL beakers containing 5.24 mL of a 3 % w/v CMCs solution obtained by dissolving 0.3 g CMCs in 10 mL distilled water (Figure 5.1).

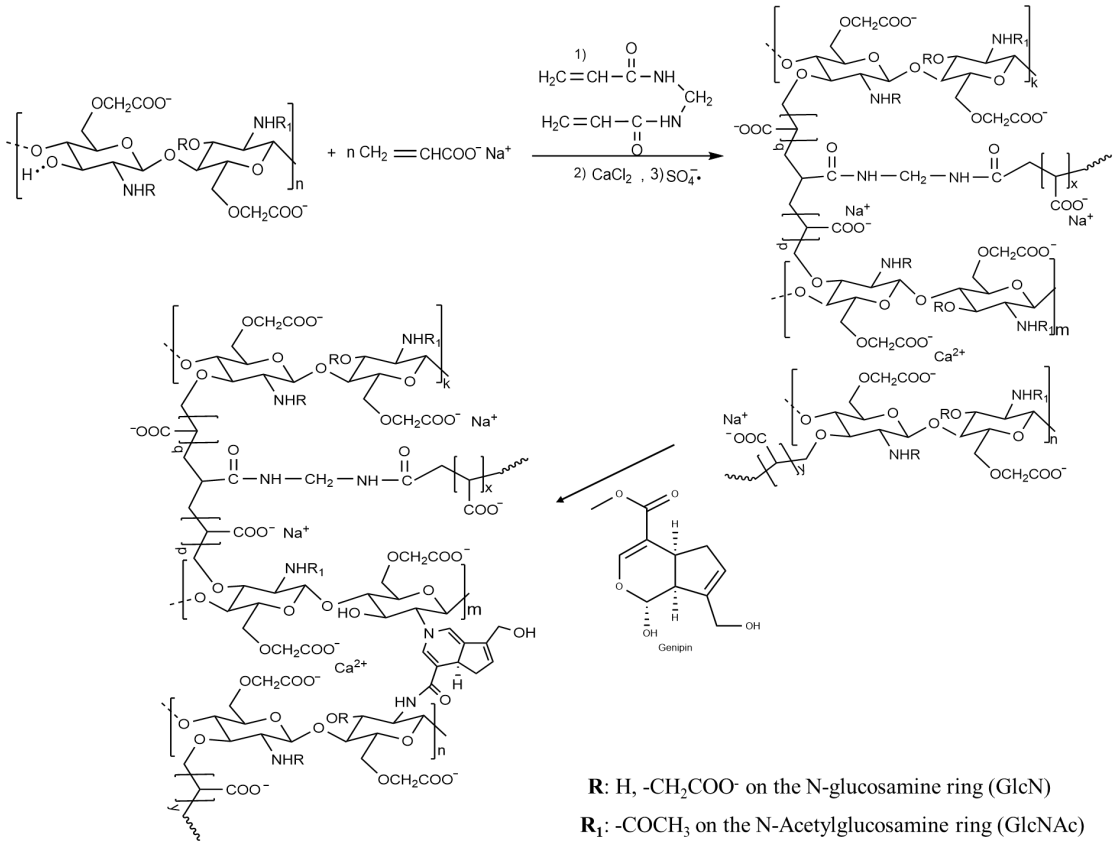

Scheme 2 **Synthesis mechanism of the interpenetrated polymer networks (IPNs) of sodium polyacrylate-co-carboxymethyl chitosan (NaPA-CMCs), crosslinked by N,N'-methylene-bis-acrylamide, and genipin**

The solutions were stirred at 200 rpm for 30 min. The pH was adjusted to 5 by adding 1M NaOH aqueous solution. Suspensions of sodium acrylate (NaA) and carboxymethyl chitosan were obtained. They were labeled NaA_1/CMCs, NaA_2/CMCs, NaA_3/CMCs, and NaA_4/CMCs, respectively. 15 mol % MBA was introduced into each solution along with 3 % $CaCl_2$ to crosslink the polymers. The stirring speed was adjusted to 600 rpm in an ice bath for 1 h to solubilize the reagents completely. The initiator solutions were prepared by dissolving the respective masses of KPS/SMS (0.149 g: 0.21 g, 0.119 g: 0.168 g, 0.089 g: 0.126 g, and 0.059 g: 0.084 g) in 1 mL of distilled water and stored at 4 °C until use. The initiator solutions were introduced into the NaA/CMC suspensions at 200 rpm for 3 min. Subsequently, these different mixtures were introduced into 10 mL latex-free syringes and placed in a freezer at -18 °C for 24 h to complete the cryopolymerization stage to obtain $NaPA_1$-CMCs, $NaPA_2$-CMCs, $NaPA_3$-CMCs, and $NaPA_4$-CMCs cryogel samples. The cryogels were thawed at room temperature, placed in 100 mL beakers containing 50 mL

of 50 % ethanol, and stirred at 150 rpm for 5 h to remove unreacted chemical species. The cryogels were then placed in a solution of genipin (1 mmol/L) under agitation for 1 h and then in an oven at 70 °C for 30 min. The cryogels were washed with 600 mL of distilled water and freeze-dried. The cryogels were cut to the following dimensions: height 1.5 cm, diameter 1.3 cm, and stored in a desiccator until use.

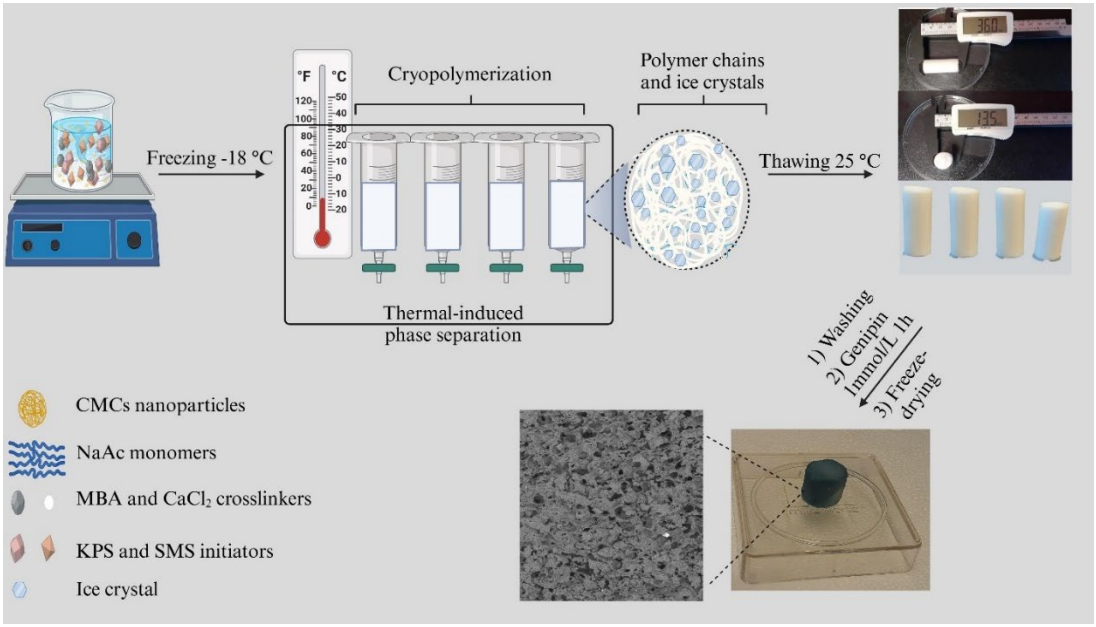

Figure 5.1 Production of cryogels: cryopolymerization temperature -18 °C, thawing 25 °C

5.5.2.2 Characterization of cryogel materials

The chemical modifications of chitosan and the structure of NaPA-CMC cryogels were investigated using Fourier transform infrared (FTIR) spectroscopy. Spectra were acquired in the wavelength range 4000-500 cm^{-1} at room temperature on a Nicolet IS10 FTIR Spectrometer (Thermo Scientific) equipped with a Diamond/ZnSe Crystal. Proton nuclear magnetic resonance (^1H NMR) of the CMCs dissolved in the binary solvent D_2O was performed using a Bruker ASCEND 400 MHz NMR spectrometer. Simultaneously, thermogravimetric analysis (TGA) of the polymer and NaPA-CMC cryogels was performed on a Perkin-ELMER (Pyris Diamond) Thermoanalyzer. The TG/DTG analysis was completed over a 25–900 °C temperature range with an increment of 10 °C / min in a nitrogen atmosphere. The Zeta potential of NaPA/CMC suspensions at pH 5 and particle

size distribution were assessed by dynamic light scattering (DLS) using a ZETASIZER NanoSeries model ZEN3600. For cryogels, the BET surface area (m^2/g) was determined by the Brunauer-Emmett-Teller method by measuring nitrogen adsorption at 77 K between 0 and 1 atm pressure, the average pore diameter by the Barrett, Joyner, and Halenda (BJH) method, and the micropore surface area by the Dubinin-Radushkevich method. A Micromeritics ASAP 2020 instrument was used for the analysis. The surface morphology was studied by scanning electron microscopy (SEM), and elemental analysis of the cryogels by energy dispersive X-ray spectroscopy (EDX) was performed using a Hitachi SU1510 Scanning Electron Microscope equipped with an Oxford EDX detector. The swelling, porosity, and surface charge of NaPA-CMC adsorbents were also studied. The point of zero charge (pH_{PZC}) of the cryogel materials was investigated by pH derivation [43]. The samples were immersed in a 0.01 M NaCl solution for 24 h at 22 °C with moderate stirring using an orbital shaker incubator (LAB-LINE instrument model 3528). The pH of the solutions was stabilized with 1M NaOH and 1M HCl solutions, and the study was completed in the pH range of 2-12. The solutions were filtered at the end of the tests, and the final pH was measured. Plotting ΔpH versus $pH_{initial}$ enabled the determination of pH_{PZC}, which is the pH at which $pH_{final} = pH_{initial}$. The liquid displacement method was used to determine the porosities of the cryogels [44]. Anhydrous ethanol was used as a solvent to complete the experiments. The cryogel samples tested were 1.5 cm high and 1.3 cm in diameter. The porosities of the cryogel samples were calculated using Equation 5.1, where ρ = 0.785 g/cm^3 is the density of the solvent, V (cm^3) is the volume of the samples, and m_1 and m_2 are the sample masses recorded before and after the test, respectively.

$$P(\%) = \left(m_2 - m_1\right) \Big/ \rho V \times 100 \qquad \text{Equation 5.1}$$

5.5.3 Measurements of swelling capacity and effect of pH

Swelling of the cryogels was investigated at room temperature (22 ± 1 °C) by immersing the cryogel samples in 50 mL of distilled water previously adjusted to pH between 7 and 8.5. The contact time was between 0 and 20 s, and the dry cryogel sample (W_{dry}) mass was between 25 and 80 mg before each bath contact. Excess water on the outer surface of the

samples was removed by lightly wiping with blotting paper. The mass of the swollen cryogels (W_{sw}) was determined, and the swelling capacity, SW (%), was calculated using Equation 5.2.

$$SW\,(\%) = \frac{W_{SW} - W_{dry}}{W_{dry}} \times 100 \qquad \text{Equation 5.2}$$

where W_{dry} (g) and W_{sw} (g) are the masses of swollen and dry cryogels, respectively. All swelling tests were repeated three times for each cryogel.

5.5.4 Batch adsorption experiments

Batch adsorption tests were performed in FLX solutions with concentrations ranging from 10 to 50 ppm, prepared from a standard solution of 1000 ppm. To accomplish this, precise volumes of aliquots were withdrawn from the standard solution and diluted in a mixture of demineralized water, and 5 % methanol (95:5). Subsequently, 50 mL of each resulting solution was transferred into 125 mL Pyrex flasks. The effects of parameters such as contact time (between 0 and 300 min), initial concentration (between 0 and 200 ppm), pH (between 7 and 8.5), and temperature (between 25 and 50 °C) on the adsorption capacity of the cryogel adsorbents tested were investigated by shaking the samples in an Orbital Shaker at 250 rpm. The removal efficiency and adsorption capacity were calculated using Equations 5.3 and 5.4, respectively:

$$\%R = (C_0 - C_t) / C_0 \times 100 \qquad \text{Equation 5.3}$$

$$q_e = \left(C_0 - C_e\right) \times V \Big/ m \qquad \text{Equation 5.4}$$

where $\%\,R$ is the removal efficiency, and q_e is the amount of FLX adsorbed by the beads at equilibrium (mg.g^{-1}). where C_0 is the initial concentration of FLX (ppm), V (mL), and m (g).

The experimental data were fitted to three kinetic models: the pseudo-first-order model (Equation 5.5), pseudo-second-order model (Equation 5.6), and intraparticle model (Equations 5.7 and 5.8) to study the adsorption kinetics of FLX on the cryogels.

$$q_t = q_e(1 - e^{-k_1 t})$$ Equation 5.5

$$q_t = k_2 q_e^2 t / 1 + k_2 q_e t$$ Equation 5.6

$$q_t = k_1 t^{1/2} \quad 0 \le t \le t_1$$ Equation 5.7

$$q_t - q_{t=t_1} = k_2 (t - t_1)^{1/2} \quad t_1 < t \le t_2$$ Equation 5.8

where k_1 (mg.g $^{-1}$. min$^{-1/2}$) : intraparticle diffusion constant, k_2 (mg.g $^{-1}$. min$^{-1/2}$) : intraparticle diffusion constant.

Adsorption equilibrium experiments were conducted to examine the adsorption isotherms that could provide information on the nature and mechanism of adsorption involved in the process. Cryogels were placed in contact with 50 mL of FLX solutions of different concentrations (0 to 200 ppm) at a temperature and pH level for which the removal efficiencies were maximized during a specific time required to reach equilibrium. The contact time was determined from kinetic experiments, and the samples were agitated at 250 rpm. The experimental data were fitted to the Langmuir and Freundlich isotherm models (Equations 5.9 and 5.10).

$$q_e = q_{\max} K_L C_e / 1 + K_L C_e$$ Equation 5.9

$$q_e = K_F C_e^{1/n}$$ Equation 5.10

where q_{max} (mg.g^{-1}) is the maximum monolayer adsorption capacity, K_F (mg.g^{-1}) is the Freundlich isotherm constant, C_e (mg.L^{-1}) is the equilibrium concentration, and 1/n is the Freundlich intensity parameter, which relates to the surface heterogeneity or intensity of the adsorption driving force.

The separation factor R_L (Equation 5.11) is a dimensionless constant calculated from the Langmuir constant K_L. This is used to discuss the favorability of the adsorption process.

Depending on the value of R_L, the adsorption process is unfavorable if $R_L > 1$, linear if $R_L = 1$, favorable if $0 < R_L < 1$, and reversible if $R_L = 0$ [43].

$$R_L = 1/\left(1 + K_L . C_0\right)$$ Equation 5.11

where C_0 (ppm) is the initial concentration and K_L ($L.mg^{-1}$) is the Langmuir isotherm constant.

The samples were analyzed using the method described by Camiré et al. to determine the residual concentration of FLX after adsorption [45] A HPLC instrument fitted with a DAD iodine bar detector (Shimadzu i-Series Plus) was used in this study. A C18 reverse phase column (XB-C18, 100 Å, 150 ×3 mm, particle size 2.6 µm, Phenomenex, Kinetex) was used as the stationary phase. In contrast, the mobile phase was a binary solvent (ACN/H_3PO_4 0.1 %, 60:40).

Statistical analysis of the experimental data fitted to the kinetic models and adsorption isotherms was determined, and their optimization was performed using the OriginPro 2024 software (OriginLab Corporation, Northampton, USA). The statistical parameters used to assess the quality of the fits were R^2 and the root mean square error (*RMSE*) using Equations 5.12 and 5.13.

$$R^2 = \sum (q_{mean} - q_{cal})^2 \Big/ \sum (q_{cal} - q_{mean})^2 + \sum (q_{cal} - q_{\exp})^2$$ Equation 5.12

$$RMSE = \sqrt{1/N_{\exp} \sum (q_{\exp} - q_{cal})^2}$$ Equation 5.13

where q_{exp} ($mg.\ L^{-1}$) is the experimental adsorption capacity, q_{mean} ($mg.\ L^{-1}$) is the average experimental adsorption capacity; q_{cal} ($mg.\ L^{-1}$) is the calculated adsorption capacity; N_{exp} is the number of data points [46].

5.5.5 Desorption experiments

The viability of an adsorbent can be studied based on its ability to be recycled and reused over several cycles. This aspect can be assessed for the $NaPA_4$-CMCs cryogel by adsorption/desorption tests. The desorption was completed by treating the cryogel in a

beaker containing 50 mL of a 1:1 v/v HCl (0.1 M)/methanol mixture for 3 h under gentle agitation (100 rpm) at room temperature. The amount of FLX desorbed was assessed by HPLC using the method described previously. Desorption efficiency (%) was calculated using Equation 5.14.

$$Desorption = \left(C_{des} / C_{ads} \right) \times 100 \quad \text{Equation 5.14}$$

where C_{ads} (ppm) and C_{des} (ppm) are the quantities of FLX adsorbed and desorbed onto the cryogel, respectively.

If the adsorbent is to be reused, it is first treated in a 0.1 M NaOH solution for 1 h under gentle agitation (100 rpm) to regenerate the active sites on the surface of the cryogel polymer chains and guarantee adsorption efficiency. This was followed by thoroughly washing the cryogel with distilled water until the pH of the wash water was neutral and drying at room temperature for 24 h. This sample was then subjected to an adsorption test in 50 mL of a 50 ppm FLX solution, 25 °C, 250 rpm, and 300 min. Three adsorption/desorption cycles were performed during this experiment to determine the reusability of the cryogel.

5.6 Results and discussion

5.6.1 Characterization of carboxymethyl chitosan and cryogel adsorbents

The Zeta potential of the NaA/CMC suspensions and the particle size of the CMCs in the suspensions were determined using DLS analysis. Results presented in Table 5.1 indicate that at pH 5, the ZP of the suspensions was negative. This confirmed the deprotonation of the carboxylic acid groups of acrylic acid and the formation of sodium acrylate as the monomer. At pH 5, the suspensions appear to contain nanoparticles of different sizes, as shown in Figure SI1. This indicates that pH 5 is close to the isoelectric point of the polymer, where precipitation occurs [19].

Figure 5.2a shows the FTIR spectra of the cryogel precursors, highlighting the characteristic bands. The synthesis of CMCs from chitosan was confirmed by the presence

of absorption bands at 1580 cm^{-1} attributed to the asymmetric C=O stretching vibration of the carboxylate groups (COO^-, which overlaps with the N-H bending vibration of the amine groups, and that at 1400 cm^{-1} associated with the symmetric C=O stretching vibration of the carboxylate groups $-COO^-$ [47,48]. The characteristic bands of AA and MBA were observed in the range of [3101-2850 cm^{-1}] attributed to the symmetrical and asymmetrical CH_2 stretching vibrations, C-H stretching vibration, and -C=CH. The C=O stretching vibration at 1700 cm^{-1} was attributed to the carboxyl groups, whereas the band at 1656 cm^{-1} was attributed to the C=O stretching vibration of the carbonyl group of amide I. The bands between 1634 cm^{-1} and 1625 cm^{-1} are associated with the C=C stretching vibration. The band around 1430 cm^{-1} is attributed to the $-CH=CH_2$ bending vibration [30,49,50]. The characteristic absorption bands of genipin were observed at 1680 cm^{-1}, 1620 cm^{-1}, 1442 $cm^{-1,}$ and 1300 $cm^{-1,}$ which are attributed to the C=O stretching vibration of the ester groups, the stretching vibration of the C=C bonds of the heterocycle, asymmetric bending of the methyl, and C-O-C stretching of the heterocycle, respectively [51] y. The spectra in Figure 5.2b show those of the cryogels produced and have a high degree of similarity. Stabilizing the pH to 5 using 1M NaOH during cryogel preparation affected acrylic acid, leading to deprotonation, as confirmed by the absence of the 1700 cm^{-1} band. The polymerization of sodium acrylate and its cross-linking by MBA was confirmed by the disappearance of the bands associated with the CH_2 bending vibration, C-H stretching, and -C=CH between 3101 and 2850 cm^{-1} as well as the $-CH=CH_2$ bending vibration around 990 and 975 cm^{-1} [52–54]. The appearance of the band at 1448 cm^{-1} was attributed to CH_2 deformation vibration, which also validates this. The formation of the interpenetrating polymer chain network was confirmed by the 1538 and 1634 cm^{-1} absorption bands, which were attributed to the cross-linking of sodium poly(acrylate) by MBA and carboxymethyl chitosan by genipin [51,55]. The displacement and disappearance of the bands representing the -C-O stretch C3-OH secondary alcohol and C6-OH primary alcohol of the CMCs between 1104 and 1030 cm^{-1}, along with the emergence of new bands at 1114 and 1042 cm^{-1}, are indicative of the grafting of NaPA onto the oxygen atoms of carbons C3 and C6, where the substitution of the carboxymethyl groups did not occur. In addition, the formation of inter- and intramolecular hydrogen

bonds established by the -COO^- groups substituted on the primary alcohol C6-OH also influenced the observed decreased absorption band intensity.

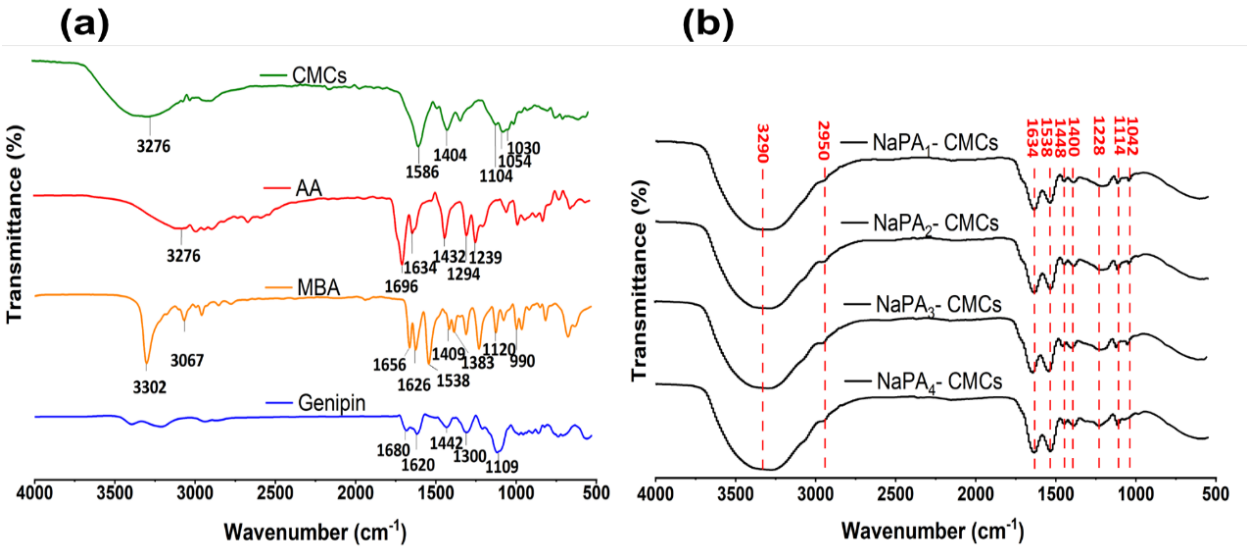

Figure 5.2 **FTIR spectra of: (a) carboxymethyl chitosan (CMCs), acrylic acid (AA), N,N-Methylenebis (acrylamide) (MBA), and genipin and (b) sodium polyacrylate-co-carboxymethyl chitosan cryogel prepared with 3% CMCs and 50 % acrylic acid (NaPA1-CMCs), 40 % acrylic acid ($NaPA_2$-CMCs), 30% acrylic acid ($NaPA_3$-CMCs), and 20 % acrylic acid ($NaPA_4$-CMCs)**

The ^{1}H NMR spectrum revealed characteristic signals, indicating a change in the chemical structure of chitosan (Figure 5.3a). The signals between 4.5 and 4 ppm were attributed to the resonance of the protons of the carboxymethyl groups substituted on the C3 and C6 carbons of D-glucosamine (GlcN) and N-acetyl-D-glucosamine (GlcNAc) [56]. In comparison, the signal at 3.23 ppm corresponds to the resonance of the protons of the carboxymethyl groups substituted on the amine groups of the GlcN units of chitosan [56,57]. This information corroborates the results of the FTIR analysis and confirms the synthesis of carboxymethyl chitosan.

The low-pressure ($P/P_0 < 1$) BET method was used to obtain Type II isotherms of the cryogels, as shown in Figure 5.3b. These isotherms suggest that the cryogels possessed micropores [58] and the micropore volume was approximately 2 x 10^{-3} $cm^3.g^{-1}$ for all the samples (see Table 5.1). Analysis of the pore diameter revealed mesopores with diameters ranging from 2 to 50 nm for all the samples, while the specific surface area was between

41 and 75 m^2/g. The results of cryogel porosity determination are shown in Figure 5.3d, and the corresponding data are presented in Table 5.1.

Table 5.1 Data from the analysis of the specific surface area, pore size, porosity, point of zero charges of cryogel materials NaPA1-CMCs, NaPA2-CMCs, NaPA3-CMCs, and NaPA4-CMCs and the zeta potential of initial suspensions of cry-ogels NaPA1-CMCs, NaPA2-CMCs, $NaPA_3$-CMCs, and $NaPA_4$-CMCs at pH = 5

Samples	S_{BET} (m^2/g)	Adsorption average pore diameter (nm)	Micropore volume $x10^{-3}$ (cm^3/g)	Porosity (%) (n=3)	Zeta Potential (mV) pH =5	pH_{ZPC}
$NaPA_1$-CMCs	41.6	18.7	2.1	43 ± 1.0	-15.2	4.7
$NaPA_2$-CMCs	49.7	11.7	2.2	57 ± 0.6	-9.8	4.8
$NaPA_3$-CMCs	56.5	9.5	1.9	62 ± 0.4	-8.9	4.6
$NaPA_4$-CMCs	74.9	15.4	1.7	85 ± 1.6	-8.9	4.6

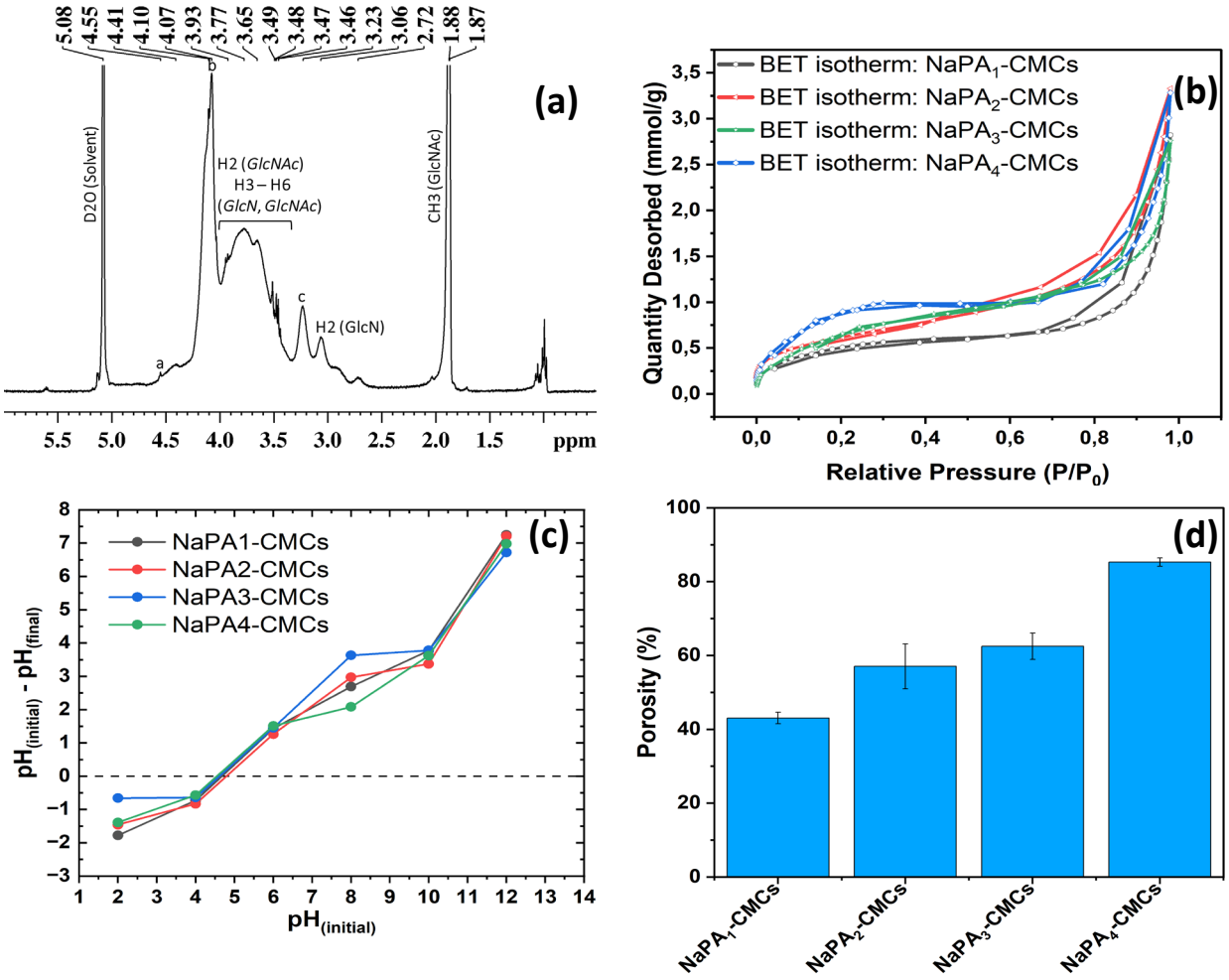

Figure 5.3 **Characterization of carboxymethyl chitosan and cryogel materials (NaPA$_1$-CMCs, NaPA$_2$-CMCs, NaPA$_3$-CMCs, and NaPA$_4$-CMCs: (a) ^{1}H NMR analysis of carboxymethyl chitosan (CMCs) at room temperature in the D_2O solvent, (b) BET adsorption/desorption isotherms of cryogel materials, (c) point of zero charge curves of cryogel materials, pH studied between 2 and 12, (d) porosity of cryogel materials in anhydrous ethanol at rest for 60 min at 22 °C (n=3)**

NaPA$_4$-CMC cryogels had a higher porosity (85 %) than the other cryogels. This is because the ice crystals formed after freezing the water, which acts as a porogen and leads to the formation of macropores. However, the ice crystals formed cause the cryogel precursors to be expelled into the spaces available between the crystals, where the polymerization of sodium acrylate and cross-linking of polymer chains ensure the formation of fine micro- and mesoporous walls in the macropore network. This improves the specific surface area of the materials. Determination of the zero-charge point of the cryogels revealed the value of this parameter is pH_{PZC} = 4.7 for the NaPA$_1$-CMCs, 4.8 for

the $NaPA_2$-CMCs sample, and 4.6 for the $NaPA_3$-CMCs and $NaPA_4$-CMCs samples (Figure 5.3c, and Table 5.1). This implies that the surface charge of the cryogels is positive when the pH of the medium is below pH_{PZC} and negative otherwise [43]. This was due to the ionization of the chemical amine and carboxylic acid functions of the polymer chains on the surface of the cryogels. This is particularly interesting for the adsorption of FLX (pKa = 9.8) when the pH of the medium is $pH_{PZC} < pH_{solution} < pKa_{FLX}$ because this molecule is in the cationic form under these conditions.

The thermal stability of the cryogels was studied using TG/DTG analysis. The obtained thermograms are shown in Figure SI2, and the data obtained are listed in Table 5.2. The thermograms reveal the two-stage decomposition profiles for all samples. Before that, we have between 50 °C and 150 °C the evaporation of water and moisture adsorbed in the cryogenic network owing to the presence of hydrophilic groups on the polymer chains. During this stage, there was a mass loss between 9.5 % and 13.6 %. The first stage of decomposition is between 242 and 407.6 °C, resulted in the most significant mass loss (between 23.6 and 41.8 %), which could be attributed to the cleavage of the glucoside bonds, structural degradation of the glucosamine units, degradation of the acrylamide part, and breakage of the NaPA chains. The second stage of decomposition occurs above 600 °C, with a mass loss of between 1.9 % and 6.2 %, which can be attributed to pyrolysis, which produces volatile hydrocarbons and inorganic residues. The $NaPA_4$-CMCs sample was the most thermally stable at 900 °C, with a mass loss of 69.9 %, which was lower than those of the other cryogels at the same temperature.

Table 5.2 Thermogravimetric analysis of cryogels NaPA1-CMCs, NaPA2-CMCs, NaPA3-CMCs and NaPA4-CMCs, Heat from 25 °C to 900 °C at 10 °C/min, cool from 900 °C to 25 °C at 200 °C/min, in a nitrogen atmosphere

Samples	Moisture elimination		1st decomposition		2nd decomposition		Tmax	WL	Inorganic residues W (%)	Total WL (%)
	T (°C)	WL (%)	T (°C)	WL (%)	T (°C)	WL (%)	(°C)	(%) at T_{max}	at 900°C	at 900°C
$NaPA_1$-CMCs	58.5 - 141.8	9.8	256.3 – 407.6	41.8	700.9 – 760.7	4.4	389.6	22.8	21.9	78.1
$NaPA_2$-CMCs	56.1 - 142.8	9.5	242.5 – 393.4	30.8	710.3 – 768.7	6.2	375.3	30.8	26.3	73.7
$NaPA_3$-CMCs	50.2 – 144.5	13.6	242.4 – 395.7	29.9	615.6 – 663.4	1.4	379.5	30	27.8	72.2
$NaPA_4$-CMCs	52.5 - 147.8	11	272.2 – 389.6	23.6	637.2 – 696.9	1.9	372.7	23.6	30.1	69.9

T (°C) and **T_{max} (°C)**: temperature and maximum temperature, **W (%)** and **WL (%)**: weight and weight loss, respectively.

The surface morphology was studied by SEM analysis, and the counter ions (Na^{+} and $Ca^{2+)}$ present in the cryogels were identified and quantified by elaborate EDX analysis. The results are presented in Figure 5.4, which shows the micrographs of the different cryogels, a map showing the distribution of these counter ions in these materials, and the EDX spectra on which the relative quantification associated with the intensity of the peaks of these chemical elements is based.

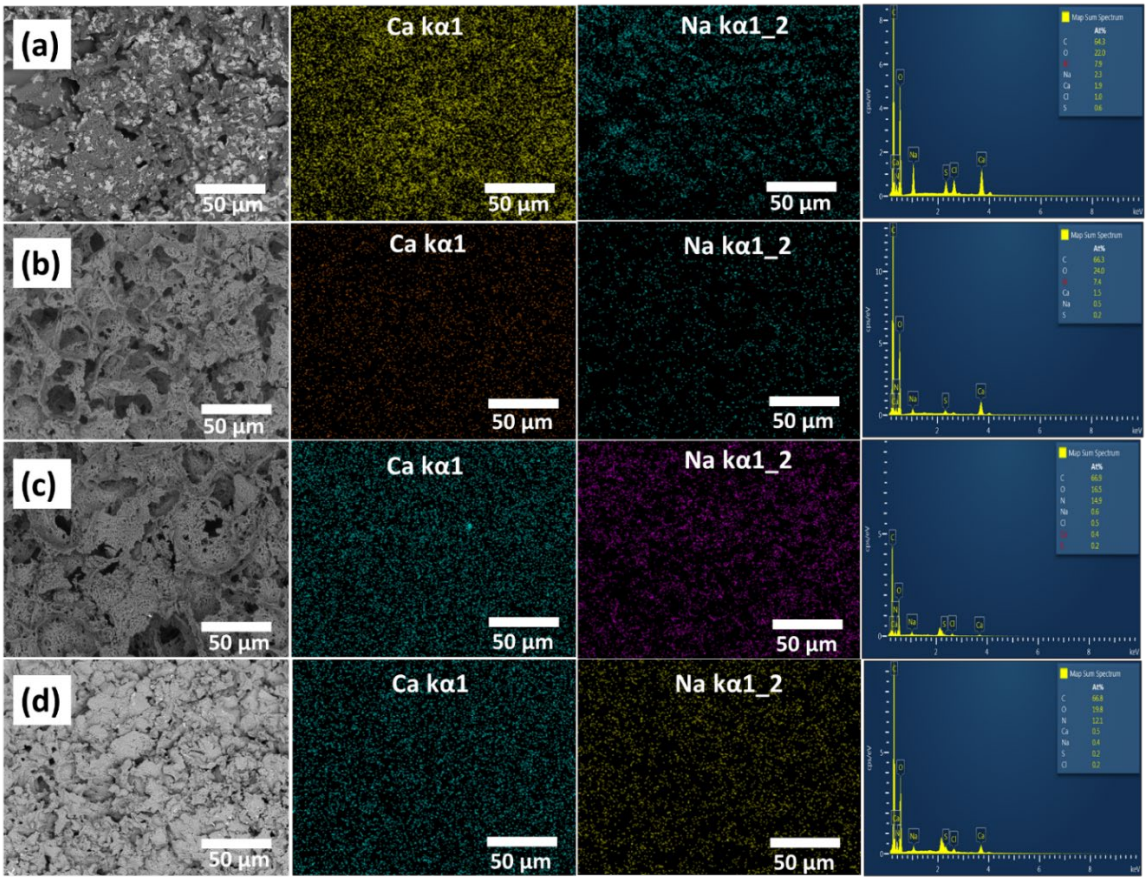

Figure 5.4 SEM micrographs and EDS analysis of sodium and calcium loaded in cryogels: a) $NaPA_1$-CMCs, b) $NaPA_2$-CMCs, c) $NaPA_3$-CMCs and d) $NaPA_4$-CMCs

The micrographs demonstrate that the materials have a porous structure with pores of various sizes. Macroporosity is highly developed and is believed to be a consequence of cryopolymerization. This technique has proven effective for the fabrication of macroporous materials in numerous studies. This is due to the freezing of the solvent, mainly water, which forms ice crystals and occupies spaces in the polymer chain network

during polymerization at temperatures below 0 °C. They act as porogens, leaving the spaces previously occupied in the network free when thawed at the end of the process [39,59]. The counter-ions identified and quantified by EDX analysis result from chemical cross-linking by $CaCl_2$ and residual chemical reagents that were not eliminated even after washing with distilled water. The mapping indicated they were well distributed in the different cryogels and could interact with deprotonated carboxyl groups. Quantification of the EDX spectra revealed that their proportions were more significant in the $NaPA_1$-CMCs sample.

5.6.2 Effect of pH on swelling kinetics

The study of cryogel swelling provides key information on water diffusion into the pore network and its interaction with the polymer chains. Figure 5.5 shows the swelling profiles of the cryogel materials under various pH conditions.

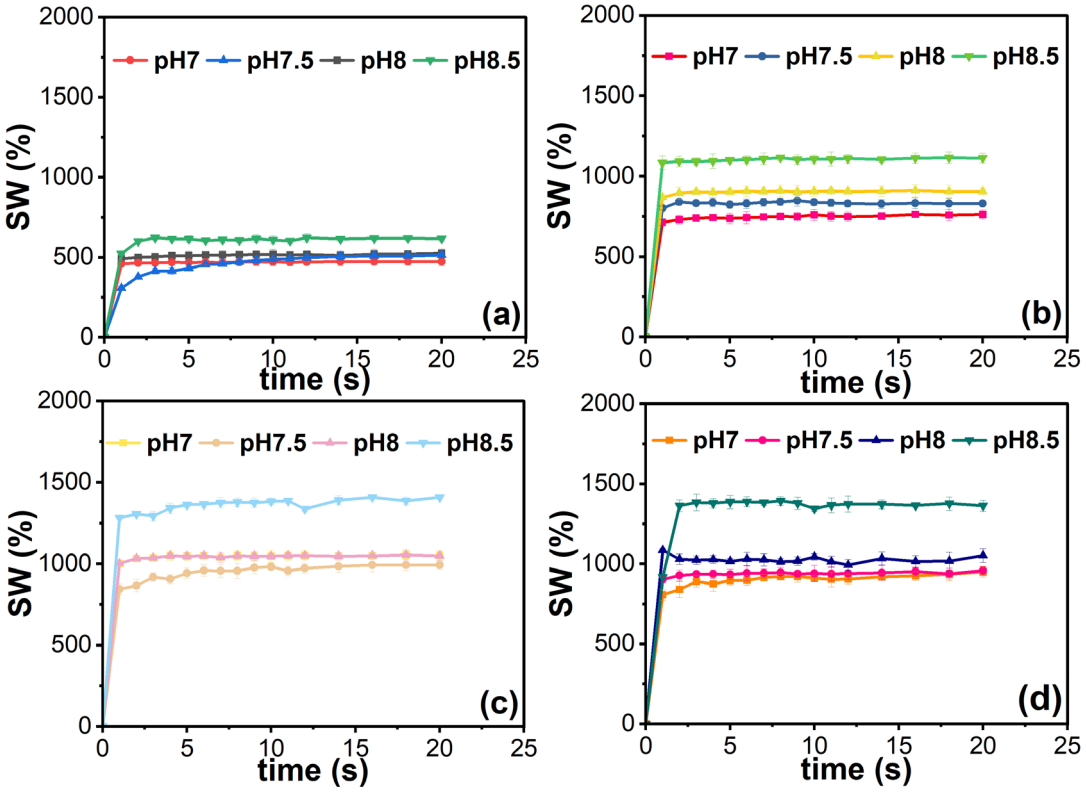

Figure 5.5 Dynamic swelling profiles of cryogels and effect of pH (a) NaPA1-CMCs, (b) $NaPA_2$-CMCs, (c) $NaPA_3$-CMCs, and (d) $NaPA_4$-CMCs

Spontaneous water absorption into the cryogel pore network was observed, and adsorption equilibrium was reached after 10 s. This is linked to the good diffusion of water through the porous structure of the cryogels and the availability of hydrophilic groups (OH, NH_2, and COO^-). On the other hand, the presence of Na^+ and Ca^{2+} counter ions create a difference in the chemical potential at the cryogel/solvent interface and generates osmotic pressure, which causes the monoliths to swell [60]. The pH of the bath and the osmotic pressure influence the swelling capacity and kinetics as swelling increases with the pH of the bath. The swelling of the cryogels increased as a function of the bath pH from 7 to 8.5. The $NaPA_3$-CMCS and $NaPA_4$-CMCS samples had the best swelling rates, which could be due to the higher proportion of counter ions in these samples, as shown by EDX analysis, and to the lower concentration of monomers used in their preparation, which could suggest a higher cross-linking density of the interpenetrated polymer networks.

5.6.3 Effect of pH, temperature, initial concentration, and contact time on fluoxetine adsorption

The adsorption performance of macroporous cryogels is influenced by several physicochemical parameters. In this study, the effects of different parameters (pH, temperature, initial concentration, and contact time) on the ability of cryogels to remove FLX were investigated. The pH studied varied from 7 to 8.5, the temperature from 25 to 50 °C, the contact time from 0 to 300 min and the initial concentration from 0 to 200 ppm. The dose of adsorbent 0.5 mg/ml, the volume 50 mL and the stirring speed 250 rpm were kept constant. In selected experimental trials, the fixed parameter values were: t=300 min, T=25 °C, C=50 ppm and pH=8.5.

Varying pH affects the surface charge of the adsorbents and the ionic or non-ionic state of the adsorbates, which involves the adsorption equilibrium and, therefore, the removal efficiency. The results of the investigation of the effects of pH are shown in Figure 5.6a. The FLX removal efficiency of the cryogels increased as the solution pH increased from 7 to 8.5. An elimination rate of over 77 % was obtained at pH 8.5 for the $NaPA_4$-CMCs cryogel, which was the best adsorbent for the different pH values studied. This could be explained by this material's good specific surface area and excellent porosity compared with other cryogels, which favors better solution diffusion through the interpenetrating

network. In this case, ionized FLX (pKa = 9.8) > pH solution could establish electrostatic interactions with the ionized functional groups ($-COO^-$) on the surface of the polymer chains, as suggested by the study of the surface charge of the cryogels tested.

The effect of temperature on FLX removal by cryogels is shown in Figure 5.6b. A decrease in removal efficiency was observed with increasing temperature from 25 °C to 50 °C for all adsorbents. The best removal rates were observed at 25 °C, and the $NaPA_4$-CMCs cryogel stands out as the one that removes the most FLX, with a yield that decreases significantly from 70.5 % at 25 °C to 49.9 % at 50 °C. An increase in the temperature had a negative effect on the adsorption of FLX. This suggests that the intensity of the binding forces involved in FLX adsorption, particularly van der Waals, hydrogen bonding, and electrostatic interactions, decreases with increasing temperature. However, it should be noted that this decrease in the quantity of FLX eliminated with increasing temperature is attributed to an exothermic process. The thermodynamic study will be completed in a later section, and the thermodynamic parameters obtained will be used to validate this statement.

Figure 5.6c illustrates the results of the initial concentration effect investigation on the ability of the cryogels to eliminate FLX. A rapid increase in the quantity eliminated was observed up to a concentration of 100 ppm, above which the adsorbed quantity was low. This phenomenon was observed across all the cryogels tested and can be attributed to the availability of active sites on the surface of the cryogels, which interact with FLX. At higher concentrations, the saturation of the binding sites could explain the lower adsorption levels. It is important to consider contact time as a factor in adsorption kinetics when analyzing adsorption equilibrium. The effects of this parameter on adsorption capacity are shown in Figure 5.6d. We observed that for all adsorbents, the quantity of FLX eliminated increased with contact time. Furthermore, rapid adsorption was observed for all the cryogels, particularly up to 50 min for the $NaPA_1$-CMCs and $NaPA_2$-CMCs cryogels, with quantities removed of 49.6 $mg.g^{-1}$ and 58.8 $mg.g^{-1}$, respectively. For the $NaPA_3$-CMCs and $NaPA_4$-CMCs cryogels, it was observed up to 90 min with quantities removed of 71.1 $mg.g^{-1}$ and 76.1 $mg.g^{-1}$, respectively. Following these contact times, the quantity of adsorbed FLX remained largely constant, indicating that equilibrium was

achieved. The rapid adsorption of FLX can be attributed to its low resistance to mass transfer during external diffusion and surface diffusion through macropores. Furthermore, the rapid diffusion of the solvent, as demonstrated by the swelling kinetics of the cryogels, their porosity, and the excellent interconnected pore network that developed during the manufacturing process, likely contributed to the rapid transfer of FLX to the active sites. Rapid external diffusion and mass transfer through the network of interconnected macropores during the first hour of contact could explain the observed quantities of FLX adsorbed, as the concentration gradient would be the driving force for FLX diffusion, and there would be good affinity between the FLX molecules and the sorption sites on the polymer chains of the cryogels. $NaPA_4$-CMCs showed excellent adsorption performance compared with the other cryogels tested (77.4 ± 2.1 mg.g^{-1}) after 300 min of contact. This could be due to the high porosity and good specific surface area of this sample compared with the other adsorbents tested.

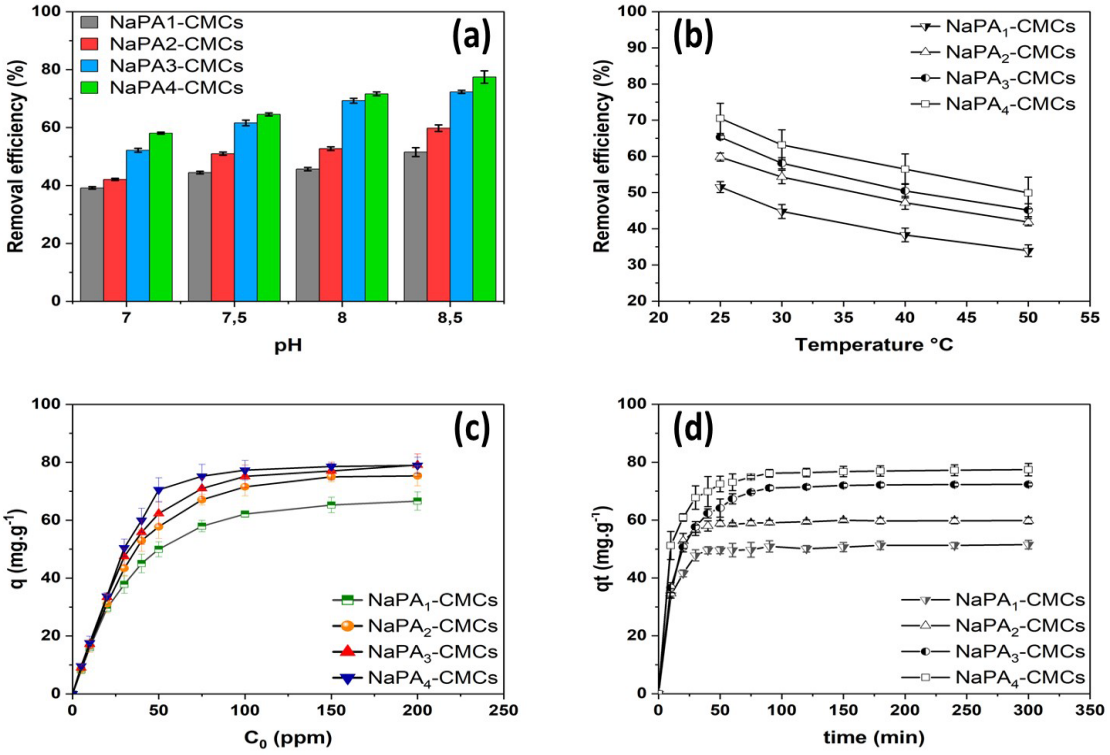

Figure 5.6 Investigation of the effect of physicochemical parameters in the adsorption capacity of NaPA1-CMCs, NaPA2-CMCs, NaPA3-CMCs and NaPA4-CMCs cryogels 0.5 mg.mL-1, Volume 50 mL, 250 rpm: a) pH from 7 to 8.5, b) temperature from 25 °C to 50 °C, c) initial concentration

5.6.4 Adsorption kinetics

The geometric, chemical, and energetic heterogeneity of adsorbents with porous surfaces make it difficult to describe the kinetics of the adsorption process. Nevertheless, three main stages of the adsorption process have been identified in the literature. The first two stages were attributed to the transport of the adsorbent, whereas the third stage was attributed to the reaction on the active sites [61]. It is important to elucidate which of these steps controls the adsorption kinetics. This sometimes requires additional information obtained from the study of the adsorption equilibrium, which may or may not confirm the choice of step or the synergy between these steps, limiting the process. The most commonly used models in the literature, namely the pseudo-first-order (PFO), pseudo-second-order (PSO), and intraparticle diffusion (IPD) kinetic models [62], were fitted to the experimental FLX adsorption data using nonlinear regression. The data were selected from tests performed with cryogel $NaPA_4$-CMCs, which demonstrated the best ability to eliminate this contaminant (Figure 5.7). The results of the analysis are presented in Table 5.3. It can be seen that the PFO and PSO models have good determination coefficients ($R^2 > 0.99$). Although the R^2 value is greater for the PSO model than for the PFO model, and the RMSE parameter is lower than that of the PFO model, it can be seen that the theoretical value $q_e calc = 75.6 \pm 0.3$ mg.g^{-1} obtained from the PFO model is very close to the experimental value $q_e exp = 77.4 \pm 2.1$ mg.g^{-1}. This suggests the PFO model fits the experimental data on FLX adsorption kinetics. This result does not allow us to draw any conclusions about the nature of the adsorption mechanism and the step that limits the process, especially as in the literature, it is noted that the adsorbent diffusion step is slower than the adsorption itself [62]. This suggests that diffusion or diffusion-reaction synergy could control the process. However, according to Rudzinski et al., mass transfer from the solution to the adsorbent surface controls the adsorption rate if the PFO model fits the experimental data well [61]. However, the experimental conditions studied favor complete ionization of the carboxyl groups on the surface of the polymer chains. In this case, FLX elimination was mainly achieved through electrostatic interactions on the cryogel surface.

Internal diffusion is the mass-transfer stage, as highlighted by the stepwise intraparticle diffusion model [63]. The simulation of this model was completed, and the optimal

partitioning of the adsorption kinetics data Figures 5.7b-f was determined by evaluating the statistical parameters. The results are presented in Table 5.4. Analysis of these results shows that the optimal division of the kinetics data (Figure 5.7c) gives the best statistical parameters (R^2 = 0.915, *RMSE* = 6.91 step 1 and R^2 =0.910, *RMSE* = 0.07 step 2) at $0 \leq t \leq 90$ min and $90 < t \leq 300$ min. The rate constant of step 1 (K_1 = 8.83 ± 0.39 mg.g^{-1}. min$^{-1/2}$) was very large compared to that of step 2 (K_2 = 0.81 ± 0.04 mg.g^{-1}. min$^{-1/2}$ x 10^{-1}). This indicates that stage 1 internal diffusion prior to equilibrium is faster than that in stage 2. This could be attributed to the concentration gradient and excellent porosity of this adsorbent, which facilitated the rapid diffusion of FLX through the macroporous structure. The value of the rate constant K_2 suggests minimal diffusion of FLX. This implies a slow mass transfer from macropores to micropores, which would reduce the adsorptive capacity of the NaPA$_4$-CMCs cryogel.

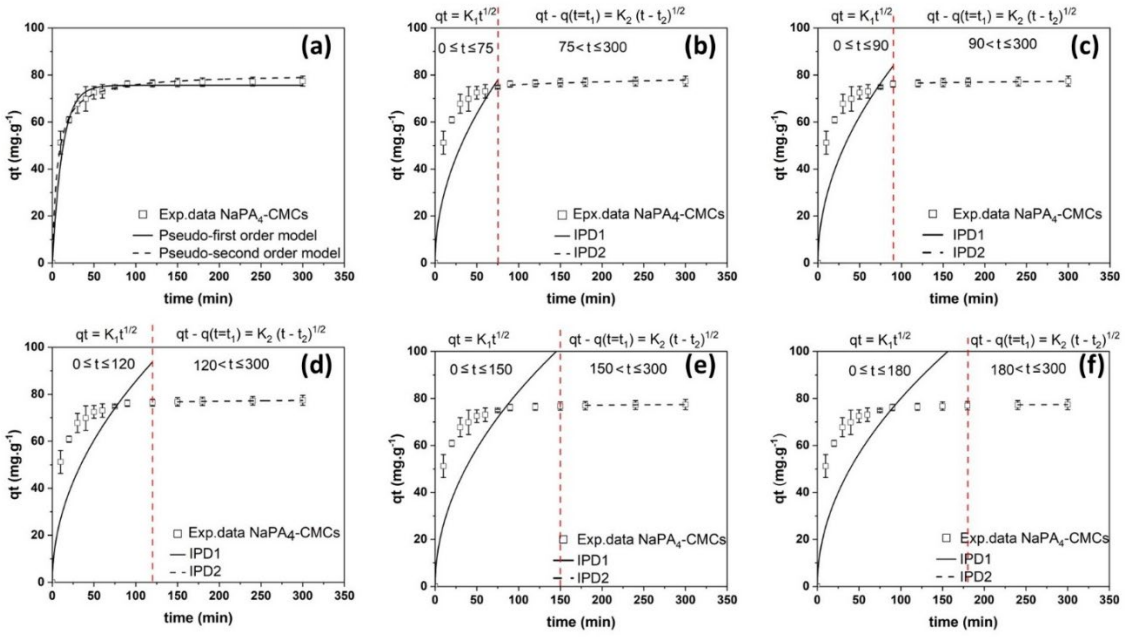

Figure 5.7 Fitting of pseudo-first-order, pseudo-second-order (a), and intraparticle diffusion kinetic models (b, c, d, e, and f) to experimental data of adsorption of fluoxetine in the NaPA4-CMCs cryogel 0.5 mg.mL^{-1}, t = 300 min, pH = 8.5, T = 25 °C, C$_0$ = 50 ppm

.

Table 5.3 Pseudo-first order and pseudo-second-order kinetic parameters for fluoxetine adsorption on NaPA4-CMCs

Sample	PFO model				PSO model			
$NaPA_4$-CMCs	Constants				Constants			
q_e exp ($mg.g^{-1}$)	q_e calc ($mg.g^{-1}$)	K_1 ($min^{-1} \times 10^{-2}$)	R^2	RMSE	q_e calc ($mg.g^{-1}$)	K_2 ($g/mg \cdot min \times 10^{-3}$)	R^2	RMSE
77.4 (2.1)*	75.6 (0.3)*	8.3 (0.4)	0.998	0.848	80.5 (0.4)*	2 (0.1)*	0.999	0.485

* Standard error in parentheses

Table 5.4 Intraparticle diffusion kinetic parameters for fluoxetine adsorption on NaPA4-CMCs

	Stage 1			Stage 2		
Time (min)	K_1 ($mg.g^{-1} \cdot min^{-1/2}$)	R^2	RMSE	K_2 ($mg.g^{-1} \cdot min^{-1/2} \times 10^{-1}$)	R^2	RMSE
75	8.98 (0.43)*	0.920	6.99	1.98 (0.05)*	0.472	0.21
90	8.83 (0.39)	0.915	6.91	0.81 (0.04)	0.910	0.07
120	8.55 (0.40)	0.882	7.77	0.71(0.02)	0.972	0.02
150	8.30 (0.43)	0.837	8.73	0.50 (0.05)	0.909	0.04
180	7.99 (0.46)	0.771	9.94	0.39 (0.15)	0.790	0.04

* Standard error in parentheses

5.6.5 Adsorption isotherms

The adsorption process can be modeled using two-parameter empirical equations, the most widely used of which are the Langmuir and Freundlich models [46,64]. The Langmuir model suggests that the sorption sites have the same affinity for the adsorbent, characterized by uniform binding energies, implying monolayer adsorption with no interaction between the adsorbates on adjacent active sites. The Freundlich model suggests multilayer adsorption on a heterogeneous surface with possible interactions between adsorbates [46,65]. These models were fitted to the experimental adsorption equilibrium data for the $NaPA_4$-CMCs adsorbent, which has been completed (Figure 5.8). The results are presented in Table 5.5. The performance of this cryogel in removing FLX depended on its initial concentration. The amount adsorbed at equilibrium increased with increasing initial concentration, up to 100 ppm. Above this concentration, the amount of FLX removed at equilibrium varied very little. This indicates that equilibrium was reached, and all available sorption sites were saturated. It can be seen that increasing temperature has a negative effect on the adsorption capacity of FLX. In addition, Table 5.5 shows that the value of the Langmuir constant (K_L) decreases with increasing temperature, indicating that the adsorption process is exothermic [66]. The values of the separation factor, $0 < R_L < 1$, indicate that the adsorption of FLX on cryogel $NaPA_4$-CMCs is favorable. The maximum adsorption capacity, q_{max} = 80.6 ± 3.4 $mg.g^{-1}$ was obtained at 25°C. The results demonstrated that the Langmuir isotherm model best fit the adsorption equilibrium data for FLX on this cryogel. The *RMSE* error function values for the Langmuir model were lower than those obtained from the Freundlich model, and $R^2 \geq 0.977$ values were higher, indicating the best fit of the Langmuir isotherm model to the adsorption equilibrium data.

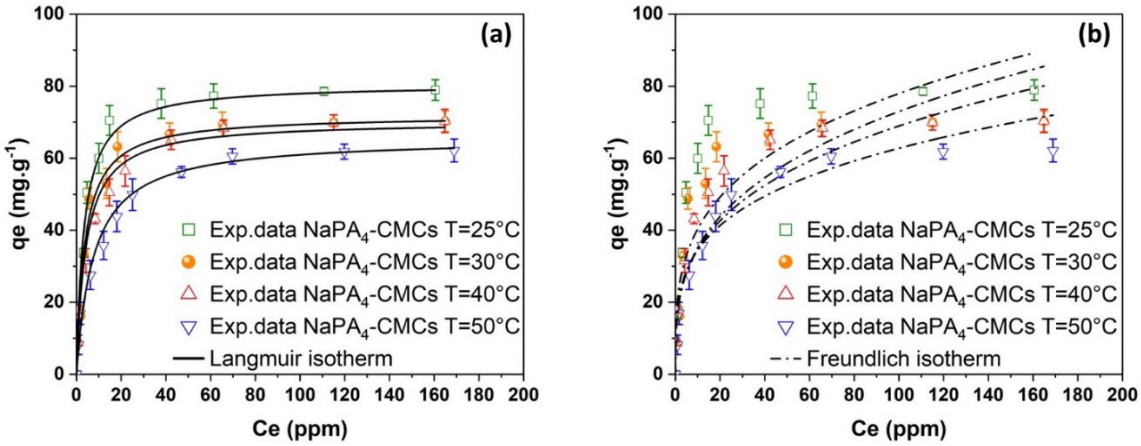

Figure 5.8 **Non-linear fit of the isotherm models to experimental data of fluoxetine adsorption in the NaPA4-CMCs cryogel: a) Langmuir model, b) Freundlich model, initial concentration from 5 to 200 ppm, 0.5 mg.mL^{-1} adsorbent, t = 300 min, pH = 8.5, T = 25 °C and 250 rpm**

Table 5.5 Langmuir and Freundlich isotherm parameters for fluoxetine adsorption on NaPA4-CMCs

	Langmuir isotherm parameters					Freundlich isotherm parameters			
Temperature (°)	**q_{max} ($mg.g^{-1}$)**	**K_L ($L.mg^{-1}$)**	**R_L**	**R^2**	**RMSE**	**K_F ($mg.g^{-1}$)**	**n**	**R^2**	**RMSE**
25	80.6 (3.4)*	0.29 (0.05)*	0.06	0.977	3.33	20.87 (2.53)*	3.49 (0.34)*	0.961	4.55
30	71.9 (2.1)	0.27 (0.03)	0.07	0.988	2.12	17.40 (2.52)	3.34 (0.38)	0.947	4.79
40	70.3 (2.5)	0.24 (0.03)	0.08	0.985	1.92	16.92 (2.44)	3.15 (0.37)	0.929	4.53
50	65.6 (1.4)	0.13 (0.01)	0.13	0.996	0.82	18.92 (3.14)	3.84 (0.58)	0.973	2.23

* Standard error in parentheses

5.6.6 Thermodynamic parameters

The determination of the thermodynamic parameters provides additional information that can be used to discuss the nature of the adsorption mechanism. These are Gibbs energy $\Delta G°$ (kJ.mol^{-1}), enthalpy $\Delta H°$ (kJ.mol^{-1}), and entropy $\Delta S°$ (J.mol^{-1}. K^{-1}) [67,68]. The type of adsorbate-adsorbent interaction determines whether adsorption is physical or chemical. Physical adsorption occurs when there are weak interactions such as van der Waals, hydrogen bonding, hydrophobic, and π-π interactions. In contrast, chemisorption occurs when strong interactions such as covalent bonding exist. The thermodynamic parameters were calculated using the laws of thermodynamics in equations 5.15-17.

$$\Delta G° = - R T \, Ln(Kc) \qquad \text{Equation 5.15}$$

$$\Delta G° = \Delta H° - T \, \Delta S° \qquad \text{Equation 5.16}$$

$$Ln\left(Kc \right) = -\Delta H°/RT + \Delta S°/R \qquad \text{Equation 5.17}$$

where K_C is the equilibrium constant, T (Kelvin) is the temperature, and R = 8.314 J.mol^{-1}. K^{-1}is the universal gas constant. The Gibbs energy was calculated using the following equation x, and the van't Hoff equation was used to determine the enthalpy, with the slope ($-\Delta H°/R$) and the intercept ($\Delta S°/R$) of the graph of K_C versus $1/T$. K_C is a dimensionless quantity calculated from the Langmuir constant K_L (L mg^{-1}) because the Langmuir model provides the best description of the adsorption equilibrium data of FLX on the NaPA$_4$-CMCs cryogel. To achieve this, the K_L constant was multiplied by a factor of 10^6, considering that the density of water is 1000 g.L^{-1}, which gives the values of the dimensionless K_C constant [66,67,69].

The results of the thermodynamic parameter calculations are presented in Table 5.6. It can be observed that the enthalpy value is negative ($\Delta H° < 0$), indicating that the increase in temperature reduces the efficiency of the NaPA$_4$-CMCs cryogel in eliminating FLX. This is characteristic of an exothermic adsorption process dominated by physisorption at low temperatures. In the literature, the absolute value of enthalpy is used to discuss the nature of the adsorption process. When the value is between 40 kJ.mol^{-1} < $\Delta H°$ < 80 kJ.mol^{-1}, the

adsorption process is physical, whereas when the value is between 80 kJ.mol^{-1} < $\Delta H°$ < 400 kJ.mol^{-1}, the adsorption process is chemical.

Table 5.6 Thermodynamic parameters of fluoxetine adsorption on NaPA4-CMCs

Temperature (K)	K_L (L.mg^{-1})	Kc (dimensionless)	ΔG° (kJ.mol^{-1})	ΔH° (kJ.mol^{-1})	ΔS° (J.mol^{-1}.K^{-1})
298	0.29	290000	-31.16	-24.26	23.89
303	0.27	270000	-31.50		
313	0.24	240000	-32.24		
323	0.13	130000	-31.62		

5.6.7 Desorption and reuse

The entropy provides information on the distribution and organization of the adsorbate at the solution/adsorbent interface. The calculated value of entropy is positive ($\Delta S° > 0$), indicating a random organization of FLX at the solution/$NaPA_4$-CMCs interface. For Gibbs energy, physisorption and chemisorption were characterized by Gibbs free energy change (ΔG°) values between - 20 kJ.mol^{-1} < $\Delta G°$ < 0 kJ.mol^{-1}, and - 400 kJ.mol^{-1} < $\Delta G°$ < - 80 kJ.mol^{-1} respectively [70–75]. In this case, the Gibbs energy is ΔG° < 0 kJ.mol^{-1}, with values between - 31.6 and - 31.1 kJ.mol^{-1} for the temperatures studied. These values are between those attributed to physisorption and chemisorption, indicating that the adsorption process of FLX on the $NaPA_4$-CMCs cryogel is favorable and may be attributed to the synergy between the main physisorption mechanism and chemisorption.

The regeneration of the adsorbent represents a crucial stage in the process because the efficiency, environmental impact, and overall cost of the adsorbent can influence its viability. A variety of extraction solvents, including water, acetonitrile, methanol, and ethanol, have been employed in the existing literature for the chemical regeneration of adsorbents containing FLX [42,45]. Although water is an environmentally friendly solvent, it is unsuitable for the desorption of FLX because of its hydrophobic nature. This is evidenced by the value of the octanol/water coefficient, log K_{OW} = 4.17 [76], which

indicates that the molecule is highly insoluble in water (14 mg L^{-1} at 25 °C) [77]. Acetonitrile has been demonstrated to be a more efficacious solvent; however, its high cost precludes its use at this stage [42]. Consequently, methanol and ethanol are attractive alternatives to acetonitrile.

The results of FLX desorption from the $NaPA_4$-CMCs cryogel and its reuse under the experimental adsorption conditions mentioned in the methodology section are presented in Figure 5.9.

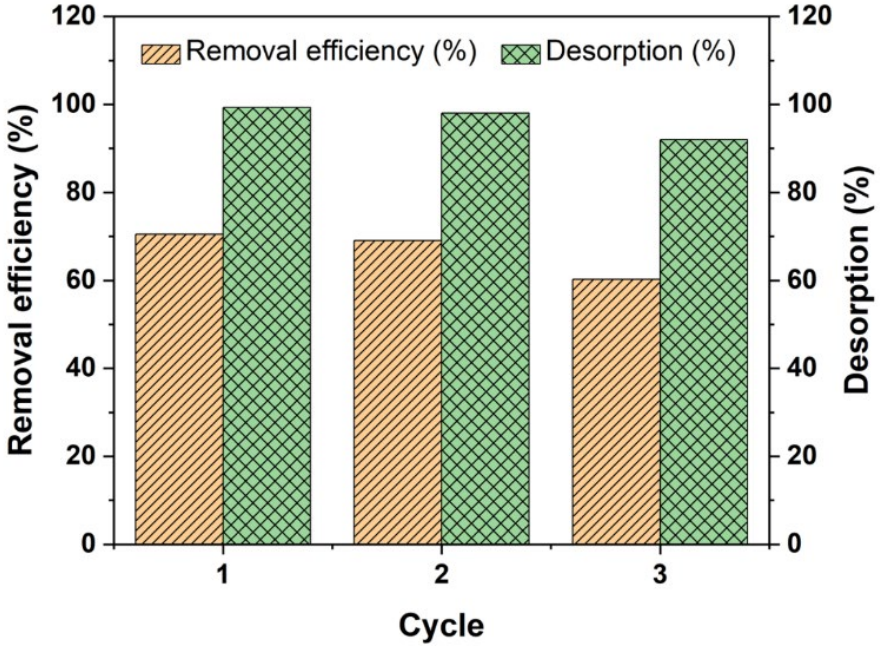

Figure 5.9 Regeneration and reusability of $NaPA_4$-CMCs cryogel after three cycles of adsorption/desorption: adsorbent dose 0.5 mg.mL^{-1}, initial concentration 50 ppm, pH 8.5, temperature 25 °C, contact time 300 min and 250 rpm for adsorption, HCl (0.1 M) / Methanol 1:1 v/v extraction solvent, time 3h, 100 rpm for desorption and NaOH (0.1 M), 1h for reactivation of adsorption sites

This result reveals that the binary solvent HCl (0.1 M) / methanol (1:1 v/v) used for desorption is adequate to remove the FLX bound to the sorption sites. This was justified by the yield of desorbed FLX, which was greater than 91 % for each desorption cycle. This could be explained by the protonation of the NH_2 and COO^- chemical functions on the interpenetrating polymer chains of the $NaPA_4$-CMCs monolith, which prevents electrostatically attractive interactions between the COO^- active sites and ionized FLX and

favors repulsion between the NH^{3+} groups and ionized FLX. When this adsorbent was reused, the FLX removal efficiency was greater than 60 %, although a decrease of approximately 14.5 % was observed after three adsorption/desorption cycles. This efficiency underlines the importance of the cryogel pre-treatment step carried out in the 0.1 M NaOH solution, which would reactivate the sorption sites by deprotonation of the COOH groups on the polymer chains. The decrease in adsorption performance could be explained by the competition between the Na^+ ions supplied by the NaOH solution during cryogel reactivation and ionized FLX. Na^+ ions would interact with sorption sites by establishing electrostatic interactions.

5.6.8 Proposed mechanism for the adsorption of fluoxetine on interpenetrated macroporous cryogel NaPA$_4$-CMCs

The study of adsorption isotherms and kinetic models provided information on the adsorption mechanism involved. However, this particular case did not allow us to precisely elucidate the mechanism governing the adsorption of FLX on the cryogels produced. The study of the thermodynamic parameters provided further insight, indicating that physisorption is the primary adsorption mechanism involved in the process. This is a plausible assumption, given the surface properties, including the chemical functions that have been identified through the characterization of the cryogels and the chemistry of the target molecule. The potential adsorption mechanism is illustrated in Figure 5.10.

The surface reaction is dominated by electrostatic interactions, hydrogen bonds, hydrophobes, and π-π electron donor-acceptor interactions (EDA interactions). The ionization of FLX and the negative surface charge of the cryogel attributed to the COO^- functional groups favor electrostatic adsorbate/adsorbent interactions. At the same time, the highly electronegative fluorine atoms of FLX could form hydrogen bonds with the hydrogen atoms of the free hydroxyl OH and amine NH_2 groups. These functional groups and the double bonds of genipin are π electron donors that can bind FLX through π–π EDA interactions with the aromatic rings of FLX and pi electron acceptors. Similar observations were made for the adsorption of FLX on carbon-based adsorbents [42,78]. Hydrophobic interactions can also occur between the hydrophobic sites of the cryogel and those of FLX.

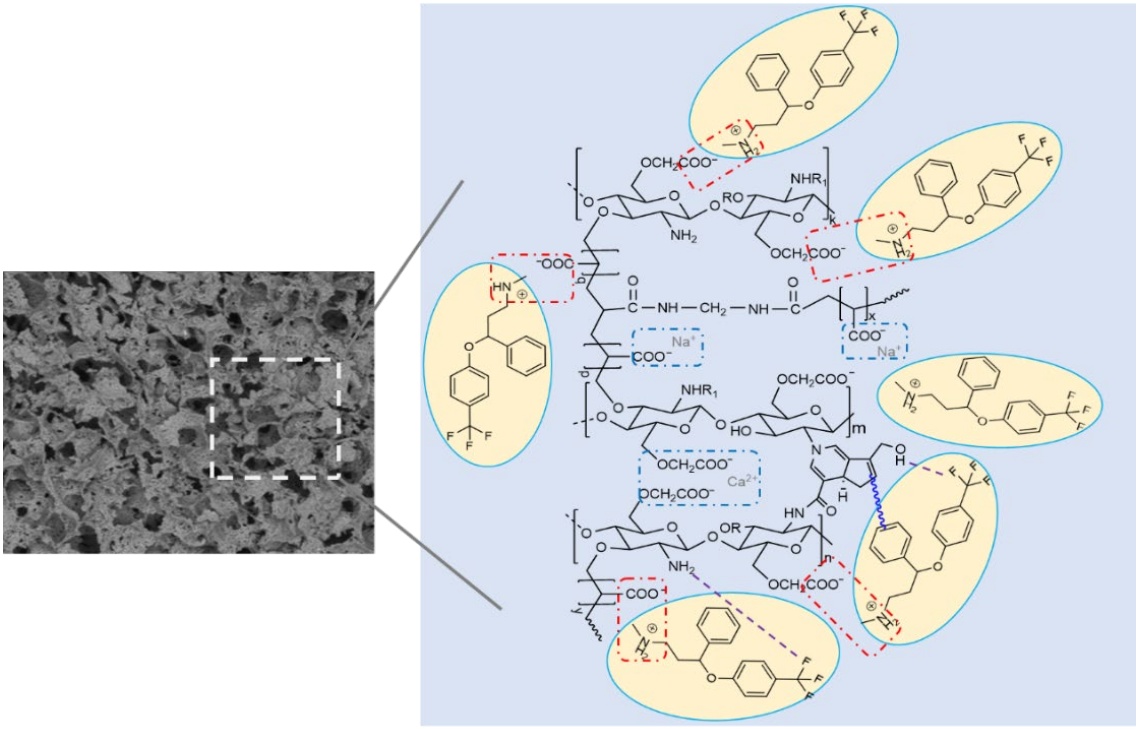

Figure 5.10 The potential adsorption mechanism of fluoxetine adsorption in the macroporous interpenetrated polymer network of NaPA4-CMCS cryogel at pH 8.5 and temperature 25 °C

5.6.9 Comparison with other sorbents developed in the literature

A comparative study of the adsorption of fluoxetine in aqueous solution between various adsorbents reported in the literature and the cryogel NaPA4-CMCs having presented more ability to retain this adsorbate was carried out. The results are reported in Table 5.7.

Table 5.7 Comparison of different adsorbents used for fluoxetine removal

Adsorbents	q_{max} ($mg.g^{-1}$)	Contact time (min)	Number of reuse cycles	Removal efficiency (%)	References
Activated carbon PBFG4	105.5	360	-	-	[79]
Granular activated carbon (GAC)	233.5	1800	-	-	[15]
PS800-10$ZnCl_2$	28.4	420	-	-	[79]
Nanocomposite XCM	90.9	120	4	24	[80]
Nanocomposite PCM	114.9	120	4	50	[80]
PHB4 (PEG/ O-CMCs, 3:3)	112.6	180	5	65	[19]
PHB5(PEG/N,O-CMCs 0:3)	109.3	180	5	65	[19]
NaPA4-CMCs cryogel	80.6	300	3	60	This work

5.7 Conclusion

The present study consisted of manufacturing macroporous cryogels by the cryopolymerization method from sodium acrylate/carboxymethyl chitosan solutions in the first instance and testing them for fluoxetine adsorption in batch mode in an aqueous solution in the second instance. Monoliths with a network of interpenetrating polymers stable in aqueous solution were obtained and coded as $NaPA_1$-CMCs, $NaPA_2$-CMCs, $NaPA_3$-CMCs, and $NaPA_4$-CMCs, considering the proportions of acrylic acid used in their manufacture. These materials were characterized using various analytical techniques that provided information on cryogel chemistry, surface morphology, thermal stability, and specific surface area. The swelling capacity of the hydrogels showed rapid swelling kinetics and an increase in swelling as the pH increased from 7 to 8.5. Determination of the pH at the zero-charge point revealed that the cryogel surface was negatively charged and could establish electrostatic interactions with FLX when the pH was between $pH_{PZC} < pH_{solution} < pKa_{FLX}$.

The effects of the parameters (temperature, pH, initial concentration, and contact time) on the FLX adsorption performance of the manufactured cryogels were investigated. Increasing the pH from 7 to 8.5 increased the adsorption performance of the cryogels, while the removal efficiency decreased with increasing temperature. Increasing the initial concentration improves the adsorption capacity, and above 100 ppm, it is stable, which implies that the available sorption sites have been exhausted. Analysis of the contact time as a function of the quantity of FLX adsorbed showed relatively faster adsorption for the $NaPA_1$-CMCs and $NaPA_2$-CMCs adsorbents compared to the $NaPA_3$-CMCs and $NaPA_4$-CMCs adsorbents. The study of these physicochemical parameters highlighted the $NaPA_4$-CMCs cryogel, which showed a greater ability to eliminate FLX. Therefore, modeling of the adsorption kinetics and the adsorption equilibrium was completed using experimental data on the adsorption of FLX on the $NaPA_4$-CMCs cryogel.

Modeling of the kinetics using pseudo-first-order and pseudo-second-order models revealed that the experimental data correlated well with the two models ($R^2 > 0.99$). The *RMSE* error function of the pseudo-second-order model was closer to zero, and the deviation between q_{cal} and q_{exp} of the pseudo-first-order model was smaller than that of

the pseudo-second-order model, suggesting that the pseudo-first-order model is better suited for describing the experimental kinetics data. The stepwise intraparticle diffusion study showed that the division $0 \leq t \leq 90$ min, step 1, and $90 < t \leq 300$ min, step 2 best described the internal diffusion step. The rate constants associated with these steps were $K_1 > K_2$, suggesting faster internal diffusion of FLX through the macropores and mesopores in the first step and almost no diffusion in the micropores. Modeling of the adsorption process by the Langmuir isotherm and Freundlich isotherm revealed that the Langmuir model fitted the experimental adsorption data well, as $R^2 \geq 0.977$ was higher than that of the Freundlich model. At the same time, the error functions $RMSE < 3.4$ were lower than those obtained from the Freundlich model. The maximum adsorption capacity was $q_{max} = 80.6 \pm 3.4$ mg.g^{-1} and the values of the separation factor R_L were between $0 < R_L < 1$, suggesting that the adsorption process was favorable.

This was validated by the values of negative Gibbs energy ($\Delta G° < 0$), which suggests synergy between physisorption and chemisorption during the adsorption process. The adsorption process is exothermic because $\Delta H° < 0$, and the absolute values of this thermodynamic parameter indicate that physisorption is the primary mechanism governing adsorption. The entropy $\Delta S° > 0$ suggested a random organization of FLX at the solution / $NaPA_4$-CMCs interface. The binary solvent HCl (0.1 M) / methanol 1:1 v/v) used for FLX desorption proved to be effective, which is justified by a desorption rate of approximately 91% after three cycles. The adsorption efficiency remained above 60% after three cycles, although there was a significant drop of approximately 14.5% in the adsorption performance of this cryogel.

5.8 Acknowledgments

The authors would like to thank the Natural Sciences and Engineering Research Council of Canada (NSERC), grant no. RGPIN-2016-04844, for financial support and the University of Quebec at Trois-Rivières for providing space, materials, and equipment to complete this research.

5.9 Declaration of Competing Interest

The authors have no financial or non-financial interests to disclose.

5.10 References

[1] C. Leong, K. Kowalec, S. Eltonsy, J.M. Bolton, M.W. Enns, Q. Tan, M. Yogendran, D. Chateau, J.A. Delaney, J. Sareen, J. Falk, R. Spiwak, S. Logsetty, S. Alessi-Severini, Psychotropic Medication Use Be-fore and During COVID-19: A Population-Wide Study, Front Pharmacol 13 (2022) 886652. https://doi.org/10.3389/FPHAR.2022.886652/BIBTEX.

[2] T. Oskotsky, I. Marić, A. Tang, B. Oskotsky, R.J. Wong, N. Aghaeepour, M. Sirota, D.K. Stevenson, Mortality Risk Among Patients With COVID-19 Prescribed Selective Serotonin Reuptake Inhibitor Anti-depressants, JAMA Netw Open 4 (2021) e2133090–e2133090. https://doi.org/10.1001/JAMANETWORKOPEN.2021.33090.

[3] N. Diaz-Camal, J.D. Cardoso-Vera, H. Islas-Flores, L.M. Gómez-Oliván, A. Mejía-García, Consumption and occurrence of antidepressants (SSRIs) in pre- and post-COVID-19 pandemic, their environmental impact and innovative removal methods: A review, Science of The Total Environment 829 (2022) 154656. https://doi.org/10.1016/J.SCITOTENV.2022.154656.

[4] C. Leong, K. Kowalec, S. Eltonsy, J.M. Bolton, M.W. Enns, Q. Tan, M. Yogendran, D. Chateau, J.A. Delaney, J. Sareen, J. Falk, R. Spiwak, S. Logsetty, S. Alessi-Severini, Psychotropic Medication Use Before and During COVID-19: A Population-Wide Study, Front Pharmacol 13 (2022) 886652. https://doi.org/10.3389/FPHAR.2022.886652/BIBTEX.

[5] E. Yavuz-Guzel, A. Atasoy, İ.E. Gören, N. Daglioglu, Impact of COVID- 19 pandemic on antidepressants consumptions by wastewater analysis in Turkey, Science of the Total Environment 838 (2022). https://doi.org/10.1016/j.scitotenv.2022.155916.

[6] AGMR, Rapport sur le marché mondial des antidépresseurs 2021 : implications et croissance du COVID-19 jusqu'en 2030, 2021, (n.d.).

[7] A. Singh, D. Saidulu, A.K. Gupta, V. Kubsad, Occurrence and fate of antidepressants in the aquatic environment: Insights into toxicological effects on the aquatic life, analytical methods, and removal techniques, J Environ Chem Eng 10 (2022) 109012. https://doi.org/10.1016/J.JECE.2022.109012.

[8] C. Castillo-Zacarías, M.E. Barocio, E. Hidalgo-Vázquez, J.E. Sosa-Hernández, L. Parra-Arroyo, I.Y. López-Pacheco, D. Barceló, H.N.M. Iqbal, R. Parra-Saldívar, Antidepressant drugs as emerging contaminants: Occurrence in urban and non-urban waters and analytical methods for their detection, Science of the Total Environment 757 (2021). https://doi.org/10.1016/j.scitotenv.2020.143722.

[9] C. Castillo-Zacarías, M.E. Barocio, E. Hidalgo-Vázquez, J.E. Sosa-Hernández, L. Parra-Arroyo, I.Y. López-Pacheco, D. Barceló, H.N.M. Iqbal, R. Parra-Saldívar, Antidepressant drugs as emerging contaminants: Occurrence in urban and non-urban waters and analytical methods for their detection, Science of The Total Environment 757 (2021) 143722. https://doi.org/10.1016/J.SCITOTENV.2020.143722.

[10] A. Lajeunesse, S.A. Smyth, K. Barclay, S. Sauvé, C. Gagnon, Distribution of antidepressant residues in wastewater and biosolids following different treatment processes by municipal wastewater treatment plants in Canada, Water Res 46 (2012) 5600–5612. https://doi.org/10.1016/J.WATRES.2012.07.042.

[11] P. Arnnok, R.R. Singh, R. Burakham, A. Pérez-Fuentetaja, D.S. Aga, Selective Uptake and Bioaccumulation of Antidepressants in Fish from Effluent-Impacted Niagara River, Environ Sci Technol 51 (2017) 10652–10662. https://doi.org/10.1021/ACS.EST.7B02912/SUPPL_FILE/ES7B02912_SI_001.PDF.

[12] K. Nowakowska, J. Giebułtowicz, M. Kamaszewski, A. Adamski, H. Szudrowicz, T. Ostaszewska, U. Solarska-Dzięciołowska, G. Nałęcz-Jawecki, P. Wroczyński,

A. Drobniewska, Acute exposure of zebrafish (Danio rerio) larvae to environmental concentrations of selected antidepressants: Bioaccumulation, physiological and histological changes, Comparative Biochemistry and Physiology Part C: Toxicology & Pharmacology 229 (2020) 108670. https://doi.org/10.1016/J.CBPC.2019.108670.

[13] J.M. Orozco-Hernández, L.M. Gómez-Oliván, G.A. Elizalde-Velázquez, K.E. Rosales-Pérez, J.D. Cardoso-Vera, G. Heredia-García, H. Islas-Flores, S. García-Medina, M. Galar-Martínez, Fluoxetine-induced neurotoxicity at environmentally relevant concentrations in adult zebrafish Danio rerio, Neurotoxicology 90 (2022) 121–129. https://doi.org/10.1016/J.NEURO.2022.03.007.

[14] D. Correia, I. Domingues, M. Faria, M. Oliveira, Chronic Effects of Fluoxetine on Danio rerio: A Biochemical and Behavioral Perspective, Applied Sciences (Switzerland) 12 (2022) 2256. https://doi.org/10.3390/APP12042256/S1.

[15] B. Silva, M. Martins, M. Rosca, V. Rocha, A. Lago, I.C. Neves, T. Tavares, Waste-based biosorbents as cost-effective alternatives to commercial adsorbents for the retention of fluoxetine from water, Sep Purif Technol 235 (2020). https://doi.org/10.1016/j.seppur.2019.116139.

[16] S. Aydın, F. Bedük, A. Ulvi, M.E. Aydın, Simple and effective removal of psychiatric pharmaceuticals from wastewater treatment plant effluents by magnetite red mud nanoparticles, Science of The Total Environment 784 (2021) 147174. https://doi.org/10.1016/J.SCITOTENV.2021.147174.

[17] S.S. Ray, R. Gusain, N. Kumar, Water purification using various technologies and their advantages and disadvantages, Carbon Nanomaterial-Based Adsorbents for Water Purification (2020) 37–66. https://doi.org/10.1016/B978-0-12-821959-1.00003-9.

[18] I.O. Saheed, W. Da Oh, F.B.M. Suah, Chitosan modifications for adsorption of pollutants – A review, J Hazard Mater 408 (2021) 124889. https://doi.org/10.1016/J.JHAZMAT.2020.124889.

[19] G.R.N. Nkana, A. Lajeunesse, B. Chabot, P. Nguyen-Tri, Design of porous spherical biomaterials from carboxymethyl chitosan for removal of fluoxetine in aqueous medium, J Environ Chem Eng 12 (2024) 112228. https://doi.org/10.1016/J.JECE.2024.112228.

[20] P. Mohammadzadeh Pakdel, S.J. Peighambardoust, A review on acrylic based hydrogels and their applications in wastewater treatment, J Environ Manage 217 (2018) 123–143. https://doi.org/10.1016/j.jenvman.2018.03.076.

[21] X. Qi, L. Wu, T. Su, J. Zhang, W. Dong, Polysaccharide-based cationic hydrogels for dye adsorption, Colloids Surf B Biointerfaces 170 (2018) 364–372. https://doi.org/10.1016/j.colsurfb.2018.06.036.

[22] G. Crini, Recent developments in polysaccharide-based materials used as adsorbents in wastewater treatment, Prog Polym Sci 30 (2005) 38–70. https://doi.org/10.1016/J.PROGPOLYMSCI.2004.11.002.

[23] M. Jamali, A. Akbari, Facile fabrication of magnetic chitosan hydrogel beads and modified by interfacial polymerization method and study of adsorption of cationic/anionic dyes from aqueous solution, J Environ Chem Eng 9 (2021). https://doi.org/10.1016/j.jece.2021.105175.

[24] A. Ayub, Z.A. Raza, M.I. Majeed, M.R. Tariq, A. Irfan, Development of sustainable magnetic chitosan biosorbent beads for kinetic remediation of arsenic contaminated water, Int J Biol Macromol 163 (2020) 603–617. https://doi.org/10.1016/j.ijbiomac.2020.06.287.

[25] M. Jamali, A. Akbari, Facile fabrication of magnetic chitosan hydrogel beads and modified by interfacial polymerization method and study of adsorption of cationic/anionic dyes from aqueous solution, J Environ Chem Eng 9 (2021) 105175. https://doi.org/10.1016/J.JECE.2021.105175.

[26] M. Jalilzadeh, S. Şenel, Removal of Cu(II) ions from water by ion-imprinted magnetic and non-magnetic cryogels: A comparison of their selective Cu(II)

removal performances, Journal of Water Process Engineering 13 (2016) 143–152. https://doi.org/10.1016/j.jwpe.2016.08.010.

[27] S. Ghayempour, M. Montazer, A modified microemulsion method for fabrication of hydrogel Tragacanth nanofibers, Int J Biol Macromol 115 (2018) 317–323. https://doi.org/10.1016/J.IJBIOMAC.2018.04.037.

[28] S. Butylina, S. Geng, K. Oksman, Properties of as-prepared and freeze-dried hydrogels made from poly(vinyl alcohol) and cellulose nanocrystals using freeze-thaw technique, Eur Polym J 81 (2016) 386–396. https://doi.org/10.1016/J.EURPOLYMJ.2016.06.028.

[29] M. Khan, I.M.C. Lo, A holistic review of hydrogel applications in the adsorptive removal of aqueous pollutants: Recent progress, challenges, and perspectives, Water Res 106 (2016) 259–271. https://doi.org/10.1016/j.watres.2016.10.008.

[30] M.Y. Shi, L.J. Jiang, C.J. Yu, X.R. Dong, Q.Y. Yu, M.M. Yao, S.S. He, Z.W. Yue, F.L. Yao, H. Zhang, H. Sun, J.J. Li, A robust polyacrylic acid/chitosan cryogel for rapid hemostasis, Sci China Technol Sci 65 (2022) 1029–1042. https://doi.org/10.1007/S11431-021-1986-9/METRICS.

[31] A. Baimenov, D.A. Berillo, S.G. Poulopoulos, V.J. Inglezakis, A review of cryogels synthesis, characterization and applications on the removal of heavy metals from aqueous solutions, Adv Colloid Interface Sci 276 (2020). https://doi.org/10.1016/j.cis.2019.102088.

[32] V. Rac, S. Lević, B. Balanč, B. Olalde Graells, G. Bijelić, PVA Cryogel as model hydrogel for iontophoretic transdermal drug delivery investigations. Comparison with PAA/PVA and PAA/PVP interpenetrating networks, Colloids Surf B Biointerfaces 180 (2019) 441–448. https://doi.org/10.1016/j.colsurfb.2019.05.017.

[33] S. Zhao, D. Wang, S. Zhu, X. Liu, H. Zhang, 3D cryogel composites as adsorbent for isolation of protein and small molecules, Talanta 191 (2019) 229–234. https://doi.org/10.1016/J.TALANTA.2018.08.068.

[34] Z. Li, L. Yang, H. Cao, Y. Chang, K. Tang, Z. Cao, J. Chang, Y. Cao, W. Wang, M. Gao, C. Liu, D. Liu, H. Zhao, Y. Zhang, M. Li, Carbon materials derived from chitosan/cellulose cryogel-supported zeolite imidazole frameworks for potential supercapacitor application, Carbohydr Polym 175 (2017) 223–230. https://doi.org/10.1016/j.carbpol.2017.07.089.

[35] H. Zhang, F. Zhang, J. Wu, Physically crosslinked hydrogels from polysaccharides prepared by freeze-thaw technique, React Funct Polym 73 (2013) 923–928. https://doi.org/10.1016/j.reactfunctpolym.2012.12.014.

[36] O.E. Zaborina, R.G. Gasanov, A.S. Peregudov, V.I. Lozinsky, Cryostructuring of polymeric systems. 38. The causes of the covalently-crosslinked cryogels formation upon the homopolymerization of N,N-dimethylacrylamide in moderately-frozen aqueous media, Eur Polym J 61 (2014) 226–239. https://doi.org/10.1016/j.eurpolymj.2014.10.006.

[37] M. Jalilzadeh, S. Şenel, Removal of Cu(II) ions from water by ion-imprinted magnetic and non-magnetic cryogels: A comparison of their selective Cu(II) removal performances, Journal of Water Process Engineering 13 (2016) 143–152. https://doi.org/10.1016/J.JWPE.2016.08.010.

[38] M.Y. Kim, T.G. Lee, Removal of Pb(II) ions from aqueous solutions using functionalized cryogels, Chemosphere 217 (2019) 423–429. https://doi.org/10.1016/J.CHEMOSPHERE.2018.10.021.

[39] S. Bratskaya, Y. Privar, A. Slobodyuk, D. Shashura, D. Marinin, A. Mironenko, V. Zheleznov, A. Pestov, Cryogels of carboxyalkylchitosans as a universal platform for the fabrication of composite materials, Carbohydr Polym 209 (2019) 1–9. https://doi.org/10.1016/j.carbpol.2018.12.094.

[40] M. Jalilzadeh, S. Şenel, Removal of Cu(II) ions from water by ion-imprinted magnetic and non-magnetic cryogels: A comparison of their selective Cu(II) removal performances, Journal of Water Process Engineering 13 (2016) 143–152. https://doi.org/10.1016/J.JWPE.2016.08.010.

[41] M.Y. Kim, T.G. Lee, Removal of Pb(II) ions from aqueous solutions using functionalized cryogels, Chemosphere 217 (2019) 423–429. https://doi.org/10.1016/j.chemosphere.2018.10.021.

[42] A. Lago, B. Silva, T. Tavares, Biowaste valorization on pharmaceuticals and pesticides abatement in aqueous environments, Sustainable Materials and Technologies 39 (2024). https://doi.org/10.1016/j.susmat.2023.e00792.

[43] B.C. Melo, F.A.A. Paulino, V.A. Cardoso, A.G.B. Pereira, A.R. Fajardo, F.H.A. Rodrigues, Cellulose nanowhiskers improve the methylene blue adsorption capacity of chitosan-g-poly(acrylic acid) hydrogel, Carbohydr Polym 181 (2018) 358–367. https://doi.org/10.1016/j.carbpol.2017.10.079.

[44] C. Che, L. Liu, X. Wang, X. Zhang, S. Luan, J. Yin, X. Li, H. Shi, Surface-Adaptive and On-Demand Antibacterial Sponge for Synergistic Rapid Hemostasis and Wound Disinfection, ACS Biomater Sci Eng 6 (2020) 1776–1786. https://doi.org/10.1021/ACSBIOMATERIALS.0C00069/ASSET/IMAGES/LARGE/AB0C00069_0004.JPEG.

[45] A. Camiré, B. Chabot, A. Lajeunesse, Sorption Capacities of a Lignin-Based Electrospun Nanofibrous Material for Pharmaceutical Residues Remediation in Water, Sorption in 2020s (2019). https://doi.org/10.5772/INTECHOPEN.88621.

[46] J. Wang, X. Guo, Adsorption isotherm models: Classification, physical meaning, application and solving method, Chemosphere 258 (2020). https://doi.org/10.1016/j.chemosphere.2020.127279.

[47] R.K. Farag, R.R. Mohamed, Synthesis and characterization of carboxymethyl chitosan nanogels for swelling studies and antimicrobial activity, Molecules 18 (2013) 190–203. https://doi.org/10.3390/molecules18010190.

[48] F.G.L. Medeiros Borsagli, A.A.P. Mansur, P. Chagas, L.C.A. Oliveira, H.S. Mansur, O-carboxymethyl functionalization of chitosan: Complexation and adsorption of Cd (II) and Cr (VI) as heavy metal pollutant ions, React Funct Polym 97 (2015) 37–47. https://doi.org/10.1016/j.reactfunctpolym.2015.10.005.

[49] M.N.M. Ismael, A. El Nemr, E.S.H. El Ashry, H. Abdel Hamid, Removal of Hexavalent Chromium by Cross-Linking Chitosan and N,N'-Methylene Bis-Acrylamide, Environmental Processes 7 (2020) 911–930. https://doi.org/10.1007/s40710-020-00447-2.

[50] H. Geng, Preparation and characterization of cellulose/N,N'-methylene bisacrylamide/graphene oxide hybrid hydrogels and aerogels, Carbohydr Polym 196 (2018) 289–298. https://doi.org/10.1016/j.carbpol.2018.05.058.

[51] F.A. Whitehead, S.A. Young, S. Kasapis, Swelling behaviour and glass transition in genipin-crosslinked chitosan systems, Int J Biol Macromol 164 (2020) 3075–3083. https://doi.org/10.1016/j.ijbiomac.2020.08.178.

[52] A. Sávio, G. Magalhães, M.P.A. Neto, M.N. Bezerra, N.M.P.S. Ricardo, J.P.A. Feitosa, Application of FTIR in The Determination of Acrylate Content in Poly(Sodium Acrylate-co-Acrylamide) Superabsorbent Hydrogels, 2012.

[53] R. Di Maggio, S. Dirè, E. Callone, L. Bergamonti, P.P. Lottici, R. Albatici, R. Rigon, N. Ataollahi, Super-adsorbent polyacrylate under swelling in water for passive solar control of building envelope, SN Appl Sci 2 (2020). https://doi.org/10.1007/s42452-019-1814-4.

[54] M. Zhang, Z. Cheng, T. Zhao, M. Liu, M. Hu, J. Li, Synthesis, characterization, and swelling behaviors of salt-sensitive maize bran-poly(acrylic acid)

superabsorbent hydrogel, J Agric Food Chem 62 (2014) 8867–8874. https://doi.org/10.1021/jf5021279.

[55] Y. Liu, Z. Cai, L. Sheng, M. Ma, Q. Xu, Y. Jin, Structure-property of crosslinked chitosan/silica composite films modified by genipin and glutaraldehyde under alkaline conditions, Carbohydr Polym 215 (2019) 348–357. https://doi.org/10.1016/j.carbpol.2019.04.001.

[56] X.G. Chen, H.J. Park, Chemical characteristics of O-carboxymethyl chitosans related to the preparation conditions, Carbohydr Polym 53 (2003) 355–359. https://doi.org/10.1016/S0144-8617(03)00051-1.

[57] F.R. de Abreu, S.P. Campana-Filho, Characteristics and properties of carboxymethylchitosan, Carbohydr Polym 75 (2009) 214–221. https://doi.org/10.1016/J.CARBPOL.2008.06.009.

[58] N. Hwang, A.R. Barron, OpenStax-CNX module: m38278 1 BET Surface Area Analysis of Nanoparticles * This work is produced by OpenStax-CNX and licensed under the Creative Commons Attribution License 3.0 †, n.d. http://cnx.org/content/m38278/1.1/.

[59] O. Okay, V.I. Lozinsky, Synthesis and structure–property relationships of cryogels, Advances in Polymer Science 263 (2014) 103–157. https://doi.org/10.1007/978-3-319-05846-7_3.

[60] L. Chen, Y. Du, R. Huang, Novel pH, ion sensitive polyampholyte gels based on carboxymethyl chitosan and gelatin, Polym Int 52 (2003) 56–61. https://doi.org/10.1002/pi.997.

[61] W. Rudzinski, W. Plazinski, Theoretical description of the kinetics of solute adsorption at heterogeneous solid/solution interfaces. On the possibility of distinguishing between the diffusional and the surface reaction kinetics models, Appl Surf Sci 253 (2007) 5827–5840. https://doi.org/10.1016/j.apsusc.2006.12.038.

[62] J. Wang, X. Guo, Adsorption kinetic models: Physical meanings, applications, and solving methods, J Hazard Mater 390 (2020). https://doi.org/10.1016/j.jhazmat.2020.122156.

[63] J. Wang, X. Guo, Rethinking of the intraparticle diffusion adsorption kinetics model: Interpretation, solving methods and applications, Chemosphere 309 (2022). https://doi.org/10.1016/j.chemosphere.2022.136732.

[64] M. Mozaffari Majd, V. Kordzadeh-Kermani, V. Ghalandari, A. Askari, M. Sillanpää, Adsorption isotherm models: A comprehensive and systematic review (2010−2020), Science of the Total Environment 812 (2022). https://doi.org/10.1016/j.scitotenv.2021.151334.

[65] M.A. Al-Ghouti, D.A. Da'ana, Guidelines for the use and interpretation of adsorption isotherm models: A review, J Hazard Mater 393 (2020) 122383. https://doi.org/10.1016/J.JHAZMAT.2020.122383.

[66] H.N. Tran, S.J. You, H.P. Chao, Thermodynamic parameters of cadmium adsorption onto orange peel calculated from various methods: A comparison study, J Environ Chem Eng 4 (2016) 2671–2682. https://doi.org/10.1016/j.jece.2016.05.009.

[67] X. Zhou, X. Yu, J. Hao, H. Liu, Correction to the thermodynamic calculation using the Langmuir isotherm model by Saeed et al. (2022), J Hazard Mater 435 (2022). https://doi.org/10.1016/j.jhazmat.2022.129014.

[68] T. Chen, T. Da, Y. Ma, Reasonable calculation of the thermodynamic parameters from adsorption equilibrium constant, J Mol Liq 322 (2021). https://doi.org/10.1016/j.molliq.2020.114980.

[69] J. López-Luna, L.E. Ramírez-Montes, S. Martinez-Vargas, A.I. Martínez, O.F. Mijangos-Ricardez, María, C.A. González-Chávez, R. Carrillo-González, Fernando, A. Solís-Domínguez, C. Cuevas-Díaz, Virgilio Vázquez-Hipólito, Linear and nonlinear kinetic and isotherm adsorption models for arsenic removal

by manganese ferrite nanoparticles, SN Appl Sci 1 (2019). https://doi.org/10.1007/s42452-019-0977-3.

[70] H.N. Tran, S.-J. You, H.-P. Chao, Thermodynamic parameters of cadmium adsorption onto orange peel calculated from various methods: A comparison study, n.d.

[71] A. Zarrouk, B. Hammouti, H. Zarrok, S.S. Al-Deyab, M. Messali, A.-M. Almounawwara, S. Arabia, Temperature Effect, Activation Energies and Thermodynamic Adsorption Studies of L-Cysteine Methyl Ester Hydrochloride As Copper Corrosion Inhibitor In Nitric Acid 2M, 2011. www.electrochemsci.org.

[72] Donahue1965, (n.d.).

[73] G. Moretti, F. Guidi, G. Grion, Tryptamine as a green iron corrosion inhibitor in 0.5 M deaerated sulphuric acid, Corros Sci 46 (2004) 387–403. https://doi.org/10.1016/S0010-938X(03)00150-1.

[74] M.H.W. b Gamal K. Gomma a, Schiff bases as corrosion inhibitors for aluminum in hydrochloric acid solution, Mater Chem Phys 39 (1995) 209–213.

[75] R.D.M.A.J. and B.K. William Durnie1, Development of a Structure-Activity Relationship for Oil Field Corrosion Inhibitors, J Electrochem Soc 146 (1999).

[76] A.D.M. Silva, D.F. Fernandes, S.A. Figueiredo, O.M. Freitas, C. Delerue-Matos, Fluoxetine and Nutrients Removal from Aqueous Solutions by Phycoremediation, Int J Environ Res Public Health 19 (2022). https://doi.org/10.3390/ijerph19106081.

[77] R. Langer, Polymer Systems for Controlled Release of Macromolecules, Immobilized Enzyme Medical Bioreactors, and Tissue Engineering, in: Advances in Chemical Engineering, 1994: pp. 1–50. https://doi.org/10.1016/S0065-2377(08)60212-4.

[78] S. Román, J.M.V. Nabais, B. Ledesma, C. Laginhas, M.M. Titirici, Surface interactions during the removal of emerging contaminants by hydrochar-based adsorbents, Molecules 25 (2020). https://doi.org/10.3390/molecules25092264.

[79] G. Jaria, V. Calisto, M.V. Gil, M. Otero, V.I. Esteves, Removal of fluoxetine from water by adsorbent materials produced from paper mill sludge, J Colloid Interface Sci 448 (2015) 32–40. https://doi.org/10.1016/J.JCIS.2015.02.002.

[80] H.H. Farghal, M. Nebsen, M.M.H. El-Sayed, Eco-friendly Biopolymer/Activated Charcoal Magnetic Nanocomposites with Enhanced Stability and Adsorption Properties for Water Treatment Applications, J Polym Environ 31 (2023) 5338–5354. https://doi.org/10.1007/s10924-023-02959-y.

Chapitre 6 - Article 3

6.1 Avant-propos

Le titre du troisième article scientifique est: «Removal of fluoxetine by adsorption in a fixed-bed column using a hybrid cryogel based on sodium poly(acrylate) / carboxymethyl chitosan ». Il a été soumis à la revue scientifique Journal of Environmental Management en 2025.

Les auteurs et leurs coordonnées correspondantes sont, dans l'ordre:

Gilbert Romeo Nkana Nkana : Étudiant au Doctorat en sciences et génie des matériaux lignocellulosiques, Institut d'Innovations en Écomatériaux, Écoproduits et Écoénergies à base de biomasse (I2E3), Université du Québec à Trois-Rivières, 3351 Boulevard des Forges, CP.500, Trois-Rivières, Québec, Canada, G9A 5H7
Courriel : Gilbert.Nkana@uqtr.ca

Phuong Nguyen-Tri, Ph.D. : Directeur de thèse
Professeur au Département de biochimie, chimie, physique et sciences forensiques et chercheuse à l'Institut de recherche sur l'hydrogène, Université du Québec à Trois-Rivières, 3351 Boulevard des Forges, C.P. 500, Trois-Rivières, Québec, Canada, G9A 5H7.
Courriel: Phuong.Nguyen-Tri@uqtr.ca

Bruno Chabot, Ph.D. Co-Directeur de thèse et auteur pour la correspondance Institut d'Innovation en Écomatériaux, Écoproduits et Écoénergies à basse de biomasse, Université du Québec à Trois-Rivières, 3351 Boulevard des Forges, C.P. 500, Trois-Rivières, Québec, Canada, G9A 5H7
Courriel: bruno.Chabot@uqtr.ca

Contribution des auteurs: Gilbert Nkana est l'auteur principal de cet article. Il a mené toutes les expériences scientifiques et réalisé les développements associés. M. Nguyen-Tri est directeur de recherche et M. Chabot est co-directeur de cette recherche. Le directeur et le co-directeur ont participé à la révision et à la correction du manuscrit.

6.2 Résumé

Le développement d'adsorbants alternatifs respectueux de l'environnement capables d'éliminer les produits pharmaceutiques, en particulier les antidépresseurs dans les milieux aqueux est un défi actuel. Dans cette étude, un cryogel hybride d'acrylate de sodium et de carboxyméthylchitosane (NaPA-CMCs) a été synthétisé à l'aide d'une méthode de cryogélation et testé pour l'élimination des antidépresseurs dans une colonne à lit fixe. La fluoxétine (FLX) a servi de contaminant cible, tandis que le citalopram (CIT) et la venlafaxine (VEN) ont été utilisés pour des tests d'adsorption compétitive. Les effets du pH, du débit (Q), de la hauteur du lit (H) et de la concentration initiale (C0) sur les courbes de percée ont été étudiés. Le taux d'élimination maximal de la FLX (59 %) a été obtenu lorsque les paramètres expérimentaux étaient les suivants : pH 8,5, H 0,4 cm, Q 1,5 mL/min et C_0 10 ppm. L'adsorption compétitive a révélé une affinité plus élevée du FLX pour la surface du cryogel hybride (9,98 mg/g) par rapport au CIT (4 mg/g) et au VEN (2,17 mg/g). Le pH_{PZC} 7,1 du cryogel hybride, le pKa 9,8 du FLX et le pH des solutions peuvent expliquer les interactions électrostatiques entre les sites de sorption et le FLX ionisé. Les modèles de Thomas et Yoon-Nelson décrivent avec précision les données d'adsorption expérimentales ($R^2 > 0,97$ et RMSE < 0,062). Le taux d'élimination était de 17,76 % après quatre cycles d'adsorption/désorption. Le cryogel NaPA-CMCs présente un potentiel pour éliminer les antidépresseurs de l'eau.

6.3 Abstract

The development of environmentally friendly alternative adsorbents capable of removing pharmaceuticals, particularly antidepressants, from aqueous environments is a current challenge. In this study, hybrid cryogel of sodium acrylate and carboxymethyl chitosan (NaPA-CMCs) was synthesized using cryogelation method and tested for antidepressant removal in a fixed-bed column. Fluoxetine (FLX) served as the target contaminant, with citalopram (CIT) and venlafaxine (VEN) used for competitive adsorption tests. The effects of pH, flow rate (Q), bed height (H), and initial concentration (C_0) on breakthrough curves were studied. Maximum FLX removal rate (59 %) was obtained when experimental parameters were pH 8.5, H 0.4 cm, Q 1.5 mL/min and C_0 10 ppm. Competitive adsorption

revealed a higher affinity of FLX for the surface of hybrid cryogel (9.98 mg/g) compared to CIT (4 mg/g) and VEN (2.17 mg/g). The pH_{PZC} 7.1 of the hybrid cryogel, the pKa 9.8 of FLX and the pH of the solutions may explain the electrostatic interactions between the sorption sites and ionized FLX. The Thomas and Yoon-Nelson models accurately describe the experimental adsorption data ($R^2 > 0.97$ and RMSE < 0.062). The elimination rate was 17.76% after four adsorption/desorption cycles. The NaPA-CMCs cryogel shows potential for removing antidepressants from water.

6.4 Introduction

Global mental health remains a major concern for the World Health Organization (WHO), with depression and anxiety affecting around 3-4 % of the world's population (Matthew Ridley https://ORCID.ORG/0000-0001-7612-7436, 2020). Additionally, the COVID-19 pandemic has worsened the already toxic environment where vulnerable populations live and, as a result, has led to increased use of psychotropic drugs such as antidepressants ("AGMR, Antidepressants Global Market Report 2021: Covid-19 Implications and Growth to 2030, 2021.,"). This situation continues even in the post-pandemic years, according to recent studies (Santomauro et al., 2021). Unfortunately, human activity contributes significantly to the entry of antidepressant residues and their metabolites into wastewater treatment plants (WWTPs). They have also been detected in WWTP effluents and other environmental matrices, highlighting the ineffectiveness of conventional wastewater treatment processes. The chemical stability and biological activity of these emerging pollutants raise concerns about their environmental impact. Numerous studies have reported their ability to bioaccumulate in non-target aquatic organisms living in receiving environments (Arnnok et al., 2017; Singh et al., 2022a). Their toxicological effects on the aquatic ecosystem are well documented and reveal their ability to cause behavioral changes in many aquatic species (Correia et al., 2023; Gould et al., 2021; Singh et al., 2022b; Wang et al., 2023). They can affect physiological functions and disrupt reproduction, which is likely to cause imbalances throughout the food web (Campos et al., 2016; Correia et al., 2022; Eisenreich et al., 2017; Orozco-Hernández et al., 2022). In the long term, this could adversely affect the availability of certain fish resources for human consumption. The detection, measurement, and efficient elimination of antidepressants

from wastewater are therefore urgent environmental issues to maintain the stability of aquatic ecosystems.

Various biological and physico-chemical processes have been developed by researchers to remove antidepressants from aqueous environments (Diaz-Camal et al., 2022; Fernandes et al., 2019; Köse et al., 2024; Lajeunesse et al., 2013; Singh et al., 2022b; Zhao et al., 2017a). Most have shown promising results but face limitations like antidepressants' persistence harming microorganisms that degrade them, producing toxic by-products, complex processes, and high costs. These treatment techniques include phytoremediation using selectively cultivated microorganisms, photocatalysis, photochemical oxidation, electrocatalysis, ozonation, electro-peroxone systems, and photoelectro-Fenton systems (Gornik et al., 2020; Melin et al., 2021; Méndez-Arriaga et al., 2011; Pan et al., 2022; Silva et al., 2022; Zhao et al., 2017b). It is therefore imperative to develop advanced treatment technologies that are more simple, effective, inexpensive, and generate less toxic by-products. In the context of sustainable development, adsorption is an attractive, simple, and inexpensive technology that has proven itself in the removal of a wide range of pharmaceutical products (Escudero-Curiel et al., 2021; Jaria et al., 2015; Juang et al., 2026; Nkana et al., 2024a). This technique uses two mechanisms, determined by the bonding forces involved in adsorption. These are physisorption, which involve low-energy interactions between the adsorbate and the adsorbent, and chemisorption, which involves stronger bonds. It should be noted that there are several treatment methods in the literature, including batch treatment and continuous fixed-bed treatment, which are the most widely studied for the removal of pollutants from aqueous media. Batch adsorption enables the treatment of small volumes of wastewater with low pollutant loads. This is a limitation of this method, as it cannot be scaled up to industrial levels. However, it enables the evaluation of the feasibility and efficiency of adsorption for a specific adsorbate-adsorbent system, as demonstrated in our previous study of the NaPA-CMCs-Fluoxetine cryogel system (Nkana et al., 2024a).

Continuous fixed-bed adsorption enables the treatment of larger volumes of wastewater containing high concentrations of pollutants. This method is better suited for industrial applications, which is especially relevant to our interests, as the main goal of this study is

to develop an adsorbent material that can potentially be used for the antidepressant removing in water solution (Patel, 2021). This process involves placing the adsorbent in a column and steadily injecting the pollutant-containing solution at a controlled flow rate, either upstream or downstream. It is important to optimize several factors, such as pH, flow rate, initial adsorbate concentration at the column inlet, column height, particle size, etc., that ensure the column functions properly and prevent premature exhaustion of the adsorbent. For that, breakthrough curve data is required. The breakthrough curve of an adsorbate in a dynamic adsorption system represents the ratio of influent concentration to effluent concentration over time. Analyzing breakthrough curves helps us to understand adsorption dynamics, enabling the design and optimization of adsorption systems. In this case, modelling breakthrough curves is an important step in analysing dynamic adsorption data. The Thomas and Yoon-Nelson models are the most commonly used in the literature for adjusting breakthrough curves (Thomas H, 1944; Yoon and Nelson, 1984).

Research studies have shown that activated carbon, titanium dioxide nanoparticles, and cation exchange resins are used to adsorb antidepressant residues in aqueous media (Choi et al., 2020; Maršálek and Švidrnoch, 2020). However, the regeneration and reuse of these adsorbents generate additional costs, prompting the exploration of alternatives like biopolymer-based options such as cryogels. Cryogels are three-dimensional porous materials produced by cryogelation or cryotopic gelation. This technique involves in situ radical polymerization of a solution of a water-soluble monomer/polymer and a cross-linking agent in the presence of an initiator system at a temperature below zero. The formation of ice crystals expels the reactants into microspaces between the formed crystals (cryoconcentration), leading to a sharp increase in concentration in these microspaces where cryopolymerization takes place. The developed macroporosity is created by ice crystals, which leave open spaces (pores) after the cryogel thaws (Baimenov et al., 2020; Gun'ko et al., 2013; Kumar et al., 2010; Okay and Lozinsky, 2014). These materials are used for various applications, especially adsorption, due to their superior features, including a network of interconnected macropores that promotes good diffusion and excellent mass transfer, as well as their good mechanical stability (Agustin et al., 2023; Baimenov et al., 2020). The selection of monomer/polymer, crosslinker, temperature, and cryogelation time significantly influences the structural and functional properties of

cryogels (Baimenov et al., 2020; Doser et al., 2023; Lozinsky and Okay, 2014). Synthetic monomers, biopolymers, and their combinations (natural-synthetic) have been widely used to manufacture cryogels. These materials offer main advantages of being biodegradable and biocompatible; however, unlike synthetic cryogels, they exhibit poor mechanical stability. Developing hybrid cryogels enhances mechanical strength while maintaining the features of natural cryogels. It also enables new properties through the combination of biopolymers and synthetic monomers (Doser et al., 2023; Izadpanah et al., 2024; Lozinsky, 2002; Shi et al., 2022).

Several biopolymers have been used to manufacture hybrid cryogels depending on the targeted applications. These include chitosan and its derivatives, alginate, starch, xanthan gum, and cellulose (Doser et al., 2023; Lozinsky, 2002). These polysaccharides are environmentally friendly, easily accessible, inexpensive, and can be chemically altered to enhance the selectivity of cryogels (Bratskaya et al., 2019; Doser et al., 2023; Lozinsky, 2002; Phat et al., 2022). Acrylamide and its derivatives, such as acrylonitrile, acrylic acid, sodium acrylate, and their combinations, are among the most commonly used synthetic monomers for producing cryogels. Recent research reports the manufacture of hybrid cryogels developed for specific applications in the purification of biologically important molecules and the adsorption in aqueous media of pharmaceutical products such as antibiotics and antidepressants (Hamacek et al., 2023; Mourão et al., 2019; Nkana et al., 2024a).

To our knowledge, no studies have reported the continuous fixed-bed adsorption of antidepressants on hybrid cryogels, which motivates this research. This work focuses on creating a hybrid cryogel made from sodium acrylate and carboxymethyl chitosan for the ongoing fixed-bed adsorption of fluoxetine. It also involves predicting and modeling breakthrough curves within a simple operational framework, thereby enabling straightforward scalability to industrial applications. The material was characterized using FTIR spectroscopy, scanning electron microscopy coupled with energy-dispersive X-ray spectroscopy (SEM-EDX), and BET analysis. The study of swelling and surface charge was also completed. A study was conducted to investigate the effect of operating

parameters (pH, flow rate, initial concentration, and bed height). Regeneration and adsorption/desorption tests were also performed.

6.5 Materials and methods

6.5.1 Materials

Chitosan (Cs), deacetylation degree ≥75%) from shrimp shells, Chloroacetic acid ($C_2H_3ClO_2$), ≥ 99.0 %, Sodium hydroxide (NaOH), ≥ 98 %, Calcium Chloride anhydrous ($CaCl_2$), ≥ 93.0 %, Genipin ≥ 98 %, Acrylic acid anhydrous, containing 200 ppm mono methyl ether hydroquinone (MEHQ) as inhibitor 99 % (AA), N,N-Methylenebis (acrylamide) 99.0 % (MBA), Sodium metabisulfite ≥ 99.0 %, Ammonium peroxydisulfate (APS) ≥ 98.0 %, N,N,N', N'-Tetramethylethylenediamine (TEMED), Acetonitrile (ACN) (CH_3CN) ≥ 99 % for HPLC, Phosphoric acid (H_3PO_4) 85.0 % for HPLC, Isopropyl alcohol (C_3H_8O) 99.0 %, Fluoxetine hydrochloride (FLX), Venlafaxine hydrochloride (VEN) and N-Desmethylcitalopram hydrochloride (CIT), pharmaceuticals standards used as target molecules for the fixed bed column adsorption test were supplied by Sigma-Aldrich. Hydrochloric acid (HCl), 37 %, and acetic acid (CH_3COOH), 99.7 %, were provided by Acros Organic. Anhydrous ethyl alcohol (C_2H_5OH) and methanol ≥ 99.0 % were purchased from Commercial Alcohol Greenfield.

6.5.2 Methods

6.5.2.1 Synthesis of carboxymethyl chitosan

The CMCs were synthesized based on our previous work, with a few modifications (Nkana et al., 2024b). First of all, 6 g of chitosan were placed in a flask containing 80 mL of propan-2-ol for 1 h at 250 rpm at room temperature. Then, 60 mL of NaOH (0.4 g/mL) were gradually added to the mixture and stirred for 4 h. The flask was then placed at -20 °C overnight. After thawing, the flask was placed in an oil bath at 50 °C. Then, a solution of monochloroacetic acid previously prepared by dissolving 30 g in 20 mL of propan-2-ol was gradually added while stirring at 250 rpm for 30 min, and the reaction was carried out for 150 min. The mixture was left to cool to room temperature, then 200 mL of 95 %

ethanol were added to stop the reaction. The product obtained was washed with ethanol and dried under vacuum at 30 °C for 24 h. The impurities were removed by dissolving the synthesis product in 400 mL of distilled water for 6 h, followed by centrifugation at 10000 rpm. The dissolved polymer was recrystallized in 600 mL of 100 % ethanol. The CMCs were recovered after vacuum filtration and dried for 24 h under vacuum at 30 °C.

6.5.2.2 Synthesis of hybrid cryogel (NaPA-CMCs)

Sodium acrylate (NaA) was prepared by neutralizing acrylic acid with 1 M NaOH, followed by complete removal of water in a water bath at 80°C, while stirring magnetically at 100 rpm for 24 h. The NaA obtained was dried under vacuum at 45 °C. The hybrid cryogel (NaPA-CMCs) was produced following the method described in our previous work and by Cecilia Alves Mourão et al. (Mourão et al., 2019; Nkana et al., 2024a), with some modifications. Nine milliliters of a 0.3 % (m/v) CMCs solution was added to a glass vial and stirred on a magnetic stirrer set at 300 rpm. Next, 0.687 g of NaA was dissolved in the CMCs solution, and the pH was then stabilized at 7 with 1M NaOH. To cross-link the CMCs, 20 µL of 11 mM genipin was added to the mixture and left for 10 min, followed by the addition and dissolution of 0.113 g of MBA for 30 min. The mixture was degassed in an ultrasonic bath (Bransonic, CPX3800) for 3 min and then placed in a freezer for 5 min. The mixture was gently agitated (90 rpm) in an ice bath, then the co-initiators APS 0.2 % (m/v) and TEMED 0.2 % (v/v) were added, along with 100 µL of CaCl2 2 % (m/v). The volume of the mixture was made up to 10 mL, stirred for 60 seconds, and transferred to polypropylene syringes (Hsw 10/12 mL, 15.9 mm ID). The syringes were placed in a freezer at -18 °C for 24 h to complete the cryopolymerization. The cryogels obtained were slowly thawed in a cold chamber at 5 °C, then returned to room temperature and washed thoroughly with ultra-pure water to remove any unreacted monomers. The samples used for characterization were freeze-dried, while the remaining samples were maintained in a moist state following one hour of vacuum drying at room temperature.

6.5.3 Characterization of hybrid cryogel (NaPA-CMCs)

Multiple physical and chemical tests were performed to characterize the developed hybrid cryogel. This included surface morphology analysis and the identification and quantification of chemical elements using scanning electron microscopy and energy-dispersive X-ray spectroscopy (SEM/EDX) on a Hitachi SU1510 scanning electron microscope equipped with an Oxford EDX detector. Images of the material's surface were also obtained using a Keyence VHX digital microscope confocal laser scanning microscope (CLSM). The Brunauer-Emmet-Teller (BET) specific surface area, pore volume, and average pore size were determined by adsorption of N_2 at 77K and 0-1 atm using Micromeritics ASAP2020 equipment. Fourier transform infrared spectroscopy (FTIR) analysis was performed using a Nicolet IS10 FTIR Spectrometer (Thermo Scientific) at room temperature, with an acquisition interval ranging from 500 to 4000 cm^{-1}. The contact angle was measured using an FTA4000 Microdrop analyzer (First Ten Angstroms, Portsmouth, VA, USA). Zero-point charge (pH_{PZC}) was determined using the pH derivation method with a SevenMulti pH meter (Mettler-Toledo AG 8603) and a Lab-Line 3528 orbital shaker incubator. The liquid displacement method was used to evaluate the porosity of the material. The study of swelling as a function of time was completed. The protocols for the three previous analyses are described in the Supplementary Information (SI) document.

6.5.4 Study of the adsorption of fluoxetine in continuous flow on hybrid cryogel (NaPA-CMCs)

The adsorption experiments of ionized FLX on the hybrid cryogel were carried out in continuous mode, using a downward flow and a simple system consisting mainly of a peristaltic pump (Cole-Parmer IL 60648 1-100 RPM) with adjustable flow rate, a column (Transparent PVC Rigid Tubing) supplied by Meccanixity, with the following characteristics: height: 35 cm, internal diameter: 20 mm and external diameter: 25 mm (Figure 1). FLX solutions of different concentrations at the column inlet (10, 20 and 40 ppm) were tested, as were the pH (5.5, 7, and 8.5), the bed height in the column (0.2 cm, 0.4 cm and 0.8 cm), and the flow rate (1.5, 2 and 2.5 mL/min). Samples were taken at regular intervals and analyzed using a UV-Vis spectrometer (Agilent Cary 60 UV-Vis) at

a maximum wavelength of 230 nm to obtain the absorbance values of the initial and final FLX solutions. The residual concentrations of FLX were determined using a calibration curve (absorbance versus concentration). Each adsorption experiment was repeated three times. All adsorption experiments were carried out at room temperature (20 ± 2 °C).

Preliminary competitive adsorption tests of three antidepressants on synthetized cryogel were conducted. This investigation provided insight into the selectivity potential of the developed hybrid cryogel towards these three pharmaceuticals (VEN, FLX, CIT). The operating conditions of the column were as follows adsorbent bed height 0.2 cm, influent pH 8.5, flow rate 1.5 mL/min, and the initial concentration of each solute in the influent at the inlet was 10 ppm. Samples collected at regular intervals were analyzed using high-performance liquid chromatography equipment with a Diode Array Detector (DAD) and a C18 column (XB-C18, 100 Å, 150 × 3 mm, particle size 2.6 µm, Phenomenex Kinetex). The mobile phase was a mixture of 10 mM phosphate buffer pH 3.0/ acetonitrile 60:40 (v/v), with an elution flow rate of 0.3 $mL.min^{-1}$. The analysis time was 10 min, and the retention times were 2.62 min for VEN, 4.96 min for FLX, and 3.11 min for CIT, respectively. Using the iodine bar detector, the maximum area under the peaks at the maximum wavelengths associated with each of these molecules (224 nm, 230 nm, and 238 nm) was obtained for VEN, FLX, and CIT, respectively.

The adsorption performance on cryogels was investigated using non-linear regressions (C_t/C_0) versus (t), which correspond to the breakthrough curves. It should be noted that the breakthrough time (t_b) and the exhaustion time (t_e) correspond to the operating time when $C_t/C_0 = 0.05$ and $C_t/C_0 = 0.95$, respectively. The total amount of pollutants adsorbed in the column at a specific flow rate and concentration q_{total} (mg), the adsorption capacity at equilibrium $q_{e.exp}$ (mg/g), the total amount of pollutant entering the column W_{total} (mg) and the total adsorption percentage P (%) were determined from equations 6.1, 2, 3 and 4.

$$q_{total} = (Q/1000)\int_{t=0}^{t=t_{total}} C_t \, dt$$ Equation 6.1

$$q_{e.\exp} = q_{total}/m$$ Equation 6.2

$$W_{total} = Q.C_0.t_{total}/1000$$ Equation 6.3

$$P(\%) = (q_{total}/W_{total}) \times 100$$ Equation 6.4

The regeneration tests of the 0.4 cm high hybrid cryogel following the adsorption of FLX (40 ppm), conducted at pH 8.5 with a flow rate of 1.5 mL/min, were carried out by washing the material within the column using 50 mL of a solvent (containing 5 % methanol and 0.1 M HCl) at the same flow rate used during adsorption. Distilled water was then introduced into the column until the pH of the effluent was neutral. The material was subjected to another adsorption cycle by placing it in contact with the FLX solution (40 ppm, pH = 8.5) at a flow rate of 1.5 mL/min. Four adsorption cycles and three desorption cycles were performed.

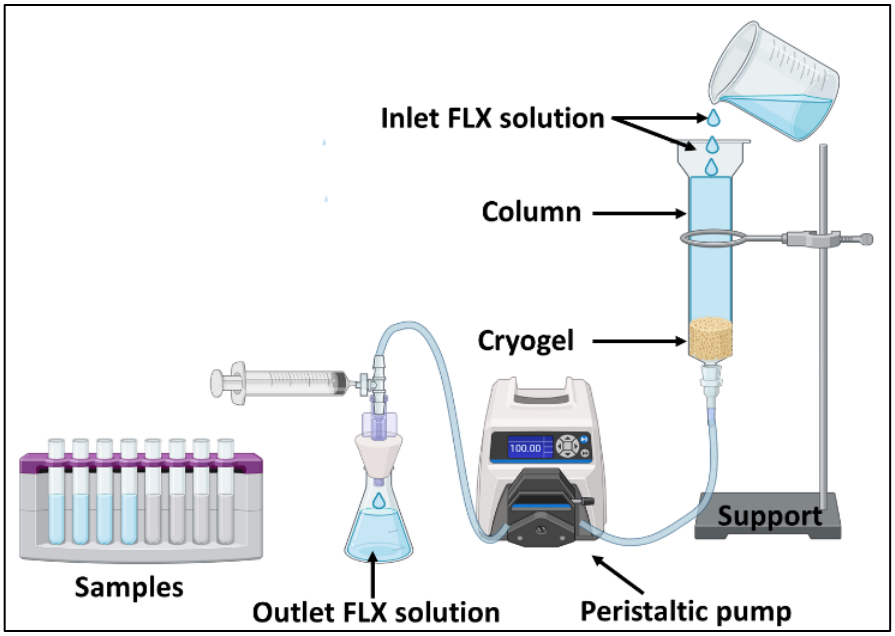

Figure 6.1 Experimental setup for continuous flow adsorption of fluoxetine on the NaPA-CMCs hybrid cryogel

6.5.5 Adsorption process modeling

Modelling the adsorption process is an important step in gaining a deeper understanding of the adsorption dynamics in the column. Two widely used empirical models for describing dynamic adsorption on a fixed bed have been fitted to the experimental data. These are the Thomas and Yoon-Nelson models, represented by equations 6.5 and 6.6, respectively. The Thomas model is used to study dynamic adsorption kinetics within the column. It effectively describes adsorption processes where diffusion limitations have minimal impact on mass transfer. It enables estimation of the adsorption rate constant and the amount of contaminant adsorbed per gram of adsorbent. This model assumes that the adsorption equilibrium is adequately described by the Langmuir isothermal model and that the adsorption kinetics of the process follow the reversible pseudo-second-order model (Thomas and HENRY THOMAS Vol, 1944). The Yoon-Nelson model is used to predict the time required for the effluent concentration to reach 50 % of the influent concentration. This model assumes that the decrease in the probability of contaminant adsorption is proportional to both the probability of adsorption and the probability of breakthrough in the fixed bed. This results in zero breakthroughs at the start of adsorption, followed by a gradual decrease in the adsorption probability and saturation of the adsorbent at the end (Yoon and Nelson, 1984).

$$C_t/C_0 = 1/\left(1+\exp\left(K_{Th}\left[\left(q_0\, m\right)/Q - C_0\, t\right]\right)\right) \qquad \text{Equation 6.5}$$

$$C_t/C_0 = 1/\left(1+\exp\left[K_{YN}\left(\tau - t\right)\right]\right) \qquad \text{Equation 6.6}$$

Where K_{Th} (mL/mg.min) is Thomas' constant, q_0 (mg/g) is the equilibrium adsorption capacity, Q (mL/min) is the influent flow rate, m (g) is the mass of adsorbent, t (min) is the time, C_0 (ppm) is the concentration at the column inlet, C_t (ppm) is the effluent concentration, K_{YN} (min^{-1}) is the Yoon-Nelson rate constant, and τ (min) is the time required for the concentration of the adsorbate at the column outlet to be equal to 50% of the concentration of the adsorbate entering the column. These parameters were derived from modeling using the non-linear regression method with OriginPro 2025b software.

The statistical parameters used to assess the quality of the fits were R^2 and the root mean square error (*RMSE*) using equations 6.7 and 6.8.

$$R^2 = 1 - \frac{\sum_{n-1}^{n} \left(q_{e.\exp.n} - q_{e.cal.n}\right)^2}{\sum_{n-1}^{n} \left(q_{e.\exp.n} - \overline{q}_{e.\exp.n}\right)^2} \qquad \text{Equation 6.7}$$

$$RMSE = \sqrt{\frac{1}{n-1} \sum_{n-1}^{n} \left(q_{e.\exp.n} - q_{e.cal.n}\right)^2} \qquad \text{Equation 6.8}$$

6.6 Results and discussions

6.6.1 Characterization of the hybrid cryogel

FTIR analysis was performed based on the vibration frequencies observed in the spectra. Figure 6.2f shows the infrared spectra of sodium acrylate (NaA), sodium carboxymethyl chitosan (NaCMCs), the hybrid cryogel before adsorption (NaPA-CMCs1), and after adsorption (NaPA-CMCs2) of FLX, respectively. The NaA spectrum shows bands between 3089-2981 cm^{-1}, which are attributed to the C-H stretching of the = CH_2 and CH_2 groups. The band at 1636 cm^{-1} corresponds to the C=C stretching vibration. Those at 1545 cm^{-1} and 1437 cm^{-1} correspond to the asymmetric and symmetric stretching of COO- groups, confirming the deprotonation of the carboxyl groups initially present in acrylic acid. The bands on the NaCMCs spectrum are identified at 1594 cm^{-1} and correspond to the overlap of the bands associated with the asymmetric COO- elongation of the carboxyl groups and the N-H deformation of the primary amine groups, while the band at 1418 cm^{-1} is attributed to the symmetric elongation of COO-, confirming the carboxymethylation of chitosan (Anitha et al., 2009). The band at 1306 cm^{-1} is assigned to C-O stretching, while those at 1140-1062 cm^{-1} correspond to C-O-C and C-OH stretching. It should be noted that the bands attributed to the C=C and C-H stretching of the =CH_2 and CH_2 groups observed in the NaA monomer spectrum have disappeared in the NaPA-CMCs1 spectrum, which would confirm the polymerization of NaA. This shows a band at 1645 cm^{-1}, characteristic of amide I, indicating the formation of covalent bonds following the cross-linking of sodium polyacrylate (NaPA) with MBA and NaCMCs with genipin on the

primary amine. The band observed at 1548 cm^{-1} corresponds to the overlap between the band attributed to the asymmetric COO- elongation and the N-H elongation of amide II linked to the formation of the network after cross-linking of the polymer chains by MBA. The new band at 1452 cm^{-1} corresponds to the -CH_2- deformation of the methylene groups of MBA. The band at 1323 cm^{-1} is attributed to the C-N elongation of amide III, which confirms the cross-linking of the polymer chains.

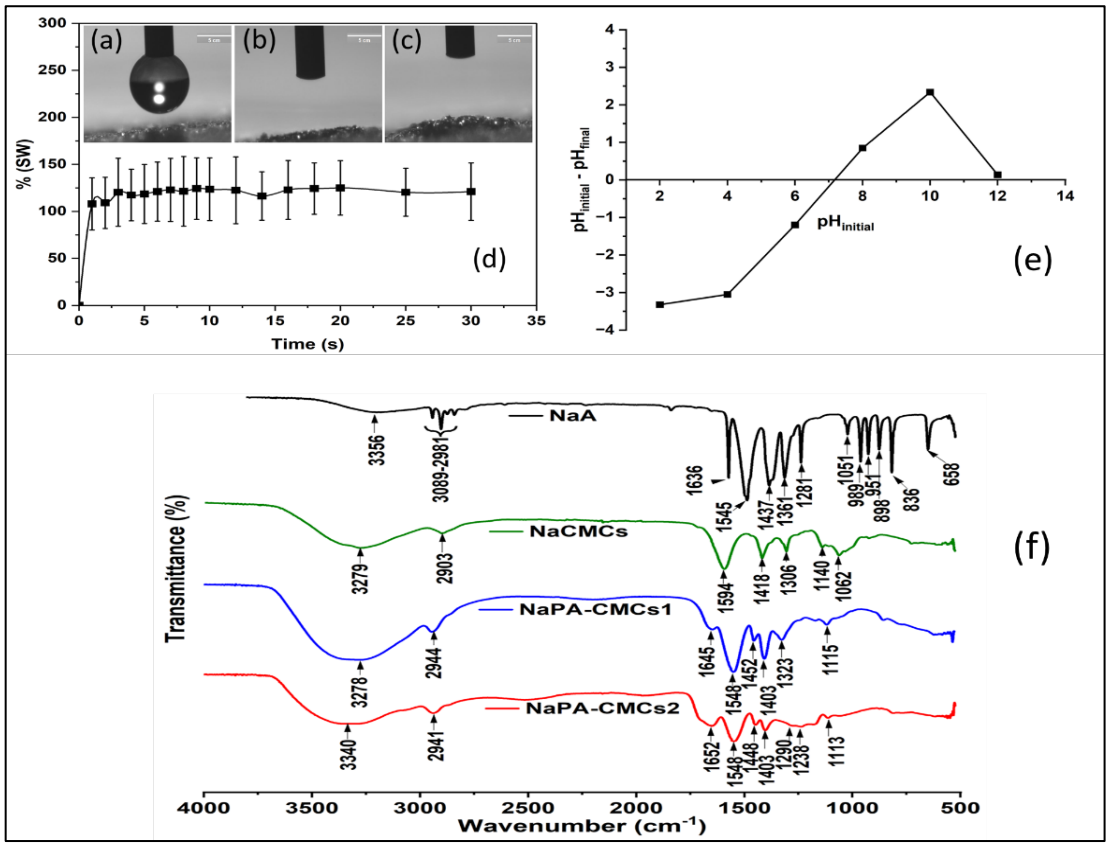

Figure 6.2 **Contact angle measurement: (a) deposition of the microdrop of water, (b) instant absorption, (c) swelling, (d) swelling rate, (e) Zero-point charge of NaPA-CMCs1 and (f) FTIR spectra of sodium acrylate (NaA), Carboxymethyl chitosan (NaCMCs), hybrid cryogel before and after fluoxetine adsorption (NaPA-CMCs1 and NaPA-CMCs2)**

The vibration of the polycyclic skeleton of genipin in the polymer network corresponds to the band at 1115 cm^{-1}. The spectrum of NaPA-CMCs2 shows a broader and moderately intense band at 1652 cm^{-1}, compared to the band at 1645 cm^{-1}. The upward shift of the latter is thought to be due to a change in the chemical environment of the C=O carbonyl groups of the amides formed by the covalent bonds between MBA and genipin with the

polymer chains. This change is thought to be the result of hydrogen bonds formed between the C=O groups and the protonated amine -$NH3^+$ of FLX. The decrease in the intensity of the bands at 1548 cm^{-1} and 1403 cm^{-1} observed in the spectrum could suggest electrostatic interactions between the protonated FLX and the COO- groups of the polymer network of the hybrid cryogel. It should be noted that the broad bands observed in the 3500-3100 cm^{-1} range on the different spectra are attributed to O-H and N-H stretching associated with hydrogen bonds.

The analysis of the pH at which the total charge of the hybrid cryogel surface is zero (PZC) was completed using the pH derivation method Figure 6.2e. This reveals that $pH_{PZC} = 7.1$, which implies that for a $pH_{solution}$ value < pH_{PZC}, the surface of the material is positive and, conversely, it is negative. It should be noted that the surface charge depends mainly on the functional groups (COO^- and NH_2) present in the polymer network of the cryogels, which may or may not carry a charge depending on the $pH_{solution}$ and their pKa. This indicates that the optimal pH range for electrostatic interactions between the ionized FLX and the surface of the hybrid cryogel is $pH_{PZC} < pH_{solution} < pKa_{FLX} = 9.8$.

Table 6.1 BET surface area, pore volume, average pore width, porosity, point of zero charge, and average surface roughness of NaPA-CMCs1 hy-brid cryogel

*S_{BET} (m^2/g)	Pore volume x 10^{-3} (cm^3/g)	Average pore width (nm)	Porosity (%) (n=3)	PH_{PZC}	*Sa (µm)
61.1	83.4	545.7	98.3 ± 0.07	7.1	19.2

*S_{BET}: BET Surface Area *Sa: Average Surface Roughness

The analysis of the swelling behavior of the hybrid cryogel allowed us to determine its water absorption capacity. This was further supported by FTIR analysis of the hybrid cryogel (NaPA-CMCs1), which confirmed the presence of hydrophilic groups (OH, NH2, and COO-) within the polymer network. Figure 6.2d shows that the swelling rate increases rapidly, reaching a maximum of 123.5 ± 33.4 % after 10 seconds. This could be explained by the porous structure of the material created through cryopolymerization, which can be seen in the microscopy images (Figure 6.3.) and is supported by the porosity value and

BET analysis results shown in Table 6.1. This porous structure promotes the rapid diffusion of water into the monolith and the dissociation of COONa ionic groups, resulting in an ionic potential difference between the interior of the polymer network and the external aqueous medium. The high osmotic pressure causes substantial water absorption to balance the ionic potential. All these factors could explain why it is impossible to measure the contact angle of the water micro droplet on the surface of the material, as observed in Figures 6.2a, b, and c. As soon as the microdroplet of water is deposited, the cryogel absorbs it instantly and swells.

SEM and CLSM analyses were employed to examine the morphology, porosity, and distribution of the polymer material within the hybrid cryogel. The SEM micrographs and 2D CLSM image of the NaPA-CMCs1 cryogel as shown in Figures 6.3a, b, c and d show a homogeneous distribution of the polymer matrix within the material. There are interconnected open cavities that form a honeycomb structure with surface irregularities. In the 3D CLSM image in Figure 6.3i, the internal structure of the sample analyzed in depth (212 μm) reveals dark red cavities extending from the surface to the depth studied. This suggests that the hybrid cryogel has open pores. Additionally, the measured average surface roughness value (19.2 μm) provides information about surface irregularities. The rough and macroporous structure observed could facilitate the molecular diffusion and adsorption of FLX. A similar observation has been reported for granular activated carbon (Tansel and Nagarajan, 2004). Mapping the chemical elements on the surface of the analyzed samples (EDS layered images) offers only indicative insights into their presence and amounts. However, it also helps illustrate how height influences the hybrid cryogel's capacity to immobilize ionized FLX. Based on the proportions of fluorine, a chemical element in the FLX structure. In Figures 6.3e and e1, 6.3f and f1, 6.3g and g1, 6.3h and h1, we observe that the NaPA-CMCs1 sample contains no fluorine. In contrast, the NaPA-CMCs2 sample shows an increase in fluorine content with increasing cryogel height (0.1 % at 0.2 cm, 7.3 % at 0.4 cm, and 8.6 % at 0.8 cm). This could be explained by the increase in the density of active sites in the polymer network as the height increases.

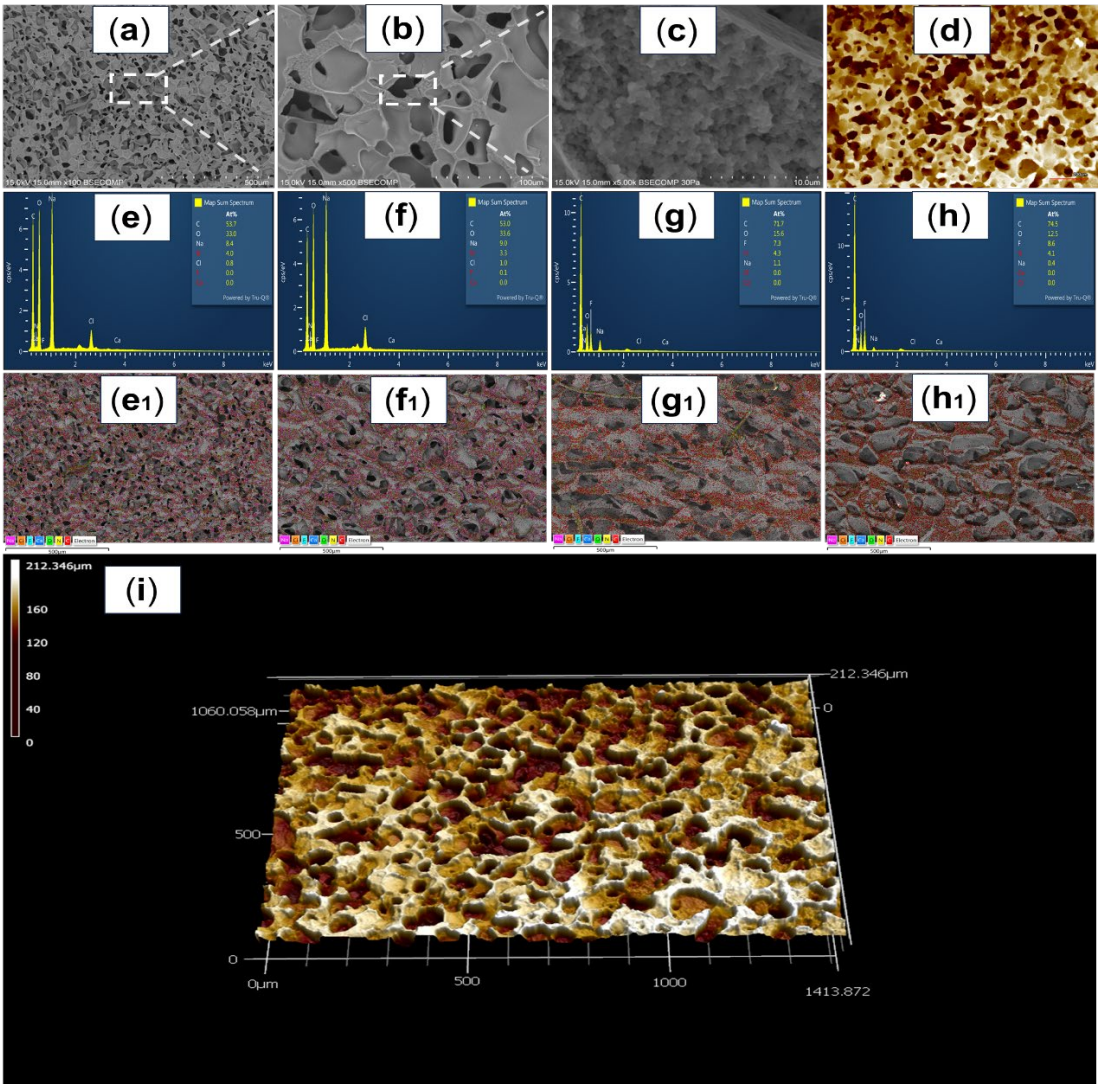

Figure 6.3 **SEM micrographs of NaPA-CMCs1 with magnification of : (a) X100, (b) X500 and (c) X5000; (d) 2D image of NaPA-CMCs1 obtained by CLSM analysis; EDS layered images and map spectrum of : NaPACMCs1 (e) and (e1), NaPA-CMCs2 at different heights (f), (f1) 0.2 cm, (g), (g1) 0.4 cm, and (h), (h1); 0.8 cm; (i) 3D image of NaPA-CMCs1 obtained by CLSM analysis**

6.6.2 Effects of operational parameters on FLX adsorption in a fixed bed column of NaPA-CMCs hybrid cryogel

Numerous studies in the literature provide comprehensive information regarding the impact of volumetric flow rate, initial concentration, bed height, and influent pH on the dynamic adsorption performance within fixed beds for an extensive range of pollutants, including pharmaceutical residues (Chu and Hashim, 2023; Feizi et al., 2021; Puga et al.,

2022). These parameters affect the kinetics and adsorption capacity in the column during operation. Dynamic adsorption tests of FLX on a NaPA-CMCs hybrid cryogel fixed bed were carried out, and the effects of these parameters on the breakthrough curves were examined. Results are reported in Figure 6.4. and Table 6.2.

6.6.2.1 Effect of influent flow rate

Figure 6.4a shows the effect of flow rate on the breakthrough curves with an inlet FLX concentration of 40 ppm, a bed height of 0.4 cm, and an influent pH of 8.5. As the flow rate increases from 1.5, 2, and 2.5 mL/min, the breakthrough curves become steeper. The breakthrough occurs more quickly as the flow rate increases with decreasing from 193.5 min at 1.5 mL/min to 42.7 min at 2.5 mL/min. The same pattern applies to the exhaustion time, which drops from 665.9 minutes to 268.7 minutes at these flow rates. Additionally, there is a decrease in adsorption capacity, from 33.98 mg/g to 15.82 mg/g. This could be explained by the longer contact time between the influent and the fixed bed of NaPA-CMCs hybrid cryogel when the flow rate is lower. This improved the diffusion of FLX into the polymer network, reaching active sites on the surface and within the material, where increased interaction enhanced adsorption. The higher flow rate resulted in a shorter residence time, which limited mass transfer, explaining the early breakthrough and exhaustion observed, the steeper slope of the breakthrough curve, and the lower removal efficiency of 35.94 %. The high influent flow rate limits the sorption capacity of the column (Hussain et al., 2011).

6.6.2.2 Effect of pH

The pH of the solution is a factor that also influences the adsorption efficacy of various adsorbents. Depending on the functional groups in these materials' structures, the surface of many cryogels exhibits greater affinity for pharmaceutical molecules in ionic form. Figure 6.4b shows the effect of FLX solution’s pH. The effect of pH 5.5, 7 and 8.5 at an initial FLX concentration at the inlet of 40 ppm, a flow rate of 1.5 mL/min and a bed height of 0.4 cm has been investigated. The results reveal that breakthrough and exhaustion are delayed when the pH of the influent is 8.5 (195 min and 665.9 min, respectively), compared to pH 5.5 (96.1 min and 391.9 min, respectively). Additionally,

the adsorption capacity of 33.98 mg/g and the removal rate of 52.45 % are higher at a pH of 8.5. On the other hand, the PZC value showed that above pH 7.1, the cryogel's surface becomes negative due to the deprotonation of carboxyl groups on the polymer chains. This promotes electrostatic interactions between the ionized FLX and the carboxylate groups. The increase in adsorption capacity with increasing pH of the FLX solution at the inlet can therefore be explained by a better affinity between the adsorbate and adsorbent at pH 8.5.

6.6.2.3 Effect of bed height

Figure 6.4c shows the effect of the bed height of the NaPA-CMCs hybrid cryogel of 0.2, 0.4, and 0.8 cm at an initial FLX concentration at the inlet of 40 ppm, a flow rate of 1.5 mL/min, and an influent pH of 8.5 on the dynamic adsorption performance was also studied. It was observed that the breakthrough curves had a steeper slope for the smallest bed (0.2 cm). Breakthrough and exhaustion are rapid, at 101.8 min and 334.1 min, respectively. Opposite results were observed for the tallest bed (0.8 cm), where breakthrough and exhaustion are delayed, at 339.1 min and 888 min, respectively. As the height increases, the adsorption capacity increases from 22.77 mg/g for 0.2 cm to 34.56 mg/g for 0.8 cm with respective removal efficiencies of 42.18 % and 58.18 %. Increasing the bed height increases the density of active sites capable of capturing FLX. Thus, for a bed height of 0.8 cm, there are more adsorption sites available, which improves the adsorption capacity and delays both breakthrough and exhaustion of the adsorbent. This could suggest that the influence of axial dispersion is predominant over FLX mass transfer when the height of the NaPA-CMCs cryogel fixed bed is low due to the low density of binding sites (Auta and Hameed, 2013).

6.6.2.4 Effect of initial concentration

Figure 6.4d presents the study of the effect of the initial concentration of FLX at the inlet (10 ppm, 20 ppm and 40 ppm at a flow rate of 1.5 mL/min, a fixed bed height of 0.4 cm, and an influent pH of 8.5. The results reveal that breakthrough and exhaustion occur rapidly for the highest concentration and are delayed for the lowest concentration. Furthermore, the adsorption capacity increases with increasing concentration, while the

removal rate decreases. This trend has been observed for the removal of pharmaceuticals in aqueous media by other adsorbent systems (Aichour et al., 2019; Feizi et al., 2021; Jaria et al., 2019). This could be justified by the fact that the driving force associated with the concentration gradient is greater when the FLX concentration is high, promoting faster diffusion and higher mass transfer of FLX into the polymer network of the cryogel. This would lead to increased contact and interaction between FLX molecules and binding sites.

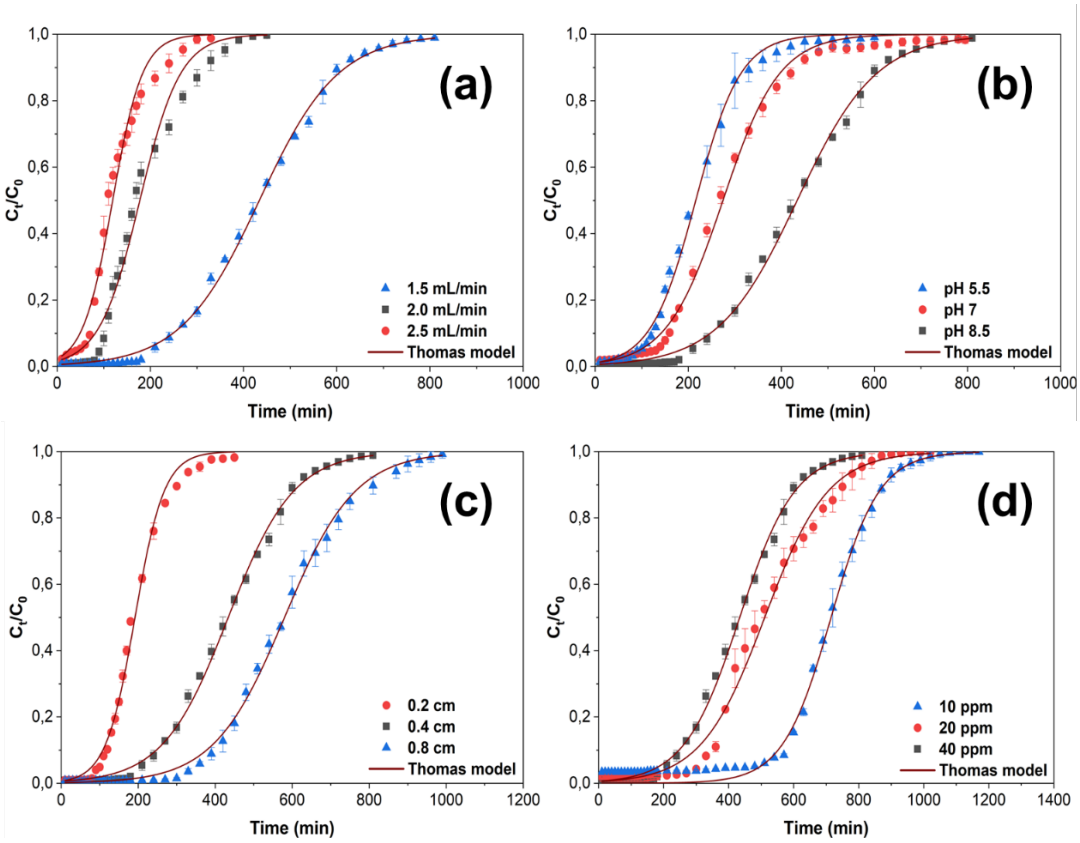

Figure 6.4 **Breakthrough curves and adjustment of the Thomas model to dynamic adsorption data of FLX on a fixed bed of NaPA-CMCs hybrid cryogel under different operating conditions: a) flow rate 1.5, 2, and 2.5 mL/min; b) pH 5.5, 7, and 8.5; c) bed height 0.2, 0.4, and 0.8 cm; d) initial concentration 10, 20, and 40 ppm**

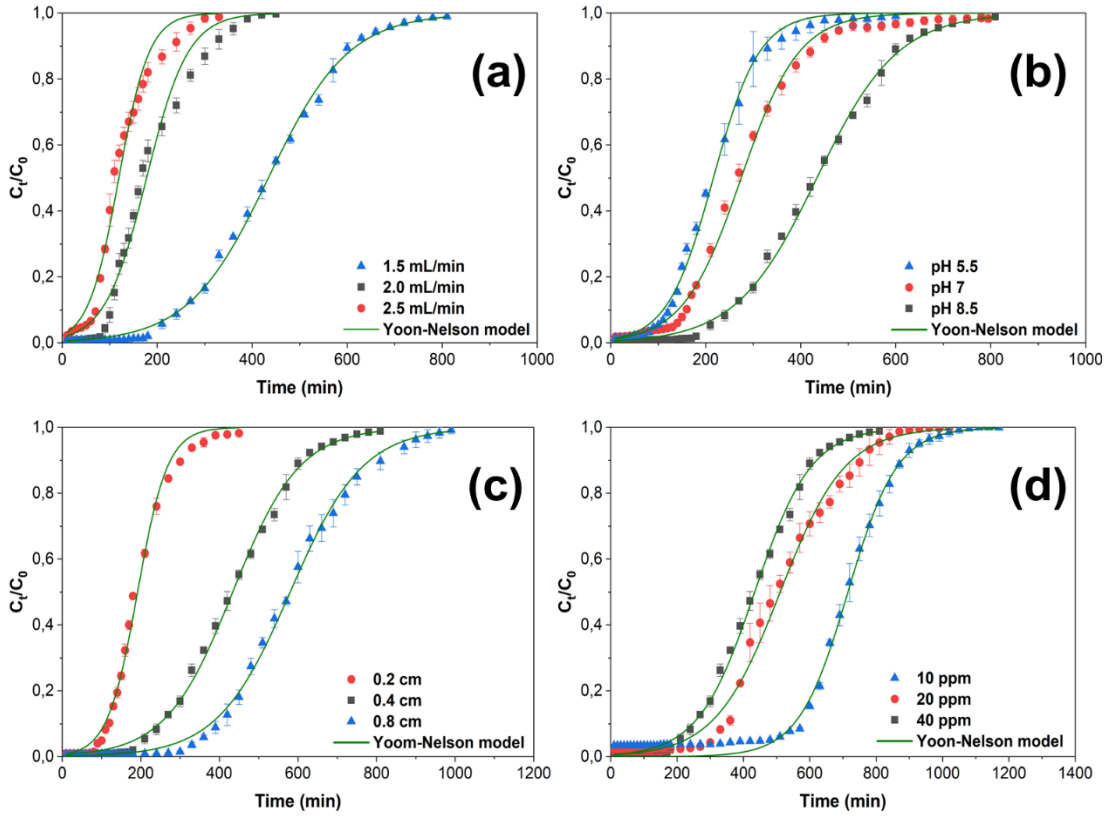

Figure 6.5 **Breakthrough curves and fitting of the Yoon-Nelson model to the dynamic adsorption data of FLX on the fixed bed of NaPA-CMCs hybrid cryogel under different operational conditions: a) flow rate 1.5, 2 and 2.5 mL/min; b) pH 5.5, 7 and 8.5; c) bed height height 0.2, 0.4 and 0.8 cm; (d) initial concentration 10, 20 and 40 ppm.**

Table 6.2 Column performance indicators for FLX removal under different operational conditions

C_0 (ppm)	H (cm)	Q (mL/min)	pH	t_b (min)	t_e (min)	q_{total} (mg)	$q_{e.exp}$ (mg/g)	W_{total} (mg)	P (%)
40	0.4	1.5	5.5	96.1	391.9	12,77	17.03	36.00	35.47
40	0.4	1.5	7	133.9	481.5	16.45	21.93	47.70	34.48
40	0.4	1.5	8.5	193.5	665.9	25.49	33.98	48.60	52.45
40	0.4	2	8.5	182.2	664.7	14.43	19.25	36.00	40.08
40	0.4	2.5	8.5	42.7	268.7	11.86	15.82	33.00	35.94
40	0.2	1.5	8.5	101.8	334.1	11.39	22.77	27.00	42.18
40	0.8	1.5	8.5	339.1	888.0	34.56	34.56	59.40	58.18
20	0.4	1.5	8.5	199.9	806.3	15.20	20.26	30.60	49.67
10	0.4	1.5	8.5	474.73	929.0	10.36	13.81	17.55	59.03

6.6.3 Modeling breakthrough curves

In this study, the Thomas and Yoon-Nelson models were used to analyze experimental data on the dynamic adsorption of FLX in a fixed-bed column of NaPA-CMCs cryogel. The aim of this analysis is to understand how this contaminant behaves in the porous structure of the adsorbent material under various operating conditions during dynamic adsorption. The breakthrough curves obtained were modeled (Figures 6.4 and 6.5), and the parameters associated with each of the models studied were listed in Table 6.3.

6.6.3.1 Thomas model

Thomas' model provides access to parameters that answer questions related to the performance and operation of the column. Adjusting this model to the experimental dynamic adsorption data for FLX obtained in this study (Figure 6.4) enabled the prediction of the adsorption capacity and rate constant reported in Table 3. The results demonstrate that, across all tested operating conditions, the coefficient of determination (R^2) exceeds 0.98 and the root mean square error (RMSE) is below 0.052. This means that the Thomas

model accurately describes the experimental dynamic adsorption data of FLX on the fixed bed of NaPA-CMCs hybrid cryogel. Furthermore, there is a small difference between the theoretical values q_0 and the experimental values $q_{e,exp}$ of the adsorption capacity, which confirms the validity of this model in this case. This result is consistent with that reported in our earlier work on batch adsorption of FLX on a cryogel made from the same precursors, where the Langmuir isothermal model provided a better fit to the experimental adsorption data (Nkana et al., 2024a). Table 6.3 shows a decrease in the apparent Thomas rate constant as the flow rate decreases, while increasing the pH, bed height, and initial concentration at the column inlet. This suggests that increasing the flow rate limits the external and internal diffusion resistance of FLX, while increasing the bed height has the opposite effect. At a pH of 8.5, it is assumed that the hydration layer created by the ion-dipole interactions between the carboxylate groups of the polymer network and the water molecules of the solution at the surface of the cryogel could act as a diffusion barrier, preventing the transport of FLX into the pores of the cryogel (resistance of the external fluid film). This could explain the decrease in the rate constant, which could also be justified by the diffusion resistance of the macro- and micropores (MD LeVan et al., 1999). The increase in concentration at the column inlet leads to a greater concentration gradient, which increases the flow of FLX to the external boundary layer. As the active sites become saturated, mass transfer would become low, suggesting overall slow kinetics.

The adsorption capacity of FLX on the NaPA-CMCs cryogel fixed bed increases as the influent pH, initial concentration, and fixed bed height increase. However, it decreases with increasing flow rate. This result implies that the optimal column operating parameters for adsorption on the fixed bed are pH 8.5, a bed height of 0.8 cm, an initial concentration of 10 ppm, and an influent flow rate of 1.5 mL/min. This is attributed to the activation of carboxyl groups, which facilitate electrostatic interactions, an increased density of binding sites, a concentration gradient that enhances the diffusion of FLX, and a longer contact time in the column.

6.6.3.2 Yoon-Nelson model

The adjustment of the Yoon-Nelson model allowed for the analysis of data from the breakthrough curves of dynamic adsorption of FLX on a fixed bed of NaPA-CMCs hybrid

cryogel under various experimental conditions. The results are shown in Figure 6.5, and the model parameter values are listed in Table 6.3. They show that R^2 values exceed 0.98 and RMSE values are under 0.052, with only slight differences between the experimental and theoretical adsorption capacities. This suggests that the Yoon-Nelson model can adequately describe the dynamic adsorption process of FLX on the NaPA-CMCs hybrid cryogel fixed bed under the experimental operating conditions. The gradual decrease in K_{YN} values when the initial concentration of FLX increases could be explained by the significant flow of FLX towards the surface of the cryogel, which causes rapid saturation of the binding sites and a slowdown in mass transfer. The greater concentration gradient is thought to be responsible for faster breakthrough of FLX into the bed, which could explain why the τ values decrease as the concentration increases. Increasing the bed height and the pH of the influent gradually decreases the K_{YN} values and increases the τ values, while increasing the flow rate has the opposite effect. This could indicate that increasing the pH to 8.5 increases FLX-cryogel interactions, while increasing the bed height provides more adsorbent material. This leads to increased adsorption, delays breakthrough and reduces the overall effective adsorption rate. In the case of flow rate, the increase leads to very limited contact times between FLX and the cryogel binding sites, causing rapid breakthrough and a gradual decrease in time τ as well as a gradual increase in K_{YN}.

Table 6.3 Results of the adjustment of the Thomas model and the Yoon-Nelson model to experimental data on the dynamic adsorption of FLX on a fixed bed of NaPA-CMCs hybrid cryogel

Parameters				Thomas model				Yoon-Nelson model			
C_0 (ppm)	H (cm)	Q (mL/min)	pH	q_0 (mg/g)	K_{Th} (mL/mg.min)	R^2	RMSE	K_{YN} (min^{-1})	τ (min)	R^2	RMSE
40	0.4	1.5	5.5	17.29	0.5185	0.9971	0.0228	0.0207 ± 0.0006	216.07 ± 1.97	0.9971	0.0228
40	0.4	1.5	7.0	21.96	0.4125	0.9970	0.0234	0.0164 ± 0.0005	274.57 ± 2.33	0.9970	0.0234
40	0.4	1.5	8.5	34.71	0.2942	0.9982	0.0165	0.0117 ± 0.0002	433.92 ± 2.04	0.9982	0.0165
40	0.4	2.0	8.5	18.93	0.5735	0.9824	0.0515	0.0286 ± 0.0016	177.56 ± 3.48	0.9824	0.0515
40	0.4	2.5	8.5	15.88	0.7825	0.9817	0.0500	0.0312 ± 0.0021	119.14 ± 2.23	0.9817	0.0500
40	0.2	1.5	8.5	23.01	0.6575	0.9949	0.0283	0.0262 ± 0.0011	191.78 ± 1.93	0.9949	0.0283
40	0.8	1.5	8.5	34.79	0.2715	0.9981	0.0162	0.0108 ± 0.0002	580.86 ± 3.65	0.9981	0.0162
20	0.4	1.5	8.5	20.43	0.5125	0.9955	0.0276	0.0102 ± 0.0003	510.78 ± 1.93	0.9955	0.0276
10	0.4	1.5	8.5	14.29	1.3460	0.9955	0.0268	0.0134 ± 0.0005	714.97 ± 3.10	0.9955	0.0268
10*	0.2	1.5	8.5	9.98	1.8750	0.9933	0.0281	0.0188 ± 0.0008	322.31 ± 2.74	0.9933	0.0281
10**	0.2	1.5	8.5	2.17	3.9050	0.9818	0.0457	0.0039 ± 0.0026	72.42 ± 1.81	0.9818	0.0457
10***	0.2	1.5	8.5	4.00	5.2510	0.9707	0.0610	0.0531 ± 0.0053	133.57 ± 2.06	0.9707	0.0610

Operating conditions for simultaneous adsorption of FLX*, VEN**, and CIT*** and parameters of the Thomas and Yoon-Nelson models

6.6.4 Competitive adsorption of fluoxetine, venlafaxine, and citalopram on a fixed bed of NaPA-CMCs hybrid cryogel

A dynamic adsorption test of three targeted antidepressants was conducted under the operating conditions specified in section 6.5.4. Figure 6.6 shows the breakthrough curve and the fit of the non-linear Thomas and Yoon-Nelson models. The column exhaustion times for each target solute are 468 min for FLX, 178.5 min for CIT, and 127 min for VEN, while their equilibrium adsorption capacities are 9.98 mg/g, 4 mg/g, and 2.17 mg/g, respectively. The Thomas and Yoon-Nelson models fit the breakthrough curves well (R^2 > 0.97 et RMSE < 0.062). These results suggest an affinity for the cryogel in the following order: FLX > CIT > VEN. This phenomenon may be attributed to the fact that, despite the molecules being in an ionic state in solution and the cryogel surface exhibiting a negative charge, electrostatic interactions are not the sole factors promoting the sorption of solutes. Furthermore, the lipophilic characteristics of these pharmaceuticals (Table SI1) would promote hydrophobic interactions with the less polar regions of the cryogel polymer chains. This could justify the order of affinity, which suggests a dominant hydrophobic effect.

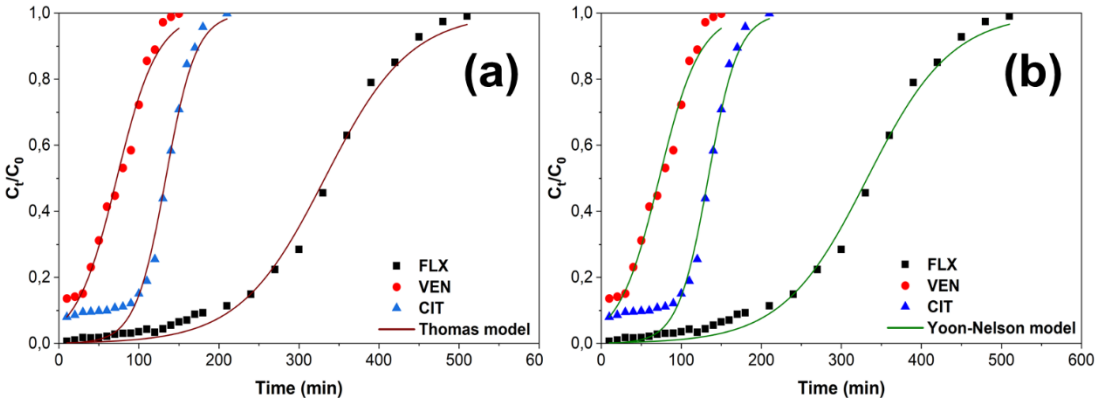

Figure 6.6 Breakthrough curves for the simultaneous adsorption of FLX, VEN and CIT on a fixed bed of NaPA-CMCs hybrid cryogel and adjustment to models: a) Thomas and b) Yoon-Nelson

6.7 Proposed mechanism of targeted antidepressant adsorption

The presence of NH_2, OH, and COO^- groups in the polymer network makes NaPA-CMCs cryogel generally hydrophilic. These functional groups contribute to the formation of hydrogen bonds with the donor or acceptor groups of the targeted antidepressants. FLX, CIT, and VEN exhibit high, moderate, and low lipophilicity, respectively, which could explain FLX's greater affinity for the relatively nonpolar areas of the cryogel, where hydrophobic interactions are more likely to occur. Furthermore, electrostatic interactions under experimental conditions where solution pH < pKa of each antidepressant would be predominant during the sorption of solutes on the negatively charged surface of the cryogel. It is also assumed that donor-acceptor Π-Π interactions occur between the aromatic ring of the target pharmaceuticals and the cryogel. Based on the physicochemical properties of the targeted antidepressants and the results of characterizing the NaPA-CMCs hybrid cryogel, adsorption mechanisms have been proposed (Figure 6.7).

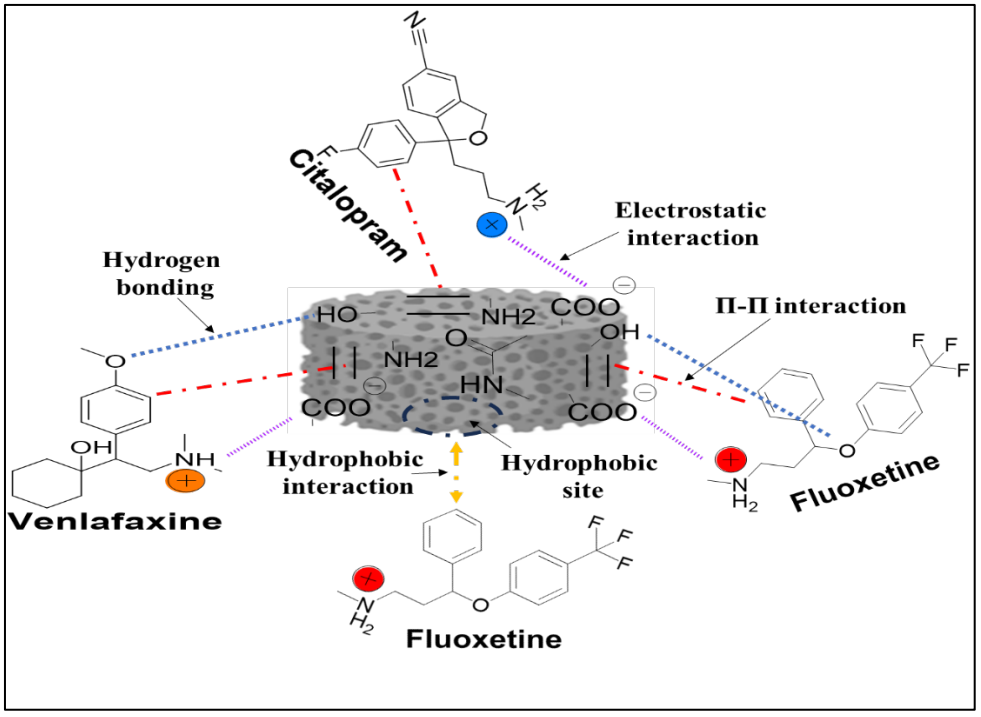

Figure 6.7 Proposed scheme of the dynamic adsorption mechanism of fluoxetine, venlafaxine and citalopram on the hybrid cryogel NaPA-CMCs

6.8 Regeneration of the adsorbent NaPA-CMCs

The effectiveness of a dynamic treatment system depends on both the adsorption performance of the adsorbent and the effectiveness of the regeneration method, which can extend the operational life of the adsorbent through adsorption-desorption cycles. Figure 6.8 shows the results from four consecutive dynamic adsorption cycles, each followed by desorption, using the conditions outlined in section 6.5.4. The results reveal a decrease in the sorption rate (% P) from 52.5 % (first adsorption) to 17.8 % (fourth adsorption) with a minimum desorption capacity of 54 %. This could suggest that although the composition of the eluant allowed for effective desorption after the first adsorption (89.9 %), the flow rate and/or total volume of solvent used for FLX desorption were no longer suitable for optimal desorption. A decrease in elution flow rate and treatment of the cryogel with a larger volume of desorption solvent would promote optimal timing and more efficient regeneration.

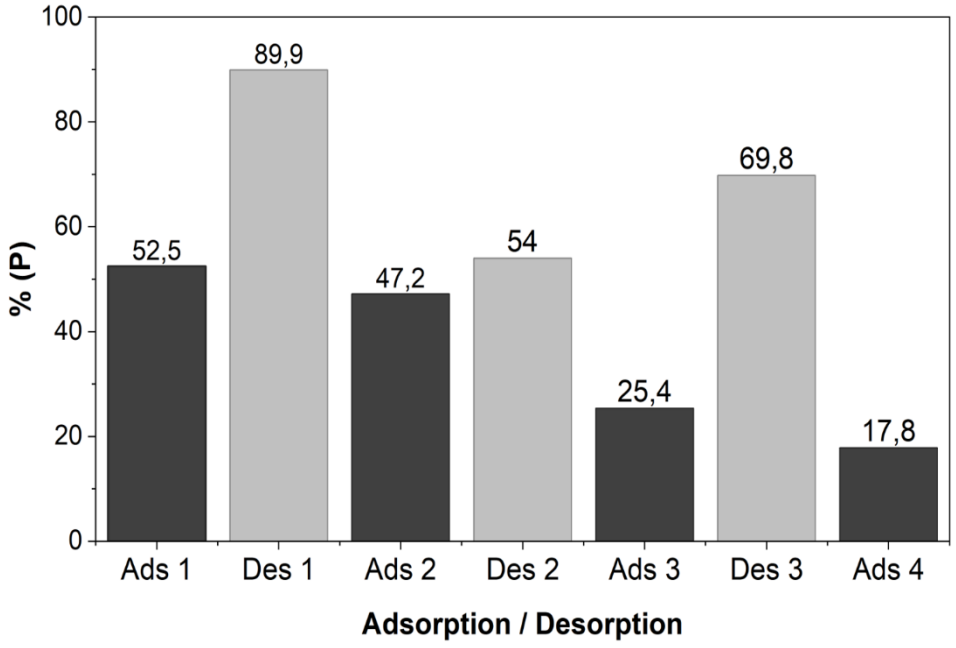

Figure 6.8 Adsorption (Ads) and Desorption (Des) cycles of fluoxetine on NaPA-CMCs hybrid cryogel

6.9 Conclusion

This work addresses the removal of emerging contaminants, particularly antidepressants, from aqueous media by adsorption on a hybrid cryogel. The aim was to manufacture the cryogel through cryopolymerization using sodium acrylate and carboxymethyl chitosan in the first stage, and then to conduct continuous adsorption tests on a fixed-bed column using a simple device in the second stage. The material obtained has a macroporous structure with relatively well-distributed open pores that form an interconnected network. Investigation of the effect of operating parameters on the efficiency of the dynamic adsorption system reveals that a pH of 8.5 is optimal for FLX adsorption, as this molecule is ionized in its current state. The negatively charged surface of the hybrid cryogel promotes electrostatic interactions. Increasing the flow rate limits the contact time between FLX and the hybrid cryogel, causing early breakthrough and exhaustion of the adsorbent. Increasing the initial concentration leads to rapid saturation of the active sites, delaying breakthrough and exhaustion, while the equilibrium adsorption capacity increases with increasing bed height.

The Thomas and Yoon-Nelson models accurately describe the experimental breakthrough curve data. The cryogel developed achieves FLX removal levels greater than 50 % for a solution pH of 8.5, a bed height of 0.8 cm, an initial concentration of 10 ppm, and a flow rate of 1.5 mL/min. This suggests that the synergistic action of different adsorption mechanisms, depending on the properties of the cryogels and the target antidepressants, contributes to their removal from the aqueous medium. This justifies the greater affinity of the cryogel for FLX compared to CIT and VEN.

This work demonstrates the potential of the NaPA-CMCs hybrid cryogel as a simple and effective alternative for solving the problem of wastewater contamination by antidepressants, and more specifically by FLX. This material could be used as a potential antidepressant sensor in aqueous media, particularly in the pharmaceutical industry and hospitals. A drop in efficiency was observed during the regeneration of the hybrid cryogel. It would be advisable to reduce the flow rate during the desorption process to increase contact time and to test larger volumes of desorption solutions for more efficient regeneration. For future work, the investigation of the effect of column operating

parameters on the simultaneous adsorption of the three targeted antidepressants will be completed. The regeneration of the hybrid cryogel will be optimized, and dynamic adsorption tests with real wastewater containing antidepressants will be conducted. The information gathered from this study indicates that the macroporous NaPA-CMCs hybrid cryogel is a promising adsorbent that could be a potential candidate for water purification applications, particularly in removing antidepressants originating from the pharmaceutical industry and hospitals.

6.10 Acknowledgments

The authors thank the Natural Sciences and Engineering Research Council of Canada (NSERC), grant no. RGPIN-2022-03510, for financial support, and the University of Quebec at Trois-Rivières for providing space, materials, and equipment to complete this research.

6.11 Declaration of Competing Interest

The authors have no financial or non-financial interests to disclose.

6.12 Declaration of generative AI and AI-assisted technologies in the writing process

During the preparation of this work, the author(s) used [Grammarly, DeepL] in order to [improve the English language quality]. After using this tool/service, the author(s) reviewed and edited the content as needed and take full responsibility for the content of the published article.

6.13 References

- AGMR, Antidepressants Global Market Report 2021: Covid-19 Implications and Growth to 2030, 2021. URL https://www.researchandmarkets.com (accessed 8.12.25).
- Agustin, M.B., Lehtonen, M., Kemell, M., Lahtinen, P., Oliaei, E., Mikkonen, K.S., 2023. Lignin nanoparticle-decorated nanocellulose cryogels as adsorbents for

pharmaceutical pollutants. J Environ Manage 330. https://doi.org/10.1016/j.jenvman.2022.117210

- Aichour, A., Zaghouane-Boudiaf, H., Mohamed Zuki, F.B., Kheireddine Aroua, M., Ibbora, C.V., 2019. Low-cost, biodegradable and highly effective adsorbents for batch and column fixed bed adsorption processes of methylene blue. J Environ Chem Eng 7, 103409. https://doi.org/10.1016/J.JECE.2019.103409
- Anitha, A., Divya Rani, V. V., Krishna, R., Sreeja, V., Selvamurugan, N., Nair, S. V., Tamura, H., Jayakumar, R., 2009. Synthesis, characterization, cytotoxicity and antibacterial studies of chitosan, O-carboxymethyl and N,O-carboxymethyl chitosan nanoparticles. Carbohydr Polym 78, 672–677. https://doi.org/10.1016/j.carbpol.2009.05.028
- Arnnok, P., Singh, R.R., Burakham, R., Pérez-Fuentetaja, A., Aga, D.S., 2017. Selective Uptake and Bioaccumulation of Antidepressants in Fish from Effluent-Impacted Niagara River. Environ Sci Technol 51, 10652–10662. https://doi.org/10.1021/ACS.EST.7B02912
- Auta, M., Hameed, B.H., 2013. Coalesced chitosan activated carbon composite for batch and fixed-bed adsorption of cationic and anionic dyes. Colloids Surf B Biointerfaces 105, 199–206. https://doi.org/10.1016/J.COLSURFB.2012.12.021
- Baimenov, A., Berillo, D.A., Poulopoulos, S.G., Inglezakis, V.J., 2020. A review of cryogels synthesis, characterization and applications on the removal of heavy metals from aqueous solutions. Adv Colloid Interface Sci 276. https://doi.org/10.1016/j.cis.2019.102088
- Bratskaya, S., Privar, Y., Slobodyuk, A., Shashura, D., Marinin, D., Mironenko, A., Zheleznov, V., Pestov, A., 2019. Cryogels of carboxyalkylchitosans as a universal platform for the fabrication of composite materials. Carbohydr Polym 209, 1–9. https://doi.org/10.1016/j.carbpol.2018.12.094
- Campos, B., Rivetti, C., Kress, T., Barata, C., Dircksen, H., 2016. Depressing Antidepressant: Fluoxetine Affects Serotonin Neurons Causing Adverse Reproductive Responses in Daphnia magna. Environ Sci Technol 50, 6000–6007. https://doi.org/10.1021/ACS.EST.6B00826/SUPPL_FILE/ES6B00826_SI_001.PDF

- Choi, J.W., Bediako, J.K., Zhao, Y., Lin, S., Sarkar, A.K., Han, M., Song, M.H., Cho, C.W., Yun, Y.S., 2020. Adsorptive removal of cationic tricyclic antidepressants using cation-exchange resin. Environmental Science and Pollution Research 27, 24760–24771. https://doi.org/10.1007/S11356-019-06549-1/FIGURES/6
- Chu, K.H., Hashim, M.A., 2023. Adsorptive removal of pharmaceutical contaminants: Accurate description of tailing breakthrough curves. J Environ Chem Eng 11, 111025. https://doi.org/10.1016/J.JECE.2023.111025
- Correia, D., Domingues, I., Faria, M., Oliveira, M., 2023. Effects of fluoxetine on fish: What do we know and where should we focus our efforts in the future? Science of The Total Environment 857, 159486. https://doi.org/10.1016/J.SCITOTENV.2022.159486
- Correia, D., Domingues, I., Faria, M., Oliveira, M., 2022. Chronic Effects of Fluoxetine on Danio rerio: A Biochemical and Behavioral Perspective. Applied Sciences (Switzerland) 12, 2256. https://doi.org/10.3390/APP12042256/S1
- Diaz-Camal, N., Cardoso-Vera, J.D., Islas-Flores, H., Gómez-Oliván, L.M., Mejía-García, A., 2022. Consumption and occurrence of antidepressants (SSRIs) in pre- and post-COVID-19 pandemic, their environmental impact and innovative removal methods: A review. Science of the Total Environment 829. https://doi.org/10.1016/j.scitotenv.2022.154656
- Doser, G., Su, E., Okay, O., 2023. Effects of cryogenic condition and chemistry on the properties of synthetic and biopolymer cryogels. React Funct Polym 190, 105635. https://doi.org/10.1016/J.REACTFUNCTPOLYM.2023.105635
- Eisenreich, B.R., Greene, S., Szalda-Petree, A., 2017. Of fish and mirrors: Fluoxetine disrupts aggression and learning for social rewards. Physiol Behav 173, 258–262. https://doi.org/10.1016/J.PHYSBEH.2017.02.021
- Escudero-Curiel, S., Penelas, U., Sanromán, M.Á., Pazos, M., 2021. An approach towards Zero-Waste wastewater technology: Fluoxetine adsorption on biochar and removal by the sulfate radical. Chemosphere 268, 129318. https://doi.org/10.1016/J.CHEMOSPHERE.2020.129318
- Feizi, F., Sarmah, A.K., Rangsivek, R., 2021. Adsorption of pharmaceuticals in a fixed-bed column using tyre-based activated carbon: Experimental investigations and

numerical modelling. J Hazard Mater 417, 126010. https://doi.org/10.1016/J.JHAZMAT.2021.126010

- Fernandes, M.J., Moreira, M.M., Paíga, P., Dias, D., Bernardo, M., Carvalho, M., Lapa, N., Fonseca, I., Morais, S., Figueiredo, S., Delerue-Matos, C., 2019. Evaluation of the adsorption potential of biochars prepared from forest and agri-food wastes for the removal of fluoxetine. Bioresour Technol 292, 121973. https://doi.org/10.1016/J.BIORTECH.2019.121973
- Gornik, T., Kovacic, A., Heath, E., Hollender, J., Kosjek, T., 2020. Biotransformation study of antidepressant sertraline and its removal during biological wastewater treatment. Water Res 181, 115864. https://doi.org/10.1016/J.WATRES.2020.115864
- Gould, S.L., Winter, M.J., Norton, W.H.J., Tyler, C.R., 2021. The potential for adverse effects in fish exposed to antidepressants in the aquatic environment. Environ Sci Technol 55, 16299–16312. https://doi.org/10.1021/ACS.EST.1C04724
- Gun'ko, V.M., Savina, I.N., Mikhalovsky, S. V., 2013. Cryogels: Morphological, structural and adsorption characterisation. Adv Colloid Interface Sci. https://doi.org/10.1016/j.cis.2012.11.001
- Hamacek, H.S.D.R., Bresolin, I.T.L., Fioravante, I.F., Bueno, S.M.A., 2023. Synthesis and characterization of chitosan-polyacrylamide cryogels for the purification of human IgG by IMAC. Process Biochemistry 131, 199–209. https://doi.org/10.1016/J.PROCBIO.2023.06.021
- Hussain, S., Aziz, H.A., Isa, M.H., Ahmad, A., Van Leeuwen, J., Zou, L., Beecham, S., Umar, M., 2011. Orthophosphate removal from domestic wastewater using limestone and granular activated carbon. Desalination 271, 265–272. https://doi.org/10.1016/J.DESAL.2010.12.046
- Izadpanah, A., Nemati, S., Nojavan, S., 2024. A comprehensive review on synthesis and applications of cryogel-based sorbents in solid-phase extraction techniques. TrAC - Trends in Analytical Chemistry. https://doi.org/10.1016/j.trac.2024.117899
- Jaria, G., Calisto, V., Gil, M.V., Otero, M., Esteves, V.I., 2015. Removal of fluoxetine from water by adsorbent materials produced from paper mill sludge. J Colloid Interface Sci 448, 32–40. https://doi.org/10.1016/J.JCIS.2015.02.002

- Jaria, G., Calisto, V., Silva, C.P., Gil, M.V., Otero, M., Esteves, V.I., 2019. Fixed-bed performance of a waste-derived granular activated carbon for the removal of micropollutants from municipal wastewater. Science of The Total Environment 683, 699–708. https://doi.org/10.1016/J.SCITOTENV.2019.05.198
- Juang, R.-S., Fan, C.-C., Fu, C.-C., 2026. Efficient removal of diclofenac and phosphate anions from aqueous solutions using electrospun quaternized chitosan/poly(vinyl alcohol) fibrous membranes. Sep Purif Technol 380, 135454. https://doi.org/10.1016/J.SEPPUR.2025.135454
- Köse, K., Yalçın Kehribar, D., Goodarzi, V., Uzun, L., 2024. Strategies for the detection, removal and elimination of antidepressants. Int J Environ Anal Chem. https://doi.org/10.1080/03067319.2021.2019726
- Kumar, A., Mishra, R., Reinwald, Y., Bhat, S., 2010. Cryogels: Freezing unveiled by thawing, NUMBER.
- Lajeunesse, A., Blais, M., Barbeau, B., Sauvé, S., Gagnon, C., 2013. Ozone oxidation of antidepressants in wastewater -Treatment evaluation and characterization of new by-products by LC-QToFMS. Chem Cent J 7, 1–11. https://doi.org/10.1186/1752-153X-7-15/FIGURES/7
- Lozinsky, V.I., 2002. Cryogels on the basis of natural and synthetic polymers: preparation, properties and application. Russian Chemical Reviews 71, 489–511. https://doi.org/10.1070/RC2002V071N06ABEH000720
- Lozinsky, V.I., Okay, O., 2014. Basic Principles of Cryotropic Gelation. Advances in Polymer Science 263, 49–101. https://doi.org/10.1007/978-3-319-05846-7_2
- Maršálek, R., Švidrnoch, M., 2020. The adsorption of amitriptyline and nortriptyline on activated carbon, diosmectite and titanium dioxide. Environmental Challenges 1, 100005. https://doi.org/10.1016/J.ENVC.2020.100005
- MATTHEW RIDLEY HTTPS://ORCID.ORG/0000-0001-7612-7436, G.R.H.O.-0002-1662-5457, F.S.H.O.-0002-8022-6725, A.V.P., 2020. Poverty, depression, and anxiety: Causal evidence and mechanisms. Science (1979) 370.
- MD LeVan, G.Carta, CM Yon, 1999. Adsorption and Ion Exchange. McGrawHill , New York.

- Melin, V., Salgado, P., Thiam, A., Henríquez, A., Mansilla, H.D., Yáñez, J., Salazar, C., 2021. Study of degradation of amitriptyline antidepressant by different electrochemical advanced oxidation processes. Chemosphere 274, 129683. https://doi.org/10.1016/J.CHEMOSPHERE.2021.129683
- Méndez-Arriaga, F., Otsu, T., Oyama, T., Gimenez, J., Esplugas, S., Hidaka, H., Serpone, N., 2011. Photooxidation of the antidepressant drug Fluoxetine (Prozac®) in aqueous media by hybrid catalytic/ozonation processes. Water Res 45, 2782–2794. https://doi.org/10.1016/J.WATRES.2011.02.030
- Mourão, C.A., Marcuz, C., Haupt, K., Bueno, S.M.A., 2019. Polyacrylamide-alginate (PAAm-Alg) and phospho-L-tyrosine-linked PAAm-Alg monolithic cryogels: Purification of IgG from human serum. Journal of Chromatography B 1129, 121783. https://doi.org/10.1016/J.JCHROMB.2019.121783
- Nkana, G.R.N., Chabot, B., Nguyen-Tri, P., 2024a. Adsorption of fluoxetine in aqueous environments: Development of macroporous cryogels based on sodium poly(acrylate) and carboxymethyl chitosan. React Funct Polym 205. https://doi.org/10.1016/j.reactfunctpolym.2024.106069
- Nkana, G.R.N., Lajeunesse, A., Chabot, B., Nguyen-Tri, P., 2024b. Design of porous spherical biomaterials from carboxymethyl chitosan for removal of fluoxetine in aqueous medium. J Environ Chem Eng 12, 112228. https://doi.org/10.1016/J.JECE.2024.112228
- Okay, O., Lozinsky, V.I., 2014. Synthesis and structure–property relationships of cryogels. Advances in Polymer Science 263, 103–157. https://doi.org/10.1007/978-3-319-05846-7_3
- Orozco-Hernández, J.M., Gómez-Oliván, L.M., Elizalde-Velázquez, G.A., Rosales-Pérez, K.E., Cardoso-Vera, J.D., Heredia-García, G., Islas-Flores, H., García-Medina, S., Galar-Martínez, M., 2022. Fluoxetine-induced neurotoxicity at environmentally relevant concentrations in adult zebrafish Danio rerio. Neurotoxicology 90, 121–129. https://doi.org/10.1016/J.NEURO.2022.03.007
- Pan, C., Zhu, F., Wu, M., Jiang, L., Zhao, X., Yang, M., 2022. Degradation and toxicity of the antidepressant fluoxetine in an aqueous system by UV irradiation. Chemosphere 287, 132434. https://doi.org/10.1016/J.CHEMOSPHERE.2021.132434

- Patel, H., 2021. Comparison of batch and fixed bed column adsorption: a critical review. International Journal of Environmental Science and Technology. https://doi.org/10.1007/s13762-021-03492-y
- Phat, L.N., Nguyen, H.C., Khoa, B.D.D., Khang, P.T., Tien, D.X., Thang, T.Q., Trung, N.K., Nam, H.M., Phong, M.T., Hieu, N.H., 2022. Synthesis and surface modification of cellulose cryogels from coconut peat for oil adsorption. Cellulose 29, 2435–2447. https://doi.org/10.1007/s10570-022-04427-7
- Puga, A., Moreira, M.M., Pazos, M., Figueiredo, S.A., Sanromán, M.Á., Delerue-Matos, C., Rosales, E., 2022. Continuous adsorption studies of pharmaceuticals in multicomponent mixtures by agroforestry biochar. J Environ Chem Eng 10, 106977. https://doi.org/10.1016/J.JECE.2021.106977
- Santomauro, D.F., Mantilla Herrera, A.M., Shadid, J., Zheng, P., Ashbaugh, C., Pigott, D.M., Abbafati, C., Adolph, C., Amlag, J.O., Aravkin, A.Y., Bang-Jensen, B.L., Bertolacci, G.J., Bloom, S.S., Castellano, R., Castro, E., Chakrabarti, S., Chattopadhyay, J., Cogen, R.M., Collins, J.K., Dai, X., Dangel, W.J., Dapper, C., Deen, A., Erickson, M., Ewald, S.B., Flaxman, A.D., Frostad, J.J., Fullman, N., Giles, J.R., Giref, A.Z., Guo, G., He, J., Helak, M., Hulland, E.N., Idrisov, B., Lindstrom, A., Linebarger, E., Lotufo, P.A., Lozano, R., Magistro, B., Malta, D.C., Månsson, J.C., Marinho, F., Mokdad, A.H., Monasta, L., Naik, P., Nomura, S., O'Halloran, J.K., Ostroff, S.M., Pasovic, M., Penberthy, L., Reiner, R.C., Reinke, G., Ribeiro, A.L.P., Sholokhov, A., Sorensen, R.J.D., Varavikova, E., Vo, A.T., Walcott, R., Watson, S., Wiysonge, C.S., Zigler, B., Hay, S.I., Vos, T., Murray, C.J.L., Whiteford, H.A., Ferrari, A.J., 2021. Global prevalence and burden of depressive and anxiety disorders in 204 countries and territories in 2020 due to the COVID-19 pandemic. The Lancet 398, 1700–1712. https://doi.org/10.1016/S0140-6736(21)02143-7
- Shi, M.Y., Jiang, L.J., Yu, C.J., Dong, X.R., Yu, Q.Y., Yao, M.M., He, S.S., Yue, Z.W., Yao, F.L., Zhang, H., Sun, H., Li, J.J., 2022. A robust polyacrylic acid/chitosan cryogel for rapid hemostasis. Sci China Technol Sci 65, 1029–1042. https://doi.org/10.1007/S11431-021-1986-9/METRICS
- Silva, A.D.M., Fernandes, D.F., Figueiredo, S.A., Freitas, O.M., Delerue-Matos, C., 2022. Fluoxetine and Nutrients Removal from Aqueous Solutions by

Phycoremediation. Int J Environ Res Public Health 19. https://doi.org/10.3390/ijerph19106081

- Singh, A., Saidulu, D., Gupta, A.K., Kubsad, V., 2022a. Occurrence and fate of antidepressants in the aquatic environment: Insights into toxicological effects on the aquatic life, analytical methods, and removal techniques. J Environ Chem Eng 10. https://doi.org/10.1016/j.jece.2022.109012
- Tansel, B., Nagarajan, P., 2004. SEM study of phenolphthalein adsorption on granular activated carbon. Advances in Environmental Research 8, 411–415. https://doi.org/10.1016/S1093-0191(02)00126-0
- Thomas, H.C., HENRY THOMAS Vol, B.C., 1944. Heterogeneous Ion Exchange in a Flowing System.
- Wang, W., Zhang, J., Hu, M., Liu, X., Sun, T., Zhang, H., 2023. Antidepressants in wastewater treatment plants: Occurrence, transformation and acute toxicity evaluation. Science of The Total Environment 903, 166120. https://doi.org/10.1016/J.SCITOTENV.2023.166120
- Yoon, Y.H., Nelson, J.H., 1984. Application of Gas Adsorption Kinetics I. A Theoretical Model for Respirator Cartridge Service Life. Am Ind Hyg Assoc J 45, 509–516. https://doi.org/10.1080/15298668491400197
- Zhao, Y., Yu, G., Chen, S., Zhang, S., Wang, B., Huang, J., Deng, S., Wang, Y., 2017. Ozonation of antidepressant fluoxetine and its metabolite product norfluoxetine: Kinetics, intermediates and toxicity. Chemical Engineering Journal 316, 951–963. https://doi.org/10.1016/J.CEJ.2017.02.032

Chapitre 7 - Article 4

7.1 Avant-propos

Le titre du quatrième article scientifique est: « Design of a Sodium Acrylate/Carboxymethyl-Chitosan-Based Imprinted Cryogel for the Selective Adsorption of Fluoxetine in Continuous Mode » Il a été soumis à la revue scientifique Advanced Materials Interfaces en 2025.

Les auteurs et leurs coordonnées correspondantes sont, dans l'ordre:

Gilbert Romeo Nkana Nkana : Étudiant au Doctorat en sciences et génie des matériaux lignocellulosiques, Institut d'Innovations en Écomatériaux, Écoproduits et Écoénergies à base de biomasse (I2E3), Université du Québec à Trois-Rivières, 3351 Boulevard des Forges, CP.500, Trois-Rivières, Québec, Canada, G9A 5H7
Courriel : Gilbert.Nkana@uqtr.ca

Mostafa Eesaee : Chercheur postdoctoral
Département de biochimie, chimie, physique et sciences forensiques et chercheuse à l'Institut de recherche sur l'hydrogène, Université du Québec à Trois-Rivières, 3351 Boulevard des Forges, C.P. 500, Trois-Rivières, Québec, Canada, G9A 5H7.
Courriel: Mostafa Eeasaee@uqtr.ca

Phuong Nguyen-Tri, Ph.D. : Directeur de thèse
Professeur au Département de biochimie, chimie, physique et sciences forensiques et chercheuse à l'Institut de recherche sur l'hydrogène, Université du Québec à Trois-Rivières, 3351 Boulevard des Forges, C.P. 500, Trois-Rivières, Québec, Canada, G9A 5H7.
Courriel: Phuong.Nguyen-Tri@uqtr.ca

Bruno Chabot, Ph.D. Co-Directeur de thèse et auteur pour la correspondance Institut d'Innovation en Écomatériaux, Écoproduits et Écoénergies à basse de biomasse, Université du Québec à Trois-Rivières, 3351 Boulevard des Forges, C.P. 500, Trois-Rivières, Québec, Canada, G9A 5H7
Courriel: bruno.Chabot@uqtr.ca

Contribution des auteurs: Gilbert Nkana est l'auteur principal de cet article. Il a mené toutes les expériences scientifiques et réalisé les développements associés. M. Eesaee a contribué à la rédaction et à la traduction de l'article. M. Nguyen-Tri est directeur de

recherche et M. Chabot est co-directeur de cette recherche. Le directeur et le co-directeur ont participé à la révision et à la correction du manuscrit.

7.2 Résumé

La FLX présent dans les milieux aquatiques menace les écosystèmes, ce qui nécessite des méthodes d'élimination efficaces. Dans cette étude, un cryogel imprimé a été fabriqué à l'aide de la FLX comme modèle. Les cavités imprimées dans le réseau polymère du cryogel servent de sites de reconnaissance sélectif pour le FLX. Les cryogels imprimés et non imprimés ont été caractérisés par microscopie électronique à balayage (MEB), microscopie confocale à balayage laser (CLSM), spectroscopie infrarouge à transformée de Fourier (FTIR) et analyse de surface BET (Brunauer-Emmett-Teller). Le degré de gonflement et la charge de surface ont été mesurés. Des tests d'adsorption continue de la FLX ont été réalisés à l'aide de colonnes à lit fixe remplies de cryogels non imprimés (NIC1/NaPA-CMCs) et imprimés (MIC2/NaPA-CMCs) dans des conditions définies (10-40 ppm, 1,5-2,5 ml/min, pH 8,5, 0,4 cm, 20 ± 2 °C). Le profil de percée s'est accentué à mesure que la concentration et le débit augmentaient. Les données d'adsorption correspondaient aux modèles de Thomas et de Yoon-Nelson, et les paramètres indiquaient une cinétique lente, limitée par la diffusion et régie par la diffusion interne. L'élimination sélective de la FLX a été testée par adsorption compétitive avec le CIT. Le cryogel imprimé a adsorbé 24,96 mg/g et 22,04 mg/g de FLX sous (40 ppm, 1,5 mL/min) et (20 ppm, 1,5 mL/min), respectivement. La FLX a montré une plus grande affinité pour les surfaces MIC2/NaPA-CMCs, avec une efficacité d'élimination supérieure à celle des NIC1/NaPA-CMCs.

7.3 Abstract

FLX in aquatic environments threatens ecosystems, necessitating efficient removal methods. In this study, an imprinted cryogel was fabricated using FLX as a template. The cavities imprinted within the cryogel's polymer network serve as selective recognition sites for FLX. The imprinted and non-imprinted cryogels were characterized by scanning electron microscopy (SEM), confocal laser scanning microscopy (CLSM), Fourier-

transform infrared spectroscopy (FTIR), and BET (Brunauer-Emmett-Teller) surface analysis. Swelling degree and surface charge were measured. Continuous FLX adsorption tests used fixed-bed columns packed with non-imprinted (NIC1/NaPA-CMCs) and imprinted (MIC2/NaPA-CMCs) cryogels under defined conditions (10–40 ppm, 1.5–2.5 mL/min, pH 8.5, 0.4 cm, 20 ± 2 °C). The breakthrough profile steepened as concentration and flow rate increased. The adsorption data fit the Thomas and Yoon–Nelson models, and parameters indicated slow, diffusion-limited kinetics governed by internal diffusion. Selective FLX removal was tested via competitive adsorption with CIT. The imprinted cryogel adsorbed 24.96 mg/g and 22.04 mg/g FLX under (40 ppm, 1.5 mL/min) and (20 ppm, 1.5 mL/min), respectively. FLX showed greater affinity for MIC2/NaPA-CMCs surfaces, with higher removal efficiency than NIC1/NaPA-CMCs.

7.4 Introduction

Antidepressants are psychotropic pharmaceuticals classified as emerging contaminants, detected at trace levels ($ng \cdot L^{-1}$) in environmental media [1]. They exhibit biorecalcitrance, persistence, and tissue accumulation in aquatic organisms from contaminated environments [2–4]. Fluoxetine (FLX), an antidepressant in the selective serotonin reuptake inhibitors family, treats depressive disorders [5–7]. It is lipophilic and stable, with an octanol-water partition coefficient of 4.05-4.6 [8]. Increasing human and animal consumption of these medications contributes to environmental release of the original compounds or their metabolites [9,10]. Conventional wastewater treatment methods in wastewater treatment plants (WWTPs) do not remove these micropollutants before discharge into receiving waters [11]. These molecules adsorb onto sediments where they accumulate [12]. Effective removal of antidepressant residues from wastewater is essential, as bioamplification risks in the trophic network may cause harmful effects on species in receiving environments [4,13]. The main toxic effects include behavioral and reproductive disruptions, alterations to physiological functions, and severe dysfunctions in the trophic network [14,15].

The stability of these molecules requires advanced treatment processes for effective removal. Promising methods include photocatalysis, electrocatalysis, ozonation, electro-

peroxone systems, and photoelectro-Fenton processes [16–19]. Although effective, these techniques are energy-intensive, costly, may generate toxic by-products, and are complex to operate. Adsorption stands out for its efficiency and flexibility in removing organic compounds from aqueous media [20–22] a. It enables the development of adsorbent materials that effectively interact with such molecules. In a sustainable development context, adsorption is promising because it is simple, easy to implement, low-energy, and uses precursors that are often abundant, inexpensive, and derived from biomass.

Several bio-based adsorbents have been developed, but one approach is increasingly attractive due to its material properties. Cryogelation produces stable, flexible cryogels with highly porous structures from monomer and/or polymer precursors without toxic solvents [23–25]. The macroporous structure and composites promote rapid molecular diffusion within the open and interconnected pore network. These materials can be chemically modified for target molecule selectivity and produced in various shapes, advantageous for filtration systems [26,27]. They effectively eliminate both organic and inorganic pollutants [25,28]. They have been developed from biodegradable, biocompatible polymers (cellulose, alginate, chitosan) and synthetic monomers (acrylamide, acrylonitrile, acrylic acid, sodium acrylate, and derivatives). Combining biopolymers and synthetic polymers has created hybrid cryogels with enhanced properties from both materials [29–31].

Incorporating a template molecule during fabrication and then removing it creates specific cavities that match the template molecule. This approach has enabled molecularly imprinted cryogels with selective removal potential for the target molecule in complex systems [26,32]. Such an approach enhances cryogels' adsorption capacity for target molecules, such as FLX.

To our knowledge, no study has reported a molecularly imprinted hybrid cryogel for selective FLX removal from aqueous media. This work aims to use FLX as a template molecule in fabricating an imprinted cryogel from sodium acrylate and carboxymethylchitosan. We characterized imprinted and non-imprinted cryogels using scanning electron microscopy (SEM), confocal laser scanning microscopy (CLSM),

Fourier-transform infrared spectroscopy (FTIR), and BET analysis. We analyzed the materials' swelling degree and surface charge by determining the point of zero charge.

We conducted continuous-flow adsorption tests of FLX on the developed materials and evaluated the selective adsorption potential of the imprinted cryogel through competitive adsorption between FLX and citalopram (CIT), another antidepressant in the same family.

7.5 Experimental

7.5.1 Materials

Chitosan (Cs) with a deacetylation degree ≥ 75 % derived from shrimp shells, chloroacetic acid ($C_2H_3ClO_2$, ≥ 99.0 %), sodium hydroxide (NaOH, ≥ 98 %), anhydrous calcium chloride ($CaCl_2$, ≥ 93.0%), genipin (≥ 98 %), and anhydrous acrylic acid containing 200 ppm MEHQ (99 %, AA) were purchased from Sigma-Aldrich. N,N-methylenebis(acrylamide) (MBA, 99.0 %), sodium metabisulfite (≥ 99.0 %), ammonium persulfate (APS, ≥ 98.0 %), N,N,N',N'-tetramethylethylenediamine (TEMED), isopropyl alcohol (C_3H_8O, 99.0 %), and fluoxetine hydrochloride (FLX), used as the pharmaceutical standard for the fixed-bed adsorption tests, were also from Sigma-Aldrich. Hydrochloric acid (HCl, 37 %) was obtained from Acros Organics. Anhydrous ethanol (C_2H_5OH) and methanol (≥ 99.0 %) were purchased from Commercial Alcohol Greenfield. All solutions were prepared with ultrapure Milli-Q water.

7.5.2 Method

7.5.2.1 Synthesis of carboxymethyl chitosan

Building on our previous research, CMCs were synthesized with slight methodological modifications [33]. First, 6 g of chitosan was added to a flask with 80 mL propan-2-ol and stirred at 250 rpm for 1 h at room temperature. Then, 60 mL NaOH solution (0.4 g/mL) was added and the mixture stirred for 4 h. The flask was stored at −20 °C overnight. After thawing, it was placed in an oil bath at 50 °C. A solution of monochloroacetic acid (30 g in 20 mL propan-2-ol) was added and stirred at 250 rpm for 30 min. The reaction proceeded for 150 min. After cooling, 200 mL of 95 % ethanol was added to stop the

reaction. The product was washed with ethanol and vacuum-dried at 30 °C for 24 h. Impurities were removed by dissolving the product in distilled water, centrifuging at 10,000 rpm, and filtering the supernatant. The dissolved polymer was recrystallized with 600 mL of pure ethanol, isolated by vacuum filtration, and dried under vacuum at 30 °C for 48 h.

7.5.2.2 Synthesis of the non-imprinted hybrid cryogel (NIC1/NaPA-CMCs)

Sodium acrylate (NaA) was prepared by neutralizing acrylic acid with 1 M NaOH, heating the solution in an 80 °C water bath at 100 rpm for 24 h until water evaporated, and drying it under vacuum at 45 °C. The NIC1/NaPA-CMCs cryogel was synthesized following our previous methodology and that of Mourão et al. [29,33] with minor modifications. In a glass vial, 9 mL of 0.3 % (m/v) NaCMCs solution was stirred at 300 rpm. Then, 0.687 g NaA was dissolved in the NaCMCs solution, and pH was adjusted to 7 with 1 M NaOH. For crosslinking, 20 µL of 11 mM genipin was added for 10 min, followed by dissolution of 0.113 g MBA for 30 min. The mixture was degassed for 3 min in an ultrasonic bath (Bransonic CPX3800), frozen for 5 min, and stirred at 90 rpm in an ice bath. Co-initiators APS (0.2 % m/v), TEMED (0.2 % v/v), and 100 µL of 2 % (m/v) $CaCl_2$ were added. The final volume was adjusted to 10 mL, stirred for 60 s, and transferred to polypropylene syringes (Hsw 10/12 mL, 15.9 mm ID). Cryopolymerization proceeded at −18 °C for 24 h. The cryogels were thawed at 5 °C, then at room temperature, and washed with ultrapure water. Samples for characterization were freeze-dried; others were stored hydrated after 1 h of vacuum drying at room temperature.

7.5.2.3 Synthesis of the molecularly imprinted hybrid cryogel (MIC1/NaPA-CMCs)

The MIC1/NaPA-CMCs cryogel was prepared using FLX as the template. In a 0.3 % (m/v) NaCMCs solution stirred at 300 rpm, 0.687 g NaA and 0.1 mg FLX were dissolved for 90 min. After pH adjustment to 7 with 1 M NaOH, 20 µL of 11 mM genipin and 0.113 g MBA were added and stirred for 30 min. The mixture was degassed and cooled to 4 °C. Co-initiators APS (0.2 % m/v) and TEMED (0.2 % v/v) were added under stirring, followed by 100 µL of 2 % (m/v) $CaCl_2$. The volume was adjusted to 10 mL with water,

briefly stirred, and transferred to syringes. Cryopolymerization proceeded at −18 °C for 24 h. The MIC1/NaPA-CMCs was inserted into a clear PVC rigid tube column (Meccanixity; height 35 cm, inner diameter 20 mm, outer diameter 25 mm) connected to a Masterflex peristaltic pump (Cole-Parmer) to remove the template molecule. Distilled water (5 mL) was added to the column for 1 min to promote swelling. Subsequently, the FLX extraction solvent (5% methanol/0.1 M HCl, 1:1 v/v) was pumped through the cryogel at 1 mL/min to the outlet. Samples were collected from the column outlet over 10-120 min and analyzed by UV-Vis spectrophotometry at 230 nm until no FLX was detected in the effluent. The resulting material was annotated MIC2/NaPA-CMCs.

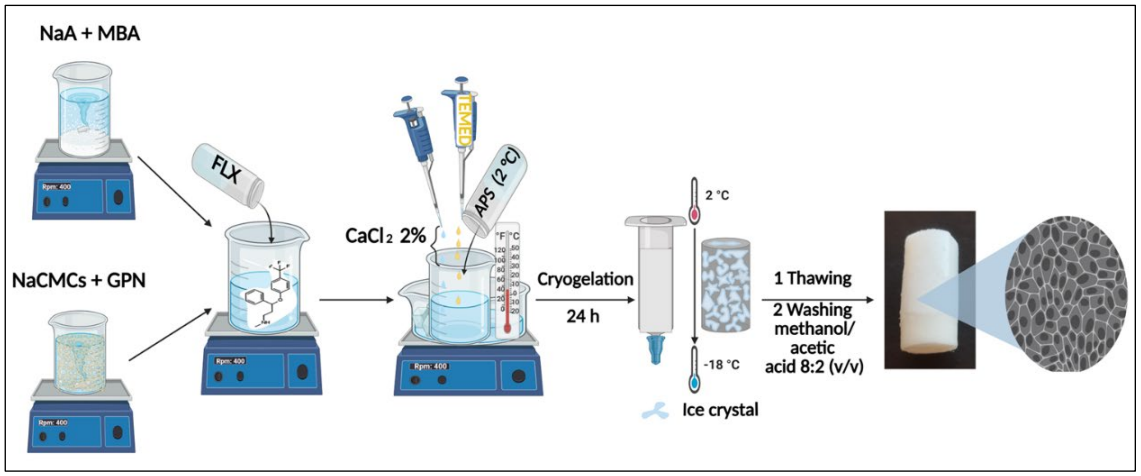

Figure 7.1 Manufacturing steps of the hybrid cryogel based on sodium acrylate (NaA) and sodium carboxymethyl chitosan (NaCMCs) by cryopolymerization

7.5.3 Characterization of the hybrid cryogels MIC/NaPA-CMCs and NIC/NaPA-CMCs

Various analytical techniques were employed to characterize the MIC/NaPA-CMCs and NIC/NaPA-CMCs cryogels. These included FTIR analysis using a Nicolet IS10 FTIR spectrometer at room temperature (500 - 4000 cm^{-1}), surface morphology analysis by SEM using a Hitachi SU 1510 Microscope, and surface images obtained using a Keyence VHX digital microscope. The specific surface area was determined by the BET method, measuring nitrogen adsorption at 77 K using a Micromeritics ASAP2020 instrument.

The point of zero charge (pH_{PZC}) was determined using the pH drift method [33]. Samples were placed in beakers with 20 mL of 0.01 M NaCl solution. The initial pH was adjusted with NaOH and HCl to obtain values between 2 and 12. The beakers were placed in a Lab-Line 3528 orbital shaker for 24 h at 22 °C. After filtration, the final pH was measured using a Mettler-Toledo pH meter. The pH_{PZC} is defined as the pH at which the change in pH (initial pH minus final pH) is zero.

The degree of swelling was determined following Marcuz C. et al. (2021) [34]. A cryogel sample (m_1, g) was weighed, immersed in 50 mL distilled water (pH 7, 20 ± 2 °C) for 10 s. The saturated cryogel was blotted and weighed (m_2, g). The experiment was repeated three times, and the swelling ratio (%) SW was calculated using Equation 7.1:

$$\%\,Sw = \frac{m_2 - m_1}{m_1} \times 100$$

Equation 7.1

7.5.3.1 Continuous-flow adsorption study of fluoxetine on hybrid MIC2/NaPA-CMCs and NIC1/NaPA-CMCs cryogels

Continuous adsorption tests in a fixed-bed column were conducted in downflow mode using the same column/pump system used in section 7.5.2.3 for FLX extraction. The factors to evaluate the adsorption capacity of the cryogel beds were pH 8.5, bed height 0.4 cm, flow rates of 1.5, 2, and 2.5 mL/min, and initial concentrations of 10, 20, and 40 ppm. Water samples were collected regularly and analyzed using a UV-Vis spectrometer (Agilent Cary 60 UV-Vis) at 230 nm to determine the absorbance of the initial and final FLX solutions. All experiments were at room temperature (20 ± 2 °C).

From the data, breakthrough curves ((C_t/C_0) versus t) were plotted, and column operating parameters were determined, including total FLX adsorbed at a flow rate q_{total} (mg) and equilibrium adsorption capacity $q_{e.exp}$ (mg/g), represented by Equations (2) and (3). The breakthrough time, t_b (min), and the exhaustion time, t_e (min), are defined as the points at which the ratio C_t/C_0 reaches 0.05 and 0.95, respectively.

$$q_{total} = \left(\frac{Q}{1000}\right)\int_{t=0}^{t=t_{total}} C_t dt$$

Equation 7.2

$$q_{e.\exp} = \frac{q_{total}}{m}$$

Equation 7.3

Where Q is the flow rate (mL/min), C_0 (ppm) is the initial FLX concentration at the column inlet, C_t (ppm) is the FLX concentration in the effluent at the outlet, m (g) is the mass of cryogel adsorbent, and t_{total} (min) is the column operating time.

The Thomas and Yoon-Nelson models (Equations 7.4 and 7.5) were used to fit the experimental data. The underlying assumptions of these models state that adsorption follows pseudo-second-order kinetics for the former, and that the probability of breakthrough is proportional to the probability of adsorption for the latter [35,36].

$$\frac{C_t}{C_0} = \frac{1}{1+\exp\left(K_{th}\left[\frac{q_0 m}{Q} - C_0 t\right]\right)}$$

Equation 7.4

$$\frac{C_t}{C_0} = \frac{1}{1+\exp\left(K_{YN}(\tau - t)\right)}$$

Equation 7.5

Where K_{Th} (L/mg·min) is the Thomas rate constant, q_0 (mg/g) is the equilibrium adsorption capacity, K_{YN} (min^{-1}) is the Yoon-Nelson rate constant, and τ (min) is the time corresponding to 50 % breakthrough.

The quality of fit of experimental data by both models was determined using a statistical software (OriginPro 2025), specifically the coefficient of determination (R^2) and the root mean square error (RMSE).

7.5.3.2 Preliminary competitive adsorption study of fluoxetine and citalopram in continuous flow on MIC2/NaPA-CMCs and NIC1/NaPA-CMCs cryogels

A mixed solution of FLX and CIT (10 ppm each) was prepared with 5 % methanol and pH adjusted to 8.5 with 1 M NaOH. Competitive adsorption on NIC1/NaPA-CMCs and

MIC2/NaPA-CMCs cryogel beds was performed in continuous mode at an initial concentration of 10 ppm, a bed height of 0.4 cm, and a flow rate of 1.5 mL/min. Effluent samples were collected and analyzed using a Shimadzu i-Series Plus liquid chromatography system with a diode array detector (DAD). Separation used a C18 column (XB-C18, 100 Å, 150 × 3 mm, 2.6 µm) with phosphate buffer (10 mM) and acetonitrile mobile phase. The elution flow rate was 0.3 mL/min, with CIT and FLX retention times of 3.11 and 4.96 min, respectively, for a total analysis time of 10 min. Maximum absorption was at 230 nm for FLX and 238 nm for CIT. Equations 7.6, 7.7, and 7.8 determined distribution coefficients, selectivity coefficients, and relative selectivity coefficients.

$$K_d = \frac{q_{e.\exp}}{C_e}$$ Equation 7.6

$$K = \frac{K_{d\,FLX}}{K_{dCIT}}$$ Equation 7.7

$$K' = \frac{K_{MIC/NaPA-CMCs}}{K_{NIC/NaPA-CMCs}}$$ Equation 7.8

Where K_d (L/g) is the distribution coefficient, C_e (ppm) is the equilibrium concentration, K_{dFLX} (L/g) and K_{dCIT} (L/g) are the distribution coefficients of FLX and CIT, $K_{MIC/NaPA-CMCs}$ and $K_{NIC/NaPA-CMCs}$ are the selectivity coefficients of the imprinted and non-imprinted cryogels, and K' is the relative selectivity coefficient.

7.6 Results and discussion

7.6.1 Characterization of imprinted and non-imprinted hybrid cryogels

Analysis of the infrared spectra (Figure 7.2) revealed structural changes in the polymer network after polymerization in the presence of the template molecule, its extraction, and FLX-induced modifications. The MIC1/NaPA-CMCs spectrum shows a band at 1644 cm^{-1}, associated with the amide I C=O bond, linked to crosslinking of polymer chains by MBA and genipin. The intense band at 1545 cm^{-1} is attributed to asymmetric COO^-

stretching and the N–H bond of amide II. The band at 1452 cm^{-1} is attributed to CH_2 deformation, and that at 1406 cm^{-1} corresponds to symmetric COO^- stretching. The band at 1324 cm^{-1}, attributed to C–N stretching of amide III, further confirms covalent-bridge formation in the polymer network, while the band at 1114 cm^{-1} is assigned to C–O stretching.

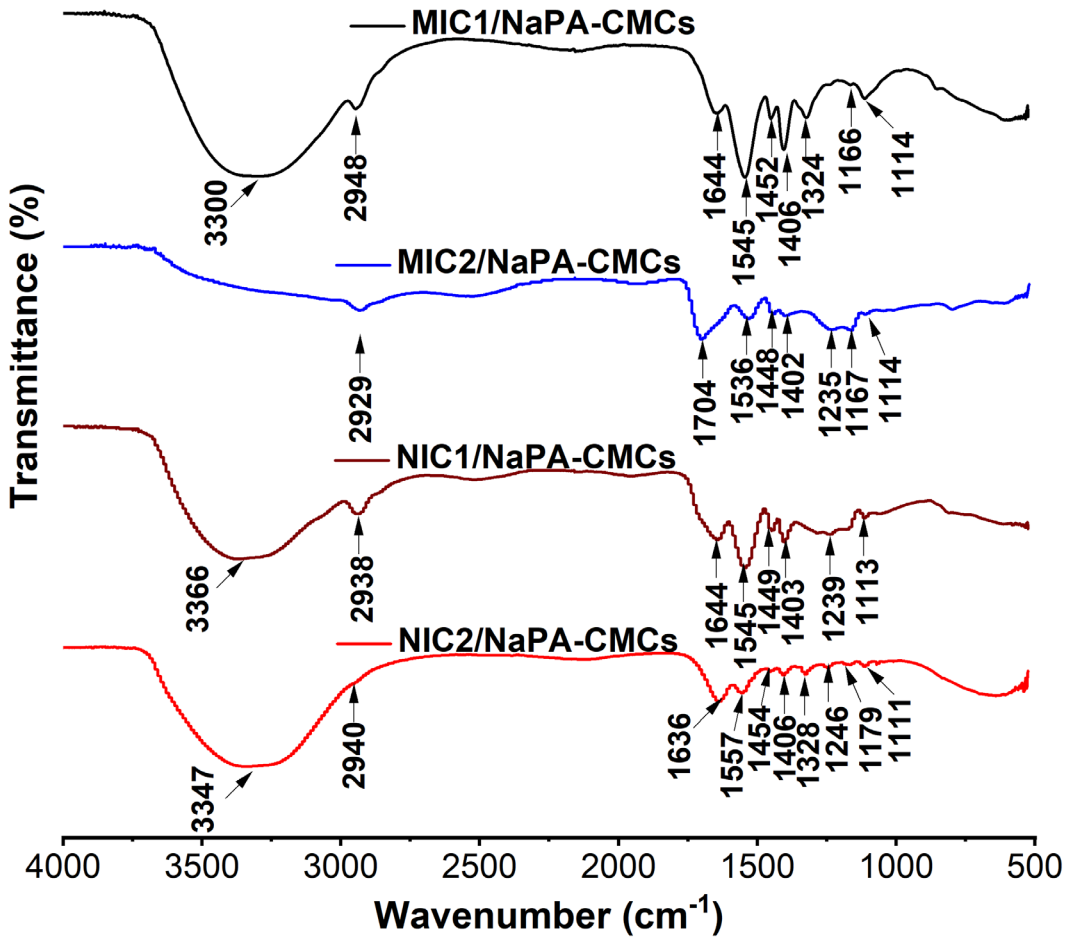

Figure 7.2 FTIR spectra of MIC1/NaPA-CMCs after printing, MIC2/NaPA-CMCs after extraction, NIC1/NaPA-CMCs and NIC2/NaPA-CMCs before and after fluoxetine adsorption

During MIC1/NaPA-CMCs formation, the functional groups COO^-, NH_2, and OH establish electrostatic interactions and hydrogen bonds with FLX, thereby modifying their chemical environment. Extraction of FLX from the polymer network alters the vibration frequencies of these groups, as observed in the MIC2/NaPA-CMCs spectrum. An intense,

broad band appears at 1704 cm^{-1}, associated with C=O stretching of carboxylic acid arising from protonation of COO^- groups during washing with the acidified solvent.

The shift of the bands at 1545 cm^{-1} and 1406 cm^{-1} toward lower frequencies and reduced intensity (to 1536 cm^{-1} and 1402 cm^{-1}, respectively) corresponds to asymmetric and symmetric COO^- stretching. A similar modification occurs for the band at 1453 cm^{-1}, which shifts to 1448 cm^{-1}. FLX adsorption on NIC1/NaPA-CMCs is confirmed by changes in the NIC2/NaPA-CMCs spectrum. The band at 1644 cm^{-1} shifts to 1636 cm^{-1}, likely due to hydrogen-bond formation between the C=O group of amide I and ionized FLX. Electrostatic interactions between COO^- groups and ionized FLX likely cause the shift of the bands at 1545 cm^{-1} and 1403 cm^{-1} to 1557 cm^{-1} and 1406 cm^{-1}, respectively, where weaker bands appear. Likewise, the bands at 1449 cm^{-1} and 1113 cm^{-1} shift to weaker bands at 1454 cm^{-1} and 1111 cm^{-1}, respectively.

Figure 7.3 shows the swelling ratio of cryogels in water. Upon contact with water, the materials swell rapidly and reach equilibrium within 10 s. The maximum swelling of MIC2/NaPA-CMCs is 117.7 ± 7.8 %, while NIC1/NaPA-CMCs reach 123.5 ± 33.4 %. The demineralized water at pH 7 keeps the MIC2/NaPA-CMCs monolith surface generally negative ($pH > pH_{PZC}$) and the NIC1/NaPA-CMCs surface generally positive ($pH < pH_{PZC}$), as indicated by surface charge analysis. This promotes repulsive electrostatic interactions between charged functional groups, which, together with osmotic force, drive rapid water diffusion through the interconnected macropore network observed in microscopy and expand the polymer networks. The increased swelling of NIC1/NaPA-CMCs compared to MIC2/NaPA-CMCs could result from FLX incorporation during polymerization, leading to the network forming around the template. Removing FLX to form printed cavities protonates COO^- groups and disrupts these interactions, reducing electrostatic repulsion between polymer chains and limiting MIC2/NaPA-CMCs swelling relative to NIC1/NaPA-CMCs.

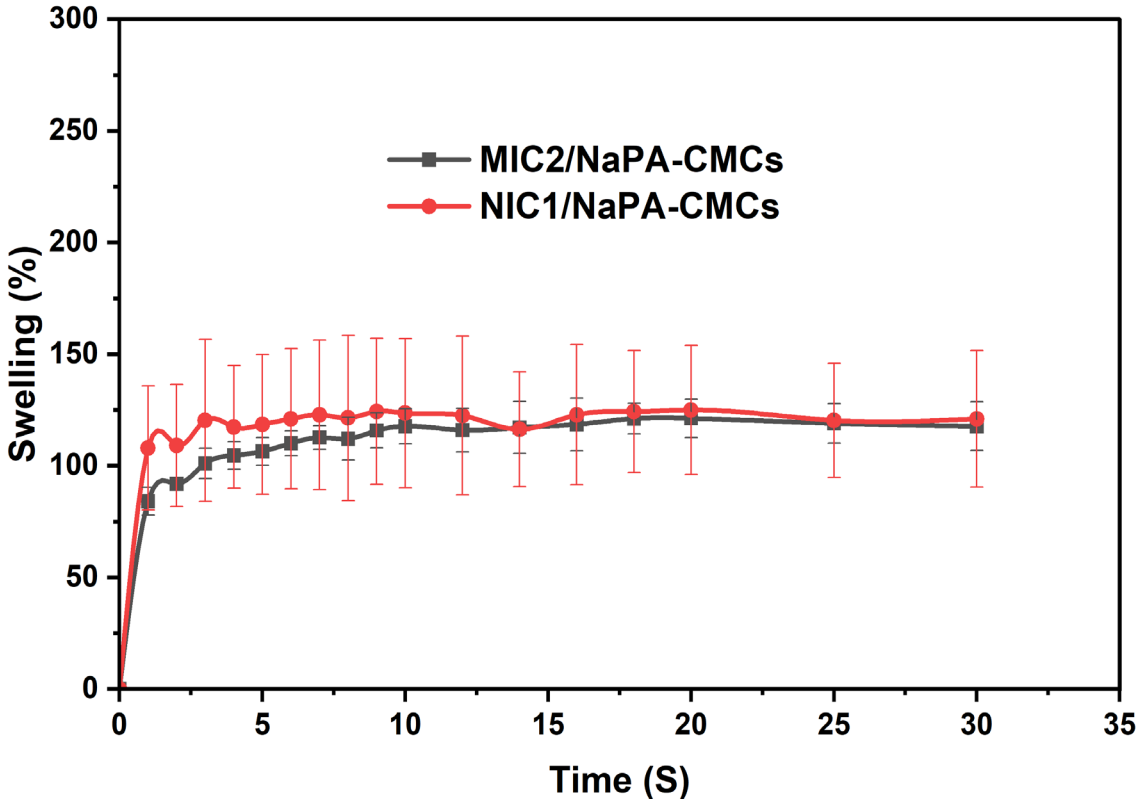

Figure 7.3 Water swelling ratio (%) of MIC2/NaPA-CMCs and NIC1/NaPA-CMCs upon contact with water. Cryogel samples were immersed in 50 mL of distilled water at pH 7 and 20 ± 2 °C for 10 s

FTIR analysis of the various cryogels confirmed the presence of polyelectrolyte within the monoliths' polymer network, with functional groups responsive to pH variation. To clarify this further, the overall surface charge of the cryogels was analyzed, along with the determination of the point of zero charge (pH_{PZC}) (Figure 7.4). The pH_{PZC} of MIC2/NaPA-CMCs is 4.9, while that of NIC1/NaPA-CMCs is 7.1. Thus, surfaces are positively charged when $pH_{solution} < pH_{PZC}$ and negatively charged when $pH_{solution} > pH_{PZC}$. Although both cryogels consist of the same polymers, the use of FLX as a template would have modified the chemical environment of the functional groups. Extraction of FLX resulted in protonation of COO^- groups trapped in imprinted cavities. Upon immersion in an acidified aqueous environment, protonation occurs on fewer COO^- groups, which may explain the lower pH_{PZC} of MIC2/NaPA-CMCs compared to NIC1/NaPA-CMCs.

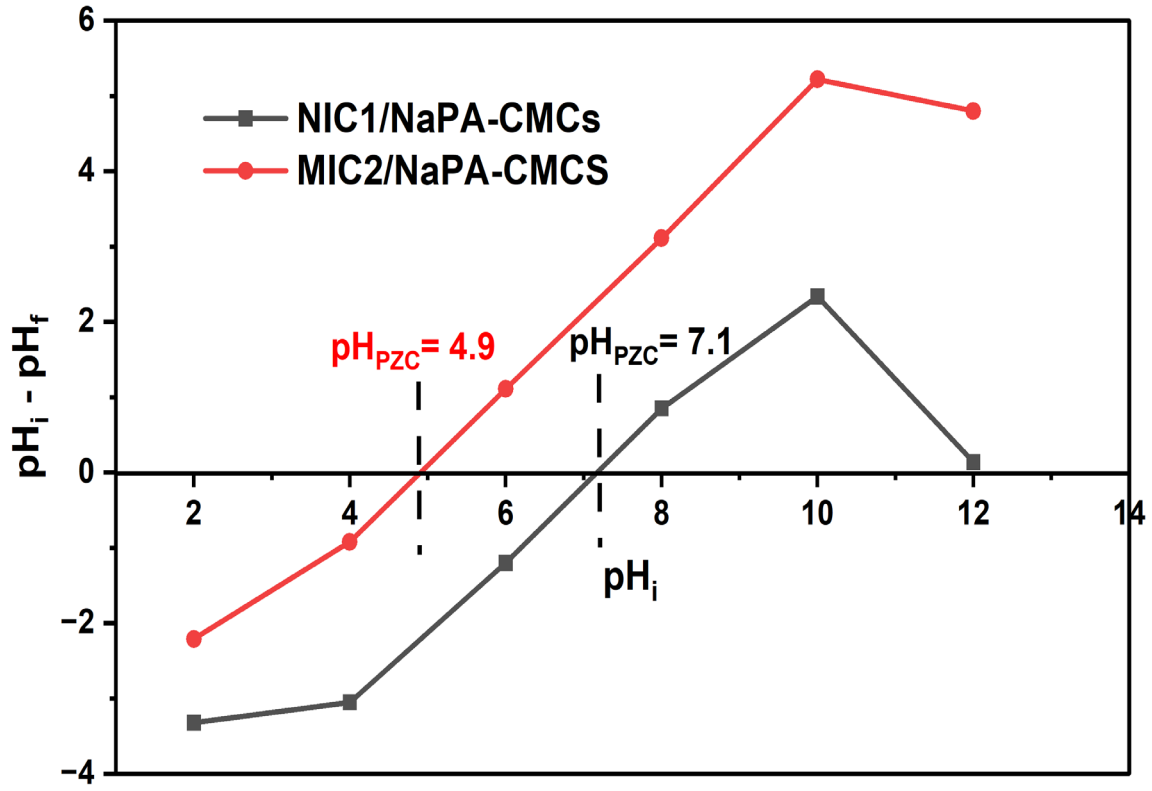

Figure 7.4 Point of zero charge of MIC2/NaPA-CMCs and NIC1/NaPA-CMCs. Tests were carried out at room temperature

The extraction of FLX from the MIC1/NaPA-CMC polymer network forms printed cavities. Fig. 5 shows UV spectra of extraction-solvent samples recovered at the column outlet from 10 to 120 min. The spectra show a marked decrease in FLX absorption after 120 min of elution. This indicates that the extraction solvent (5 % methanol/0.1 M HCl, 1:1 v/v) protonates carboxylate groups on the polymer chains, cancelling electrostatic interactions, and disrupts hydrogen bonds between polymer hydrogen-donor groups and the FLX hydrogen-acceptor group. This likely causes changes in the chemical environment around these donor groups on the MIC2/NaPA-CMCs monolith, as indicated by shifts in vibration frequencies between this cryogel and MIC1/NaPA-CMCs in FTIR analysis.

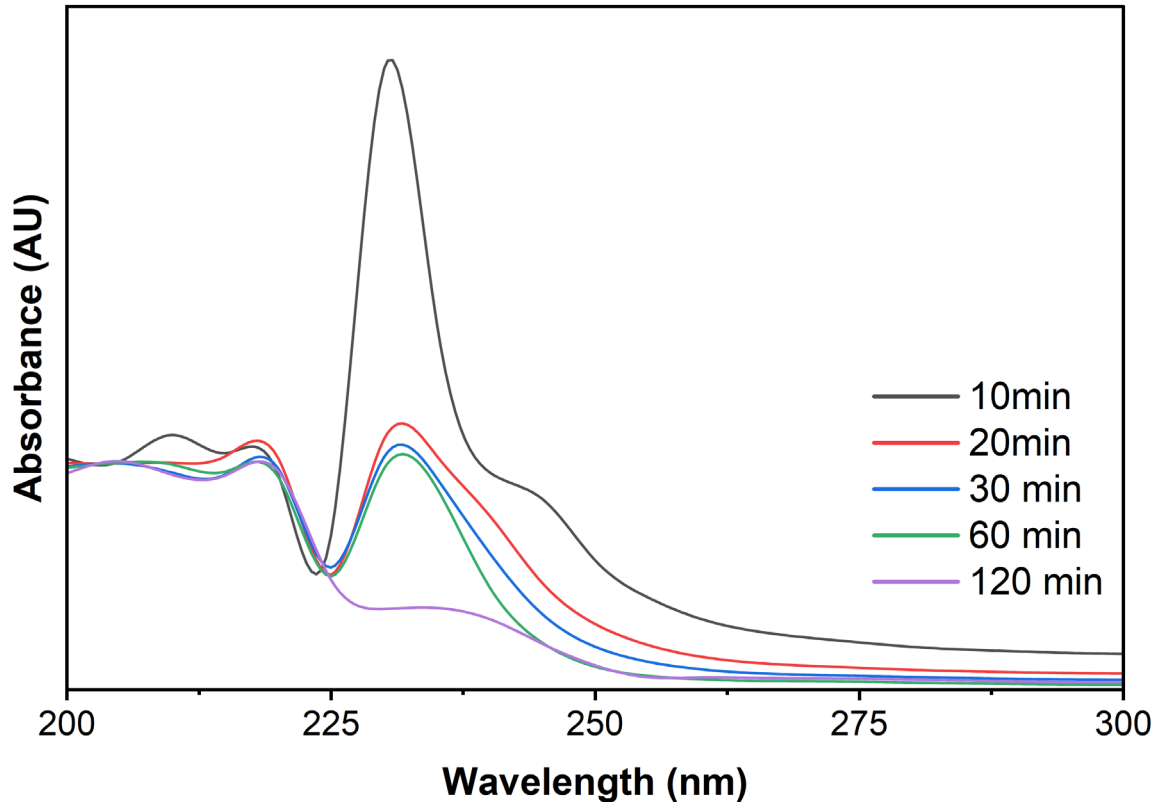

Figure 7.5 UV spectra of solution samples recovered after washing MIC1/NaPA-CMCs cryogel at different extraction times

The morphology, pore distribution, and roughness were analyzed by SEM and CLSM (Figure 7.6). The micrographs show a porous structure with a homogeneous distribution of interconnected pores. The 3D images reveal that at depths of 324.9 µm for MIC2/NaPA-CMCs and 212.3 µm for NIC1/NaPA-CMCs, the internal structure contains open cavities, which may accelerate FLX diffusion within the polymer network during adsorption. The material surfaces are irregular, with average roughness values of 19.2 µm for NIC1/NaPA-CMCs and 31.5 µm for MIC2/NaPA-CMCs. BET analysis gives specific surface areas of 61.1 $m^2 \cdot g^{-1}$ for NIC1/NaPA-CMCs and 36.8 $m^2 \cdot g^{-1}$ for MIC2/NaPA-CMCs. The pore volumes are 0.083 $cm^3 \cdot g^{-1}$ for NIC1/NaPA-CMCs and 0.187 $cm^3 \cdot g^{-1}$ for MIC2/NaPA-CMCs, with pore diameters of 547.7 nm and 203.3 nm, respectively.

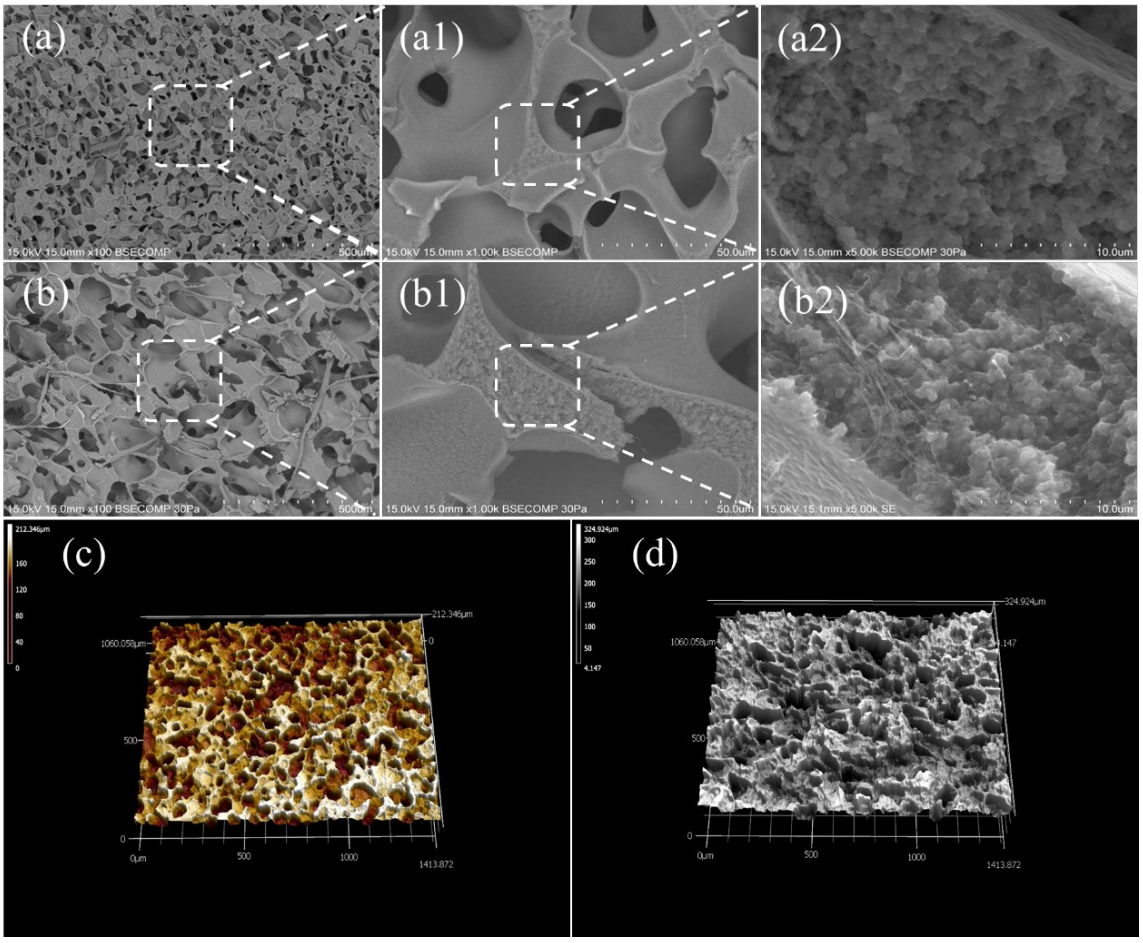

Figure 7.6 SEM micrographs of NIC1/NaPA-CMCs: (a) ×100, (a_1) ×1000, (a_2) ×5000; MIC2/NaPA-CMCs: (b) ×100, (b_1) ×1000, (b_2) ×5000; and 3D CLSM images of (c) NIC1/NaPA-CMCs and (d) MIC2/NaPA-CMCs

7.6.2 Effect of operating parameters on the fluoxetine adsorption capacity of NIC1/NaPA-CMCs and MIC2/NaPA-CMCs cryogel beds

Breakthrough curves represent system behavior during dynamic adsorption and quantify column performance during FLX adsorption. In the breakthrough curves (Figure 7.7), initial concentration variation shows similar effects on NIC1/NaPA-CMCs and MIC2/NaPA-CMCs. Higher inlet concentrations lead to earlier breakthrough and faster exhaustion of cryogel beds. For NIC1/NaPA-CMCs, breakthrough time (t_b) decreased from 477.8 min to 159.1 min, and exhaustion time (t_e) from 963.6 min to 654.9 min. For MIC2/NaPA-CMCs, breakthrough time decreased from 465.8 min to 137.1 min and exhaustion time from 946 min to 564.2 min, as shown in Tables 7.1 and 7.2. Rapid

adsorption-front movement produces a sharper breakthrough profile. Higher concentration gradients overcome liquid-film resistance and increase mass transfer between FLX solution and the cryogel-bed surface. The active sites reach saturation earlier at higher FLX concentrations, consistent with Saravanan et al. (2018) [37] for pollutant removal using biomass.

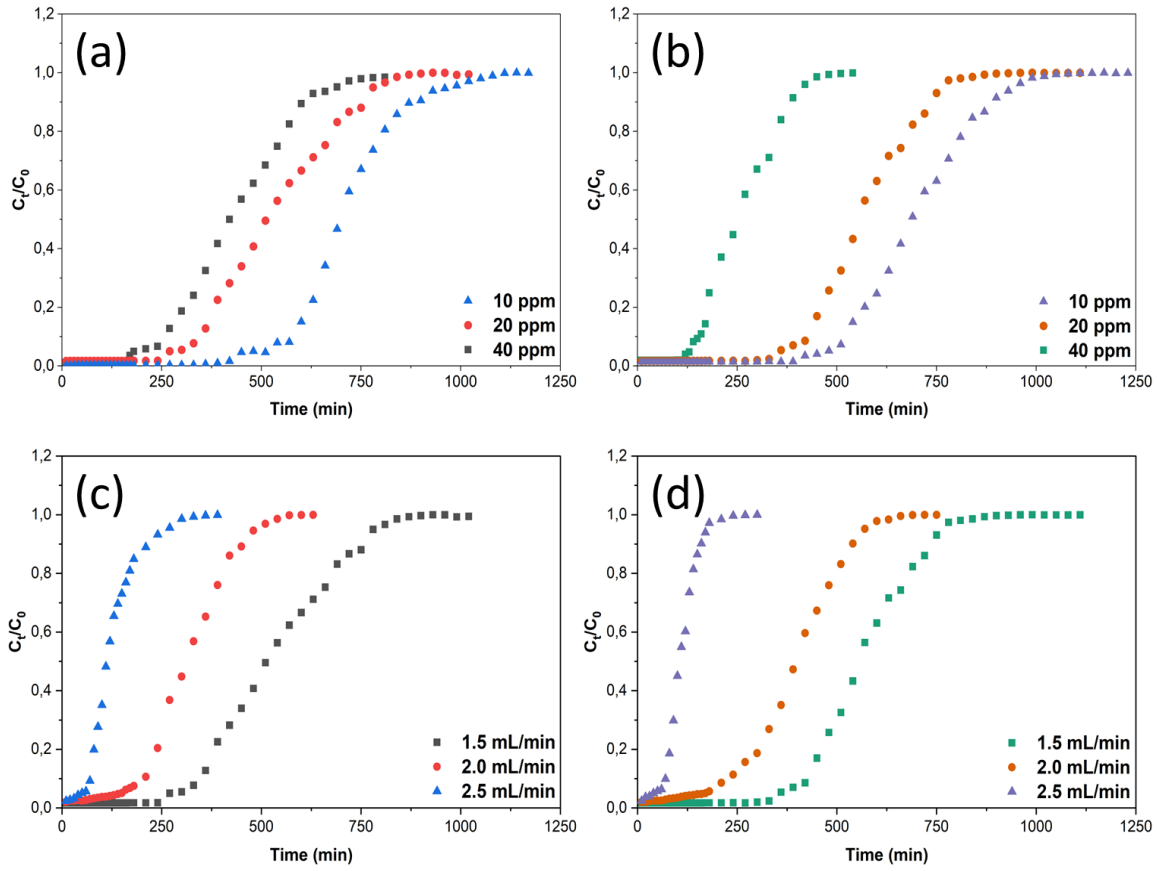

Figure 7.7 Breakthrough curves of FLX in a fixed-bed cryogel column under different operating conditions: a) concentration (NIC1/NaPA-CMCs), b) concentration (MIC2/NaPA-CMCs), c) flow rate (NIC1/NaPA-CMCs), d) flow rate (MIC2/NaPA-CMCs), at pH 8.5, bed height 0.4 cm, and temperature 20 ± 2 °C

Increasing the flow rate accelerated breakthrough and exhaustion for both NIC1/NaPA-CMCs and MIC2/NaPA-CMCs (Tables 7.1 and 7.2). At 1.5 mL·min^{-1}, FLX solution flows more slowly through cryogel beds than at 2 and 2.5 mL·min^{-1}, allowing molecules more time to diffuse through pores and reach active sites [22,38]. Consequently, adsorption

capacity decreased from 20.61 mg·g^{-1} to 7.79 mg·g^{-1} for NIC1/NaPA-CMCs and from 22.04 mg·g^{-1} to 6.61 mg·g^{-1} for MIC2/NaPA-CMCs.

The adsorption-test pH (8.5) promotes electrostatic interactions between ionized FLX (pKa 9.8) and the negatively charged NIC1/NaPA-CMCs and MIC2/NaPA-CMCs surfaces via COO^- groups along polymer chains, as indicated by pH_{PZC} results.

Table 7.1 Performance indicators of FLX adsorption by NIC1/NaPA-CMCs cryogel bed under different operational conditions

C (ppm)	Q (mL/min)	pH	H (cm)	q_{tot} (mg)	$q_{e.exp}$ (mg/g)	t_b (min)	t_e (min)
10	1.5	8.5	0.4	10.51	14.02	477.8	963.6
20	1.5	8.5	0.4	15.46	20.61	269.2	779.9
40	1.5	8.5	0.4	22.20	29.60	159.1	654.9
20	2.0	8.5	0.4	13.71	18.28	147.3	482.2
20	2.5	8.5	0.4	5.84	7.79	49.0	268.4

Table 7.2 Performance indicators of FLX adsorption by MIC2/NaPA-CMCs cryogel bed under different operational conditions

C (ppm)	Q (mL/min)	pH	H (cm)	q_{tot} (mg)	$q_{e.exp}$ (mg/g)	t_b (min)	t_e (min)
10	1.5	8.5	0.4	10.23	13.64	465.8	946
20	1.5	8.5	0.4	16.53	22.05	334.6	760.6
40	1.5	8.5	0.4	18.72	24.96	137.1	564.2
20	2.0	8.5	0.4	15.32	20.43	170.8	568.9
20	2.5	8.5	0.4	4.96	6.61	39.6	171.9

7.6.3 Modeling of breakthrough curves

Modeling breakthrough curves is an essential step for predicting column operating parameters by fitting models to experimental data. It also allows evaluation of the adsorption dynamics in a fixed-bed column. For this purpose, the Thomas and Yoon-Nelson models were used, as they are advantageous for describing overall adsorption kinetics. The data processing and modeling were carried out using Origin 2025 software.

7.6.3.1 Thomas model

A nonlinear adjustment of the Thomas model to experimental continuous adsorption data of FLX fit the data well (Figure 7.8). The predicted parameters appear in Tables 7.3 and 7.4. Results indicate robust fits across initial concentration and flow rate. The R^2 values

exceed 0.98, with RMSE values near zero. The minimal difference between experimental ($q_{e,exp}$) and theoretical (q_0) adsorption capacities supports the model's validity.

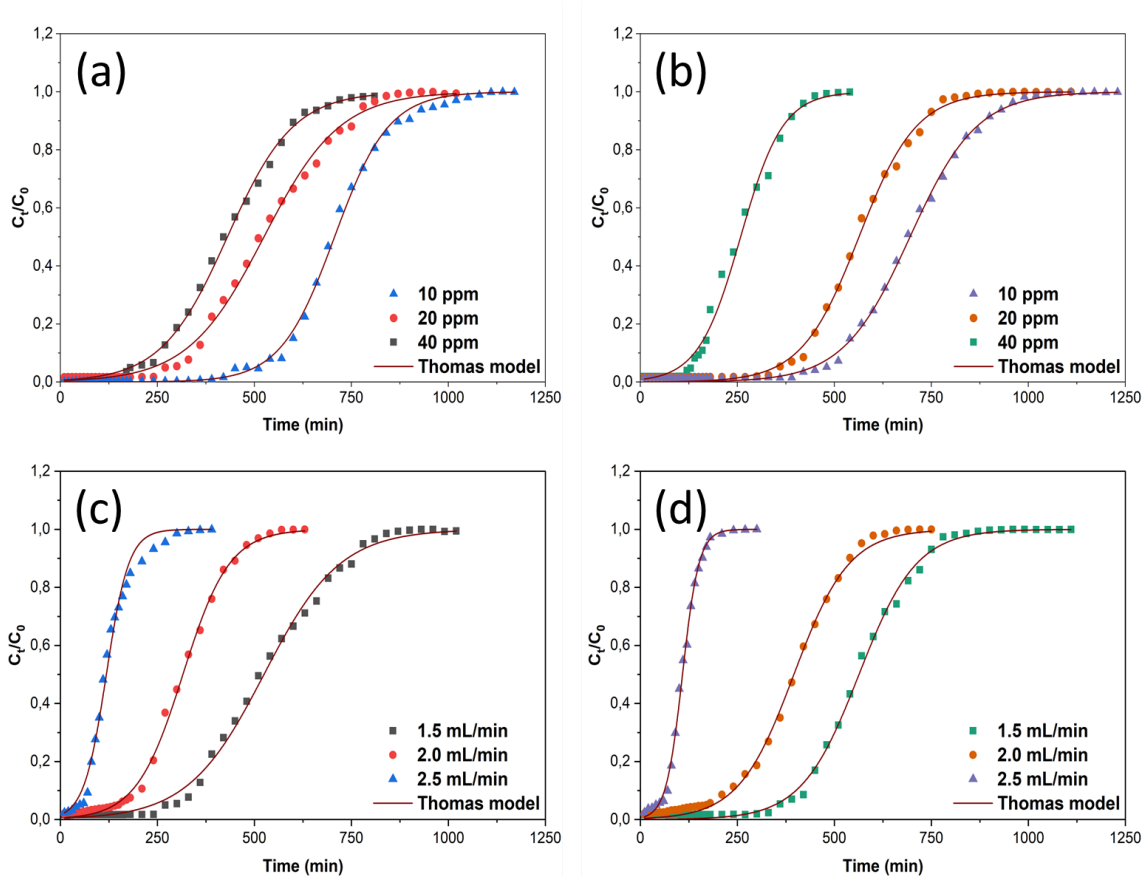

Figure 7.8 Adjustment of the Thomas model to FLX dynamic adsorption data in a fixed bed of NIC1/NaPA-CMCs and MIC2/NaPA-CMCs

The Thomas constant K_{Th} ($mL \cdot mg^{-1} \cdot min^{-1}$) decreases with increasing FLX inlet concentration and with reduced flow rate. This decrease indicates mass transfer limited by internal diffusion, although concentration gradients rise. External diffusion occurs faster, and surface sites saturate before internal pore sites. The apparent adsorption kinetics is slow and limited by internal diffusion. Higher concentration increases the FLX mass flux to active sites, thereby increasing adsorption. A similar behavior is observed for acetaminophen adsorption [39].

7.6.3.2 Yoon-Nelson model

A nonlinear adjustment of the Yoon–Nelson model fits the experimental adsorption data. The simulation results for different column conditions are shown in Figure 7.9, with the model parameters listed in Tables 7.3 and 4. R^2 values above 0.98 and RMSE values near 0 confirm the model captures FLX adsorption on the cryogels. The parameter τ and Yoon–Nelson constant K_{YN} (min^{-1}) decrease with increasing initial FLX concentration and flow rate, indicating faster saturation and shorter breakthrough times.

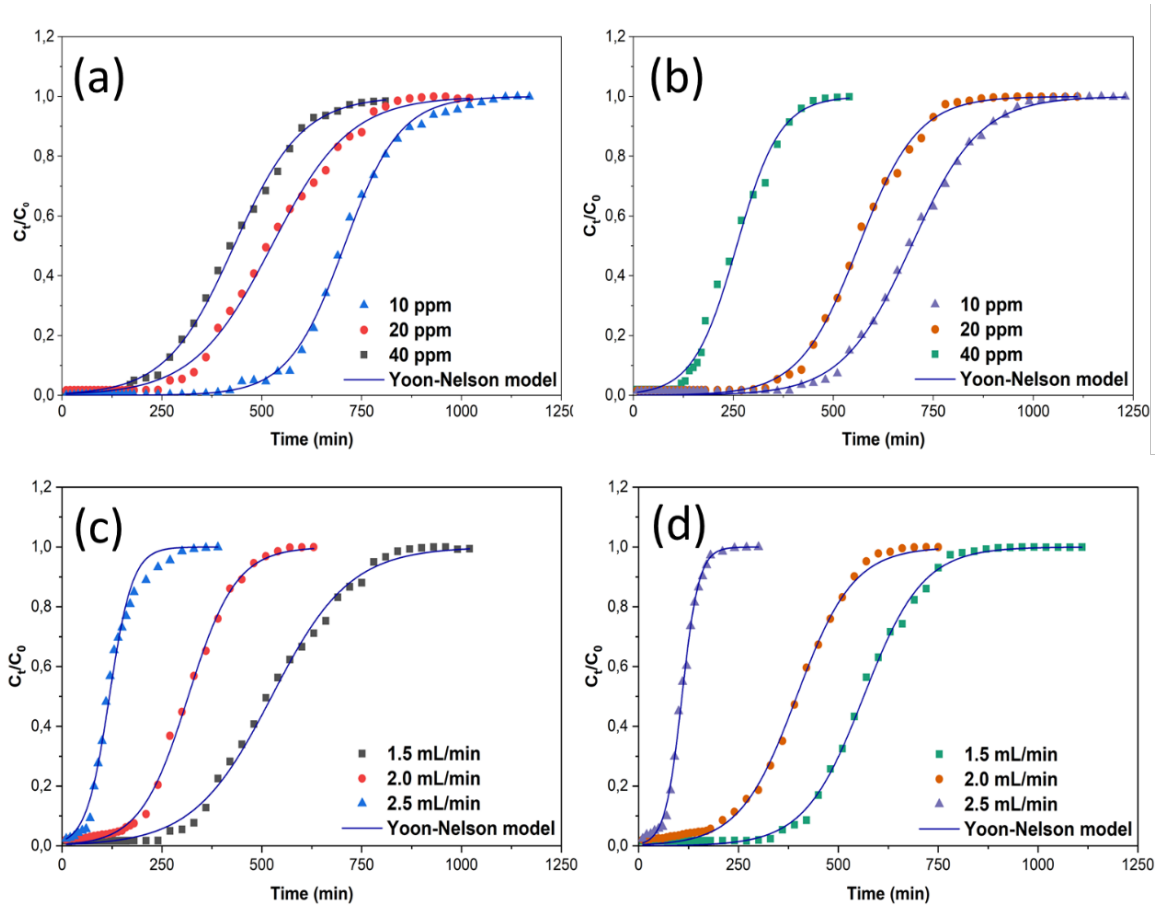

Figure 7.9 Adjustment of the Yoon-Nelson model to FLX dynamic adsorption data in a fixed bed of NIC1/NaPA-CMCs and MIC2/NaPA-CMCs

Table 7.3 Adjustment of Thomas and Yoon-Nelson models for NIC1/NaPA-CMCs

	Parameters			Thomas model				Yoon-Nelson model			
C (ppm)	Q (mL/min)	pH	H (cm)	K_{Th} (mL/mg.min)	q_0 (mg/g)	R^2	RMSE	K_{YN} (min^{-1})	τ (min)	R^2	RMSE
10	1.5	8.5	0.4	1.43 ± 0,03	14.13 ± 0.03	0.998	0.015	0.014 ± 2.42 $x10^{-4}$	706.48 ± 1.74	0.998	0.015
20	1.5	8.5	0.4	0.51 ± 0.01	20.98 ± 0.10	0.997	0.020	0.010 ± 2.46 $x10^{-4}$	524.50 ± 2.70	0.997	0.020
40	1.5	8.5	0.4	0.28± 0.06	30.27 ± 0.21	0.998	0.016	0.011 ± 3.15 $x10^{-4}$	433.82 ± 1.99	0.998	0.016
20	2.0	8.5	0.4	0.83 ± 0.02	16.83 ± 0.09	0.998	0.017	0.017 ± 3.80 $x10^{-4}$	315.60 ± 1.72	0.998	0.017
20	2.5	8.5	0.4	1.73 ± 0.09	7.89 ± 0.11	0.990	0.039	0.034 ± 18.40 $x10^{-4}$	118.30 ± 1.63	0.990	0.039

Table 7.4 Adjustment of Thomas and Yoon-Nelson models for MIC2/NaPA-CMCs

	Parameters			Thomas model				Yoon-Nelson model			
C (ppm)	Q (mL/min)	pH	H (cm)	K_{Th} (mL/mg.min)	q_0 (mg/g)	R^2	RMSE	K_{YN} (min^{-1})	τ (min)	R^2	RMSE
10	1.5	8.5	0.4	1.160 ± 0.020	13.90 ± 0.03	0.999	0.013	0.012 ± 1.96 $x10^{-4}$	694.81 ± 1.64	0.999	0.013
20	1.5	8.5	0.4	0.675 ± 0.017	22.53 ± 0.08	0.998	0.017	0.013 ± 3.13 $x10^{-4}$	563.35 ± 195	0.998	0.017
40	1.5	8.5	0.4	0.295 ± 0.011	25.77 ± 0.33	0.992	0.035	0.01 ± 4.48 $x10^{-4}$	322.21 ± 4.18	0.992	0.035
20	2.0	8.5	0.4	0.703 ± 0.017	21.09 ± 0.11	0.998	0.018	0.014 ± 3.32 $x10^{-4}$	395.55 ± 1.99	0.998	0.018
20	2.5	8.5	0.4	2.355 ± 0.074	7.23 ± 0.05	0.997	0.021	0.047 ± 14.90 $x10^{-4}$	108.44 ± 0.75	0.997	0.021

7.6.4 The study of selective adsorption of imprinted and non-imprinted cryogels

A preliminary adsorption test was conducted using fluoxetine (FLX) and citalopram (CIT), antidepressants in the selective serotonin reuptake inhibitor class that coexist in aquatic environments. Their properties are presented in Table 7.5. CIT shares physicochemical properties with FLX, such as pKa, log K_{ow}, and log K_d. The mixed solution prepared according to Section 7.5.5 was contacted with NIC1/NaPA-CMCs and MIC2/NaPA-CMCs beds to assess selective FLX adsorption. The solution pH was adjusted to 8.5, below both molecules' pKa, ensuring their cationic protonation. This promotes electrostatic interactions with the materials' negatively charged surfaces, as shown by point-of-zero-charge analysis. The adsorbed amounts of FLX and CIT are shown in Figure 7.10.

Table 7.5 Physico-chemical characteristics of fluoxetine and citalopram [8,40]

Chemical	Fluoxetine (FLX)	Citalopram (CIT)
Molecular structure	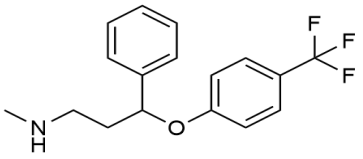	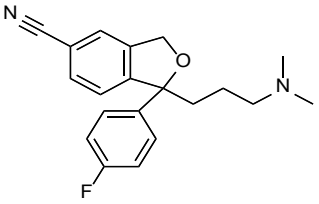
Molecular formula	$C_{17}H_{18}F_3NO$	$C_{20}H_{21}FN_2O$
Molecular weight	309.32 g/mol	405.30 g/mol
pKa	9.80	9.78
Water solubility	0.0017 mg/mL	0.0059 mg/mL
Log Kow	4.17	3.76
Log K_d	3.9	3.6

The amount of FLX adsorbed onto MIC2/NaPA-CMCs (13.78 mg·g^{-1}) is higher than onto NIC1/NaPA-CMCs (9.98 mg·g^{-1}), while CIT adsorption onto MIC2/NaPA-CMCs is significantly lower than FLX. This indicates FLX's stronger affinity for the imprinted cavities. The selectivity coefficient calculations in Table 7.6 show higher FLX adsorption than CIT for both materials. The selectivity coefficient of MIC2/NaPA-CMCs exceeds that of NIC1/NaPA-CMCs, with K′ > 1, confirming FLX's stronger affinity for MIC2/NaPA-CMCs active surface. It is believed that during adsorption, FLX, being more hydrophobic than CIT with a higher sorption coefficient, orients toward memory sites (imprinted cavities), which saturate rapidly, then toward non-imprinted binding sites in the polymer network. FLX binds through electrostatic, hydrophobic, hydrogen-bonding, and π-π interactions. CIT competes with FLX only at sites outside imprinted cavities.

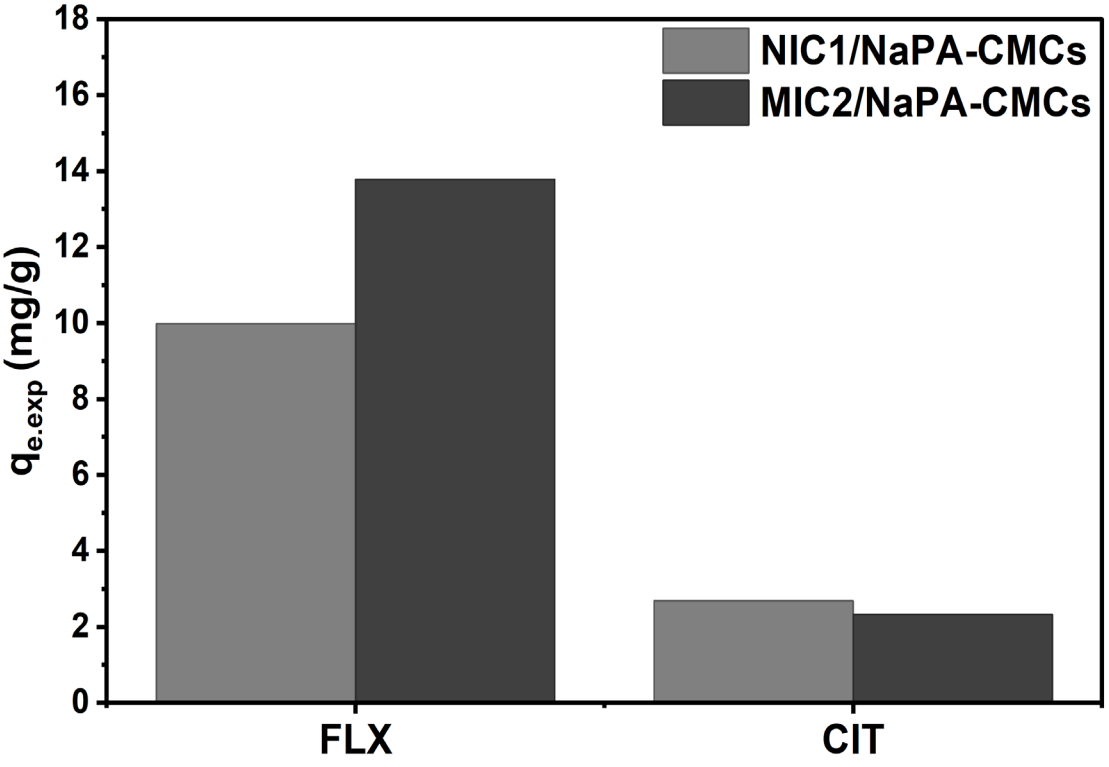

Figure 7.10 Adsorbed amounts of fluoxetine and citalopram on NIC1/NaPA-CMCs and MIC2/NaPA-CMCs

Table 7.6 The distribution coefficient, selectivity, and relative selectivity coefficients

	NIC1/NaPA-CMCs			MIC2/NaPA-CMCs			
	$q_{e.exp}$	K_d	K	$q_{e.exp}$	K_d	K	K'
FLX	9.98	0.998	-	13.78	1.38	-	-
CIT	2.67	0.27	3.7	2.33	0.23	5.92	1.6

7.7 Conclusion

The presence of antidepressant residues, such as FLX, in aquatic environments poses ecological risks. Developing molecularly imprinted cryogels that selectively bind this contaminant mitigates these risks, as FLX often coexists with other pharmaceutical pollutants, such as CIT.

In this study, FLX served as the template molecule to create memory cavities in the polymer network. The macroporous monoliths NIC1/NaPA-CMCs and MIC2/NaPA-CMCs were characterized and subjected to FLX adsorption tests. The selective adsorption capacity of MIC2/NaPA-CMCs was preliminarily evaluated by competitive adsorption with CIT.

Results show that both NIC1/NaPA-CMCs and MIC2/NaPA-CMCs effectively removed FLX across experimental conditions. The adsorbed quantities were 24.96 $mg \cdot g^{-1}$ for MIC2/NaPA-CMCs and 29.6 $mg \cdot g^{-1}$ for NIC1/NaPA-CMCs at 40 ppm initial concentration and 1.5 $mL \cdot min^{-1}$ flow rate. Exhaustion times ranged from 170 to 964 min.

A continuous-flow adsorption study of FLX on both cryogels showed that initial concentration and flow rate shaped the breakthrough curves. The Thomas and Yoon–Nelson models effectively described the adsorption data. Internal diffusion proved the rate-limiting step.

FLX exhibited stronger affinity for MIC2/NaPA-CMCs' active surface than for CIT, and the imprinted cryogel showed higher potential for selective FLX removal than NIC1/NaPA-CMCs. This material could eventually support FLX preconcentration in various samples.

7.8 Acknowledgments

The authors would like to thank the Natural Sciences and Engineering Research Council of Canada (NSERC), grant no. RGPIN-2022-03510, for financial support, and the University of Quebec at Trois-Rivières for providing space, materials, and equipment to complete this research

7.9 Declaration of Competing Interest

The authors have no financial or non-financial interests to disclose.

7.10 Declaration of generative AI and AI-assisted technologies in the writing process

During the preparation of this work, the author(s) used [Grammarly, DeepL] to [improve the English language quality]. After using this tool/service, the author(s) reviewed and edited the content as needed and take full responsibility for the content of the published article.

7.11 Reference

[1] A. Lajeunesse, C. Gagnon, S. Sauvé, Determination of Basic Antidepressants and Their N-Desmethyl Metabolites in Raw Sewage and Wastewater Using Solid-Phase Extraction and Liquid Chromatography−Tandem Mass Spectrometry, Anal Chem 80 (2008) 5325-5333. https://doi.org/10.1021/AC800162Q.

[2] A.M. Christensen, S. Faaborg-Andersen, F. Ingerslev, A. Baun, Mixture and single-substance toxicity of selective serotonin reuptake inhibitors toward algae

and crustaceans, Environ Toxicol Chem 26 (2007) 85-91. https://doi.org/10.1897/06-219R.1.

[3] S.L. Gould, M.J. Winter, W.H.J. Norton, C.R. Tyler, The potential for adverse effects in fish exposed to antidepressants in the aquatic environment, Environ Sci Technol 55 (2021) 16299-16312. https://doi.org/10.1021/ACS.EST.1C04724.

[4] P. Arnnok, R.R. Singh, R. Burakham, A. Pérez-Fuentetaja, D.S. Aga, Selective Uptake and Bioaccumulation of Antidepressants in Fish from Effluent-Impacted Niagara River, Environ Sci Technol 51 (2017) 10652-10662. https://doi.org/10.1021/ACS.EST.7B02912.

[5] Antidepressant Use by Country 2025, (n.d.). https://worldpopulationreview.com/country-rankings/antidepressant-use-by-country (accessed September 29, 2025).

[6] L.J.G. Silva, C.M. Lino, L.M. Meisel, A. Pena, Selective serotonin reuptake inhibitors (SSRIs) in the aquatic environment: An ecopharmacovigilance approach, Science of The Total Environment 437 (2012) 185-195. https://doi.org/10.1016/J.SCITOTENV.2012.08.021.

[7] K. Köse, D. Yalçın Kehribar, V. Goodarzi, L. Uzun, Strategies for the detection, removal and elimination of antidepressants, Int J Environ Anal Chem 104 (2024) 323-354. https://doi.org/10.1080/03067319.2021.2019726.

[8] Fluoxetine: Uses, Interactions, Mechanism of Action | DrugBank Online. https://go.drugbank.com/drugs/DB00472 (accessed August 15, 2025).

[9] Pratishtha Khurana, R.K. Das, S. Kaur Brar, From prescription to pollution: environmental behavior and breakdown of fluoxetine, Environ Sci (Camb) (2025). https://doi.org/10.1039/D5EW00636H.

[10] C. Castillo-Zacarías, M.E. Barocio, E. Hidalgo-Vázquez, J.E. Sosa-Hernández, L. Parra-Arroyo, I.Y. López-Pacheco, D. Barceló, H.N.M. Iqbal, R. Parra-Saldívar, Antidepressant drugs as emerging contaminants: Occurrence in urban and non-

urban waters and analytical methods for their detection, Science of the Total Environment 757 (2021). https://doi.org/10.1016/j.scitotenv.2020.143722.

[11] S. Suárez, M. Carballa, F. Omil, J.M. Lema, How are pharmaceutical and personal care products (PPCPs) removed from urban wastewaters, Rev Environ Sci Biotechnol 7 (2008) 125-138. https://doi.org/10.1007/s11157-008-9130-2.

[12] A. Lajeunesse, S.A. Smyth, K. Barclay, S. Sauvé, C. Gagnon, Distribution of antidepressant residues in wastewater and biosolids following different treatment processes by municipal wastewater treatment plants in Canada, Water Res 46 (2012) 5600-5612. https://doi.org/10.1016/j.watres.2012.07.042.

[13] D. Correia, I. Domingues, M. Faria, M. Oliveira, Effects of fluoxetine on fish: What do we know and where should we focus our efforts in the future, Science of The Total Environment 857 (2023) 159486. https://doi.org/10.1016/J.SCITOTENV.2022.159486.

[14] P. Arnnok, R.R. Singh, R. Burakham, A. Pérez-Fuentetaja, D.S. Aga, Selective Uptake and Bioaccumulation of Antidepressants in Fish from Effluent-Impacted Niagara River, Environ Sci Technol 51 (2017) 10652-10662. https://doi.org/10.1021/ACS.EST.7B02912.

[15] A. Singh, D. Saidulu, A.K. Gupta, V. Kubsad, Occurrence and fate of antidepressants in the aquatic environment: Insights into toxicological effects on the aquatic life, analytical methods, and removal techniques, J Environ Chem Eng 10 (2022). https://doi.org/10.1016/J.JECE.2022.109012.

[16] A. Lajeunesse, M. Blais, B. Barbeau, S. Sauvé, C. Gagnon, Ozone oxidation of antidepressants in wastewater -Treatment evaluation and characterization of new by-products by LC-QToFMS, Chem Cent J 7 (2013) 1-11. https://doi.org/10.1186/1752-153X-7-15/FIGURES/7.

[17] M.J. Benotti, B.D. Stanford, E.C. Wert, S.A. Snyder, Evaluation of a photocatalytic reactor membrane pilot system for the removal of pharmaceuticals

and endocrine disrupting compounds from water, Water Res 43 (2009) 1513-1522. https://doi.org/10.1016/J.WATRES.2008.12.049.

[18] J.-W. Kwon, K.L. Armbrust, Degradation of Citalopram by Simulated Sunlight, 2005.

[19] J.J. García-Galán, A. Anfruns, R. Gonzalez-Olmos, S. Rodríguez-Mozaz, J. Comas, UV/H2O2degradation of the antidepressants venlafaxine and O-desmethylvenlafaxine: Elucidation of their transformation pathway and environmental fate, J Hazard Mater 311 (2016) 70-80. https://doi.org/10.1016/J.JHAZMAT.2016.02.070.

[20] D. Bonenfant, M. Mimeault, P. Niquette, R. Hausler, Adsorption study of a commonly used antidepressant drug, fluoxetine hydrochloride, onto a crosslinked β-cyclodextrin-carboxymethylcellulose polymer, Water Science and Technology 66 (2012) 224-230. https://doi.org/10.2166/WST.2012.112.

[21] R. Guillossou, J. Le Roux, R. Mailler, E. Vulliet, C. Morlay, F. Nauleau, J. Gasperi, V. Rocher, Organic micropollutants in a large wastewater treatment plant: What are the benefits of an advanced treatment by activated carbon adsorption in comparison to conventional treatment? Chemosphere 218 (2019) 1050-1060. https://doi.org/10.1016/J.CHEMOSPHERE.2018.11.182.

[22] M.J. Ahmed, B.H. Hameed, Removal of emerging pharmaceutical contaminants by adsorption in a fixed-bed column: A review, Ecotoxicol Environ Saf 149 (2018) 257-266. https://doi.org/10.1016/J.ECOENV.2017.12.012.

[23] A. Izadpanah, S. Nemati, S. Nojavan, A comprehensive review on synthesis and applications of cryogel-based sorbents in solid-phase extraction techniques, TrAC - Trends in Analytical Chemistry 180 (2024). https://doi.org/10.1016/j.trac.2024.117899.

[24] A. Kumar, R. Mishra, Y. Reinwald, S. Bhat, Cryogels: Freezing unveiled by thawing, 2010.

[25] V.M. Gun'ko, I.N. Savina, S. V. Mikhalovsky, Cryogels: Morphological, structural and adsorption characterisation, Adv Colloid Interface Sci 187-188 (2013) 1-46. https://doi.org/10.1016/j.cis.2012.11.001.

[26] J. Wang, Q.M. Wang, L.L. Tian, C. Yang, S.H. Yu, C. Yang, Research Progress of the Molecularly Imprinted Cryogel, Chinese Journal of Analytical Chemistry 43 (2015) 1777-1784. https://doi.org/10.1016/S1872-2040(15)60878-7.

[27] M.Y. Shi, L.J. Jiang, C.J. Yu, X.R. Dong, Q.Y. Yu, M.M. Yao, S.S. He, Z.W. Yue, F.L. Yao, H. Zhang, H. Sun, J.J. Li, A robust polyacrylic acid/chitosan cryogel for rapid hemostasis, Sci China Technol Sci 65 (2022) 1029-1042. https://doi.org/10.1007/S11431-021-1986-9/METRICS.

[28] R. Dobritoiu, S. Patachia, A study of dyes sorption on biobased cryogels, Appl Surf Sci 285 (2013) 56-64. https://doi.org/10.1016/J.APSUSC.2013.07.164.

[29] C.A. Mourão, C. Marcuz, K. Haupt, S.M.A. Bueno, Polyacrylamide-alginate (PAAm-Alg) and phospho-L-tyrosine-linked PAAm-Alg monolithic cryogels: Purification of IgG from human serum, Journal of Chromatography B 1129 (2019) 121783. https://doi.org/10.1016/J.JCHROMB.2019.121783.

[30] M.V. Dinu, A.I. Cocarta, E.S. Dragan, Synthesis, characterization and drug release properties of 3D chitosan/clinoptilolite biocomposite cryogels, Carbohydr Polym 153 (2016) 203-211. https://doi.org/10.1016/J.CARBPOL.2016.07.111.

[31] S. Bratskaya, Y. Privar, A. Slobodyuk, D. Shashura, D. Marinin, A. Mironenko, V. Zheleznov, A. Pestov, Cryogels of carboxyalkylchitosans as a universal platform for the fabrication of composite materials, Carbohydr Polym 209 (2019) 1-9. https://doi.org/10.1016/j.carbpol.2018.12.094.

[32] E. Yeşilova, B. Osman, A. Kara, E. Tümay Özer, Molecularly imprinted particle embedded composite cryogel for selective tetracycline adsorption, Sep Purif Technol 200 (2018) 155-163. https://doi.org/10.1016/j.seppur.2018.02.002.

[33] G.R.N. Nkana, B. Chabot, P. Nguyen-Tri, Adsorption of fluoxetine in aqueous environments: Development of macroporous cryogels based on sodium poly(acrylate) and carboxymethyl chitosan, React Funct Polym 205 (2024). https://doi.org/10.1016/j.reactfunctpolym.2024.106069.

[34] C. Marcuz, C. Alves Mourão, K. Haupt, S.M. Alves Bueno, Performance of phospho-L-tyrosine immobilized onto alginate/polyacrylamide-based cryogels: Effect of ligand coupling on human IgG adsorption and Fab fragments separation, Journal of Chromatography B 1165 (2021) 122530. https://doi.org/10.1016/J.JCHROMB.2021.122530.

[35] H.C. Thomas, B.C. HENRY THOMAS Vol, Heterogeneous Ion Exchange in a Flowing System, 1944.

[36] Y.H. Yoon, J.H. Nelson, Application of Gas Adsorption Kinetics I. A Theoretical Model for Respirator Cartridge Service Life, Am Ind Hyg Assoc J 45 (1984) 509-516. https://doi.org/10.1080/15298668491400197.

[37] A. Saravanan, P.S. Kumar, M. Yaswanthraj, Modeling and analysis of a packed-bed column for the effective removal of zinc from aqueous solution using dual surface-modified biomass, Particulate Science and Technology 36 (2018) 934-944. https://doi.org/10.1080/02726351.2017.1329243;SUBPAGE:STRING:ACCESS.

[38] L. Sheng, Y. Zhang, F. Tang, S. Liu, Mesoporous/microporous silica materials: Preparation from natural sands and highly efficient fixed-bed adsorption of methylene blue in wastewater, Microporous and Mesoporous Materials 257 (2018) 9-18. https://doi.org/10.1016/J.MICROMESO.2017.08.023.

[39] L. Yanyan, T.A. Kurniawan, M. Zhu, T. Ouyang, R. Avtar, M.H. Dzarfan Othman, B.T. Mohammad, A.B. Albadarin, Removal of acetaminophen from synthetic wastewater in a fixed-bed column adsorption using low-cost coconut shell waste pretreated with NaOH, HNO3, ozone, and/or chitosan, J Environ Manage 226 (2018) 365-376. https://doi.org/10.1016/J.JENVMAN.2018.08.032.

[40] Citalopram: Uses, Interactions, Mechanism of Action | DrugBank Online. https://go.drugbank.com/drugs/DB00215 (accessed August 15, 2025).

Chapitre 8 - Conclusions

8.1 Conclusions générales

Les antidépresseurs sont des contaminants émergents biorécalcitrants, persistants et bioactifs qui échappent aux procédés de traitement conventionnels des eaux usées dans les STEP, ce qui en fait des vecteurs de contamination des milieux aquatiques. Les effets chroniques négatifs des antidépresseurs sur le biote aquatique non ciblé vivant dans les milieux récepteurs sont une source de préoccupation d'autant plus qu'une toxicité synergique et/ou cumulée est de plus en plus évoquée. Cela représente un défi environnemental complexe pour éviter, à long terme, le déséquilibre du réseau trophique et la disparition de certaines espèces aquatiques. Les moyens existants pour leur élimination efficace sont marqués par de nombreuses insuffisances, ce qui motive la recherche et le développement de solutions plus vertes, simples, durables et économiques. Les matériaux fonctionnels biosourcés et leurs composites se démarquent comme des alternatives viables et crédibles pour l'élimination des contaminants de l'eau. Les regards se tournent de plus en plus vers des matériaux hydrogélifiés et cryogélifiés pour leur architecture poreuse, ainsi que pour leurs nombreuses propriétés exceptionnelles, idéales pour développer des systèmes multifonctionnels et intelligents capables d'éliminer efficacement les antidépresseurs dans les milieux aqueux.

Dans ce sens, cette thèse a porté sur le développement des hydrogels sphériques biosourcés de carboxyméthylchitosane et de cryogels hybrides monolithiques partiellement biosourcés combinant le carboxyméthylchitosane avec le poly(acrylate) de sodium pour éliminer les antidépresseurs notamment la FLX dans une solution aqueuse contenant 5 % de méthanol. La méthode d'extrusion électrostatique suivit de la gélification dans un bain de $CaCL_2$ et une stabilisation par la génipine a été l'approche adoptée pour élaborer les hydrogels sphériques poreux tandis que la cryopolymérisation a été adoptée pour élaborer les cryogels hybrides monolithiques avec ou sans cavités mémoires. Les cavités mémoire ont été introduites dans le réseau polymère du cryogel hybride par l'ajout de la FLX, molécule modèle, dans la solution de polymères avant la cryopolymérisation, suivie de son extraction par lavage avec le solvant (5% de

méthanol/0,1 M HCl, 1:1 v/v). Le but a été d'investiguer dans un premier temps la capacité d'adsorption en mode discontinu des hydrogels sphériques et des cryogels hybrides sans cavités mémoire puis, de retenir le matériau dont l'échafaudage tridimensionnel n'a pas été affecté par les cycles d'adsorption/désorption. Ce matériau (cryogel hybride) a ensuite été appliqué à des essais d'adsorption en mode dynamique. L'adsorption compétitive avec le CIT et la VEN a été étudiée, et une étude de la sélectivité des cryogels hybrides dotés ou non de cavités mémoire a enfin été effectuée.

Les différentes analyses et interprétations des résultats ont permis d'établir les conclusions suivantes :

- La caractérisation du produit de synthèse par spectroscopie FTIR et analyse ^{1}H RMN a confirmé le greffage des groupes carboxyméthyles sur la structure du chitosane avec un degré de substitution de 1,78 et 1,12 pour les dérivées N,O-CMCs et O-CMCs respectivement. La méthode d'extrusion électrostatique (7.5 kV), gélification dans un bain de $CaCl_2$/éthanol 70 % et stabilisation avec la génipine 1mM a permis de fabriquer avec succès des hydrogels sphériques de taille homogène. Visuellement, la formation des ponts covalents entre les chaînes de polymère a été confirmée par la couleur bleue des billes. Les hydrogels fabriqués étaient hydrophiles, présentaient une grande capacité de gonflement et une charge de surface globalement négative. L'analyse de la morphologie a révélé une structure poreuse avec une surface spécifique de 38,69 m^2/g pour la plus élevée. Les tests d'adsorption en batch réalisés ont indiqué une meilleure efficacité d'élimination de la FLX lorsque la concentration initiale augmentait, avec les conditions où le pH était fixé à 8,5 et la température à 30 °C pendant un contact de 180 min. La modélisation du processus d'adsorption a indiqué une cinétique du pseudo-second ordre avec une diffusion interne rapide dans les macropores comme l'a indiqué la constante de diffusion intraparticulaire dans la première phase du processus. L'isotherme de Langmuir s'adaptait mieux aux données d'adsorption ($R^2 > 0.99$) et une synergie d'interactions physiques dont les interactions électrostatiques étaient responsables de l'adsorption. L'échantillons PHB4 et PHB5 se sont démarqués comme les meilleurs adsorbants et les essais d'adsorption/désorption effectués sur ces matériaux ont montré la fragilité des

échafaudages même si après cinq cycles l'efficacité d'élimination de la FLX était supérieure à 65 %

- Pour améliorer la stabilité des hydrogels, l'approche de fabrication a été modifiée et l'ajout d'un polymère synthétique dans le réseau polymère a été effectué. La cryopolymérisation de la combinaison acrylate de sodium/carboxyméthylchitosane a permis d'obtenir des monolithes. Ceux-ci ont une architecture macroporeuse dotée d'un réseau de pores interconnectés avec une surface spécifique de 74,9 m^2/g et une porosité de 85 ± 1,6 % pour la plus élevée (NaPA4-CMCs). Un gonflement rapide au contact de l'eau a été observé et leur charge de surface était globalement négative lorsque le pH de la solution est supérieur aux points de charge nulle identifiés. L'adsorption en batch a été réalisée sur les différents cryogels élaborés. L'échantillon NaPA4-CMCs a montré la meilleure efficacité d'élimination de la FLX à pH 8.5 avec une capacité d'adsorption maximale de 80,6 ± 3,4 mg/g. La diffusion dans les macropores et les mésopores était rapide; le processus d'adsorption était favorable, exothermique et physique. Au bout de trois cycles d'adsorption/désorption, les performances du NaPA4-CMCs demeuraient supérieures à 60 % et aucun signe d'effondrement de la structure monolithique n'a été observé.
- Les cryogels hybrides ont été appliqués à l'adsorption continue dans une colonne à lit fixe, à flux descendant, à l'aide d'un montage simple. L'analyse des paramètres de fonctionnement a indiqué un rendement d'élimination de la FLX de 59 % lorsque ceux-ci étaient fixés comme suit : pH 8.5, hauteur du monolithe 0.4 cm, le débit 1.5 mL/min et la concentration initiale 10 ppm. Les essais d'adsorption compétitives ont indiqué une meilleure affinité de la FLX avec la surface du cryogel hybride par rapport à la VEN et le CIT. Le profil de percée étaient bien décrit par les modèles de Thomas et de Yoon-Nelson et la désorption en mode dynamique méritent d'être optimisée car une chute significative de l'efficacité d'adsorption de la FLX a été noté après quatre cycles d'adsorption/désorption (17.76 %).
- Le développement du cryogel à empreinte moléculaire a été effectué dans le but de comparer l'efficacité d'adsorption dynamique du cryogel à empreinte

moléculaire par rapport au cryogel non imprimé et d'évaluer sa sélectivité d'adsorption de la FLX dans un milieu aqueux complexe. Lorsque les paramètres de fonctionnement de la colonne étaient pH 8.5, débit 1.5 mL/min, la hauteur du monolithe 0.4 cm, le cryogel non imprimé (NIC1/NaPA-CMCs) et le cryogel à empreinte moléculaire (MIC2/NaPA-CMCs) avaient des capacités d'adsorption très proches (14.02 mg/g et 13.64 mg/g). Alors que, dans les mêmes conditions l'adsorption compétitive avec le CIT, le monolithe MIC2/NaPA-CMCs a été meilleur pour l'adsorption sélective de la FLX par rapport au monolithe NIC1/NaPA-CMCs comme l'a indiqué les valeurs de $q_{e.exp}$ (13.78 mg/g et 9.98 mg/g). Ainsi, le MIC2/NaPA-CMCs serait plus adéquat pour élimination la FLX dans les environnements aqueux complexe par rapport au NIC1/NaPA-CMCs grâce aux cavités mémoires introduite.

8.2 Contributions au domaine

Les contributions au domaine de cette thèse résident donc dans :

1. La gélification des gouttelettes chargées de carboxyméthylchitosane a été réalisée avec succès dans un bain contenant 70 % d'éthanol, ce qui n'avait jusqu'ici pas été démontré.
2. La fabrication d'un cryogel hybride à empreinte moléculaire selon l'approche évoquée dans nos travaux est un point qui, à notre connaissance, n'a jamais été réalisé dans aucune étude.
3. Cette étude montre pour la première fois l'utilisation de matériaux hydrogélifiés et cryogélifiés pour l'élimination des antidépresseurs dans des solutions aqueuses et met en lumière leur potentiel.

8.3 Travaux futurs

Cette étude a révélé le potentiel notamment de cryogel hybride doté de cavité mémoire ou non éliminer la FLX en flux continu et a montré en particulier à travers une étude préliminaire la capacité du cryogel à empreinte moléculaire à éliminer sélectivement la FLX dans un milieu aqueux contenant un polluant ayant une structure et des propriété

physico-chimiques très proches. Toutefois, de nombreux points d'ombre subsistent et leur éclaircissement fait office de perspective dans le cadre de cette recherche:

1. Optimiser adéquatement la régénération du cryogel hybride par un traitement en flux continu à l'aide d'un solvant approprié.
2. Investiguer d'autres paramètres de fonctionnement (pH, hauteur du monolithe), entre autres, au cours de l'adsorption dynamique, afin de dimensionner un filtre qui sera par la suite soumis à des tests d'adsorption dynamique à l'échelle pilote.
3. Faire les tests mécaniques du cryogel hybride afin d'étudier sa résistance aux contraintes mécaniques ainsi qu'une évaluation précise de sa perméabilité.
4. Faire des essais d'adsorption dynamique avec des eaux usées dans lesquelles coexistent plusieurs types de contaminants.

Annexe 1

Liste des publications (Articles)

Article 1: Design of porous spherical biomaterials from carboxymethyl chitosan for removal of fluoxetine in aqueous medium

Gilbert Romeo Nkana Nkana[a,b], André Lajeunesse[c], Bruno Chabot[a*], Phuong Nguyen-Tri[a,b]

[a] *Institut d'Innovations en Écomatériaux, Écoproduits et Écoénergies, Université du Québec à Trois-Rivières, 3351 boul. des Forges, C.P. 500, Trois-Rivières, QC G9A-5H7, Canada*
[b] *Laboratory of Advanced Materials for Energy and Environment, Université du Québec à Trois-Rivières, 3351 boul. des Forges, C.P. 500, Trois-Rivières, QC G9A-5H7, Canada*
[c] *Station d'épuration Jean-R. Marcotte, 12001 boul. Maurice-Duplessis, Montréal, QC, H1C-1V3, Canada*

*Corresponding author. *E-mail address:* Bruno.Chabot@uqtr.ca

Article 2: Adsorption of Fluoxetine in Aqueous Environments: Development of Macroporous Cryogels Based on Sodium Poly(Acrylate) and Carboxymethyl Chitosan

Gilbert Romeo Nkana Nkana[a,b], Bruno Chabot[a*], Phuong Nguyen-Tri[a,b]

[a] *Institut d'Innovations en Écomatériaux, Écoproduits et Écoénergies, Université du Québec à Trois-Rivières, 3351 boul. des Forges, C.P. 500, Trois-Rivières, QC G9A-5H7, Canada*
[b] *Laboratory of Advanced Materials for Energy and Environment, Université du Québec à Trois-Rivières, 3351 boul. des Forges, C.P. 500, Trois-Rivières, QC G9A-5H7, Canada*
[c] *Station d'épuration Jean-R. Marcotte, 12001 boul. Maurice-Duplessis, Montréal, QC, H1C-1V3, Canada*

*Corresponding author. *E-mail address:* Bruno.Chabot@uqtr.ca

Article 3: Removal of fluoxetine by adsorption in a fixed-bed column using a hybrid cryogel based on sodium poly(acrylate) / carboxymethyl chitosan

Gilbert Romeo Nkana Nkana[a,b], Bruno Chabot[a*], Phuong Nguyen-Tri[a,b]

[a] *Institut d'Innovations en Écomatériaux, Écoproduits et Écoénergies, Université du Québec à Trois-Rivières, 3351 boul. des Forges, C.P. 500, Trois-Rivières, QC G9A-5H7, Canada*
[b] *Laboratory of Advanced Materials for Energy and Environment, Université du Québec à Trois-Rivières, 3351 boul. des Forges, C.P. 500, Trois-Rivières, QC G9A-5H7, Canada*
[c] *Station d'épuration Jean-R. Marcotte, 12001 boul. Maurice-Duplessis, Montréal, QC, H1C-1V3, Canada*
*Corresponding author. *E-mail address: Gilbert.Nkana@uqtr.ca*

Article 4: Design of a Sodium Acrylate/Carboxymethyl-Chitosan-Based Imprinted Cryogel for the Selective Adsorption of Fluoxetine in Continuous Mode

Gilbert Romeo Nkana Nkana[1,2*], Mostafa Eesaee[1,2], Bruno Chabot[1], Phuong Nguyen Tri[1,2]

[1] *Institut d'Innovations en Écomatériaux, Écoproduits et Écoénergies, Université du Québec à Trois-Rivières, 3351 boul. des Forges, C.P. 500, Trois-Rivières, QC G9A-5H7, Canada*

[2] *Laboratory of Advanced Materials for Energy and Environment, Université du Québec à Trois-Rivières, 3351 boul. des Forges, C.P. 500, Trois-Rivières, QC G9A-5H7, Canada*

*Corresponding author. *E-mail address*: Bruno.Chabot@uqtr.ca

Liste des publications (présentations orales)

- Colloque conjoint en écotoxicologie 2021 : Conception d'un biomatériau sphérique de chitosane modifié pour l'adsorption de substances émergentes dans les eaux usées.
- Première conférence internationale sur les matériaux pour des applications environnementales et bioressources (ICM2EBA) 2022: Conception de biosorbants sphériques poreux à partir de dérivés du chitosane pour l'élimination de résidus pharmaceutiques.
- Colloque étudiant 2023 Consortium de recherche et d'innovation en bioprocédés industriels au Québec (CRIBIQ) : Conception de biomatériaux sphériques poreux à partir de carboxyméthylchitosane pour l'élimination de la FLX en milieu aqueux.
- Conférence internationale sur les matériaux pour des applications environnementales et bioressources (ICM2EBA) 2025 : Elimination of antidepressant by dynamic adsorption in a fixed-bed column of hybrid cryogel based on sodium acrylate and carboxymethyl chitosan.